Agronomy Research

Established in 2003 by the Faculty of Agronomy, Estonian Agricultural University

Aims and Scope:
Agronomy Research is a peer-reviewed international Journal intended for publication of broad-spectrum original articles, reviews and short communications on actual problems of modern biosystems engineering incl. crop and animal science, genetics, economics, farm- and production engineering, environmental aspects, agro-ecology, renewable energy and bioenergy etc. in the temperate regions of the world.

***Agronomy Research* online:**
Agronomy Research is available online at: https://agronomy.emu.ee/

Acknowledgement to Referees:
The Editors of *Agronomy Research* would like to thank the many scientists who gave so generously of their time and expertise to referee papers submitted to the Journal.

Abstracted and indexed:
SCOPUS, EBSCO, DOAJ, CABI Full Paper and Clarivate Analytics database: (Zoological Records, Biological Abstracts and Biosis Previews, AGRIS, ISPI, CAB Abstracts, AGRICOLA (NAL; USA), VINITI, INIST-PASCAL.)

Subscription information:
Institute of Technology, EMU
Fr.R. Kreutzwaldi 56,
51006 Tartu,
ESTONIA
e-mail: timo.kikas@emu.ee

ISSN 1406-894X

CONTENTS

Agronomy Research **20**(2), 241–260, 2022
https://doi.org/10.15159/AR.22.031

Efficiency of productivity potential realization of different-age sites of a trunk of grades of columnar type apple-trees

O. Havryliuk[1,*], T. Kondratenko[2], B. Mazur[1], O. Tonkha[1], Y. Andrusyk[1], V. Kutovenko[1], R. Yakovlev[1], V. Kryvoshapka[2], A. Trokhymchuk[2] and Y. Dmytrenko[1]

[1]National University of Life and Environmental Sciences of Ukraine, 15 Heroiv Oborony Str., UA03041 Kyiv, Ukraine
[2]Institute of Horticulture of National Academy of Agrarian Sciences of Ukraine, 23 Sadova Str., UA03027 Novosilky, Kyiv Region, Ukraine
[*]Correspondence: o.havryliuk@nubip.edu.ua

Received: April 15th, 2022; Accepted: May 15th, 2022; Published: May 17th, 2022

Abstract. An article provides information about buds organogenesis in plants of columnar apple cultivars in the Forest-Steppe of Ukraine (Kyiv), which allows to establish the features of this process in complex fruit formations of different ages, and their productivity and longevity. We recommend studying of apple trees productivity in the process of its formation by analyzing of rudimentary organs formation and their consistent development into vegetative and generative organs, which are elements of productivity. Studies of organogenesis different-age fruit formations of columnar apple cultivars were conducted in the northern part of the Forest-Steppe of Ukraine during 2016–2020. It was established that separate age sections of columnar apple trees trunk formed different initial productivity potential. In plants of all studied varieties and age groups, the laying of generative buds, the implementation of reproductive elements in V–IX and X–XI stages of organogenesis were more effective in older age areas of the trunk. Complex fruit formations, regardless of the trunk age where they are placed, form a high potential for productivity, which is effectively realized. The dependence of the formation and productivity potential realization on the stages of organogenesis and meteorological factors is established.

Key words: columnar apple, productivity, organogenesis, differentiation of generative buds, fruit formations.

INTRODUCTION

According to Isaeva (1989), apple productivity is the sum of all organic matter formed during the process of photosynthesis, which is often identified with yield; the latter is only an integral part of biological productivity (Rather et al., 2018; Vasylenko et al., 2021; Havryliuk et al., 2022). The transition of apple plants from vegetative to reproductive is due to the differentiation of generative buds (Duric et al., 1997; Buntsevich & Sergeeva, 2014; Kohek et al., 2015, Mazurenko et al., 2020; Zavadska et al., 2021). This process is the key in the problem of creating early fruiting plantations with regular fruiting of apple trees (Zamorskyi, 2007). Its passage occurs during the III–IV stages of organogenesis, so, according to Isaeva (1989), the above stages are considered critical, because the environmental conditions in this period on the possibility of potential components of fruiting transition to the actual laying of flowers (El-Sabagh et al., 2012; Gavryliuk et al., 2019; Mezhenskyj, 2019; Mezhenskyj et al., 2020). Differentiation of generative buds is influenced by various factors of both external and internal nature: rootstock, age and type of fruit formation, moisture, mineral and organic nutrition, timing and degree of flowering, yield load (Isaeva, 1989; Palubicki et al., 2009; Amasino, 2010; El Yaacoubi et al., 2020; Shevchuk et al., 2021a, 2021b; Miloševic et al., 2022). More details on research methods can be found in Havryliuk et al., 2022.

MATERIALS AND METHODS

The study was conducted during 2016–2020 at the Department of Horticulture named after Professor Volodymyr Levkovych Symyrenko of the National University of Life and Environmental Sciences of Ukraine. The experimental basis for the research was the planting of apple trees of the primary variety test at the Institute of Horticulture of the National Academy of Agrarian Sciences of Ukraine (IH NAAS).

The subject of research - 4 columnar type varieties of apples of Ukrainian and foreign selection (Varieties of Ukrainian selection - 'Bilosnizhka'('Bolero' × 'Reinette Symyrenko'), 'Favoryt' ('Trident' × 'Redfree'); Varieties of Russian selection - 'Valuta' (KV6 × OR38T17), 'President' (Free Pollination KV103)). The object of research is the processes of formation potential and real (economic) productivity of apple varieties formation.

The investigated orchard was laid in 2010 according to the primary variety testing method. Planting is not irrigated. Apple trees on rootstock 54–118 were planted according to the 4×1 m scheme.

The experimental site is located in the zone of the Western Forest-Steppe of Ukraine. The climate of the district is temperate continental and is characterized by mild winters and warm summers. The average annual temperature is 7.4 °C. The coldest month is January, with an average monthly temperature of minus 5.8 °C, and the warmest month is July (19.6 °C). The first autumn frosts are observed from the second decade of October. Winter begins in the second decade of November. Permanent snow cover is established in December and disappears in the second decade of March. Thawing during the winter period (December-February) lasts an average of 40 days (repeated 8 to 10 times lasting 5 days). Spring frosts are likely by mid-May.

The growing season in fruit crops, according to long-term data, begins in the first decade of April. Active growth and development of fruit plants is observed in the third decade of April. The sum of active temperatures of 10 °C and above ($\Sigma_{act}t \geq 10$ °C) is 2850 °C, the number of days with temperatures of 10 °C and above - about 160. The average annual rainfall reaches 597 mm, most of which falls from April to October (400 mm). The wettest months are the summer months - from June to August, with an average of 68–81 mm of precipitation per month. In the period from November to March, about 230 mm of precipitation falls. The average number of days with precipitation is 160.

Meteorological data for the years in research were obtained at the Vantage Pro2 Plus weather station. The hydrothermal coefficient (HTC of Selyaninov) was calculated by dividing the amount of precipitation in mm by the sum of active temperatures of 10 °C and above for the period of fruits growth and development, the obtained data were decreased 10 times.

The soil of the study area is Greyic Phaezems Albic (Tonkha et al., 2020). The content of humus in the arable soil layer (0–40 cm) is 1.84 ± 0.07%, the pH of the aqueous extract is 6.1 ± 0.15.

Instruments. The buds, in which features of organogenesis were investigated, were selected in five repetitions from complex flushes located in the middle part of the trunk of a certain age, anatomical sections of buds 30–60 μm thick were made using a freezing microtome OmE. The obtained material was investigated using a microscope MBI-6 at a magnification of 90–180 times.

Methods. The height, trunk diameter and crown width of the trees were measured. Quantitative evaluation of productivity formation of apple varieties at III–IV organogenesis stages and the effectiveness of implementation of its elements into the real yield (V–XI stages of organogenesis) were performed according to Isaeva (1989) method. SEC (statistical evaluation coefficient) was calculated as the ratio of reproductive elements number at a certain organogenesis stage to the number of buds that reached stage II of organogenesis.

Description of the Experiment. The number of reproduction elements at certain organogenesis stages was analyzed during the research. Correlation analysis of influence weather factors over 5 years on the actual number of potential fruiting points depending on organogenesis stage was also conducted.

Sample preparation: The number of buds per plant was calculated in early August. When the air temperature was less than 5 °C, the number of buds that differentiated into generative ones was counted. From the onset of subzero temperatures, anatomical and morphological analysis of the buds was performed under a microscope to determine their condition in the pre-winter period. During the IX organogenesis stage (flowering), the total number of flowers per plant was counted. At the stage X of organogenesis (in June), the number of ovaries that did not fall was counted. The number of fruits was counted at the XI stage of organogenesis.

Number of samples analyzed: four varieties of columnar-shaped type apples took part in the research. Each variety is represented by five plants (20 trees in total). On each of the trees counted the number of reproductive elements at certain stages of organogenesis, respectively, at all trunk ages (Havryliuk et al., 2022).

Statistical analysis. The strength of the connection between meteorological elements years of research and the number of reproduction elements at a certain stage of organogenesis was calculated using correlation analysis. Factor influence by the correlation coefficient is weak ≤ 0.29, moderate: 0.30–0.49, noticeable: 0.50–0.69, high: 0.70–0.89, very high: 0.90–0.99 (LSD: Least significantly difference at $P < 0.05$). Statistical processing was performed in Microsoft Excel 2016 in combination with XLSTAT.

RESULTS AND DISCUSSION

During the III–IV stages of organogenesis due to the flowers formation in the generative buds the laying of tree productivity elements occurs (Kohek et al., 2015), at this time there is already a loss of productivity potential due to vegetative buds on simple and complex rings, on which generative buds are not differentiate (buds with incomplete cycle of organogenesis) (Yareshchenko et al., 2012). Kolomiets (1976) and Kobel (1984) investigated the dependence of generative buds differentiation on meteorological conditions. Isaeva (1989) experimentally found that this process begins earlier in warm and fairly dry summers than in cold and rainy. Kondratenko (2003) found a varietal difference in the timing of generative buds differentiation, in the degree of development of the latter in the pre-winter period, as well as in the timing and duration of IX–X stages of organogenesis for traditional apple genotypes. There is currently no information on the buds organogenesis in plants of columnar apple cultivars, which would make it possible to establish the features of this process in complex rings of different ages, as well as the levels of their productivity and longevity.

Plants of columnar apple varieties differ from traditional ones by almost complete lack of lateral branching, crop formation on simple and complex rings (fruit formations) located on the trunk of the tree, as well as dwarf growth, early fruiting and high yields (Lapins, 1969; Tobutt, 1984; Zakharov, 2011). According to research, the trunk of columnar varieties is densely covered with fruit formations, their location on the main and singular tree trunk in the first 5–7 years is uniform (Fig. 1), later perennial fruit formations are formed clustered, often unevenly.

a)  b) 

Figure 1. Symmetrical placement of fruit formations on the trunk of columnar apple trees: (seven-year plants of the variety 'Valuta', 2017).

The height of plant trunks of all varieties is insignificant (about 45 cm), the height of the crown exceeds its size 4–6 times (Fig. 2).

In studies, trees of columnar varieties, on a medium-sized rootstock 54–118 differed significantly in height, trunk diameter, crown width and density of fruit formations on the trunk (Table 1). Plants of 'Valuta', 'President', 'Bilosnizhka' and 'Favoryt' varieties at the age of 10 were at the level of 2.54–2.93 m.

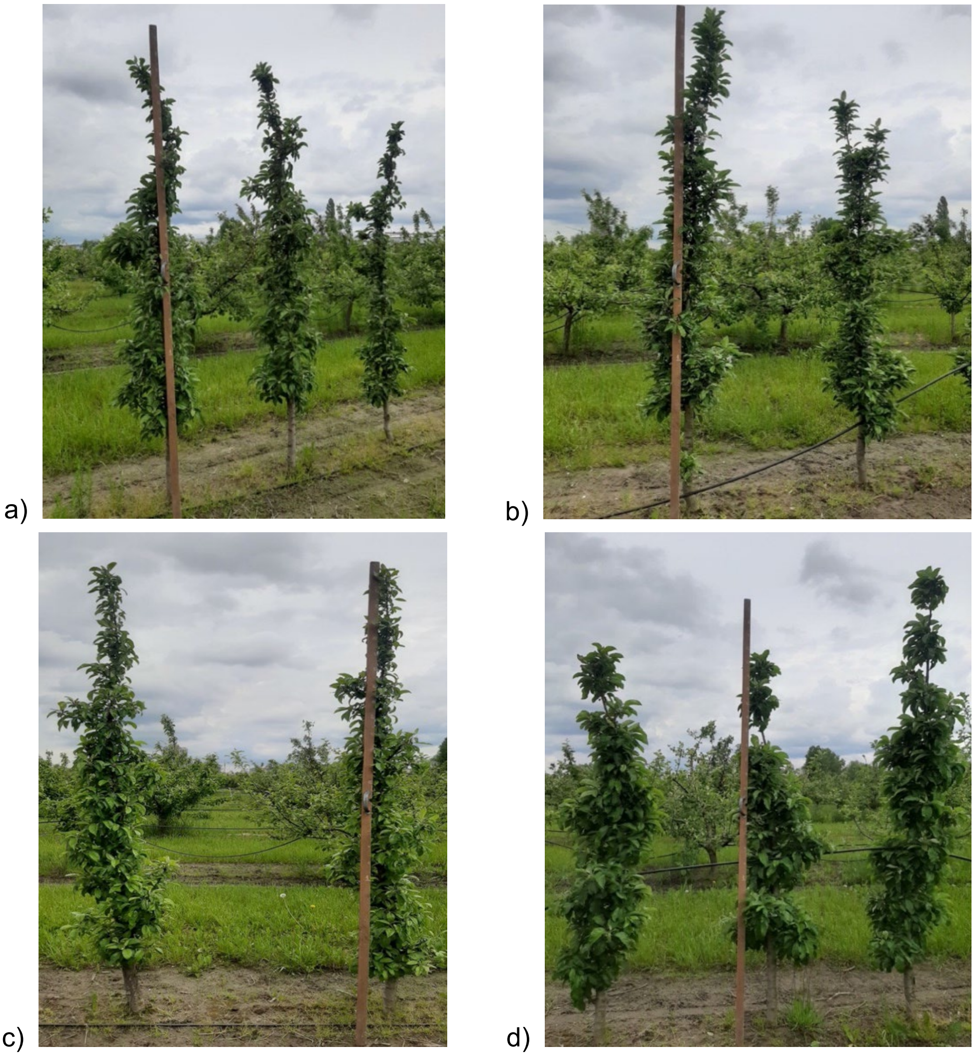

Figure 2. Height of 10-year-old plants of columnar varieties: a – ‘Valuta’; b – ‘President’; c – ‘Favoryt’; d – ‘Bilosnizhka’.

The diameter of the trunk varies between 5.63–8.00 cm. The width of the crown of columnar varieties is determined by the length of fruit formations (rings, fruit, fruit twigs) located on the trunk. This parameter in ‘Bilosnizhka’ is 20% less than in ‘President’; this is due to the increased shoot-forming ability of this variety. The largest number of buds per running meter of the trunk was placed on plants of the ‘Valuta’ variety, the smallest - on the ‘Bilosnizhka’.

Therefore, depending on the variety, such tree parameters as height, trunk diameter and crown width vary. As the height of the trees increases, the number of fruit formations on the plant increases, resulting in an increase in the potential for higher yields.

Table 1. Parameters of trees of columnar apple varieties. IH NAAS, 2019

Variety	Tree height, cm	Trunk diameter, cm	Crown width, cm	Number of buds, pcs/running m of trunk
'Bilosnizhka'	2.54[b]	6.57[b]	52.00[a]	60.47[a]
'Valuta'	2.81[a]	5.70[c]	40.33[c]	74.36[a]
'President'	2.69[b]	5.63[c]	38.67[c]	69.87[a]
'Favoryt'	2.93[a]	8.00[a]	46.00[b]	66.00[a]

Means in columns with the different letter are highly significantly different according to the Fisher's test ($P \leq 0.05$).

Anatomical and morphological analysis of buds studied columnar varieties showed that in conditions of the Forest-Steppe of Ukraine (Kyiv) at the end of July they are in the II stage of organogenesis in their development. This period corresponds to the formation of productivity potential, which is quantified by the total number of buds, which have reached this stage (Havryliuk et al., 2019). Separate age sections of tree trunks columnar apple varieties form different initial productivity potential. Thus, in seven-year-old trees of the 'Valuta' variety, the five-seven-year-old sections of the trunk had the largest share in the formation of potential productivity - 57% of the total number of buds, formed on the whole tree, were located on them (Table 2).

Table 2. Involvement of 'Valuta' tree trunks of different ages in productivity formation (%). IH NAAS, 2016–2018

Age of the trunk segment	Stage of organogenesis / Year of research											
	II			III–IV			X			XI		
	2016	2017	2018	2016	2017	2018	2016	2017	2018	2016	2017	2018
1	6.8	8.9	9.4	0.0	1.3	0.0	0.0	1.1	0.0	0.0	1.2	0.0
2	12.6	6.7	7.0	6.0	6.0	0.0	10.5	6.2	0.0	12.4	7.1	0.0
3	7.6	8.2	5.9	8.4	10.2	11.1	19.2	10.5	8.3	24.4	10.9	9.5
4	15.3	7.6	7.0	20.3	10.5	23.3	29.4	10.9	25.2	35.5	11.5	17.8
5	20.5	10.9	8.3	30.3	14.5	5.6	40.9	14.2	8.3	27.7	9.1	9.5
6	25.2	13.9	10.4	25.9	15.1	13.3	0.0	17.1	10.0	0.0	15.6	13.3
7	12.1	20.3	13.3	9.1	19.7	19.4	0.0	21.6	20.2	0.0	22.4	20.6
8		23.6	20.3		22.7	6.7		18.4	6.7		22.3	6.7
9			18.4			20.6			21.3			22.5
Total	100	100	100	100	100	100	100	100	100	100	100	100

The same pattern is observed in the following years, the oldest age areas formed the largest number of fruit formations of the total number on the tree.

During the III–IV stages of organogenesis in 2016 (mid-July-November inclusive) trees of the variety 'Valuta' laid 90 pieces/tree generative buds, the largest number of which was recorded in five to six-year sections of the trunk (Table 2). No flower buds were formed on the shoot. In 2017, trees of this variety were laid 121 pieces/tree generative buds, and in 2018 - 5 pieces/tree. The most effective differentiation of generative buds in 2017 took place on the complex rings of the eight-year-old section of the trunk, and the following year - in the four- and nine-year. The highest level of productivity potential realization at the III–IV stages of organogenesis in seven-year-old plants was observed on fruit formations located on a five-year section of the trunk, although no significant difference between three-six-year sections was found (Table 3). In eight-year-old trees, no significant difference was found between three- to eight-year-old sections of the fruit tree trunk, and three- to nine-year-old trees the following year. Over the years of research, the lowest productivity potential at the III–IV stages of organogenesis was characterized by one-year fruit formations.

In 2017, during the IX–X stages of organogenesis, were observed Frosts-damaged ovaries plants (Fig. 3). In 2018, during the IX–X stages of organogenesis, favourable meteorological conditions were observed for flowering, fertilization, and fruit growth. One-year-old fruit formations this year retained the fewest elements of reproduction during these stages; the largest - the oldest.

In 2019, 10-year-old plants showed a critically low level of flowers and fruits formation in different age areas of the trunk. At the end of the X stage of organogenesis, the most productive were complex fruit formations located on four-seven-year sections of the trunk.

Figure 3. Frosts-damaged ovaries in 'Valuta' plants (IX–X stages of organogenesis), 2017.

At the end of the XI stage of organogenesis in eight-year-old plants (2017), the largest share of fruits from the total number on the tree was recorded on three-year-old rings. The following year, the reduction during phase XI was minimal. The smallest share of formed fruits from the total harvest was observed on rings of one-year growth, the largest - on fruit formations, which are located on four-year sections of the trunk (Table 3).

A diagram is constructed according to the determined values of the shares of the influence of individual factors and their interaction with the real harvest (Fig. 4).

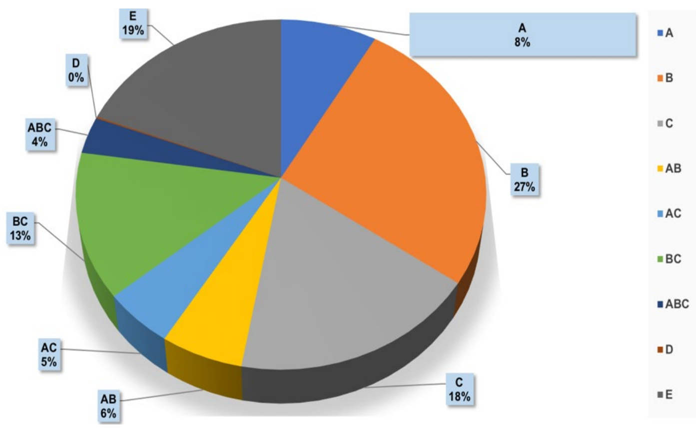

A, Age of tree section; **B**, Stage of organogenesis; **C**, Year of research; **D**, Factors not taken into account; **E**, Other factors.

Figure 4. The structure of various factors influences the real harvest formation of the variety 'Valuta', IH NAAS of Ukraine, 2016–2020.

Table 3. Participation of different age sections of the trunk in productivity formation of 'Valuta' trees at different stages of organogenesis, 2016–2020

Age of the trunk segment	The number of reproduction elements at certain stages of organogenesis (SEC)																
	Stage of organogenesis / Year of research																
	2016	2017				2018				2019				2020			
	II	III–IV	V–IX	X	XI	III–IV	V–IX	X	XI	III–IV	V–IX	X	XI	III–IV	V–IX	X	XI
1	1.000	0.000	0.000	0.000	0.000	0.068^{c}	0.340^{c}	0.083^{c}	0.067^{c}	0.000	0.000	0.000	0.000	0.258^{b}	1.300^{b}	0.298^{cd}	0.166^{dc}
2	1.000	0.387^{b}	1.834^{ab}	0.431^{b}	0.300^{b}	0.477^{b}	2.386^{b}	0.647^{ab}	0.574^{b}	0.000	0.000	0.000	0.000	0.478^{ab}	2.355^{ab}	0.553^{bcd}	0.383^{cd}
3	1.000	0.732^{a}	2.593^{a}	1.284^{a}	0.914^{a}	0.705^{ab}	3.526^{ab}	0.858^{ab}	0.696^{ab}	0.035^{ab}	0.175^{ab}	0.053^{b}	0.035^{ab}	0.342^{b}	1.745^{b}	0.263^{dc}	0.229^{cd}
4	1.000	0.847^{a}	2.903^{a}	0.969^{ab}	0.690^{ab}	0.746^{a}	3.728^{a}	1.013^{a}	0.821^{a}	0.055^{a}	0.275^{a}	0.146^{a}	0.055a	0.568^{a}	2.803^{a}	1.298^{a}	1.025^{a}
5	1.000	0.939^{a}	3.361^{a}	1.035^{ab}	0.375^{b}	0.758^{a}	3.790^{a}	0.846^{ab}	0.456^{b}	0.015^{b}	0.076^{b}	0.045^{b}	0.030^{ab}	0.456^{ab}	2.195^{ab}	0.715^{bc}	0.603^{bc}
6	1.000	0.657^{ab}	2.647^{a}	0.000	0.000	0.615^{ab}	3.073^{ab}	0.835^{ab}	0.584^{b}	0.022^{a}	0.108^{ab}	0.032^{b}	0.022^{a}	0.575^{a}	2.874^{a}	0.472^{cd}	0.381^{cd}
7	1.000	0.272^{b}	0.894^{b}	0.000	0.000	0.566^{a}	2.832^{a}	0.770^{a}	0.619^{b}	0.033^{ab}	0.166^{ab}	0.075^{ab}	0.042^{ab}	0.603^{a}	3.053^{a}	0.875^{b}	0.638^{b}
8	1.000					0.543^{ab}	2.716^{ab}	0.540^{b}	0.514^{b}	0.008^{b}	0.039^{b}	0.016^{b}	0.008^{b}	0.615^{a}	3.054^{a}	0.423^{cd}	0.327^{cd}
9	1.000									0.021^{ab}	0.104^{b}	0.049^{b}	0.028^{ab}	0.470^{ab}	2.744^{a}	0.401^{cd}	0.233^{cd}
10	1.000													0.457^{ab}	2.193^{ab}	0.369^{cd}	0.225^{cd}

Means in columns with the different letter are highly significantly different according to the Fisher's test ($P \leq 0.05$).

The diagram shows the biggest dependence of productivity potential realization of variety ‘Valuta’ on the stages of organogenesis, as during the transition of buds from stages II to III–IV on average 62.4% of potential fruiting points were lost in three years. A significant factor in the impact was the year of the study - at a certain stage of organogenesis, weather factors negatively affected the maintenance of high potential productivity. The interaction of these two factors accounted for 58% of the impact on the actual harvest. The age of the tree (the age of complex fruit formations) in the ‘Valuta’ variety had a very small effect (8%) on the actual yield.

Observations of different trunk age sections' participation in productivity formation showed its clear dependence on the stage of organogenesis. Thus, in the second year of the study (Table 3), three- to eight-year-old complex rings during stages III–IX formed the largest number of reproductive elements. However, during stage X, the level of ovarian flower buds was higher in the two-year-old rings and low in the eight-year-old. During stage XI, the largest number of ovaries is preserved by three-four-year rings. Thus, the peculiarities of the various stages of organogenesis depend on environmental conditions, which in turn have a significant impact on the potential productivity realization of the rings of different trunk parts.

The largest share in the formation of potential productivity in seven-year-old plants of variety ‘President’ at the II stage of organogenesis belonged to seven-year-old sections of the trunk (Table 4). In the following years, too, the largest numbers of vegetative buds were located in older age areas.

Table 4. Involvement of ‘President’ different ages tree trunks in productivity formation (%). IH NAAS, 2016–2019

Age of the trunk segment	Stage of organogenesis / Year of research											
	II			III–IV			X			XI		
	2016	2017	2018	2017	2018	2019	2017	2018	2019	2017	2018	2019
1	15.8	6.7	5.1	0.0	1.3	0.0	0.0	0.7	0.0	0.0	0.9	0.0
2	4.9	12.1	7.7	4.1	9.5	0.0	7.8	18.5	0.0	12.8	17.6	0.0
3	13.4	8.5	10.8	22.1	6.4	16.7	39.4	10.0	16.7	28.3	9.9	13.3
4	9.9	8.2	7.8	15.1	8.3	16.7	24.1	12.9	14.3	33.2	13.5	16.7
5	9.6	11.8	9.9	18.9	18.3	16.7	28.7	14.5	19.0	25.7	15.3	16.7
6	17.9	17.0	13.1	9.5	23.6	0.0	0.0	14.6	0.0	0.0	14.1	0.0
7	28.5	16.8	16.8	30.2	16.9	11.1	0.0	16.6	16.7	0.0	16.0	13.3
8		18.9	14.3		15.7	27.8		12.2	33.3		12.7	25.0
9			14.6			11.1			9.5			15.0
Total	100	100	100	100	100	100	100	100	100	100	100	100

During the III–IV stages of organogenesis in seven-year plantations on each tree ‘President’ was differentiated 67 pieces/tree generative buds, most of which were located in the oldest part of the trunk. The following year, trees of this variety were laid 80 generative buds, and in 2018 - 5 pieces/tree.

In the first year of the study, during the III–IV stages of organogenesis, complex rings in the two-five-year and seven-year sections of the trunk most effectively realized their potential for productivity (Table 5). In 2018, the coefficient of statistical estimation (the number of generative buds relative to their total number) was slightly higher for the five-year plot (SEC = 0.780). No differences were found between the four- and seven-year SEC plots. In the third year of the study, the effectiveness of differentiation of generative buds by age was uneven.

In 2017, three to five-year-old fruit formations of eight-year-old ‘President’ plants produced 2–3 flowers per potentially generative bud, none were formed on one-year growth. The following year, the most intense flowering was also observed on five-year-old fruit formations, and less abundant - on annuals. In the third year of the study, the number of flowers on the tree was much lower than in previous years, in one-two-year and six-year areas flowering did not occur at all.

During the X phase of organogenesis in eight-year-old ‘President’ plants, the fruits were tied in the largest number on the fruit formations of two-five-year-old sections of the trunk. Due to the frosts, there was a complete reduction of flowers and ovaries in six-seven-year areas. The following year, the intensity of fruit set was highest in the four-year period, although no significant difference in the number of ovaries between two- to eight-year-old fruit formations was found. In ten-year-old trees, there was no significant difference in the number of useful ovaries between the different age areas where the fruit was counted. The least intensive reduction of fruits during the XI stage of organogenesis was observed in 2017 and 2018 on two-five-year complex rings, in 2019 - on three-nine-year.

The calculation of the share of individual factors influences the productivity potential realization of plants variety 'President' showed that the stages of organogenesis have the greatest influence on real yield formation (65.2% of potential generative buds are lost during the transition from buds II to III–IV) also meteorological conditions during this or that stage (HTC, $\Sigma_{act}t \geq 10$) (Fig. 5.).

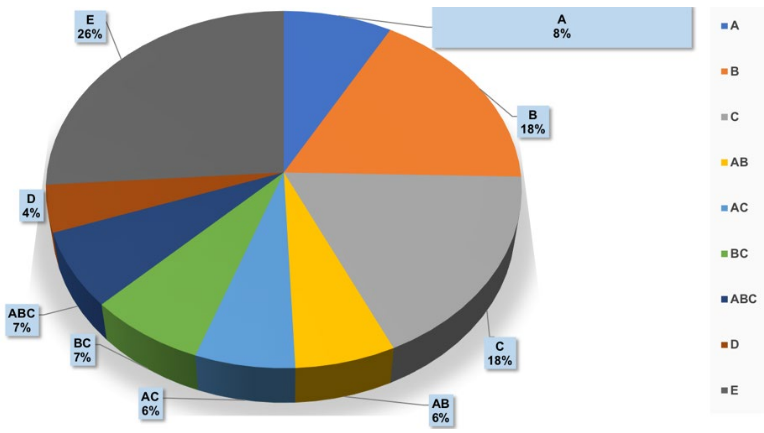

A, Age tree section; **B**, Stage of organogenesis; **C**, Year of research; **D**, Factors not taken into account; **E**, Other factors.

Figure 5. The structure of various factors influences the real harvest formation of the variety ‘President’, IH NAAS of Ukraine, 2016–2019.

The diagram shows that there is no significant difference between the ages of the trunk areas in the crop formation. We noted that from the end of the flowering phase to the end of the XI stage of organogenesis, the role of certain trunk parts in the formation of the actual harvest changes.

Table 5. Participation of different age sections of the trunk in productivity formation of 'President' trees at different stages of organogenesis, 2016–2020

Age of the trunk segment	The number of reproduction elements at certain stages of organogenesis (SEC)																
	Stage of organogenesis / Year of research																
	2016	2017				2018				2019				2020			
	II	III–IV	V–IX	X	XI	III–IV	V–IX	X	XI	III–IV	V–IX	X	XI	III–IV	V–IX	X	XI
1	1.000	0.000	0.000	0.000	0.000	0.106^{c}	0.528^{c}	0.092^{c}	0.092^{cb}	0.000	0.000	0.000	0.000	0.167^{c}	0.754^{dc}	0.147^{cb}	0.066^{cb}
2	1.000	0.483^{ab}	1.750^{ab}	0.467^{a}	0.683^{a}	0.446^{b}	2.232^{b}	1.267^{ab}	1.037^{ab}	0.000	0.000	0.000	0.000	0.252^{bc}	1.168^{cd}	0.445^{bc}	0.218^{bc}
3	1.000	0.744^{ab}	2.611^{a}	0.745^{a}	0.429^{a}	0.406^{b}	2.032^{b}	1.176^{ab}	1.010^{ab}	0.048^{a}	0.238^{a}	0.048^{a}	0.032^{a}	0.273^{bc}	1.390^{cd}	0.752^{a}	0.515^{a}
4	1.000	0.696^{ab}	2.280^{ab}	0.778^{a}	0.754^{a}	0.546^{a}	2.731^{a}	1.560^{a}	1.393^{a}	0.032^{a}	0.159^{a}	0.048^{a}	0.032^{a}	0.483^{b}	2.303^{bc}	0.986^{a}	0.552^{a}
5	1.000	0.837^{a}	3.018^{a}	0.858^{a}	0.612^{a}	0.780^{a}	3.901^{a}	0.906^{b}	0.831^{ab}	0.043^{a}	0.217^{a}	0.058^{a}	0.029^{a}	0.306^{bc}	1.444^{bcd}	0.936^{a}	0.502^{a}
6	1.000	0.391^{b}	0.888^{b}	0.000	0.000	0.726^{a}	3.631^{a}	0.765^{b}	0.646^{bc}	0.000	0.000	0.000	0.000	0.429^{b}	2.127^{bc}	0.722^{a}	0.540^{a}
7	1.000	0.536^{ab}	1.656^{ab}	0.000	0.000	0.546^{ab}	2.732^{ab}	0.848^{b}	0.691^{bc}	0.013^{a}	0.063^{a}	0.019^{a}	0.013^{a}	0.538^{ab}	2.562^{b}	0.616^{a}	0.396^{a}
8	1.000					0.410^{b}	2.050^{b}	0.518^{bc}	0.461^{bc}	0.042^{a}	0.212^{a}	0.074^{a}	0.032^{a}	0.769^{a}	3.713^{a}	0.606^{a}	0.383^{a}
9	1.000									0.017^{a}	0.085^{a}	0.034^{a}	0.017^{a}	0.576^{ab}	2.788^{ab}	0.660^{a}	0.349^{a}
10	1.000													0.431^{b}	2.081^{bc}	0.527^{bc}	0.241^{bc}

Means in columns with the different letter are highly significantly different according to the Fisher's test ($P \leq 0.05$).

Considering the formation of productivity in stages, we trace the trend of changing the participation of different age areas of the trunk (rings) in the realization of reproductive potential (Table 5). Thus, during stages III–IX in the second year of the study, complex rings placed on a four- to seven-year-old trunk section realized their potential most effectively at the end of the X stage the level of preservation of reproductive elements in two-four-year plots increased, and at the end of the XI stage six-seven-year fruit formations more intensively lost their potential. As a result, two- to five-year-old complex rings have proven to be more productive in terms of realizing their potential, and they have ensured the formation of the main crop of the tree.

In the seven-year-old 'Favoryt' plants, the largest proportion of buds that reached stage II organogenesis was located in the four-year-old trunk area (Table 6). The following year, there was a uniform placement of buds on the trunk. The oldest sections of the trunk of nine-year-old plants bore the largest number of fruit formations of the total number on the tree.

Table 6. Involvement of 'Favoryt' different ages tree trunks in productivity formation (%). IH NAAS, 2016–2019

Age of the trunk segment	Stage of organogenesis / Year of research											
	II			III–IV			X			XI		
	2016	2017	2018	2017	2018	2019	2017	2018	2019	2017	2018	2019
1	17.8	8.5	7.4	0.0	0.0	5.9	0.0	0.0	5.7	0.0	0.0	2.2
2	13.5	7.9	8.9	22.2	20.1	9.0	22.2	9.1	9.3	23.8	9.0	8.9
3	22.4	14.2	9.4	36.1	15.1	6.7	36.5	15.9	11.3	35.7	16.4	10.1
4	34.5	14.7	11.7	22.9	25.0	11.9	31.7	15.0	12.1	27.2	14.3	14.5
5	7.3	12.0	8.1	14.6	16.3	6.0	9.5	18.2	12.0	13.3	18.7	11.6
6	4.7	13.0	8.8	4.2	12.2	12.1	0.0	16.4	12.7	0.0	16.1	10.8
7	0.0	15.8	11.9	0.0	8.0	13.3	0.0	19.8	12.8	0.0	20.4	11.8
8		13.9	15.1		3.2	15.1		5.6	10.6		5.2	13.5
9			18.7			19.9			13.4			16.6
Total	100	100	100	100	100	100	100	100	100	100	100	100

The level of productivity potential realization at the III–IV stages of organogenesis in 2016 and 2018 was ambiguous; in seven-year-old plants, no significant difference was found between the plots where the generative buds were recorded (Table 7). In 2017, no significant difference was found between the two-four-year age areas, less effective differentiation of buds took place on the eight-year section of the trunk.

In 2019, the level of bud differentiation differed significantly between the age sections of the trunk, as evidenced by the different statistical coefficient, it was higher in the complex rings of older age sections of the trunk.

In eight-year-old trees at the IX stage of organogenesis, there was a low level of productivity potential realization, no significant difference between the age areas of the trunk was found. The following year, two- to six-year-old trunk plots best realized their potential, and less intensive flowering was observed on the fruits of eight-year-old plots. Ten-year-old trees bloomed more intensively on 6–9-year-old sections of the trunk.

At the X stage of organogenesis, the level of productivity potential realization differed depending on the age of the trunk area. In eight-year-old trees, there was no significant difference in the degree of fruit tying, in nine-year-old plants the intensity of fruit tying was highest in fruit-bearing six- to seven-year-old sections of the trunk, and in ten-year-olds to five-six-year.

At the XI stage of organogenesis, no significant difference in the number of tied fruits was found between the different ages of the eight-year-old plants' trunks. The following year, the oldest and youngest sections of the trunk realized their productive potential the least, no significant difference was found between other sections. In ten-year-old trees, the reduction of reproductive elements was most intense at one-year increments, and no significant difference in this factor was found between two- and nine-year-old complex fruit formations.

According to the research results and determined values of the shares of the organogenesis stages, years of research, age of the trunk, and their relationship and impact on the actual harvest, a diagram to illustrate the structure of this impact was constructed (Fig. 6).

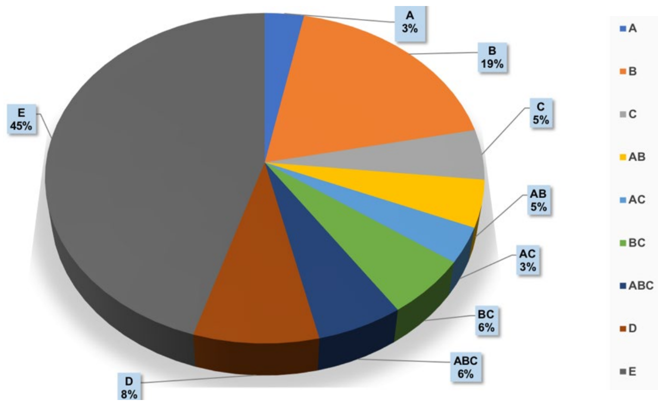

A, Age tree section; **B**, Stage of organogenesis; **C**, Year of research; **D**, Factors not taken into account; **E**, Other factors.

Figure 6. The structure of various factors influences the real harvest formation of the variety 'Favoryt', IH NAAS of Ukraine, 2016–2020.

Other factors have the most significant influence on the real harvest formation, in particular the phytosanitary condition of the plantation, etc., as well as the organogenesis stages (79.3% of buds remain at the II stage of organogenesis); the insignificant influence of age area and year of research was established.

Depending on the organogenesis stage in 'Favoryt' plants, the role of different parts of the trunk in the real productivity formation also changes. Thus, in the second year of the study (Table 7), two- to six-year-old complex rings during stages III–IX best realized their productivity potential. At the X stage of organogenesis, the realization of potential productivity was most effective in three-seven-year rings, at the XI stage - two-seven-year rings. In 'Favoryt' there are no significant jumps in the loss of rings' reproductive potential of different ages during the transition from one stage of organogenesis to another.

In the 'Bilosnizhka' variety, the greatest participation in the potential productivity formation at the II stage of organogenesis during the first two years of the study was found in six-year trunk sections, and in nine-year-old plants - in the oldest section.

Table 7. Participation of different age sections of the trunk in productivity formation of 'Favoryt' trees at different stages of organogenesis, 2016–2020

Age of the trunk segment	The number of reproduction elements at certain stages of organogenesis (SEC)																
	Stage of organogenesis / Year of research																
	2016	2017				2018				2019				2020			
	II	III–IV	V–IX	X	XI	III–IV	V–IX	X	XI	III–IV	V–IX	X	XI	III–IV	V–IX	X	XI
1	1.000	0.000	0.000	0.000	0.000	0.000	0.000	0.000	0.000	0.162^{bc}	0.812^{bc}	0.174^{bc}	0.040^{b}	0.220^{a}	0.120^{bc}	0.100^{cb}	0.000
2	1.000	0.103^{a}	0.513^{a}	0.100^{a}	0.128^{a}	0.766^{a}	3.829^{a}	0.173^{b}	0.118^{b}	0.217^{bc}	1.084^{bc}	0.231^{bc}	0.147^{a}	0.222^{a}	1.097^{bc}	0.175^{ab}	0.159^{ab}
3	1.000	0.122^{a}	0.484^{a}	0.248^{a}	0.139^{a}	0.414^{b}	2.071^{b}	0.234^{ab}	0.179^{ab}	0.154^{cb}	0.770^{cb}	0.276^{ab}	0.154^{a}	0.290^{a}	1.437^{abc}	0.179^{ab}	0.124^{bc}
4	1.000	0.085^{a}	0.396^{a}	0.148^{a}	0.096^{a}	0.521^{ab}	2.607^{ab}	0.144^{b}	0.148^{ab}	0.220^{bc}	1.100^{bc}	0.243^{bc}	0.186^{a}	0.333^{a}	1.678^{abc}	0.188^{a}	0.164^{ab}
5	1.000	0.129^{a}	0.379^{a}	0.133^{a}	0.133^{a}	0.373^{bc}	1.863^{bc}	0.228^{ab}	0.210^{ab}	0.159^{bc}	0.794^{bc}	0.333^{a}	0.197^{a}	0.384^{a}	1.911^{ab}	0.224^{a}	0.190^{a}
6	1.000	0.061^{a}	0.303^{a}	0.000	0.000	0.311^{bc}	1.556^{bc}	0.289^{ab}	0.223^{ab}	0.299^{a}	1.496^{a}	0.332^{a}	0.185^{a}	0.444^{a}	2.182^{a}	0.182^{a}	0.148^{ab}
7	1.000	0.000	0.000	0.000	0.000	0.215^{bc}	1.075^{bc}	0.326^{a}	0.241^{a}	0.245^{ab}	1.225^{ab}	0.259^{ab}	0.157^{a}	0.257^{a}	1.316^{bc}	0.171^{ab}	0.149^{ab}
8	1.000					0.094^{c}	0.469^{c}	0.083^{b}	0.073^{b}	0.233^{ab}	1.163^{ab}	0.167^{cb}	0.136^{a}	0.325^{a}	1.641^{abc}	0.184^{a}	0.147^{abc}
9	1.000									0.233^{ab}	1.165^{ab}	0.187^{bc}	0.157^{a}	0.263^{a}	1.330^{bc}	0.159^{abc}	0.142^{abc}
10	1.000													0.215^{a}	1.071^{cb}	0.111^{bc}	0.086^{cb}

Means in columns with the different letter are highly significantly different according to the Fisher's test ($P \leq 0.05$).

At the end of November, seven-year-old plants 'Bilosnizhka' formed 48 pcs/tree generative buds, the oldest age trunk sections formed the largest number of them, and none of them were formed on the shoot (Table 8).

Table 8. Involvement of ‘Bilosnizhka’ different ages tree trunks in productivity formation (%). IH NAAS, 2016–2019

Age of the trunk segment	Stage of organogenesis / Year of research											
	II			III–IV			X			XI		
	2016	2017	2018	2017	2018	2019	2017	2018	2019	2017	2018	2019
1	10.2	11.6	4.4	0.0	3.4	3.0	0.0	6.1	6.5	0.0	11.5	5.0
2	7.9	11.4	4.5	2.9	12.8	3.4	7.1	10.3	9.4	7.7	13.7	8.5
3	6.4	9.8	4.1	10.0	13.0	3.4	23.2	26.2	6.2	28.6	13.7	8.5
4	16.7	11.4	8.5	23.4	8.9	7.9	69.6	9.6	12.7	63.7	11.2	13.0
5	17.0	11.0	10.5	25.2	11.4	11.6	0.0	11.3	13.0	0.0	16.0	11.1
6	24.1	22.5	13.0	21.1	30.5	11.1	0.0	15.7	11.8	0.0	13.7	11.1
7	17.7	7.7	15.1	17.4	9.6	17.0	0.0	20.9	14.2	0.0	20.1	16.5
8		14.5	19.2		10.4	20.0		0.0	11.6		0.0	11.5
9			20.8			22.6			14.5			15.0
Total	100	100	100	100	100	100	100	100	100	100	100	100

The following year, the trees ‘Bilosnizhka’ were differentiated 68 generative buds pieces/tree, 30% of which were located on six-year trunk sections. In nine-year-old plants, generative buds formation was more efficient on the rings of the two oldest age sites (42.6%), and the total number of laid generative buds was 64 units/tree.

In the first and last years of the study, at the end of November, the lowest level of productivity potential realization was observed in the two youngest age areas, no significant difference was found between other parts of the trunk. In eight-year-old plants at stages III–IV, the highest coefficient of the statistical evaluation was in four-six-year-old complex rings (Table 9).

In the IX stage of organogenesis in eight-year-old trees ‘Bilosnizhka’ (2017), three-five-year-old trunk sections had three flowers per one potentially generative bud, and the lowest number of potential ‘fruiting points’ was located on one-year growth in three years of research. In 2018, on average, two to four flowers per one potentially generative bud were counted in all age areas, except for one-year growth. It is statistically proven that in ten-year-old plants (2019) there was no significant difference in the number of flowers per one potentially generative bud in the IX stage of organogenesis between three-nine-year-old sections of the trunk.

Due to frosts (minus 2–4 °C) at the X organogenesis stage in 2017, ‘Bilosnizhka’ trees reduced all ‘fruiting points’, which were located on six- to seven-year-olds, as well as a significant number on five-year-old trunk area. The reduction of flowers and ovaries in nine-year-old plants was less intense in five- to seven-year-old sections of the trunk. Analysis of variance proved that the intensity of reproductive elements reduction in 2019 was the lowest in two-four-year areas. A high level of ‘potential points’ of fruiting realization in the real harvest at the XI stage of organogenesis in eight-year-old trees was observed on three-four-year-old rings, on younger fruit formations the intensity of tying was lower. The highest coefficient of statistical evaluation in the following years was characterized by three-seven-year complex rings. Young fruit formations were less stable in realizing their productivity potential.

Table 9. Participation of different age sections of the trunk in productivity formation of 'Bilosnizhka' trees at different stages of organogenesis, 2016–2020

Age of the trunk segment	The number of reproduction elements per potentially generative bud at certain organogenesis stages (SEC)																
	Stage of organogenesis / Year of research																
	2016	2017				2018				2019				2020			
	II	III–IV	V–IX	X	XI	III–IV	V–IX	X	XI	III–IV	V–IX	X	XI	III–IV	V–IX	X	XI
1	1.000	0.040^{cb}	0.011^{cb}	0.000	0.000	0.183^{c}	1.000^{cb}	0.045^{c}	0.020^{c}	0.244^{cb}	1.711^{cb}	0.378^{bc}	0.137^{b}	0.217^{b}	1.022^{b}	0.094^{bc}	0.000
2	1.000	0.226^{bc}	1.774^{abc}	0.054^{cb}	0.096^{cb}	0.382^{b}	4.111^{a}	0.104^{bc}	0.078^{bc}	0.267^{bc}	1.867^{bc}	0.533^{ab}	0.233^{b}	0.296^{ab}	1.574^{ab}	0.213^{a}	0.056^{ab}
3	1.000	0.535^{ab}	3.137^{ab}	0.240^{ab}	0.288^{ab}	0.454^{b}	4.013^{a}	0.130^{b}	0.132^{ab}	0.328^{abc}	2.299^{abc}	0.706^{a}	0.456^{a}	0.340^{ab}	1.755^{ab}	0.142^{ac}	0.081^{ab}
4	1.000	0.715^{a}	3.636^{a}	0.300^{a}	0.320^{a}	0.592^{ab}	3.379^{ab}	0.149^{b}	0.158^{ab}	0.365^{a}	2.556^{ab}	0.466^{ab}	0.220^{b}	0.258^{ab}	1.383^{ab}	0.108^{bc}	0.092^{ab}
5	1.000	0.545^{ab}	3.207^{ab}	0.098^{bc}	0.128^{bc}	0.698^{a}	4.947^{a}	0.264^{a}	0.189^{a}	0.384^{a}	2.687^{a}	0.290^{bc}	0.117^{b}	0.414^{a}	1.959^{a}	0.145^{ac}	0.104^{a}
6	1.000	0.361^{bc}	1.614^{bc}	0.000	0.000	0.657^{a}	3.894^{a}	0.190^{ab}	0.158^{ab}	0.316^{abc}	2.212^{abc}	0.227^{bc}	0.091^{b}	0.378^{ab}	1.795^{ab}	0.087^{bc}	0.059^{ab}
7	1.000	0.554^{a}	0.859^{bc}	0.000	0.000	0.458^{b}	3.532^{ab}	0.187^{ab}	0.128^{ab}	0.401^{a}	2.809^{a}	0.219^{bc}	0.128^{b}	0.384^{ab}	1.878^{ab}	0.117^{bc}	0.042^{ab}
8	1.000					0.421^{b}	2.067^{bc}	0.144^{b}	0.114^{b}	0.374^{a}	2.617^{a}	0.151^{cb}	0.076^{b}	0.369^{ab}	1.841^{ab}	0.122^{bc}	0.045^{ab}
9	1.000									0.390^{a}	2.728^{a}	0.171^{bc}	0.090^{b}	0.432^{a}	2.135^{a}	0.077^{cb}	0.038^{b}
10	1.000													0.370^{ab}	1.828^{ab}	0.138^{ac}	0.021^{b}

Means in columns with the different letter are highly significantly different according to the Fisher's test ($P \leq 0.05$).

A diagram is constructed according to the determined values of the particles of individual factors influence and their interaction on the real harvest (Fig. 7).

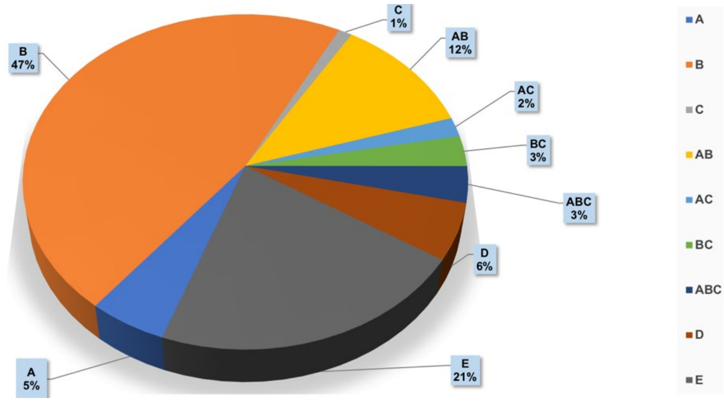

A, Age tree section; **B**, Stage of organogenesis; **C**, Year of research; **D**, Factors not taken into account; **E**, Other factors.

Figure 7. The structure of various factors influences the real harvest formation of the variety 'Bilosnizhka', 2016–2020.

The diagram shows the greatest dependence of the productivity potential realization variety 'Bilosnizhka' on organogenesis stages (58.4% of buds do not differentiate into generative ones). The age of the fruit tree has a very low impact on the final result of the production process.

During the transition of fruit formations buds of the 'Bilosnizhka' variety from one stage of organogenesis to another, there is a significant increase or decrease in the rate of reproductive potential preservation. Thus, in 2017, the largest number of generative buds was formed in the four-six-year trunk section, at the IX stage, the largest number of flowers per potentially generative bud had two-seven-year rings. At the end of the X stage of organogenesis, there was a significant loss of reproductive potential in the two- to four-year-old part of the trunk, the largest number of ovaries this year remained on the five-seven-year-old complex rings. In general, at the end of the XI stage of organogenesis, the largest number of fruits was placed on the three-seven-year section of the trunk.

Thus, in the conditions of the western Forest-Steppe of Ukraine, columnar apple cultivars react differently to environmental conditions at certain stages of organogenesis. The efficiency of generative buds differentiation of columnar varieties is influenced in one way or another by meteorological factors. For introduced varieties, the increase in the level of $\Sigma_{act}t \geq 10$, precipitation, and average daily air temperature has a negative effect on the generative potential formation at III–IV stages of organogenesis, as evidenced by the high negative correlation between the ratio of generative buds to their total number and these factors (r=-0.80–0.96). The influence of these meteorological factors on the varieties of Ukrainian selection is weak and moderate, which indicates the best adaptive properties of these varieties (Table 10).

Table 10. The correlation coefficient between SEC and weather factors during III-XI stages of organogenesis (data for 2016–2020 are processed)

Stage of organogenesis	Variety	HTC	$\Sigma_{act}t \geq 10$ °C	Σ precipitation	Average daily air temperature
III–IV	'President'	0.71	-0.91	-0.52	-0.80
	'Valuta'	0.78	-0.96	-0.60	-0.87
	'Favoryt'	0.52	-0.16	-0.69	-0.40
	'Bilosnizhka'	0.60	-0.60	-0.53	-0.61
V–IX	'President'	-0.78	0.48	-0.88	0.35
	'Valuta'	-0.75	0.45	-0.85	0.32
	'Favoryt'	-0.60	0.84	-0.31	0.88
	'Bilosnizhka'	-0.73	0.83	-0.53	0.82
X	'President'	-0.69	-0.54	-0.61	0.64
	'Valuta'	-0.81	-0.69	-0.75	0.60
	'Favoryt'	0.81	0.90	0.87	0.06
	'Bilosnizhka'	0.85	0.84	0.86	-0.27
XI	'President'	0.89	0.08	0.88	0.09
	'Valuta'	0.86	0.58	0.85	0.20
	'Favoryt'	0.38	0.65	0.39	0.80
	'Bilosnizhka'	-0.31	-0.09	-0.31	0.15

It was found that fruits reduction on plants of most of the studied columnar varieties during the XI organogenesis stage decreases with increasing $\Sigma_{act}t \geq 0$ and average daily air temperature, as well as increased rainfall. Increased precipitation (r = 0.85–0.98) had a high impact on the preservation of reproductive potential for cultivars 'President' and 'Valuta'. The increase in average daily air temperature had a positive effect on the increase in SEC in the variety 'Favoryt' (r = 0.77–0.80).

CONCLUSIONS

Individual age sections of the trunk columnar apple trees formed different initial productivity potential. In plants of all studied varieties and age groups, the laying of generative buds, the implementation of reproductive elements in V–IX and X–XI organogenesis stages were more effective in older age areas of the trunk. Complex fruit formations, regardless of the trunk age, where they are placed, form a high potential for productivity, which is effectively realized.

Differentiation of flower buds as well as the passage of V–XI stages of organogenesis depended on meteorological factors. The plants' generative potential formation of introduced varieties (III–IV stages of organogenesis) was negatively affected by the increase in $\Sigma_{act}t \geq 10$, the average daily air temperature, and the decrease in the level of HTC. The influence of these factors on the laying of flower buds on trees of domestic varieties was weak or moderate.

For plants of introduced varieties 'President' and 'Valuta', a negative correlation was found between the number of ovaries at the end of the X organogenesis stage and $\Sigma_{act}t \geq 10$ and the amount of precipitation, as well as a noticeable positive - with the average daily air temperature. With increasing rainfall during Phase XI, more ovaries remained (r = 0.85–0.98). Decreased $\Sigma_{act}t \geq 10$ and rainfall helped reduce the ovarian reduction in ‘Favoryt’ and ‘Bilosnizhka’ varieties; during the XI stage of organogenesis, the reduction was minimized by increasing the average daily air temperature.

REFERENCES

Amasino, R. 2010. Seasonal and developmental timing of flowering. *The Plant Journal* **61**, 1001–1013. https://doi.org/10.1111/j.1365-313X.2010.04148.x

Buntsevich, L. & Sergeeva, N. 2014. Morphophysiological effects of various foliar nutrition regimes in apple in the south of Russia. *Universal Journal of Plant Science* **2**(3), 63–68. https://doi.org/10.13189/ujps.2014.020301

Duric, G., Micic, N., Cerovic, R. & Plazinic, R. 1997. Degree of differentiation of generative buds as a factor of bearing in apricot. *In XI International Symposium on Apricot Culture.* Veria-Makedonia, Greece, 488, 351–356. https://doi.org/10.17660/ActaHortic.1999.488.55

El Yaacoubi, A., El Jaouhari, N., Bourioug, M, El Youssfi, L., Cherroud, S., Bouabid, R., Chaoui, M. & Abouabdillah, A 2020. Potential vulnerability of Moroccan apple orchard to climate change–induced phenological perturbations: effects on yields and fruit quality. *Int. J. Biometeorol.* **64**, 377–387. https://doi.org/10.1007/s00484-019-01821-y

El-Sabagh, A.S, Othman, S.A. & AlAbdaly, A.N. 2012. Performance of Anna apple cultivar grown on two different rootstocks in response to hydrogen cyanamide winter spraying. *World J. Agric. Sci*. **8**(1), 1–12. ISSN 1817-3047

Gavryliuk, O., Kondratenko, T. & Goncharuk, Y. 2019. Features of formation of productivity of columnar apple-tree. *Bulletin of Agricultural Science* **97**(6), 27–34. https://doi.org/10.31073/agrovisnyk201906-04

Havryliuk, O., Kondratenko, T., Mazur, B., Kutovenko, V., Mazurenko, B., Voitsekhivska, O., & Dmytrenko, Y. 2022. Morphophysiological peculiarities of productivity formation in columnar apple varieties. *Agronomy research* **20**(1), 148–160. https://doi.org/10.15159/AR.22.007

Isaeva, I.S. 1989. *Apple tree productivity*. Moscow, Russia: Moscow State University. M.V. Lomonosov, 149 pp. (in Russian).

Kobel, F. 1984. *Fruit growing on a physiological basis*. Moscow, Russia: GISL, 375 pp. (in Russian).

Kohek, Š., Guid, N., Tojnko, S., Unuk, T. & Kolmanič, S. 2015. EduAPPLE: Interactive Teaching Tool for Apple Tree Crown Formation, *HortTechnology* **25**(2), 238–246. https://doi.org/10.21273/HORTTECH.25.2.238

Kolomiets, I.A. 1976. Overcoming the frequency of fruiting apple trees. Kiev, Ukraine: *Harvest*, 240 pp. (in Ukraine).

Kondratenko, T.E. 2003. Potential productivity of apple varieties and the level of its implementation depending on the technology and growing area. *Collection of scientific works of Uman State Agrarian University "Biological sciences and problems of crop production".* Uman, Ukraine: UDAU. 470–474 (in Ukraine).

Lapins, K. 1969. Segregation of compact growth types in certain apple seedling progenies. *Canadian Journal of Plant Science* **49**(6), 765–768. doi: https://doi.org/10.4141/cjps69-130

Mazurenko, B., Honchar, L., Novytska, N. & Kalenska, S. 2020. Grain yield response of facultative and winter triticale for late autumn sowing in different weather conditions. *Agronomy research* **18**(1), 183–193. https://doi.org/10.15159/AR.20.008

Mezhenskyj, V., Kondratenko, T., Mazur, B., Shevchuk, N., Andrusyk, Y. & Kuzminets, O. 2020. Results of ribes breeding at the national university of life and environmental sciences of Ukraine. *Research for Rural Development* **35**, 22–26. https://doi.org/10.22616/rrd.26.2020.003

Mezhenskyj, V.M. 2019. Collecting sorboid plants for their horticultural merit and use in breeding work in Ukraine. *Acta Hortic.* **1259**, 25–30. https://doi.org/10.17660/ActaHortic.2019.1259.5

Miloševic, T., Miloševic, N. & Mladenovic, J. 2022.The influence of organic, organo-mineral and mineral fertilizers on tree growth, yielding, fruit quality and leaf nutrient composition of apple cv. 'Golden Delicious Reinders', *Scientia Horticulturae* **297**, 110978. https://doi.org/10.1016/j.scienta.2022.110978

Palubicki, W., Horel, K., Longay, S., Runions, A., Lane, B., Měch, R. & Prusinkiewicz, P. 2009. Self-organizing tree models for image synthesis. *ACM Transactions on Graphics (TOG*), **28**(3), 1–10. https://doi.org/10.1145/1531326.1531364

Rather, J.A., Misgar, F.A., Dar, G.A. & Qurashi, S.N. 2018. Effects of Rootstocks on Horticultural Characteristics of Various Exotic Apple Cultivars in Kashmir Climatic Conditions. *Int. J. Curr. Microbiol. App.Sci.* **7**(4), 2341–2348. https://doi.org/10.20546/ijcmas.2018.704.268

Shevchuk, L., Grynyk, I., Levchuk, L., Babenko, S., Podpriatov, H. & Kondratenko, P. 2021a. Fruit Quality Indicators of Apple (*Malus domestica Borkh*.) Cultivars Bred in Ukraine. *Journal of Horticultural Research* **29**(2), 95–106. https://doi.org/10.2478/johr-2021-0019

Shevchuk, L.M., Grynyk, I.V., Levchuk, L.M., Yareshcenko, O.M., Tereshcenko, Y. & Babenko, S.M. 2021b. Biochemical contents of highbush blueberry fruits grown in the Western Forest-Steppe of Ukraine. *Agronomy research* **19**(1), 232–249. https://doi.org/10.15159/ar.21.012

Tobutt, K.R. 1984. Breeding columnar apples varieties at East Malling. *Scientific Horticulture.* **35**, 72–77. http://www.jstor.org/stable/45128405

Tonkha, O., Menshov, O., Bykova, O., Pikovska, O. & Fedosiy, I. 2020. Magnetic methods application for the physical and chemical properties assessment of Ukraine soil. In *XIV International Scientific Conference "Monitoring of Geological Processes and Ecological Condition of the Environment"* (Nov. 2020, pp. 1–5). European Association of Geoscientists & Engineers. https://doi.org/10.3997/2214-4609.202056027

Vasylenko, O., Kondratenko, T., Havryliuk, O., Andrusyk, Y., Kutovenko, V., Dmytrenko, Y., Grevtseva, N. & Marchyshyna, Y. 2021. The study of the productivity potential of grape varieties according to the indicators of functional activity of leaves. *Potravinarstvo Slovak Journal of Food Sciences* **15**, 639–647. https://doi.org/10.5219/1638

Yareshchenko, A., Tereshchenko, Y., Pryimachuk, L., Todosyuk, E. & Mazur, B. 2012. Ribes breeding programmes in Ukraine-recent achievements. *Acta Horticulturae* **946**, 177–182. https://doi.org/10.17660/ActaHortic.2012.946.27

Zakharov, M.V. 2011. Morphology of the crown, flowering and fruiting of trees of columnar apple varieties of Ukrainian selection. *Plant Varieties Studying and Protection*, (1). https://cyberleninka.ru/article/n/morfologiya-krony-tsveteniya-i-plodonosheniya-dereviev-kolonovidnyh-sortov-yabloni-ukrainskoy-selektsii/viewer (in Ukraine).

Zamorskyi, V. 2007. The role of the anatomical structure of apple fruits as fresh cut produce. *In International Conference on Quality Management of Fresh Cut Produce*. Bangkok, Thailand. *Acta Hortic*. **746**, 509–512. https://doi.org/10.17660/ActaHortic.2007.746.64

Zavadska, O., Bobos, I., Fedosiy, I., Podpriatov, H., Komar, O., Mazur, B. & Olt, J. 2021. Suitability of various onion (*allium cepa*) varieties for drying and long-term storage. *Agronomy Research* **19**(3), 1675–1690. https://doi.org/10.15159/ar.21.117

Agronomy Research **20**(2), 261–274, 2022
https://doi.org/10.15159/AR.22.001

Assessment of power characteristics of unmanned tractor for operations on peat fields

R. Kägo[1,2,*], P. Vellak[1,2], H. Ehrpais[2,3], M. Noorma[2,3] and J. Olt[1]

[1]Estonian University of Life Sciences, Institute of Forestry and Engineering, F.R. Kreutzwaldi 56/1, EE51014 Tartu, Estonia
[2]Milrem Robotics, Betooni 1, EE11415 Tallinn, Estonia
[3]University of Tartu, Tartu Observatory, Observatooriumi 1, EE61602 Tõravere, Estonia
[*]Correspondence: riho.kago@emu.ee

Received: June 1st, 2021; Accepted: January 3rd, 2022; Published: January 11st, 2022

Abstract. In this article, power characteristics of a state-of-the-art unmanned ground vehicle (UGV) are characterised. It is demonstrated that in terms of power characteristics requirements, purpose-built computer aided autonomous UGV systems are capable of replacing systems that utilise conventional tractors in peat field operations, with milled peat extraction operations as a case study. The authors demonstrate the viability of the UGV in achieving optimal mobility capabilities in operating on peatland surface. The UGV of interest was assessed for two operations of milled peat extraction: milling and harrowing. For both operations, the power consumption of the UGV and the drawbar pull of the implements (passive miller and harrower) were measured and analysed. The required drawbar pull values of the investigated implements remained in the range of 4–8 kN, which corresponded to the drawbar power of 14–36 kW. It was found that the UGV of interest is capable of carrying out milled peat operations in terms of traction capacity. However, it was found that the power supply capacity to be insufficient, thus requiring an improved solution.

Key words: agriculture, automation, drawbar pull, drawbar power, robotic and autonomous systems, UGV.

INTRODUCTION

The introduction and vigorous implementation of Robotic and Autonomous Systems (RAS) has been going on for several decades (Lewis & Ge, 2006; Duckett et al., 2018; Roldán et al., 2018; Bonadies & Gadsden, 2019; Moysiadis et al., 2021), but so far the successful utilisation of such systems has been limited. The main constraints described as unreliable guidance systems, communications delays (Aravind et al., 2017), lack of supporting infrastructure (Hajjaj & Sahari, 2016). As well, it is noted that the overall cost of robotic systems performing agricultural tasks have not yet reached a critical cost value that supports a widespread use of these systems (Bechar & Vigneault, 2016; Bechar & Vigneault, 2017).

To conduct computer aided agricultural tasks, the first option is to equip current tractors with sensors (Reina et al., 2016) and remote-control technology (Adams, 2019), but as the RAS technology matures, it has become clear that different tasks can be performed more efficiently with the supporting autonomous capabilities (Kurita et al., 2017). Although tractors have undergone over a century of development and their design makes them universally adaptable to most tasks in agriculture, their efficiency is optimal only for certain operations (Bochtis et al., 2019).

Current autonomous functions software solutions mainly focus on fleet monitoring, particularly concerning the vehicles' position and status; however, in most cases they are not designed to automate production. Whereas UGV solutions in both military and civilian markets are focused on systems in which a single operator controls only one machine (BAE Systems, 2021; ECA Group, 2021), the capability of controlling a fleet of multiple UGV-s is not available on the market. By now, the level of autonomy is approaching the state of development that will allow the introduction of commercial off-the-shelf unmanned systems soon.

Peat fields are mostly remote areas closed to the public (Alakangas et al., 2012), therefore a safer and suitable candidate for piloting robotic systems with autonomous functions. In 2009, a robotic system with three customised autonomous tractors successfully performed peat extraction tasks (Johnson et al., 2009). This experiment, although over a decade old, demonstrated that automated milled peat extraction can be feasible.

Prerequisites for these developments are that the autonomous functions are designed in a way that supports the automation, making them the enabler of the robotic system, such as:

1. Teleoperation (Small et al., 2018).
2. Obstacle Detection and Avoidance (Zhou et al., 2012; Tabor et al., 2015).
3. Waypoint Navigation (Bayar et al., 2016; Silverberg & Xu, 2019; Madridano et al., 2021).
4. Formation Control (Kamel et al., 2020).
5. Swarming (Bayındır, 2016; Tan et al., 2016).

Depending on various factors (quality of the peat, production area size, etc.), the production of milled peat can be carried out differently (Alakangas et al., 2012):

1. re-ridging (Peco) method;
2. conveyer belt (Haku) method;
3. mechanical harvesting method;
4. vacuum harvesting method.

For all these methods, the first step is milling. In the case of milling, a thin layer of peat is removed from the deposit and left to dry. Milling usually takes place during the day, when the moisture content of the air is optimal for drying the peat. When the removed layer of peat is dry enough, the next step is to turn the peat with the operation called harrowing. Harrowing is meant to speed up the drying process even further. Depending on the weather conditions (rain, humidity, amount of solar radiation, wind), the number of turns can be 1–5. If it is no longer necessary to perform the harrowing, the peat is collected according to the method. For example, the Haku method uses a ridger, a conveyer belt collector, and trailers. The choice of method depends on various factors, such as the quality of the peat (dark peat, white peat), the surface area to be extracted, etc.

Although the different stages of operation have different energy requirements, it has become a tradition for all of these stages of operation to use general-purpose tractors with high power output and high-fuel-consumption internal combustion engines. The reason for this is that such tractors, with their versatility, are able to do carry out a variety of operations, depending on the energy needs. This versatility makes the use of tractors flexible, while for lower energy operations, large tractors are clearly oversized (Casals et al., 2016; He et al., 2019).

The underlying hypothesis of this research is that optimally designed automated UGVs can replace conventional tractors in milled peat extraction operations in terms of drawbar pull and energy consumption. To do this, the power and energy characteristics of one representative robotic system of interest are assessed by experimental setup. The robotic system of interest was chosen by the fact that it met the requirements of peatland terrain tractability and drawbar pull of the milled peat extraction implements. The novelty of the concept of utilising automated UGVs for milled peat extraction is that the fleet of conventional tractors can be replaced with a centrally controlled fleet of low-fuel-consumption robotic agents. It has been shown previously (Kägo et al., 2021) that this kind of development has the potential to reduce the demand for labour, thus lowering overall operational costs and environmental impacts.

MATERIALS AND METHODS

For the field experiments, the Multiscope by the Estonian UGV-manufacturer Milrem Robotics is used (Fig. 1) (Milrem, 2021). The platform consists of two track modules which are mechanically and electrically connected to each other. Due to the tracks, the UGV has suitable properties for moving in peatlands. The diesel-hybrid powertrain consists of a) a generator, b) a battery pack and c) two electric motors, one for each track module. As the generator constantly charges the battery pack, the batteries give out power for the electric motors which in turn generate the track propulsion. The main characteristics of the UGV are depicted in Table 1.

The control techniques applied to the UGV of interest are categorised as following (Fig. 2):

1. Remote control (Stevenson et al., 2019)
   a. Line-of-Sight remote control (LOS);
   b. Beyond-Line-of-Sight remote control (BLOS).
2. Wired control.
3. Control by AI.

‘Remote Control’ means that the UGV is controlled by the operator using an interface (one- handed, two- handed, control station).

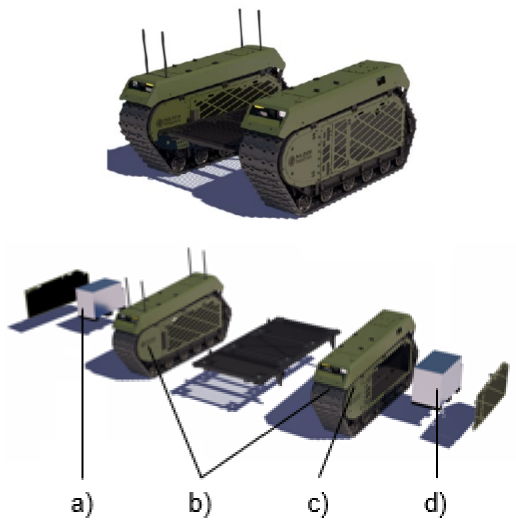

Figure 1. Structure diagram of the robotic system of interest used in the field measurement showing the position of the a) battery pack, b) track modules, c) fuel tank and d) the diesel generator.

The operator gives commands to the UGV through the interface based on direct visual observation or by using sensor information (for example, camera feed) from the

UGV sensors. The control unit can have a direct Line-of-Sight (LOS) contact with the UGV or, if the UGV is out of visual range, have a Beyond-Line-of-Sight (BLOS) contact. In the last case, the control of the UGV is conducted only based on sensor information.

The control techniques applied to the UGV of interest are categorised as following (Fig. 2):

1. Remote control (Stevenson et al., 2019)
   a. Line-of-Sight remote control (LOS);
   b. Beyond-Line-of-Sight remote control (BLOS).
2. Wired control.
3. Control by AI.

Table 1. The main characteristics of the UGV under evaluation

Name	Value
Dimensions (L×W×H)	240×200×115 cm
Maximum slope	60%
Maximum side slope	30%
Ground clearance	40–60 cm
Maximum speed	20 km h^{-1}
Net weight	1,630 kg
Payload capacity	1,200 kg
Specific ground-pressure	16.7 kPa
Maximum traction force	21 kN
Line of sight (LOS) control range	1,500 m
Engine power	(2×19 kW) 38 kW
Control	Remote Control (LOS, BLOS), wired, 'Waypoint Navigation', 'Follow Me'

'Remote Control' means that the UGV is controlled by the operator using an interface (one-handed, two-handed, control station). The operator gives commands to the UGV through the interface based on direct visual observation or by using sensor information (for example, camera feed) from the UGV sensors. The control unit can have a direct Line-of-Sight (LOS) contact with the UGV or, if the UGV is out of visual range, have a Beyond-Line-of-Sight (BLOS) contact. In the last case, the control of the UGV is conducted only based on sensor information.

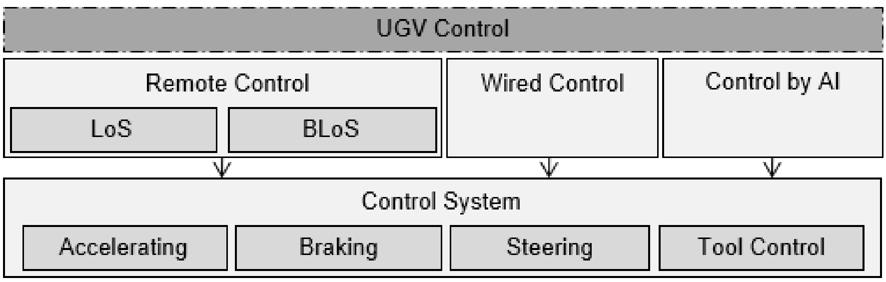

Figure 2. The control of the UGV is divided into three subcategories: a) remote control, b) wired control, c) control by AI. The control system is responsible for the d) acceleration, e) braking, f) steering, and g) tool control.

'Wired Control' is used mostly for cases, where the UGV is relatively near to the operator, for example, in operating in a maintenance area.

In cases, where the safety concerns are relatively low (for example, operating the UGV in a mostly empty peat field), the control of the UGV can be handed over to the autonomous functions (to the AI – *Artificial Intelligence*).

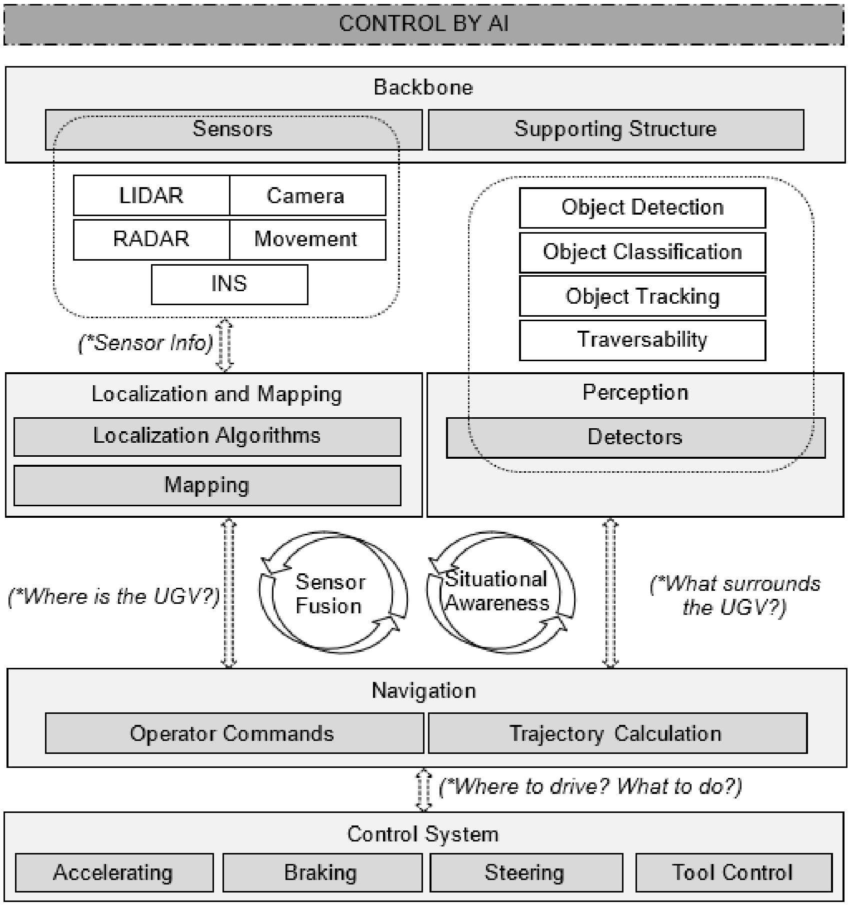

Figure 3. The 'Control by the AI' consists of five major cornerstones: a) localization and mapping, b) perception, c) navigation, d) backbone and support structure, and e) control system.

The 'Control by AI' is based on the following (Fig. 3). First, is has to be determined, where the vehicle is located. For that, localization and mapping techniques are used, which both rely on sensor information. Different types of sensors are used:

1. LIDARs (Li & Ibanez-Guzman, 2020).
2. Cameras (Chapel & Bouwmans, 2020).
3. RADARs (Javadi & Farina, 2020).
4. Vehicle movement sensors.
5. INS (Inertial Navigation System), which consist of (Konrad et al., 2018)
   a. GNSS sensor;
   b. Inertial Measurement Unit (IMU).

After the position of the vehicle is determined, it is necessary to know what it is surrounded by. For that, different types of perception techniques are used, for example:

1. Object Detection: find objects based by the output of the sensors.
2. Object Tracking (Luo et al., 2021): provide information about the location of objects over time (for example, a person in front of the UGV used in 'Follow Me' mode (Islam et al., 2019)).

3. Object Classification (Kim et al., 2021): tell the outputs of the sensor what it is. For example, in camera view, is the object a road, car, person, etc.

4. Traversablity (Aggarwal & Kumar, 2020): provide information about the surroundings around the UGV, where it can and cannot drive, and how well it is possible. Includes sensor fusion (Sock et al., 2016).

When the positioning and the surroundings are confirmed, then, based on operator input, the 'UGV Navigation Control' conducts trajectory calculations to be used by the UGV.

Based on the calculated trajectory, the 'Control System' starts moving the UGV. Basically, the vehicle control system conducts three high-level tasks: 1) accelerating, 2) braking, 3) steering. Additional tasks during the drive, such as moving the tools, are also performed by the 'Control System'.

All localization, mapping, and perception is based on an autonomous navigation backbone with support structures and various sensors (LIDARs, camera, vehicle motion sensors, RADARs, Inertial Navigation System (INS) consisting of GNSS and Inertial Measurement Unit (IMU)) (Zhu et al., 2019).

For this experiment, the UGV was controlled by the 'LOS remote control'. Although other control methods can be used, this method was chosen because this experiment (assessment of power characteristics of the UGV) does not require a high level of autonomy. The goal of the experiment was to provide evidence that the UGV of interest is capable of performing operations peat fields.

The UGV was assessed for two operations of milled peat extraction: milling and harrowing. For both operations, the power consumption of the UGV and the drawbar pull of the implements, passive miller and harrower (Fig. 4), were measured (Adamchuk et al., 2016; Bulgakov et al., 2020). The towed implements were used as if it were used by a conventional tractor–no changes were made in their dimensions or other parameters.

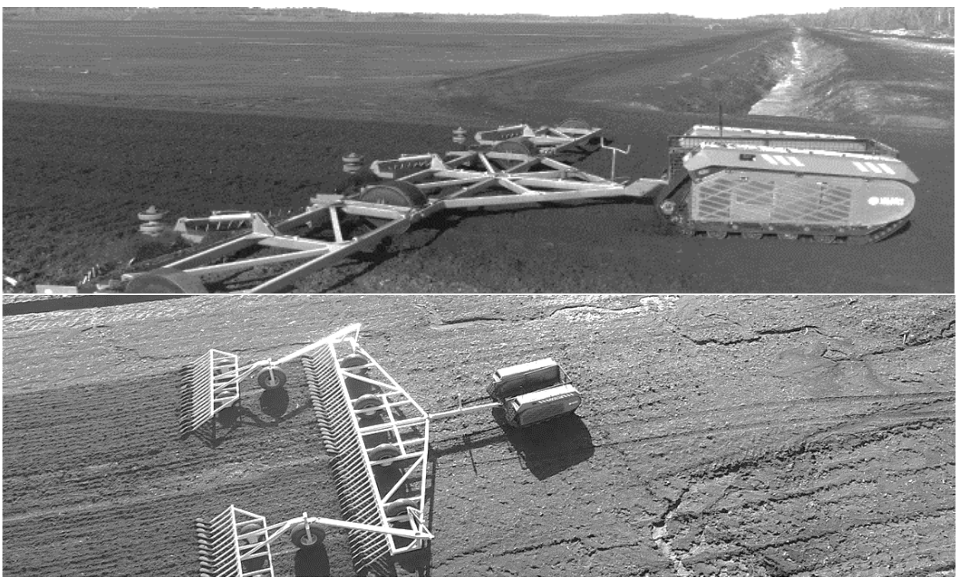

Figure 4. (up) The passive miller and (down) the harrower used in the experiment. For both implements the drawbar pull and drawbar power were determined.

The field measurements were carried out on the peat fields of Kraver AS in Viljandi County, Estonia (coordinates 58.542467, 25.860802) with ambient temperature of 10–12 °C, wind speed 2–3 m s^{-1}, no rain, relative air humidity 80%.

The data obtained from field measurements allowed the evaluation of the capability of the UGV to operate in peatland operations.

The experimental setup consists of two parts:

1. The measurement of the drawbar pull of two peat extraction implements: a) harrower, b) passive miller. The two peat extraction implement are described in Table 2.

2. The measurement of generated power by the UGV.

To measure the drawbar pull, a force transducer is connected in series between the towed implement (a passive miller and a harrower) and the drive mechanism. In this case, KAF 100 kN force transducer by A.S.T Gruppe was used (KAF-S Force Transducer, 2021). The implement is towed for at least 10 s so that the drawbar pull values can be recorded. The data is recorded with a time interval of 0.01 s. The previous procedure is repeated at varied speeds.

Table 2. The main characteristics of the towed peat extraction implements

Name	Value
Model	JLK-19S (Peatmax, 2021)
Producer	Peatmax (Finland)
Working width	12–18 m
Working depth	20 mm
Weight	1,800 kg
Name	Value
Model	84306900 (Elva EPT, 2021)
Producer	Elva EPT (Estonia)
Working width	9.5 m
Working depth	20 mm
Weight	900 kg

The values were chosen that they would correspond to the typical towing speeds for peat extraction equipment. By measuring simultaneously the drawbar pull F and operational speed v, the power consumption P_i of the implements can be determined. As the UGV was assigned to carry out milling and harrowing, the current I and the voltage U of the power system were measured. The recorded values were used to assess the draft power of the UGV.

RESULTS AND DISCUSSION

On Fig. 5 and Fig. 6, the results for the drawbar pull measurements for the passive miller and for the harrower are shown. For the sake of clarity, only two operating speed results are shown here (4 km $h^{-1}$and 14 km h^{-1}). The oscillating lines are fitted with linear trendlines which presents the mean drawbar pull. For both implements, typical values remain in the range of 4–8 kN. Note that as the implements are dragged, peaks occur, which are associated with implement getting stuck in the soil.

On Fig. 7, peak and mean drawbar pull values at different operating speeds are plotted. Note how the measurement data follows a polynomial (quadratic) dependence trendline. In this graph, two types of drawbar pull values must be distinguished:

1. 'Mean Operational Drawbar Pull' indicates the resistive forces measured during operation averaged over time.

2. 'Peak Operational Drawbar Pull' indicates the maximum force measured during the test. This short-term value provides an opportunity to optimally estimate mobility requirements.

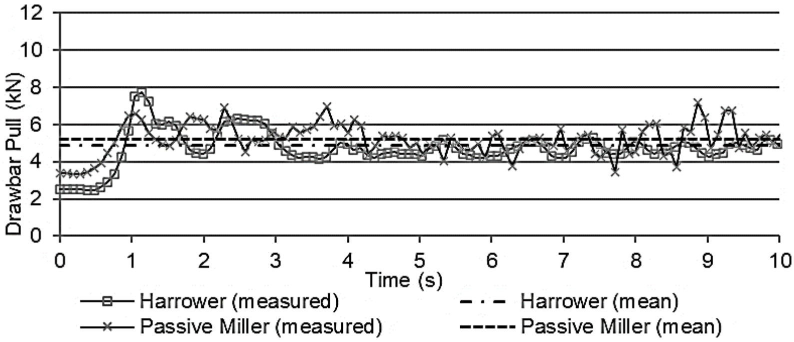

Figure 5. Measured and mean drawbar pull values for the passive miller and for the harrower at operational speed of 4 km h^{-1}. The oscillating lines (measured drawbar values) are fitted with linear trendlines which presents the mean drawbar pull.

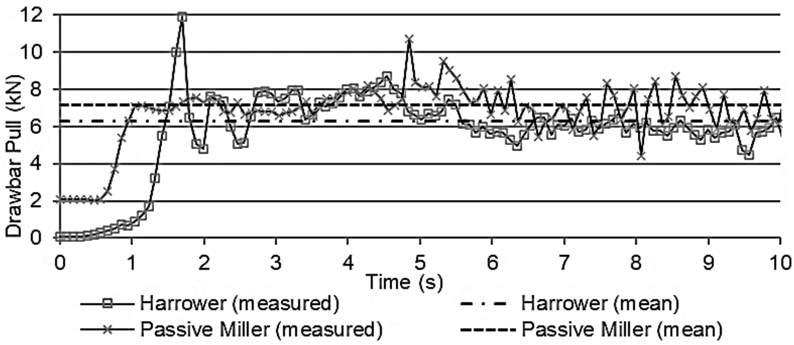

Figure 6. Measured and mean drawbar pull values for the passive miller and for the harrower at operational speed of 14 km h^{-1}. The oscillating lines (measured drawbar values) are fitted with linear trendlines which presents the mean drawbar pull.

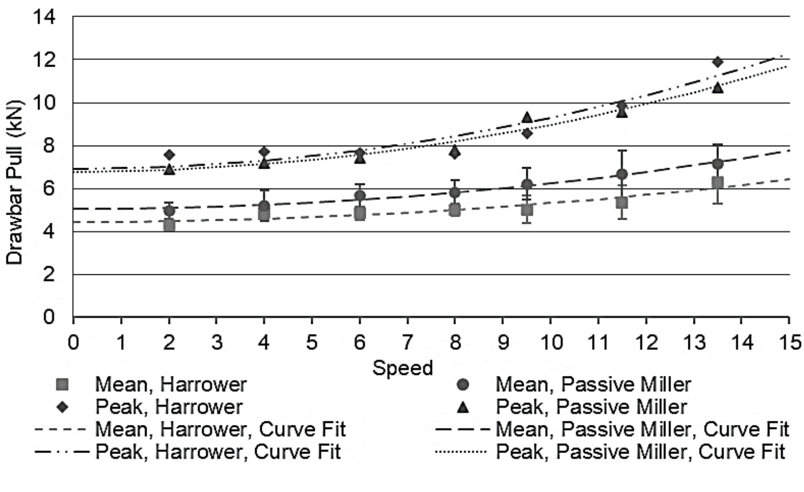

Figure 7. Mean and peak operational drawbar pull values for the passive miller and for the harrower at different operational speeds (km h^{-1}). Here, the dots present the measurement results (mean values) and the lines act as the polynomial curve fit.

Based on measured data (operational speed v and drawbar pull F), the drawbar power for a passive miller and for a harrower can be calculated. The calculated power consumption values are plotted on Fig. 8. In this graph, two types of drawbar power must be distinguished:

1. 'Mean Drawbar Power' indicates the power required during operation averaged over time.
2. 'Peak Drawbar Power' indicates the maximum power measured during the test. This short-term value provides an opportunity to optimally estimate power consumption requirements.

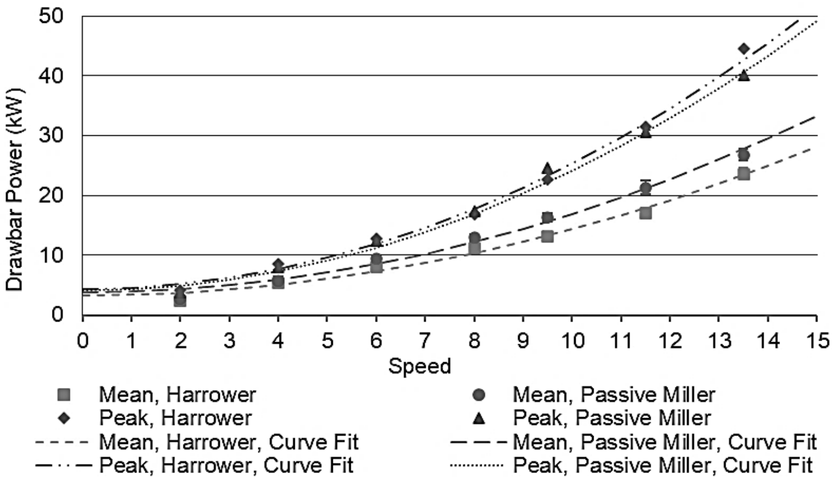

Figure 8. Mean and peak drawbar power values for the passive miller and for the harrower at different operational speeds (km h^{-1}). Here, the dots present the measurement results (mean values) and the lines act as the polynomial curve fit.

Based on measured data (current I and voltage U of the UGV power system), draft power of the UGV can be given (Figs 9 and 10).

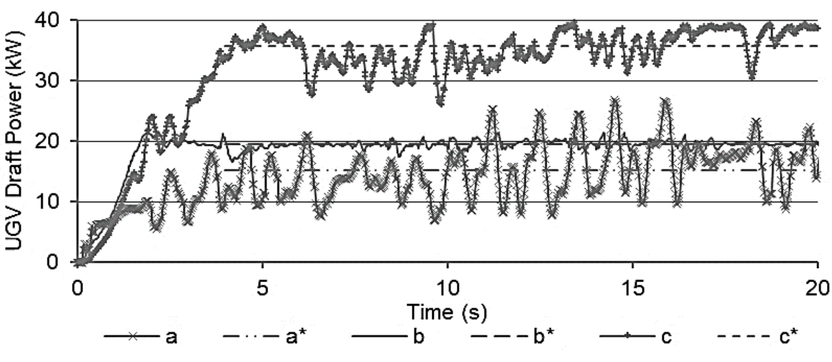

Figure 9. UGV draft power for the harrower: a) speed 5 km h^{-1}; a*) speed 5 km h^{-1} with linear trendline 15.2 kW; b) Speed 8 km h^{-1}; b*) speed 8 km h^{-1} with linear trendline 19.5 kW; c) speed 14 km h^{-1}; c*) speed 14 km h^{-1} with linear trendline 35.8 kW.

The authors observed that the robotic system of interest capable of performing in peat extraction operations. No constraining slip was detected; the traction and power output of the UGV were found to be sufficient. Also, it was found that the readiness level of autonomous functions, such as 'Waypoint Navigation' and 'Remote Control' ('Teleoperation') are sufficient.

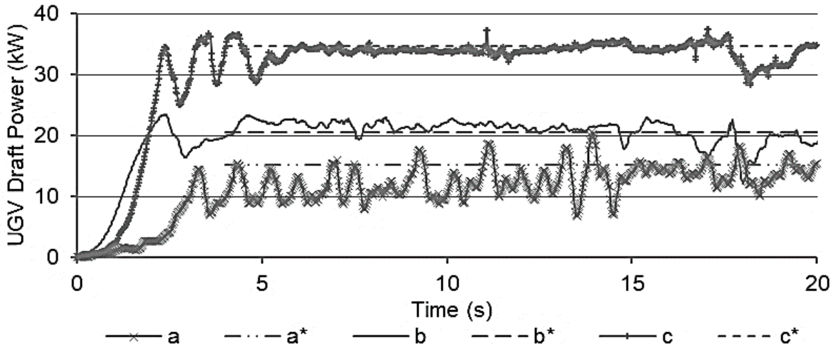

Figure 10. UGV draft power for the passive miller: a) speed 5 km h^{-1}; a*) speed 5 km h^{-1} with linear trendline 14.2 kW; b) Speed 8 km h^{-1}; b*) speed 8 km h^{-1} with linear trendline 20.6 kW; c) speed 12 km h^{-1}; c*) speed 12 km h^{-1} with linear trendline 34.7 kW.

However, the energy storage capacity requirement was not met (Ueka et al., 2013). At lower operational speeds (up to 4–5 km h^{-1}), the UGV draft power was in a suitable range to perform long-term–the generator output matched the draft power of the implements. As the operational speeds increased (up to 14 km h^{-1}), the generator lacked the capacity to maintain sufficient power output to operate in the long run. To effectively operate in peat extraction operations, the energy generation and storage capacity must be improved.

To keep a steady operational speed, the passive miller must be towed with a higher draft force. As it turns out, for both implements, the required peak draft force is roughly the same. The oscillating behaviour is caused by two reasons:

1. Steering corrections (Moriwaki, 2005).
2. Uneven resistive characteristics of the soil which results the implement getting stuck for brief moments (Shahgoli et al., 2010).

Based on the test data, the use of an alternative powertrain can be proposed (Soltani et al., 2019). Most of the traction is provided by the main source of propulsion (diesel generator, battery pack and two electric motors). Additional power can be provided by a secondary power source (such as a 'fuel cell'). This would address the issue on energy storage capacity.

When comparing the data from Fig. 8, Fig. 9, and Fig. 10, then it is shown that the use of this UGV shows a promising outlook, since for all operational speeds and for both implements, the UGV draft power exceeds the required drawbar power in the near of 10 kW. This value corresponds to the idle running power of the UGV.

Given the restriction that unauthorised personnel have limited access to the peat extraction sites, the authors of this paper state that this robotic peat extraction system has the readiness level to be safely operated, thus making it close of entering the commercial market.

In summary, additional development for this robotic system is recommended with the main challenges identified as following:

1. The development of the 'Energy Generation and Storage Capacity' to effectively operate in peat extraction operations. Additional development of the system is recommended, to provide a full 8–12 h practical work time. It can be solved based on additional batteries (Solectrac, 2021) which would also increase the mass and influence the efficiency of the system; or based on fuel cell energetics which is commercially available for that kind of situation (Mekhilef et al., 2012; US Department of Energy, 2016; Papageorgopoulos, 2019; Ma et al., 2021).

2. The further development of autonomous functions such as the 'Waypoint Navigation System' (Kurita et al., 2017; Atyabi et al., 2018) the 'Obstacle Detection and Avoidance' (Kamel et al., 2020; Badue et al., 2021).

Furthermore, possible next steps are to add other implements to the robotic peat extraction system and to validate the results based on experiment data. As implements that do not require an external power supply were investigated in this work (harrower and passive miller), the next step would be to determine the capability of the robotic system using peat implements with an external power supply (e.g. an active miller). In addition to this, current measurement results are based on standard peat extraction implement solutions - no optimisation of existing implements is done here. Fundamentally, it would be possible to optimise the peat extraction implements (for instance, reduce the width of the implements *N* times), but this would require a separate analysis.

The concept of using the UGV in milled peat extraction is derived from the idea that the known mobility requirements (low ground pressure, terrain tractability, implement drawbar pull, power requirements) in the peat extraction industry match the capabilities of the robotic system of interest. However, it must be noted that this UGV is originally not designed for peat extraction. By now, the system lacks proper safety measures in terms of operating in an environment known for its fire hazards (Tissari et al., 2006). The authors suggest adding purpose-built spark arrestors to mitigate the subject.

CONCLUSIONS

In this study, the conventional tractor-based peat extraction system was replaced by an UGV-based system. The main difference comes from the fact that the human operator is removed from the wheel, which gives an opportunity to dimension the new system for peat field work. The current state of the robotic system of interest is such that it allows the test to be repeated in each peat field with a sufficient safety level, provided that no unauthorised persons enter it.

After the requirements and experimental data analysis, it was concluded that the robotic system under study can perform peat extraction operations (milling and harrowing):

1. The power characteristics of the robotic system of interest are suitable for the milled peat extraction implements tested in this experiment (harrower and passive miller).

2. The energy demand characteristics were found sufficient for lower operational speed (up to 4–5 km h^{-1}). However, at higher operational speeds (up to 14 km h^{-1}), the power supply capacity to effectively operate in milled peat extraction operations was found to be insufficient, thus requiring an improved solution.

ACKNOWLEDGEMENTS. The authors of this article thank peat production company Kraver AS (Elar Abram), who provided access to their peat field. This research was supported by European Structural and Investment Fund project no. 2014-2020.4.02.17-0110 'Applied research on system of sensors and software algorithms for safety and driver assistance on remotely operated ground vehicles for off-road applications (1.05.2018−30.04.2021)' (NutikasUGV).

REFERENCES

Adamchuk, V., Bulgakov, V., Nadykto, V., Ihnatiev, Y. & Olt, J. 2016. Theoretical research into the powerand enegry performance of agricultural tractors. *Agronomy Research* **14**(5), 1511–1518.

Adams, B.T. 2019. Farm machinery automation for tillage, planting cultivation, and harvesting. M. Kutz, *Handbook of Farm, Dairy and Food Machinery Engineering,* pp. 115–131. Academic Press.

Aggarwal, S. & Kumar, N. 2020. Path planning techniques for unmanned aerial vehicles: A review, solutions, and challenges. *Computer Communications* **149**, 270–299.

Alakangas, E., Hölttä, P., Juntunen, M. & Vesisenaho, T. 2012. Fuel peat production technology. *Training material*, JAMK University of Applied Sciences, pp. 34–43.

Aravind, K.R., Raja, P. & Pérez-Ruiz, M. 2017. Task-based agricultural mobile robots in arable farming: A review. *Spanish Journal of Agricultural Research* **15**(1), e02R01.

Atyabi, A., MahmoudZadeh, S. & Nefti-Meziani, S. 2018. Current advancements on autonomous mission planning and management systems: An AUV and UAV perspective. *Annual Reviews in Control* **46**, 196–215.

Badue, C., Guidolini, R., Carneiro, R.V., Azevedo, P., Cardoso, V.B., Forechi, A., … De Souza, A.F. 2021. Self-driving cars: A survey. *Expert Systems with Applications* **165**, 113816.

BAE Systems 2021. https://www.baesystems.com/en/article/our-new-unmanned-ground-vehicle-takes-on-dangerous-jobs. Accessed 14.12.2021.

Bayar, G., Bergerman, M., Konukseven, E.I. & Koku, A.B. 2016. Improving the trajectory tracking performance of autonomous orchard vehicles using wheel slip compensation. *Biosystem Engineering* **146**, 149–164.

Bayındır, L. 2016. A review of swarm robotics tasks. *Neurocomputing* **172**, 292–321.

Bechar, A. & Vigneault, C. 2016. Agricultural robots for field operations: Concepts and components. *Biosystems Engineering* **149**, 94–111.

Bechar, A. & Vigneault, C. 2017. Agricultural robots for field operations. Part 2: Operations and systems. *Biosystems Engineering* **153**, 110–128.

Bochtis, D., Sørensen, C. A. & Kateris, D. 2019. Choosing a Machinery System. D. Bochtis, C. A. Sørensen, & D. Kateris, *Operations Management in Agriculture,* pp. 117–158. Academic Press.

Bonadies, S. & Gadsden, S.A. 2019. An overview of autonomous crop row navigation strategies for unmanned ground vehicles. *Engineering in Agriculture, Environment and Food* **12**(1), 24–31.

Bulgakov, V., Olt, J., Kuvachov, V. & Smolinskyi, S. 2020. A Theoretical and Experimental Study of the Traction Properties of Agricultural Gantry Systems. *Agraarteadus/Journal of Agricultural Science* **31**(1), 10–16. doi: 10.15159/jas.20.08.

Casals, L.C., Martinez-Laserna, E., Garcia, B.A. & Nieto, N. 2016. Sustainability analysis of the electric vehicle use in Europe for CO_2 emissions reduction. *Journal of Cleaner Production* **127**, 425–437.
Chapel, M.-N. & Bouwmans, T. 2020. Moving objects detection with a moving camera: A comprehensive review. *Computer Science Review* **38**, 100310.
Duckett, T., Pearson, S., Blackmore, S., Grieve, B., Chen, W.-H., Cielniak, G., … Yang, G.-Z. 2018. *Agricultural Robotics: The Future of Robotic Agriculture.* UK-RAS Network White Papers, ISSN 2398-4414. arXiv:1806.06762
ECA Group 2021. Robotic and Integrated Systems. https://www.ecagroup.com/en/robotic-and-integrated-systems. Accessed 14.12.2021.
Elva EPT 2021. http://www.elvaept.ee/?p=82&lang=et. Accessed 14.12.2021.
Hajjaj, S.S. & Sahari, K.S. 2016. Review of agriculture robotics: Practicality and feasibility. *IEEE International Symposium on Robotics and Intelligent Sensors (IRIS).* doi: 10.1109/IRIS.2016.8066090
He, P., Li, J., Fang, E., deVoil, P. & Cao, G. 2019. Reducing agricultural fuel consumption by minimizing inefficiencies. *Journal of Cleaner Production* **236**, 117619.
Islam, M.J., Hong, J. & Sattar, J. 2019. Person Following by Autonomous Robots: A Categorical Overview. *The International Journal of Robotics Research*. doi: 10.1177/0278364919881683
Javadi, S.H. & Farina, A. 2020. Radar networks: A review of features and challenges. *Information Fusion* **31**, 48–55.
Johnson, D.A., Naffin, D.J., Puhalla, J.S., Sanchez, J. & Wellington, C. K. 2009. Development and implementation of a team of robotic tractors for autonomous peat moss harvesting. *Journal of Field Robotics* **26**(6–7), 549–571.
KAF-S Force Transducer 2021. https://www.ast.de/en/products/force-measurement-technology-sensor-systems/sensors/kaf-s. Accessed 14.12.2021.
Kamel, M.A., Yu, X. & Zhang, Y. 2020. Formation control and coordination of multiple unmanned ground vehicles in normal and faulty situations: A review. *Annual Reviews in Control* **49**, 128–144.
Kim, K., Kim, C., Jang, C., Sunwoo, M. & Jo, K. 2021. Deep learning-based dynamic object classification using LiDAR point cloud augmented by layer-based accumulation for intelligent vehicles. *Expert Systems with Applications* **167**, 113861.
Konrad, T., Gehrt, J.-J., Lin, J., Zweigel, R. & Abel, D. 2018. Advanced state estimation for navigation of automated vehicles. *Annual Reviews in Control* **46**, 181–195.
Kurita, H., Iida, M., Cho, W. & Suguri, M. 2017. Rice Autonomous Harvesting: Operation Framework. *Journal of Field Robotics* **34**(6), 1084–1099.
Kägo, R., Vellak, P., Karofeld, E., Noorma, M. & Olt, J. 2021. Assessment of using state of the art unmanned ground vehicles for operations on peat fields. *Mires and Peat* **27**.
Lewis, F.L. & Ge, S.S. 2006. *Autonomous Mobile Robots.* CRC Press, 613–654.
Li, Y. & Ibanez-Guzman, J. 2020. Lidar for Autonomous Driving: The Principles, Challenges, and Trends for Automotive Lidar and Perception Systems. *IEEE Signal Processing Magazine* **37**(4), 50–61.
Luo, W., Xing, J., Milan, A., Zhang, X., Liu, W. & Kim, T.-K. 2021. Multiple object tracking: A literature review. *Artificial Intelligence* **293**, 103448.
Ma, S., Lin, M., Lin, T.-Z., Lan, T., Liao, X., Marécha, F., … Wang, L. 2021. Fuel cell-battery hybrid systems for mobility and off-grid applications A review. *Renewable and Sustainable Energy Reviews* **135**, 110119.
Madridano, Á., Al-Kaff, A., Martín, D. & de la Escalera, A. 2021. Trajectory planning for multi-robot systems: Methods and applications. *Expert Systems with Applications* **173**, 114660.
Mekhilef, S., Saidur, R. & Safari, A. 2012. Comparative study of different fuel cell technologies. *Renewable and Sustainable Energy Reviews* **16**(1), 981–989.
Milrem 2021. https://milremrobotics.com/multiscope. Accessed 14.12.2021.

Moriwaki, K. 2005. Navigation control for electric vehicles using nonlinear state feedback H∞ control. *Nonlinear Analysis: Theory, Methods & Applications*, e2257–e2268.

Moysiadis, V., Sarigiannidis, P., Vitsas, V. & Khelifi, A. 2021. Smart Farming in Europe. *Computer Science Review* **39**, 100345.

Papageorgopoulos, D. 2019. Fuel Cell R&D Overview. *Annual Merit Review and Peer Evaluation Meeting,* 29 April 2019. Crystal City, Virginia, USA

Peatmax 2021. http://peatmax.com. Accessed 14.12.2021.

Reina, G., Milella, A., Rouveure, R., Nielsen, M., Worst, R. & Blas, M.R. 2016. Ambient awareness for agricultural robotic vehicles. *Biosystem Engineering* **146**, 114–132.

Roldán, J.J., del Cerro, J., Garzón-Ramos, D., Garcia-Aunon, P., Garzón, M., de León, J. & Barrientos, A. 2018. Robots in Agriculture: State of Art and Practical Experiences. A. Neves, *Service Robots*, pp. 67–90.

Shahgoli, G., Fielke, J., Desbiolles, J. & Saunders, C. 2010. Optimising oscillation frequency in oscillatory tillage. *Soil and Tillage Research* 202–210.

Silverberg, L.M. & Xu, D. 2019. Dubins Waypoint Navigation of Small-Class Unmanned Aerial Vehicles. *Open Journal of Optimization* **8**, 59–72.

Small, N., Lee, K. & Mann, G. 2018. An assigned responsibility system for robotic teleoperation control. *International Journal of Intelligent Robotics and Applications* **2**, 81–97.

Sock, J., Kim, J., Min, J. & kWak, K. 2016. Probabilistic traversability map generation using 3D-LIDAR and camera. *IEEE International Conference on Robotics and Automation (ICRA).* 16–21 May 2016. Stockholm, Sweden.

Solectrac. 2021. https://www.solectrac.com. Accessed 14.12.2021.

Soltani, A.K., Kandidayeni, M., Boulon, L. & St-Pierre, D.L. 2019. Modular Energy Systems in Vehicular Applications. *Energy Procedia* **162**, 14–23.

Stevenson, J.D., O'Young, S. & Rolland, L. 2015. Beyond Line of Sight Control of Small Unmanned Aerial Vehicles Using a Synthetic Environment to Augment First Person Video. *Procedia Manufacturing*, 960–967.

Tabor, T., Pezzementi, Z., Vallespi, C. & Wellington, C. 2015. People in the weeds: Pedestrian detection goes off-road. *IEEE International Symposium on Safety, Security, and Rescue Robotics (SSRR).* doi: 10.1109/SSRR.2015.7442951

Tan, Y. & Zheng, Z.-Y. 2013. Research Advance in Swarm Robotics. *Defence Technology* **9**(1), 18–39.

Tissari, J.M., Yli-Tuomi, T., Raunemaa, T.M., Tiitta, P., Nuutinen, J.P., Willman, P.K., … Jokiniemi, J. 2006. Fine particle emissions from milled peat production. *Boreal Environment Research* **11**(4), 283–293.

Ueka, Y., Yamashita, J., Sato, K. & Doi, Y. 2013. Study on the Development of the Electric Tractor: Specifications and Traveling and Tilling Performance of a Prototype Electric Tractor. *Engineering in Agriculture, Environment and Food* **6**(4), 160–164.

U.S Department of Energy 2016. Fuel Cell Technologies Market Report 2016. Available at https://www.energy.gov/eere/fuelcells/downloads/2016-fuel-cell-technologies-market-report. Accessed 14.12.2021.

Zhou, S., Xi, J., McDaniel, M. W., Nishihata, T., Salesses, P. & Iagnemma, K. 2012. Self-supervised learning to visually detect terrain surfaces for autonomous robots operating in forested terrain. *Journal of Field Robotics* **29**(2), 277–297.

Zhu, S., Xiong, G. & Chen, H. 2019. Unmanned Ground Vehicle Control System Design Based on Hybrid Architecture. *2019 IEEE 8th Joint International Information Technology and Artificial Intelligence Conference (ITAIC).* Chongqing, China.

Agronomy Research **20**(2), 275–283, 2022
https://doi.org/10.15159/AR.22.030

Growth characteristics of American Ginseng (*Panax quinquefolius* L.) woods and field - cultivated at Northern Europe

A. Kronberga[1,*], I. Nakurte[2], L. Kaļāne[2], R. Abaja[2], M. Berga[2], A. Primavera[2] and I. Mežaka[2]

[1]Field and Forest, LTD, 2 Izstades Str, LV-4126 Priekuli parish, Cēsis county, Latvia
[2]Institute for Environmental Solutions, 'Lidlauks', LV-4126 Priekuļi parish, Cēsis county, Latvia
[*]Correspondence: Arta.Kronberga@fieldandforest.lv

Received: February 19th, 2022; Accepted: May 15th, 2022; Published: May 16th, 2022

Abstract. In Latvia, Northern Europe, American ginseng was grown in three forest types with different dominant species, as well as in agricultural field conditions - cultivated under artificial shade with three different types of mulches. Field cultivation yielded higher yields, root length, and root weight than wood cultivation under dominant species *Corylus avellana, Betula pendula,* and *Picea abies*. Mulching had a positive impact on ginseng growth in the field. Mulching with straw and buckwheat hulls resulted in longer and heavier roots.
In American ginseng roots, the contents of six ginsenosides were determined: Rg1, Re, Rb1, Rc, Rb2, and Rd. Re was the most abundant ginsenoside, followed by Rb1 > Rd > Rg1 = Rb2 > Rd. The total content of ginsenosides in our study did not reach the 4 percent threshold set by US Pharmacopeia.
These findings show that *Panax quinquefolium* can be grown in Northern Europe at 57°N, but it takes more than four years to achieve adequate yields and ginsenoside content.

Key words: *Panax quinquefolium*, woods - cultivated, field - cultivated, ginsenosides, Northern Europe.

INTRODUCTION

Farmers in the Nordic - Baltic region have recently expressed an increased interest in cultivating novel medicinal and aromatic plant species, such as honeysuckle (Vinogradov et al., 2020), thyme, and lavender (Nekrošiene, 2009). Additional knowledge on their adaptation to various climates, production practices, and the best varieties is, nevertheless, required.

American ginseng (*Panax quinquefolius* L.) is a native flora of Northern American hardwood forests, where it has been harvested in the wild for the last three centuries (Burkhart et al., 2021) with increasing intensity, eventually reaching over - exploitation levels. Since the late 1800s, American ginseng has been cultivated to meet the increasing demand (Mcgraw et al., 2013; Liu et al., 2021). American ginseng can be grown in temperate climates with cold winters because their seeds require cold stratification to break dormancy and germinate (Olson, 2014; Schmidt et al., 2019). The upper Midwest of the United States and Ontario, Canada are major cultivation regions (Liu et al., 2021), but there are reports of American ginseng cultivation in various Northern and Southern Hemisphere countries, such as New Zealand (Chen et al., 2020), Poland (Ligor et al., 2005), Denmark (Olson, 2014), France (Men-Olivier et al., 2006), and China (Nian He et al., 2008). American ginseng grows naturally in latitudes ranging from 30 to 50°N, and its northern limit in Canada is 53°N. Our experiments were conducted in Northern Europe under the Nemoral Climate zone at 57°N, but the proximity to the North Atlantic Ocean and the dominating west and south - west winds make winters warmer than indicated by latitude (Olson, 2014).

American ginseng can be grown in two different agroecosystems: in the forest or in an agricultural field with artificial shade. Ginseng cultivation in raised beds in agricultural fields (also known as 'field - cultivated ginseng') is the most common method of production in North America. This type of cultivation increases root yields and reduces harvesting time from 8 to 4 years (Lim et al., 2005; Roy et al., 2011; Liu et al., 2021). Mulching, soil density, bed shape, seedling density, light intensity, and other agrotechnological methods can be used to manage root size, shape, and yield (Lim et al., 2005; Roy et al., 2011).

There are two approaches for ginseng cultivation in the forest: so called 'woods cultivated' and 'wild-simulated.' The first approach is an intensively managed approach that includes raised beds, vegetation management, and soil tillage in a forest setting. The second method is to cultivate ginseng in forest soil with minimal intervention, such as site preparation before sowing seeds or planting plantlets in the forest (Burkhart et al., 2021).

Ginsenosides are unique components that contribute to the pharmacological activity of ginseng roots. Rb1, Rb2, Rc, Rd, Re, and Rg1 are the six major ginsenosides found in American ginseng (Fournier et al., 2003). The European Pharmacopoeia (01/2016:1523) does not list American ginseng. The dried root of *P. quinquefolius* is listed in the US Pharmacopeia with quality criteria of at least 4% total ginsenosides calculated on a dried basis. Climate, seasonal changes (Hao et al., 2020), light levels (Fournier et al., 2003), soil fertility and calcium content in soil (Konsler et al., 2019), mulching (Roy et al., 2011), plant population, and plant age all influence ginsenoside content (Lim et al., 2005).

Given that there are no research reports on American ginseng cultivation in Latvia, the goal of this study was to determine American ginseng cultivation potential in Latvia.

The study's main objectives were to assess root length, fresh root weight, and ginsenoside content in four-year-old roots of *Panax quinquefolius* grown in Latvia in various woods - cultivated and field - cultivation settings. Three different forest types were investigated, as well as three types of artificially shaded agricultural fields marked by different, locally available mulches.

MATERIALS AND METHODS

Seed propagation and planting

Seedlings were grown from stratified seeds purchased from a commercial supplier (Harding's wild mountain herbs). In March 2018, the seeds were sown in pots and grown in a nursery with an average moisture content of 56%, an average temperature of 16 °C, sodium lamps with light intensities ranging from 30,00 to 4,000 Lux, and a photoperiod of 16 hours.

In May 2018, plantlets were planted in three forest locations: first with dominant species *Coryllus avellana* (57°12'N 25°06'E), second with dominant species *Betula pendula* (57°14'N 25°12'E) and third with dominant species *Picea abies* (57°14'N 25°12'E). The species composition differed across the forest pilot sites (Table 1).

Table 1. Plant species in forest pilot sites

Forest layer	Dominant canopy species in woods		
	Corylus avellana	*Betula pendula*	*Picea abies*
Tree layer	*Pinus sylestris*, *Quercus robur*, *Tilia cordata*	*Betula pendula*	*Betula pendula*, *Picea abies*
Shrub layer	*Corylus avellana*, *Tilia cordata*, *Rubus idaeus*, *Acer plantonoides*, *Quercus robur*, *Padus avium*	*Amelanchier spicata*, *Rubus idaeus,* *Lonicera xylosterum,* *Picea abies*	*Amelanchier spicata*, *Lonicera xylosteum*, *Picea abies*, *Rubus idaeus*
Herb layer	*Galeobdolon luteum*, *Luzula pilosa*, *Solidago virgaurea*, *Lupinus polyphyllus*, *Fragaria vesca*, *Geum rivale*	*Aegopodium podagraria*, *Fragaria vesca*, *Dryopteris filix - mass*, *Veronica chamaedrys*, *Mycelis muralis*, *Lupinus polyphyllus*, *Equisetum sylvaticum*,	*Luzula pilosa,* *Lupinus polyphyllus*, *Solidago virgaurea*, *Fragaria vesca*, *Geum rivale*

Plantlets were planted in a shadowed system on raised soil beds in our organically certified agricultural experimental field (57°19'N 25°19'E) in June 2018. Shading was provided by wooden board roofing, with boards 10 cm wide and 2 cm apart, reducing solar radiation to 3–8 percent of full sunlight on sunny days and 6–30 percent on cloudy days. Each treatment bed measured 17 m long, 0.90 m wide, and 0.15 m tall. In both the -wood and field trials, the distance between plants was 10×15 cm. Mulch was used to cover the planting beds after they were finished. Mulching with buckwheat hulls, birch leaves, and reed (*Phragmites australis*) straws was tested.

All of the testing sites had sod-podzolic sandy loam soil. Table 2 summarises soil agrochemical properties. Because of the low pH level, granulated lime was applied at a rate of 400 kgha^{-1} in all testing locations prior to sowing. Mechanical removal and traps (on the field) were used to control slugs, and traps were used to control rodents (in the forest). If necessary, hand weeding was performed.

Table 2. Soil agrochemical characteristics in woods and cultivated field trial sites

Properties	Dominant canopy species in the woods			Mulch types on the field		
	Corylus avellana	*Betula pendula*	*Picea abies*	Buckwheat hull	Birch leaves	Straw
pH KCl	5.6	4.3	4.3	5.4	5.4	5.4
Organic matter content, %	5.2	2.5	2.5	2.5	2.5	2.5
Ca mg kg^{-1}	1138	202	202	667	667	667
P_2O_5 mg kg^{-1}	15	67	67	131	131	131
K_2O mg kg^{-1}	100	68	68	194	194	194

Plant sampling and yield assessment

In October 2021, ten four-year-old plants were randomly selected from each experimental variant. The senescing aboveground shoot was removed, and the remaining underground part was washed and dried with paper towels, root length measured, and roots weighed. They were then pooled to determine the root ginsenoside content. Prior to ginsenoside analysis, samples were dried for 20 hours at a temperature of 45 °C. Each sample was analysed in three replications.

Chemical analysis

Ginsenosides Rg1, Re, Rb1 and Rf were purchased from Sigma-Aldrich. HPLC-grade acetonitrile and methanol were supplied by Fisher Scientific (Loughborough, UK). Deionized water was obtained through a Mill-Q system, purchased from Millipore, phosphoric acid was of analytical purity.

Dried roots were pulverized by a laboratory mill. Ultrasound-assisted extraction was carried out in an ultrasonic device with a thermostat. Samples (0.5 g) were extracted with 40 mL of 50% methanol at 70.0 °C for 60 min. Samples were cooled, centrifugated for 10 min at 4,000 rpm, and filtrated through a membrane filter with a nominal pore size 0.45 μm to remove the insoluble materials. The standard solution corresponding to 0.3 mg mL^{-1} of ginsenoside Rg1, Re, Rb1 and Rf was prepared by dissolving 3 mg of reference standards in 10 mL of methanol. The solution was sonicated for 5 min and filtered through a membrane filter with a nominal pore size 0.45 μm.

Chromatographic analyses were performed on a HPLC system Agilent 1290 Infinity II series (Agilent Technologies, Germany). LC separations were achieved based on the European pharmacopeia (01/20216:1523) by using an Agilent Eclipse XDB-18 3.5 μm, 4.6×150 mm (Zorbax) column (35 °C) with water as a mobile phase A adjusted to pH 2 with phosphoric acid and acetonitrile as mobile phase B, using the following gradient program: 0–8 min (20% B); 8–40 min (20–40% B); 40–45 min (40–60% B); 45–47 min (60–95% B); 47–52 min (95% B); 52–55 min (95–20% B); 55–75 min (95–20% B) with the flow rate of 1.0 mL min^{-1}. The injection volume was 20 μL. Chromatograms were obtained on an Agilent WVD detector (Agilent Technologies, Germany) at a wavelength of 203 nm. The experimental data were handled using MassHunter Qualitative analyses 10.0 software (Agilent Technologies). For peak identification, retention times (tR) for standard solution and analysed samples were compared. The quantitative determination of sum of ginsenosides Rb1 and Rg1 in the samples expressed as percentage of dried drug was provided by inserting the related chromatographic peak areas in a mathematical equation, based on the European Pharmacopoeia.

Data analysis

T–tests were used to determine significance ($P \leq 0.05$) of mulching type under the shadowing system in field cultivation and the dominant tree species in woods - cultivation on root length and root weight. Two - way ANOVA with an ad - hoc *Tuckey test* was used to determine significance of growing conditions on composition of ginsenosides.

RESULTS AND DISCUSSION

Fresh root weight and length were significantly greater in 4-year-old field - cultivated plantlets than in 4-year-old woods-cultivated plantlets (Fig. 1). Fresh root weights among treatments ranged between 4.1 and 10.7 g in the field cultivation and 0.1 and 1.6 g in the woods cultivation, which is much less than the average fresh root weight of a 4 - year old ginseng taken in September (26.4 g) reported by Li and Wardle in Canada (Li & Wardle, 2002). Other authors have also reported that wood - cultivated ginseng has lower root weight than field - cultivated ginseng (Lim et al., 2005).

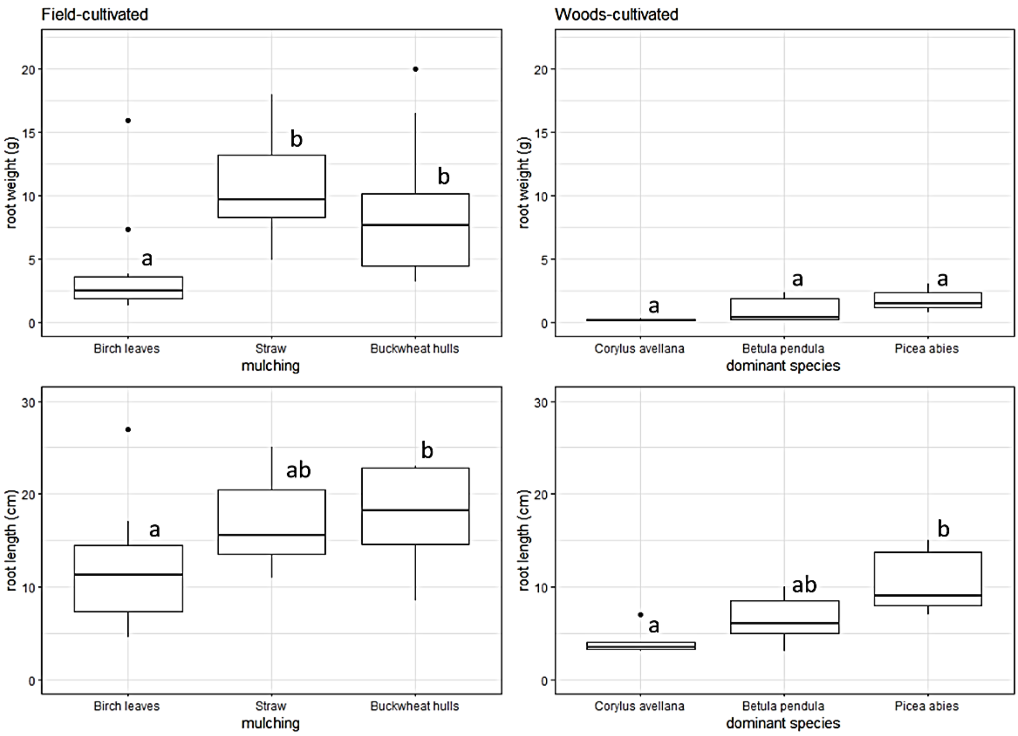

Figure 1. Boxplot of average fresh root length and weight of woods - cultivated and field - cultivated *P. quinquefolius.* Experimental variants marked with the same letter do not differ according to ad - hoc *Tuckey test* ($p > 0.05$).

The cultivation method and growing conditions are the key factors of root weight at harvest. Four years of cultivation is the minimum period required to obtain proper yield (Court et al., 1996). Oliver (1998) states that the average root weight for commercial harvesting after four years is 14 g; therefore, neither field cultivation nor woods cultivation produced sufficient root weight to meet this requirement. According to Li and Wardle (2002), American ginseng root weight increased with age (Li & Wardle, 2002), indicating that at least five years of cultivation is required in the Nordic - Baltic region to achieve the target root weight. Field cultivation yields the larger root weight, making it the more suited method for growing ginseng in Latvia.

Root length and weight were both affected by treatments within each agroecosystem. Mulch application on ginseng beds in field conditions is recommended as a common practice to mimic forest conditions and ensure more stable moisture and temperature conditions in the soil (Olson, 2014). Chopped straw is the most common mulch used by ginseng growers (Roy et al., 2011). The availability of materials and their impact on plant development, on the other hand, must be considered at each specific site. Buckwheat hulls, birch leaves, and reed straws were selected in the study based on their local availability.

The type of mulch used in field cultivation had a significant impact on root weight and length. Straw and buckwheat hull cover resulted in significantly longer root length and weight compared to birch leaf mulch and is therefore recommended for ginseng bed mulching. Ginseng cultivation was also tested in three woods with different dominant species. American ginseng naturally grows mainly in Northern American forests that are associated with *P. quinquefolium*, - *Arisaema triphyllum,* and *Acer saccharum* (Turner & McGraw, 2015). In this study three different Latvian forests with major cover species of *Betula pendula*, *Picea abies* and *Corylus avellana* were selected.

The average fresh root weight of cultivated ginseng in woods was very low - only 0.1–1.6 g - and did not differ significantly between forest types, but root length was greater in woods dominated by *Betula pendula* and *Picea abies* (Fig. 1).

This could be explained by a decrease in available nutrients in the soil, particularly phosphorus. One of the reasons for developing smaller roots is the lack of phosphorus (Choi et al., 2007). Dry conditions throughout the growing season in forest systems also contributed to lower root weight. This was most likely caused by precipitation being absorbed by the forest canopy.

While it is commonly known that forest - grown ginseng roots are more desirable on the market, they require longer time to produce - at least six years (Olson, 2014). As a result, we can conclude that a four-year period is insufficient to obtain commercially valuable *Panax quinquefolium* roots in *Corylus avellana*, *Betula pendula*, or *Picea abies* - dominated forests in Latvia. Furthermore, additional investments in improving soil composition, additional irrigation or preselecting forests with better summer moisture regime, and growing for longer seasons are suggested for the cultivation of American ginseng in woods.

P. quinquefolius roots are known to contain six characteristic active substances - ginsenosides Rg1, Re, Rb1, Rc, Rb2 and Rd. A total of 26 ginsenosides were separated and identified in analyzed samples by comparison of their retention behavior, among them 3 ginsenosides Rg1, Re and Rb1 were identified by commercially available external standards.

Six main ginsenosides (Rg1, Re, Rb1, Rc, Rb2 and Rd) were quantified by linear regression equations of standard curves, while all other ginsenosides were quantified by Rb1. All these ginsenosides were found in ginseng roots cultivated in Latvia (Table 3). All tested saponins in this study belong to the dammarane type ginsenosides. According to Zhang (2014), structurally, dammarane - ginsenosides are classified into protopanaxadiol (PPD) (Rb1, Rc, Rb2 and Rd) and protopanaxatriol (PPT) types (Rg1 and Re), according to the different positions of aglycones linked to the parent nucleus structure. The changes of PPT-/PPD - type ratio result in variance of the potency of bioactivity and further alter the overall quality of ginseng roots (Shan et al., 2014). Zhang et al. (2014) described variation of ginsenoside heterogeneity in different tissues - leaves, rhizomes, and main roots. He found that the alteration of the proportions of the two dammarane types of ginsenosides may change along with years of cultivation. Ginsenoside - Rc and Rg1 show relatively higher changing ratios during the period from 1- to 13-year-old main root samples.

Table 3. Comparison of ginsenosides in woods cultivated and field cultivated 4 year oldginseng roots

Cultivation type	Ginsenoside composition (% on dried basis)						Sum of Rg1 and Rb1, %	Sum of all ginsenosides, %
	Rg1*	Re	Rb1	Rc	Rb2	Rd		
	Field cultivated with different mulching							
Buckwheat	0.10a	0.62a	0.52a	0.06a	0.16a	0.13a	0.62a	2.42a
Birch leaves	0.11b	0.70a	0.59b	0.07a	0.07b	0.13a	0.70b	2.02b
Straw	0.03a	0.63b	0.60b	0.08a	0.21a	0.23b	0.63a	3.05c
Assinewe et al. (2003)	0.25	1.75	1.88	0.36	0.13	0.48	2.13	4.85
	Wood - cultivated with different dominant canopy species							
Corylus avellana	0.45a	0.84a	0.38a	0.13a	0.09a	n.a.	0.84a	3.09a
Picea abies	0.15b	0.51b	0.36b	0.11a	0.09a	0.04a	0.51b	1.62b
Betula pendula	0.11b	0.68c	0.57b	0.11a	0.13b	0.06a	0.68ab	2.25c
Assinewe et al. (2003)	0.94	1.42	2.81	0.42	0.09	0.29	3.75	5.78

* Under each of the growing systems, ginsenoside content indicated with the same letter in the same column do not differ according to Tuckey test ($p > 0.05$).

In Canada, Assinewe et al. (2003) found no significant difference in ginsenoside content between four-year wood - cultivated and field - cultivated ginseng roots. We also observed similar results in total ginsenosides content in both wood and field cultivated ginseng in our study. However, unlike Assinewe (2003), the total content of ginsenosides in our study did not reach the 4% threshold set by US Pharmacopeia. However, the sum of Rg1 and Rb1 exceeded the 0.4% threshold set by European Pharmacopeia for *Panax ginseng* roots.

The variance in saponins could be due to harvesting data, growth conditions, or other factors. The highest concentration of ginsenosides was found to be Re and Rb1.

These findings are partially consistent with those of other studies (Lim et al., 2005; Qu et al., 2009). According to the abovementioned authors research, ginsenoside Rb1 is the most abundant and Re is the second most abundant ginsenoside in roots. Re > Rb1 > Rd> Rg1 = Rb2 > Rd was the overall relative abundance of the six ginsenosides.

The amount of ginsenosides in the roots increases as the ginseng becomes older (Court et al., 1996; Schlag & McIntosh, 2006). The levels of accumulated ginsenosides increase rapidly in the first four years of growth, then remain steady for the next four years, with the fifth year of cultivation representing a critical transitional period in the plant's life cycle (Zhang et al., 2014).

As a result, a longer period of cultivation is recommended for ginseng, both in field and forest growing conditions, to accumulate the required amounts of ginsenosides in Latvian growing conditions and to reach sufficient root weight.

CONCLUSIONS

Cultivating American ginseng in raised beds in field settings under wooden board roofing resulted in higher yields and root lengths than woods - cultivated ginseng. Mulching had a noticeable positive effect on ginseng growth. Straw and buckwheat hull mulches are more preferable than birch leaves.

The results of this study indicate that cultivation of *P. quinquefolius* is feasible in Northern European conditions at latitude 57°N, but that more than four years of cultivation is recommended to ensure acceptable yields and ginsenoside content.

ACKNOWLEDGEMENTS. The research was supported by the EIP - Agri project 'Development of innovative technologies for cultivation and food production of ginseng (*Panax* s.p) and Chinese horseradish (*Angelica sinensis*)', No.17-00-A01620-000008.

REFERENCES

Assinewe, V.A., Baum, B.R., Gagnon, D. & Arnason, J.T. 2003. Phytochemistry of wild populations of *Panax quinquefolius* L. (North American ginseng). *Journal of Agricultural and Food Chemistry* **51**(16), 4549–4553. doi: https://doi.org/10.1021/jf030042h

Burkhart, E.P., Nilson, S.E., Pugh, C.V. & Zuiderveen, G.H. 2021. Neither Wild nor Cultivated: American Ginseng (*Panax quinquefolius* L.) Seller Surveys Provide Insights into *in situ* Planting and Husbandry. *Economic Botany* **75**(2), 126–143. doi: https://doi.org/10.1007/S12231-021-09521-8

Chen, W., Balan, P. & Popovich, D.G. 2020. Ginsenosides analysis of New Zealand - grown forest *Panax ginseng* by LC-QTOF-MS/MS. *Journal of Ginseng Research* **44**(4), 552–562. doi: https://doi.org/10.1016/J.JGR.2019.04.007

Choi, Y.E., Kim, Y.S., Yi, M.J., Park, W.G., Yi, J.S., Chun, S.R., Han, S.S. & Lee, S.J. 2007. Physiological and chemical characteristics of field-and mountain-cultivated ginseng roots. *Journal of Plant Biology* **50**(2), 198–205. doi: https://doi.org/10.1007/BF03030630

Court, W.A., Reynolds, L.B. & Hendel, J.G. 1996. Influence of root age on the concentration of ginsenosides of American ginseng (*Panax quinquefolium*). *Canadian Journal of Plant Science* **76**(4), 853–855. doi: https://doi.org/10.4141/cjps96-144

Fournier, A.R., Proctor, J.T.A., Gauthier, L., Khanizadeh, S., Bélanger, A., Gosselin, A. & Dorais, M. 2003. Understory light and root ginsenosides in forest - grown *Panax quinquefolius*. *Phytochemistry* **63**(7), 777–782. doi: https://doi.org/10.1016/S0031-9422(03)00346-7

Hao, M., Zhou, Y., Zhou, J., Zhang, M., Yan, K., Jiang, S., Wang, W., Peng, X. & Zhou, S. 2020. Cold - induced ginsenosides accumulation is associated with the alteration in DNA methylation and relative gene expression in perennial American ginseng (*Panax quinquefolius* L.) along with its plant growth and development process. *Journal of Ginseng Research* **44**(5), 747–755. doi: https://doi.org/10.1016/J.JGR.2019.06.006

Konsler, T.R., Zito, S.W., Shelton, J.E. & Staba, E.J. 2019. Lime and Phosphorus Effects on American Ginseng: II. Root and Leaf Ginsenoside Content and Their Relationship. *Journal of the American Society for Horticultural Science* **115**(4), 575–580. doi: https://doi.org/10.21273/jashs.115.4.575

Li, T.S.C. & Wardle, D. 2002. Seasonal fluctuations of leaf and root weight and ginsenoside contents of 2-, 3-, and 4-year-old american ginseng plants. *HortTechnology* **12**(2), 229–232. doi: https://doi.org/10.21273/horttech.12.2.229

Ligor, T., Ludwiczuk, A., Wolski, T. & Buszewski, B. 2005. Isolation and determination of ginsenosides in American ginseng leaves and root extracts by LC-MS. *Analytical and Bioanalytical Chemistry* **383**(7), 1098–1105. doi: https://doi.org/10.1007/S00216-005-0120-8

Lim, W., Mudge, K.W. & Vermeylen, F. 2005. Effects of Population, Age, and Cultivation Methods on Ginsenoside Content of Wild American Ginseng (*Panax quinquefolium*). *Journal of Agricultural and Food Chemistry* **53**(22), 8498–8505. doi: https://doi.org/10.1021/JF051070Y

Liu, H., Burkhart, E.P., Chen, V.Y.J. & Wei, X. 2021. Promotion of *in situ* Forest Farmed American Ginseng (*Panax quinquefolius* L.) as a Sustainable Use Strategy: Opportunities and Challenges. *Frontiers in Ecology and Evolution* **9**, 652103. doi: https://doi.org/10.3389/fevo.2021.652103

McGraw, J.B., Lubbers, A.E., Van der Voort, M., Mooney, E.H., Furedi, M.A., Souther, S., Turner, J.B. & Chandler, J. 2013. Ecology and conservation of ginseng (*Panax quinquefolius*) in a changing world. *Annals of the New York Academy of Sciences* **1286**(1), 62–91. doi: https://doi.org/10.1111/NYAS.12032

Men-Olivier, L.Le, Renault, J.H., Thepenier, P., Jacquier, M.J., Zeches-Hanrot, M. & Foucault, A.P. 2006. Purification of the Main Ginsenosides from a French Crop of *Panax Quinquefolium* L. *Journal of liquid chromatography* **18**(8), 1655–1662. doi: https://doi.org/10.1080/10826079508009302

Nekrošiene, R. 2009. Cultivation possibilities for Thyme, an important medicinal plant in Western Lithuania. *Agronomy Research*, **7**(I), 430–435.

Nian He, C., Wei Gao, W., Xue Yang, J., Bi, W., Song Zhang, X. & Jing Zhao, Y. 2008. Identification of autotoxic compounds from fibrous roots of *Panax quinquefolium* L. *Plant Soil* **318**, 63–72. doi: https://doi.org/10.1007/s11104-008-9817-8.

Oliver, A.L. 1998. Ginseng production guide for Commercial growers. Published by The Associated Ginseng Growers of British Columbia and Ministry of Agriculture, Fisheries and Food, 4.

Olson, H. 2014. *Swedish ginseng - possibilities and challenges*. Degree Project in Biology, Swedish Univerity of Agricultural Sciences, Uppsala, Sweden, 39 pp.

Qu, C., Bai, Y., Jin, X., Wang, Y., Zhang, K., You, J. & Zhang, H. 2009. Study on ginsenosides in different parts and ages of *Panax quinquefolius* L. *Food Chemistry* **115**(1), 340–346. doi: https://doi.org/10.1016/J.FOODCHEM.2008.11.079

Roy, R.C., Ball Coelho, B.R., Reeleder, R.D., Bruin, A.J., Grohs, R., White, P., Capell, B., Coelho, B., Reeleder, B.R., Grohs, A.J., White, R., Capell, P. & Ball-Coelho, B.R. 2011. Effect of planting bed shape, mulch and soil density on root yield and shape in North American ginseng (*Panax quinquefolius* L.). *Canadian Journal of Plant Science* **88**(5), 937–949. doi: https://doi.org/10.4141/CJPS07201

Schlag, E.M. & McIntosh, M.S. 2006. Ginsenoside content and variation among and within American ginseng (*Panax quinquefolius* L.) populations. *Phytochemistry* **67**(14), 1510–1519. doi: https://doi.org/10.1016/j.phytochem.2006.05.028

Schmidt, J.P., Cruse-Sanders, J., Chamberlain, J.L., Ferreira, S. & Young, J.A. 2019. Explaining harvests of wild - harvested herbaceous plants: American ginseng as a case study. *Biological Conservation* **231**, 139–149. doi: https://doi.org/10.1016/J.BIOCON.2019.01.006

Shan, S.M., Luo, J.G., Huang, F. & Kong, L.Y. 2014. Chemical characteristics combined with bioactivity for comprehensive evaluation of *Panax ginseng* C.A. Meyer in different ages and seasons based on HPLC - DAD and chemometric methods. *J. Pharm. Biomed. Anal.* **89**, 76–82. doi: https://doi.org/10.1016/j.jpba.2013.10.030

Turner, J.B. & McGraw, J.B. 2015. Can putative indicator species predict habitat quality for American ginseng? *Ecological Indicators* **57**, 110–117. https://doi.org/10.1016/J.ECOLIND.2015.04.010

Vinogradov, M., Rätsep, R. & Arus, L. 2020. Suitability of blue honeysuckle (*Lonicera caerulea* L.) cultivars of different origin for cultivation in the nordic - baltic climate. *Agronomy Research* **18** (Special Issue 4), 2785–2796. doi: https://doi.org/10.15159/AR.20.228

Zhang, Y.C., Li, G., Jiang, C., Yang, B., Yang, H.J., Xu, H.Y. & Huan, L.Q. 2014. Tissue - Specific Distribution of Ginsenosides in Different Aged Ginseng and Antioxidant Activity of Ginseng. Leaf. *Molecules* **19**, 17381–17399. doi: 10.3390/molecules191117381

Agronomy Research **20**(2), 284–288, 2022
https://doi.org/10.15159/AR.22.022

Amino acid content in rice and lentil meal for vegan and pescatarian diet

I. Lignicka*, A. Graci (Balgalve) and A.M. Zīdere - Laizāne

Felici LLC, Rigas gatve 8, LV-2164 Adazi, Adazu novads, Latvia
*Correspondence: ilva.lignicka@musli.lv

Received: December 2nd, 2021; Accepted: March 16th, 2022; Published: April 27th, 2022

Abstract. Combining different raw materials, it is possible to increase plant-based protein functionality. Traditionally lentils are combined with rice. As rice complements lentils in sulphur-containing amino acids this plant-based combination provides a complete profile of essential amino acids. The aim of this study was to compare amino acid content and scoring pattern in vegan and pescatarian quick preparation meals and analyse developed meal suitability for a vegan diet containing all needed amino acids. Results show that vegan and pescatarian quick preparation meals contain all essential amino acids at adequate amounts according to FAO`s recommendation, results showed no significant difference between samples ($p > 0.05$). These results show that combining rice and lentils it is possible to develop a meal suitable for a vegan diet that contains all needed amino acids.

Key words: essential amino acids, lentils, pescatarian, rice, vegan.

INTRODUCTION

Proteins play important role in human nutrition. Proteins are built from amino acids joined together by peptide bonds between the carboxyl and the amino group of the next amino acid. These polypeptide chains are folded into a three-dimensional structure to form protein. Dietary proteins are sources of nitrogen and essential amino acids for the body (EFSA, 2012). Proteins are made from 20 amino acids. Nine of them, histidine, threonine, valine, methionine, isoleucine, leucine, phenylalanine, lysine, and tryptophan are classified as essential for humans as they cannot be synthesized in the human body from naturally occurring precursors at a rate to meet the metabolic requirements. The remaining 11 amino acids can be made by the body from essential amino acids or glucose (EFSA, 2012; Yu & Fukagava, 2020). After food consumption, its proteins are hydrolyzed, following enzymatic digestion small peptides and amino acids are released and absorbed into the body. Amino acids have an important role in nutrition and whole-body homeostasis as they participate in many biochemical pathways for the growth, maintenance, and metabolic activity of cells and organs (Wu, 2010; Aristoy & Toldra, 2016; Yu & Fukagava, 2020). A high-quality protein provides an adequate quantity of essential amino acids that can be easily digested and utilized for protein synthesis. The amino acid profile is considered the most important among quality parameters (Kumar et al., 2021).

Low protein content and lack of essential amino acids limit plant-based protein functionality (Kumar et al., 2021). Combining different raw materials, it is possible to increase plant-based protein functionality. Traditionally lentils are combined with rice. As rice complements lentils in sulphur-containing amino acids this plant-based combination provides a complete profile of essential amino acids (Juliano, 2016). Amino acid content in rice and lentil are listed in Table 1. Since methionine can be converted to cysteine (Brosnan & Brosnan, 2006) and tyrosine can be formed by the hydroxylation of phenylalanine (Litwack, 2018), specific requirement for total methionine and cysteine and total phenylalanine and tyrosine content are also mentioned. It shows that lentils have lower methionine and cysteine (sulphur-containing amino acids) content and rice has lower lysine content than written in FAO (2013) recommendation. Data about amino acid content in lentils and rice support previously mentioned combining. Rice complements the lower amount of sulphur-containing amino acids in lentils. Lentils complement the lower lysine content in rice.

Table 1. Amino acid content in lentils and rice

Amino acid	Lentils, mg 100 g^{-1} protein[1]	Rice, mg g^{-1} protein[2]	Recommendation, mg g^{-1} protein (FAO, 2013)
Histidine	28	23	15
Isoleucine	43	42	30
Leucine	71	80	59
Lysine	69	*35*	45
Methionine + cysteine	21	43	22
Phenylalanine + tyrosine	75	85	38
Threonine	35	35	23
Tryptophan	9	11	6
Valine	49	59	39

[1] (NutrientOptimiser database, n.d.a); [2] (NutrientOptimiser database, n.d.b).

Vegans exclude many proteins rich foods and studies show that protein intake in vegan groups is lowest. Bakaloudi et al. (2021) in her study informed that total protein intake in vegan groups was the lowest compared to other diets. Tyrosine and other essential amino acids showed the lowest plasma concentrations in vegan diets compared to other diet types. It is necessary to meet daily amino acid requirements. There are not many studies on amino acid content in vegan and pescatarian meals. The aim of this study was to compare amino acid content and scoring pattern in vegan and pescatarian quick preparation meals and analyse developed meal suitability for a vegan diet containing all needed amino acids.

MATERIALS AND METHODS

For amino acid content analysis previously prepared pescatarian and vegan quick preparation meal samples were used. Two base ingredients were used - dried lentils (*Lens culinaris* L.) and rice (*Oryza sativa* L.). For vegan meal 64% of rice and 26% of green lentils were used. For pescatarian meal 69% of rice, 20% of red lentils and 2.5% freeze-dried salmon (*Salmo Salar* and *Oncorhynchus* spp) powder were used. The remaining quantity is additional ingredients such as dried vegetables and spices used to enrich the meal taste.

Amino acid content

To check amino acid content in prepared samples, one pescatarian and one vegan meal were tested. Amino acid content was determined at food quality testing laboratory. PB-136/HPLC ed. I of 06.02.2012. method for tryptophan and PB-53/HPLC ed. II of 30.12.2008. method for other proteinogenic amino acid analyses were used. Analyses were performed in triplicate.

Statistical analysis

Statistical analyses were performed with RStudio (RStudio PBA, USA). Results were evaluated using Wilcoxon signed-rank test for paired comparisons ($p = 0.05$) to determine the difference between amino acid content in vegan and pescatarian meal. Factors were defined as significant if p-value was below 0.05.

RESULTS AND DISCUSSION

Foods that are obtained from plants are usually low in one or more essential amino acids, so when consumed individually, they are considered incomplete proteins (Yu & Fukagava, 2020). The term complete protein refers to foods that contain all essential amino acids in the correct proportion to build protein in the body (Nehete et al., 2013). Lentil protein is a good source of essential amino acids leucine, lysine, threonine, and phenylalanine, but has lower content of sulphur-containing essential amino acids methionine and cysteine (Samaranayaka, 2017). Table 1 shows that rice has lower lysine content. Due to this reason during quick preparation meal development rice and lentils were used. Table 1 shows that, comparing to lentils, rice has two times higher sulphur-containing amino acid content and lentils have two times higher lysine content, showing that they are suitable for combination. Amino acid content in vegan and pescatarian quick preparation meals are listed in Table 2.

Table 2. Amino acid content in vegan and pescatarian quick preparation meals

Amino acid	Vegan meal, mg $100g^{-1}$	Pescatarian meal, mg $100g^{-1}$
Aspartic acid	1,140 ± 60	1,120 ± 60
Glutamic acid	2,120 ± 113	2,120 ± 113
Serine	580 ± 30	560 ± 30
Glycine	530 ± 26	520 ± 26
Histidine	280 ± 13	270 ± 13
Arginine	940 ± 50	900 ± 46
Threonine	430 ± 23	440 ± 23
Alanine	600 ± 33	600 ± 33
Proline	530 ± 26	510 ± 26
Tryosine	370 ± 20	360 ± 20
Valine	640 ± 33	620 ± 33
Methionine	210 ± 10	240 ± 13
Cysteine	71 ± 3	84 ± 4
Isoleucine	480 ± 26	470 ± 23
Leucine	930 ± 50	920 ± 50
Phenylalanine	610 ± 33	580 ± 30
Lysine	580 ± 30	590 ± 30
Tryptophan	100 ± 4	124 ± 5

Results show that vegan and pescatarian meals have similar amino acid content. As for essential amino acids, vegan quick preparation meal has higher histidine, valine, isoleucine, leucine, phenylalanine content, pescatarian quick preparation meal has higher methionine, lysine, and tryptophan content, however, results show no significant difference ($p > 0.05$). It could be affected by rice and lentil content, lentil type, and different additional ingredients used for taste enrichment. Freeze-dried salmon affect pescatarian quick preparation meal amino acid content. However, it has lesser importance for amino acid composition as its proteins are complete. Table 3 illustrates essential amino acid scoring pattern. Results were compared with FAO (2013) recommended amino acid scoring pattern for adults (> 18 years).

Table 3. Amino acid scoring pattern in vegan and pescatarian quick preparation meals

Amino acid	Vegan meal, mg g^{-1} protein	Pescatarian meal, mg g^{-1} protein	Recommendation, mg g^{-1} protein (FAO, 2013)
Histidine	22	21	15
Isoleucine	37	36	30
Leucine	72	71	59
Lysine	45	45	45
Methionine + cysteine	22	25	22
Phenylalanine + tyrosine	75	72	38
Threonine	33	34	23
Tryptophan	8	10	6
Valine	49	48	39

The data shows that all vegan and pescatarian quick preparation meal amino acid scoring patterns are equal or higher than recommended values. As FAO (2013) described, there may be specific cases in which it is desirable to increase the intake of specific amino acids. Supplementation of leucine, isoleucine, histidine, or threonine has been considered a good strategy to promote weight loss (Xiao & Guo, 2021). Gwin et al. (2020) data demonstrate that high compared to standard-essential amino acids ingestion enhances whole-body protein status during underfeeding, still, the effects of consuming high and standard essential amino acids on mixed muscle protein synthesis are the same during energy deficit.

CONCLUSIONS

Vegan and pescatarian quick preparation meals contain all essential amino acids at adequate amounts according to FAO`s recommendation. Results showed no significant difference between samples ($p > 0.05$). This shows that combining rice and lentils it is possible to develop a meal suitable for a vegan diet that contains all needed amino acids. It is possible to substitute lentils with other legumes such as peas and faba beans. These legumes in different varieties have similar amino acid content as lentils (Sterna et al., 2020). To consume all needed nutrients, vegans should follow protein intake and combine different raw materials to consume all essential amino acids in one meal. Protein quality is determined by comparing the relative composition of essential amino acids and their bioavailability (Siahbalaei et al., 2021). For further analysis vegan and pescatarian quick preparation meal protein and amino acid bioavailability tests should be performed. Even though the HPLC method does not consider bioavailability it can give a good indication of essential amino acid composition of a meal.

ACKNOWLEDGEMENTS. In accordance with contract No. 1.2.1.1/18/A/002 between 'Latvian Food Competence Centre' Ltd. And the Central Finance and Contracting Agency, the study is conducted by 'Felici' LLC. With support from the European Regional Development Fund (ERDF) within the framework of the project 'Latvian Food Industry Competence Centre'.

REFERENCES

Aristoy, M.C. & Toldra, F. 2016. Amino Acids: Determination. In Caballero, B., Finglas, P.M., Toldra, F. (eds) *Encyclopedia of Food and Health*. Academic Press. Cambridge. 141–148.

Bakaloudi, D.R., Halloran, A., Rippin, H.L., Oikonomidou, A.C., Dardavesis, T.I, Williams, J., Wickramasinghe, K., Breda, J. & Chourdakis, M. 2021. Intake and adequacy of the vegan diet. A sysdtematic review of the evidence. *Clinical nutrition* **40**(5), 3503–3521.

Brosnan, J.T. & Brosnan, M.E. 2006. The Sulfur-Containing Amino Acids: An Overview. *The Journal of Nutrition* **136**(6), 1636–1640.

European Food Safety Authority (EFSA). 2012. Scientific Opinion on Dietary Reference Values for protein. EFSA Panel on Dietetic Products, Nutrition and Allergies (NDA*). EFSA Journal* **10**(2), pp. 66.

FAO. 2013. Dietary protein quality evaluation in human nutrition. Report of an FAO expert consultation. FAO, Rome, pp. 66.

Gwin, J.A., Church, D.D., Hatch-McChesney, A., Howards, E.E., Carrigan, C.T., Murphy, N.E., Wilson, M.A., Margolis, L.M., Carbone, J.W., Wolfe, R.R., Ferrando, A.A. & Pasiakos, S.M. 2020. Effects og high versus standard essential amino acids intakes on whole-body protein turnover and mixed muscle protein synthesis during energy deficit: A randomized, crossover study. *Clinical Nutrition* **40**(3), 767–777.

Juliano, B.O. 2016. Rice: Role in Diet. In Caballero, B., Finglas, P.M., Toldra, F. (eds) *Encyclopedia of Food and Health*. Academic Press. Cambridge. 641–645.

Kumar, M., Tomar, M., Potkule, J., Reetu, Punia, S., Dhakane, J., Singh, S., Dhumal, S., Pradhan, P.C., 5 characterization of plant-based protein to determine its quality for food applications. *Food Hydrocolloids* **123**. 106986.

Litwack, G. 2018. Chapter 13 – Metabolism of Amino Acids. In Litwack, G. (eds) *Human Biochemistry*. Academic Press. Cambridge. 359–394.

Nehete, J.Y., Bhambar, R.S., Narkhede, M.R. & Gawali, S.R. 2013. Natural proteins: Sources, isolation, characterization, and applications. *Pharmacognosy Review* **7**(14), 107–116.

NutrientOptimiser database (n.d.a) Lentils Nutritional Value And Analysis. Retrieved from https://nutrientoptimiser.com/nutritional-value-lentils-raw

NutrientOptimiser database (n.d.b) White Rice Nutritional Value And Analysis. Retrieved from https://nutrientoptimiser.com/nutritional-value-rice-white-glutinous-unenriched-uncooked/

Samaranayaka, S. 2017. Chapter 11 – Lentil: Revival of Poor Man`s Meat. In S.R., Wanasundara, J.P.D., Scalin, L. (eds) *Sustainable Protein Sources*. Academic Press. Cambridge. 185–196.

Siahbalaei, R., Kavoosi, G. & Noroozi, M. 2021. Protein nutritional quality, amino acid profile, anti-amylase and anti-glucosidase properties of microalgae: Inhibition and mechanisms of action through *in vitro* and in silico studies. *LWT*. **150**, 112023.

Sterna, V., Zute, S., Jansone, I., Ence, E. & Strausa, E. 2020. Evaluation of various legume species and varieties grown in Latvia as raw material of plant-based protein products. *Agronomy Research* **18**(4), 2602–2612.

WHO/FAO/UNU (World Health Organization/Food and Agriculture Organization of the United Nations/United Nations University) (2007) Protein and amino acid requirements in human nutrition. Report of a joint WHO/FAO/UNU Expert Consultation. *WHO Technical Report Series*, No **935**, pp. 284.

Wu, G. 2010. Functional Amino Acids in Growth, reproduction, and Health. *Advances in Nutrition* **1**(1), 31–37.

Yu, Y.M. & Fukugawa, N.F. 2020. Chapter 2 - Protein and Amino acids. In Marriott, B.P., Birt, D.F., Stallings, V.A., Yates, V.A. (eds) *Present knowledge in nutrition. Volume 1: Basic nutrition and metabolism.* Academic Press. Cambridge. 15–35.

Xiao, F. & Guo, F. 2021. Impacts of essential amino acids on energy balance. *Molecular Metabolism*. In Press. 101393.

Agronomy Research **20**(2), 289–301, 2022
https://doi.org/10.15159/AR.22.029

Biogas production from the specialized dairy farming and porcine subsectors in Antioquia, Colombia: theoretical and technical-energy potential approach

M. Luna-del Risco[1,*], A. Jiménez Vásquez[1], J.S. Zea Fernández[1], E. Marín[1], C. Arrieta González[1], A. Cardona Vargas[2] and N.Y. Mejías Brizuela[3]

[1]Universidad de Medellin, Faculty of Engineering, Carrera 87 # 30 – 65, P.O. 050030, Medellín, Colombia
[2]Instituto Tecnológico Metropolitano de Medellín, Faculty of Engineering, Calle 73 No. 76A-354 vía el Volador, 050034, Medellín, Colombia
[3]Universidad Politécnica de Sinaloa, Energy Engineering Department, Carretera libre Mazatlán-Higuera Km 3 C.P. 82199, Sinaloa, México
[*]Correspondence: mluna@udemedellin.edu.co

Received: February 23rd, 2022; Accepted: May 1st, 2022; Published: May 11th, 2022

Abstract. In developing countries, residual biomass usage by means of anaerobic digestion offers several benefits and opportunities, such as a sustainable energy source, production of organic fertilizers and new agrobusiness models. In Latin America, Colombia is one of the most promising markets for the implementation of this technology in terms of availability of biomass and economic growth, as recently reported by local government organizations. In this paper, special attention is given to Antioquia, a department of Colombia with the largest farms of cattle and pigs, according to information reported in 2018 by the Ministry of Agriculture and Rural Development. It is estimated that manure from the porcine subsector in Antioquia has an approximate technical-energy potential of 1,896 TJ $year^{-1}$, varying from 1,611 to 2,186 TJ $year^{-1}$, corresponding to the 95% confidence interval. In the case of manure generated by the livestock subsector in Antioquia, it is estimated a theoretical energy potential of 8,566 TJ $year^{-1}$. However, traditional extensive production systems disseminate manure through the pastures turning centralization of the available residual biomass a difficult task and not senseful. Based on the local practices of the specialized dairy subsector, it is estimated that manure collected during the milking process could reached up to 25% of the total available. Biochemical conversion of this amount of biomass has an estimated technical-energy potential of 187 TJ $year^{-1}$, varying from 156 and 236 TJ $year^{-1}$, corresponding to the 95% confidence. The aim of this article is to estimate the technical-energy potential for the livestock and porcine subsectors in the Department of Antioquia, based on the available residual biomass according to local farming practices.

Key words: technical biogas potential, residual livestock biomass, porcine manure, residual biomass availability, energy matrix.

INTRODUCTION

Colombia's report presented during the United Nations Framework Convention on Climate Change (COP21), held in Paris in December 2015, makes the country responsible for 0.46% of global GHG emissions, according to data reported in 2010. Despite contributing a low percentage at a global scale compared to other countries, accumulated emissions between 1990 and 2012 place Colombia among the 40 countries with the greatest historical responsibility for generating GHG emissions. The Colombian subsectors with the highest contribution to GHG emissions are livestock, deforestation, transportation, energy generation, solid waste management, manufacturing, and construction industry, and other processes (Londoño Pineda et al., 2019; Wang et al., 2021).

Earlier studies on Residual Livestock Biomass (RLB) have been conducted and presented by the Atlas of the Energy Potential of Residual Biomass in Colombia. The study was conducted and published in 2010 by the Institute of Hydrology, Meteorology and Environmental Studies (IDEAM), the Mining and Energy Planning Unit (UPME) and the Industrial University of Santander (UIS). The report estimates that livestock activities in Colombia generates approximately 105,418.066 tons per year of manure in which the department (geographical region) of Antioquia has the largest contribution with 12,882,917 tons per year. This amount of manure represents an important environmental impact considering that animal manure produces biogas, which is considered a harmful greenhouse gas (GHG) when large amounts of it is ejected to the atmosphere without inactivation nor valorization (Marrugo et al., 2016; Pupo-Roncallo et al., 2019; Hollas et al., 2021).

Key factors such as increasing GHGs emissions due to inadequate management of RLB, the increasing trend of energy consumption during the past few years, and the possibility of decreasing dependence on fossil fuels as a pillar of the economy based on clean energy, have triggered efforts from governmental agencies, educational institutions, and public/private industries towards the use of renewable energy. Low-carbon technologies such as the bioconversion of biomass by anaerobic digestion means, are of great interest due to its low environmental impact and its positive social impact (Ramirez-Contreras & Faaij, 2018).

Energy recovery of RLB in the Department of Antioquia also contributes to the fulfillment of the Sustainable Development Goals (SDGs) approved in 2015 at the United Nations (UN) summit. This strategy aims at intensifying efforts to end poverty in all its forms, reduce inequality, and protect the environment (Kall et al., 2016; Ramirez-Contreras & Faaij, 2018; Sagastume Gutiérrez et al., 2020). For example, SDG 7 focuses on access to clean energy, in which producing biogas by means of anaerobic digestion of RLB can be an energy source for non-connected communities. It also promotes access to affordable renewable energy aiming at improving living conditions of communities in the Department of Antioquia. These renewable energy sources will provide an alternative fuel for cooking, heating, and lighting. It is estimated that the use of RLB produced by the porcine and specialized milk cattle sub-sectors through anaerobic digestion in the Department of Antioquia will help to reach the COP21 commitment established to reduce greenhouse gas emissions by 20% in relation to projected emissions by 2030 (Sagastume Gutiérrez et al., 2020).

Generally, in Colombia, not all the RLB can be collected, especially those related to cattle farming performed under traditional extensive production systems. Manure collection and centralization for energy generation are hard to achieve because farms are dispersed throughout the country.

This research focuses on the estimation of technical-energy potential by anaerobic digestion means of the Colombian livestock residual biomass. The following substrates were assessed: i) the productive system of specialized milk, which performs the temporary confinement of animals for two (2) times a day for milking. This practice facilitates the collection of 25% of the manure produced daily by the animals, and ii) biomass from the porcine sub-sector in Antioquia, in which the animals are handled in confinement.

METHODOLOGY

Main sources of information consulted for the estimation of Residual Livestock Biomass (RLB)

Different sources of information were consulted to estimate RLB, such as the census conducted by Colombian Institute of Agriculture (ICA) in 2018 for the porcine and livestock subsectors, reports form the Agricultural Assessments by Consensus, the Agricultural and Technical Assistance Municipal Units (UMATAS) and the Ministry of Agriculture (Ministerio de Agricultura, 2020).

The information reported by ICA clearly specifies the distribution of animals by age group for cattle and pigs, where the former is classified as cattle under one year old, cattle between 1 and 2 years old, cattle between 2 and 3 years old, and cattle over 3 years. In the case of the porcine subsector the classification is presented as piglets (1–60 days), weaners (61–120 days), growers (121–180 days), reproducers, females (120–240 days), breeding females (more than 240 days) and backyard pigs, which are those that remain in small-scale family farms.

In 2018, information provided by the Colombian Ministry of Agriculture specifies livestock activities in terms of milk production for each of the 125 municipalities of the Department, specifying the number of animals in traditional milking systems, dual-purpose dairies, and specialized dairies. In this study, it is considered Manure Production Rate (MPR) as an indicator of manure generated by species, according to the age of the animal and the type of activity for which it is raised (UPME, 2011). Both, the number of animals per age range and the MPR are inputs for the estimation of residual livestock biomass per species in each of Antioquia's 125 municipalities.

Estimation of RLB in the Department of Antioquia for the porcine and specialized dairy subsectors

Traditional extensive production systems in Colombia lead to the dissemination of manure through the pastures turning centralization of the available residual biomass a difficult task and not senseful. However, pasturing practices opens possibilities to produce animal products from residual sites, in which grazing enables fresh uptake of grass and herbs without energy losses and with selection of best nutrient content by the animal. Considering that grazing is an important source for feces-based nutrient networks, pathogenic risks need to be under consideration to avoid cross pollution.

Estimation of RLB in the Department of Antioquia is calculated by means of a mathematical model based on the number of animals per subsector and the Manure Production Rate (kg animal^{-1} day), which is an indicator of manure generated by species, depending on the age of the animal and the type of activity for which it is raised.

Since the porcine sub-sector establishes practices such as animal confinement and intensive production systems, it is estimated that the technical-energy potential from manure for this sub-sector only depends on the capacity of the bioconversion technology to process the available residual biomass, but it is not limited to the accessibility of it. On the other hand, since extensive production systems predominate in the livestock sector, only manure generated by the sub-sector of specialized dairies during milking, could be defined as technically usable manure. This is equivalent to 25% of the manure generated by this sub-sector.

Equation 1 presents the model used for the estimation of the residual biomass produced by the porcine and cattle sectors in the Department of Antioquia.

$$RLB = nA \times MPR \tag{1}$$

where RLB – Residual livestock biomass; nA – number of animals; MPR – manure production rate.

Theoretical estimation of the technical-energy usable potential for the porcine and specialized dairy subsectors in the Department of Antioquia

To calculate the technical-energy potential of manure generated by the porcine and dairy subsectors in the Department of Antioquia, a mathematical model was implemented based on the following variables: Residual Livestock Biomass - RLB (kg of fresh manure), Dry Matter - DM (kg DM kg^{-1} manure), Volatile Solids (kg VS kg^{-1} DM), Biochemical Methane Potential - BMP (Nm^3 CH_4 kg VS^{-1}) and Lower Calorific Value of methane, which corresponds to 35.8 MJ Nm^{-3}.

Table 1 presents bibliographic information on the characterization of cattle and pig manure for parameters such as dry matter - DM (kg DM kg DM^{-1}), volatile solids (kg VS kg DM^{-1}) and methane biochemical potential (Nm^3 CH_4 kg VS^{-1}). These values correspond to the characterization of manure produced in various countries with different climatic conditions and implementation of different conditions of animal management, including variations in the type of feed supplied.

The Center for Environmental Studies and Research - CEIAM of the Industrial University of Santander (UIS) characterized pig manure from two departments in Colombia: Antioquia (a farm located in Santa Rosa de Osos) and Valle del Cauca. Data from the characterization is presented in Table 2.

The variation in the results of the physicochemical characterization between these two samples corresponds to various factors such as, condition at the time of collection, the climate of the geographical site, quality of the food provided to animals, transport needs, herd size, manure recover facilities, among others (Jiménez Vásquez, 2021).

Table 1. Characteristics of cattle manure and pig manure

No.	Dry Matter DM kg DM kg manure^{-1}	Volatile solids kg VS kg DM^{-1}	Biochemical methane potential Nm^3 CH_4 kg VS^{-1}	Reference
	Characteristics of cattle manure			
1	0.27	0.81	0.32	(Arango Osorio et al., 2019)
2	0.17–0.26	0.71–0.87	0.17	(Pham et al., 2017)
3	0.16–0.22	0.88	0.19–0.22	(André et al., 2019)
4	0.18	0.80	0.21	(Ramírez Balaguera & Barrera Ojeda, 2017)
5	0.17	0.55	0.13	(Zhao et al., 2018)
6	0.17	0.77	0.27	(Martí Herrero, 2008)
7	0.17	0.61	0.20	(Krishna Kafle & Chen, 2016)
8	0.16	0.87	0.11	(Herrero Garcia et al., 2019)
9	0.15–0.16	0.85	0.32	(McVoitte & Clark, 2019)
10	0.16	0.84	0.33	(Li et al., 2014)
11	0.12	0.85	0.243	(Luna-Derisco et al., 2011)
	Characteristics of pig manure			
11	0.36	0.99	0.15	(Herrero Garcia et al., 2019)
12	0.28–0.33	0.71–0.76	0.32	(Galvis Pinzón & Acevedo León, 2008)
13	0.32	0.78	0.15	(Liang et al., 2020)
14	0.31	0.77	0.13	(Cabeza et al., 2016)
15	0.31	0.73	0.32	(Ramírez Balaguera & Barrera Ojeda, 2017)
16	0.31	0.87	0.32	(Krishna Kafle & Chen, 2016)
17	0.30	0.89	0.25	(Liang et al., 2017)
18	0.28	0.78	0.26	(Yang et al., 2019)
19	0.28	0.80	0.29	(J. Zhang et al., 2019)
20	0.28	0.78	0.31	(Xiao et al., 2019)
21	0.23	0.73	0.16	(Wang et al., 2018)
22	0.24–0.29	0.75–0.77	0.26–0.35	(W. Zhang et al., 2014)
23	0.3-0.8	0.7–0.8	0.175–0.35	(Luna-DelRisco et al., 2011)
24	0.19	0.77	0.35	(Li et al., 2014)

Table 2. Characterization of the residual biomass of the porcine sub-sector

Department	% Moisture	% DM	DM kg DM kg manure^{-1}	% VS	VS kg VS kg DM^{-1}
Antioquia	67.18	32.83	0.33	24.98	0.76
Valle	71.9	28.11	0.28	19.87	0.71
Average	69.54	30.47	0.31	22.42	0.73

Source: Centre for Environmental Studies and Research – CEIAM.

In Eq. 2, the mathematical model for the estimation of the technical-energy potential from RLB for the porcine and specialized milk cattle subsectors is presented.

$$EP_{RLB} = \sum_{i=1}^{n} \cdot RLBPi \cdot \%DM.VS \cdot Bo_i \cdot LCV_{CH4} \quad (2)$$

where EP_{RLB} – Technical-energy potential of residual livestock biomass (TJ year^{-1}); *RLB* – kg manure year^{-1}; *%DM* – % Dry Matter (kg DM kg manure^{-1}); *VS* – Volatile solids (kg VS kg DM^{-1}); *Bo* – Biochemical methane potential (Nm^3 Biogas kg VS^{-1}); LCV_{CH4} – Methane Lower Calorific Value (TJ Nm^{3-1}).

RESULTS AND DISCUSSION

Estimation of exploitable residual livestock biomass in the Department of Antioquia for the porcine and specialized dairy subsectors

It is estimated that manure production by the porcine sub-sector in the Department of Antioquia is approximately 1,223.056 tons per year (Table 3). From this amount, 72.13% is generated in large scale and technified systems that warranties animal confinement by physiological state and age. The remaining 27.87% is produced by backyard pigs, which are in family farms and small-scale production systems (UPME, 2011).

Table 3. Estimation of Residual Livestock Biomass (RLB) of the porcine sub-sector in the Department of Antioquia

Physiological Status	Age (days)	Number of Animals	Manure Production Rate (MPR) (kg animal $year^{-1}$)	RLB[1] (ton manure $year^{-1}$)
Piglets	1–60	583,145	102.2	59,597,419
Weaners	61–120	488,909	445.3	217,711,178
Growers	121–180	423,867	799.35	338,818,086
Reproducers	-	5,704	2,051.3	11,700,615
Females	120–240	21,187	1,971	41,759,577
Breeding females	> 240	78,916	2,693.70	212,576,029
Backyard pigs	-	253,677	1,343.81	340,893,267
Total		1,855,405	-	1,223,056,171

Source: Adapted from (UPME, 2011); [1]Technically available biomass from pigs.

According to Table 4, livestock farming operations in the Department of Antioquia, including beef cattle, specialized dairy, and dual-purpose cattle, produces a total of 13,683,706.920 tons of manure per year.

Table 4. Estimation of Residual Livestock Biomass (including beef cattle, specialized dairy and dual-purpose cattle) of the livestock farming operations in the Department of Antioquia

Livestock age (months)	Number of Animals	Manure Production Rate (MPR) (kg animal $year^{-1}$)	RLB[1] (ton manure $year^{-1}$)
< 12 months old	536,460	1,460	783,231
12–24 months old	756,146	3,285	2,483,939,610
24–36 months old	723,165	5,110	3,695,373,150
> 36 months old	1,023.008	6,570	6,721,162,560
Total	3,038.779	-	13,683,706,920

Source: Adapted from (UPME, 2011).

According to data reported in 2018 by the Agricultural Assessments by Consensus, the Municipal Agricultural Technical Assistance Units (UMATAS) and the Ministry of Agriculture, in the Department of Antioquia (MinAgricultura, 2018), there are approximately 182,166 cows destined to specialized systems of milk production with a manure production rate of 6,570 kg animal^{-1} year for a total of 1,196,830 tons of manure per year. Table 5 presents data related to manure production by the specialized dairy subsector in the Department of Antioquia.

Table 5. Municipalities with the highest manure production by the specialized dairy subsector

Municipality	Manure production (ton year^{-1})	RLB specialized dairy subsector[1] (ton manure year^{-1})
Santa Rosa de Osos	515,554	128,889
Entrerrios	166,208	41,552
Don Matías	98,550	24,638
Yarumal	90,975	22,744
Belmira	84,024	21,006
Sonsón	29,802	7,450
Medellín	24,894	6,223
Abejorral	19,881	4,970
El Carmen de Viboral	19,382	4,845
Frontino	19,283	4,821

Source: Adapted from (UPME, 2011); [1]Technically available.

Data shows that Santa Rosa de Osos and Entrerríos are the municipalities with the highest production of manure from the specialized dairy subsector with 515,554 tons and 166,208 tons per year respectively. The municipalities of Santa Rosa de Osos, Entrerrios, Don Matías, Yarumal and Belmira located in the northern sub-region of the Department of Antioquia contribute to the 79.82% of the total manure generated in the Department of Antioquia. The historical main activity of these municipalities is milk related products (Rios & Botero, 2020).

Although the specialized dairy subsector generates 1,196,830 tons of manure per year, only 25% of the manure generated in the dairies during milking can be recovered, which is approximately 299,208 tons per year of technically available manure (Ministerio de Agricultura, 2020; UPME, 2011). On the other hand, the porcine subsector in the Department of Antioquia reported a total production of 1,223,056 tons of manure per year. The available amount of this substrate has a higher technical potential than livestock manure because its productive system usually uses the confinement of the animals (Londoño et al., 2017).

The approximate sum of manure produced by the porcine sub-sector (1,223,056 tons per year) and the technically usable manure produced by the specialized dairy sub-sector (299,208 tons per year), represents a residual biomass of 1,522,264 tons per year of technically usable manure due to its collection possibilities.

Technical-energy potential of manure generated by the porcine and specialized dairy subsectors in the Department of Antioquia

Manure produced by the porcine subsector in the Department of Antioquia has a technical-energy potential of 1,896 TJ year^{-1} with a statistical variation from 1,611 to 2,186 TJ year^{-1}, corresponding to a 95% confidence interval. Backyard pigs accounts for the 27.9% of the total energy potential while the technified porcine systems represent the 72.1% (Londoño et al., 2017).

Municipalities with the highest technical-energy potential from pig manure are Don Matías (166.67 TJ year^{-1}), Medellín (144.73 TJ year^{-1}), Ebejico (129 TJ year^{-1}), Santa Rosa de Osos (121.26 TJ year^{-1}), Santo Domingo (72.13 TJ year^{-1}), San Pedro de los Milagros (68.21 TJ year^{-1}), Barbosa (64.78 TJ year^{-1}), Concordia (53.04 TJ year^{-1}), Entrerrios (49.60 TJ year^{-1}) and Angelopolis (45.08 TJ year^{-1}) (UPME, 2011).

In the Department of Antioquia, there are 182,166 cows destined for specialized milk production systems with a production of 1,196,830 tons of manure per year and an energy potential of 749 TJ year^{-1} by means of anaerobic digestion. However, since the specialized dairy farming subsector gathers milking cattle twice a day, only 25% of the total manure produced can be collected. This amount has a technical-energetic potential (anaerobic digestion) of available manure of 187 TJ year^{-1} with a variation from 156 to 236 TJ year^{-1}, corresponding to a 95% confidence interval.

For the specialized dairy subsector, the highest technical-energetic potential by means of anaerobic digestion was identified in the municipalities of Santa Rosa de Osos (80.68 TJ year^{-1}), Entrerrios (26.01 TJ year^{-1}), Don Matias (15.42 TJ year^{-1}), Yarumal (14.24 TJ year^{-1}) and Belmira (13.15 TJ year^{-1}), all located in the northern sub-region of the Department of Antioquia. The technical-energetic potential of manure produced in these municipalities is estimated at approximately 149 TJ year^{-1}, corresponding to 79.82% of the potential of the Department. The sum of the other municipalities represents less than 5 TJ year^{-1} each, where Sonson and Medellin present a potential of 4.66 TJ year^{-1} and 3.90 TJ year^{-1} respectively (Rios & Botero, 2020).

Considering data from the porcine and specialized dairy subsectors, the total exploitable technical-energetic potential is approximately 2,084 TJ year^{-1} with a statistical variation from 1,767 and 2,422 TJ year^{-1}, corresponding to a 95% confidence interval. From the estimated total technical-energetic potential, the porcine subsector represents 91.01% of the total while the specialized dairy sub-sector only presents the 8.99%. From the municipalities analyzed in this study, Santa Rosa de Osos showed the highest technical-energy potential with 201.94 TJ year^{-1}, where 60.05% is contributed by the porcine sub-sector and 39.95% of the potential by the specialized dairy sub-sector.

Don Matias, Medellin, Ebejico and Santo Domingo presented an exploitable technical-energy potential from 73 TJ year^{-1} to 182.10 TJ year^{-1}. Energy potential is primarily attributed to the porcine sector of around 91% of the total, whereas only 9% is from the specialized dairy sub-sector. Entrerríos has a total technical-energy potential of 75.61 TJ year^{-1}, where the porcine sub-sector contributes with 65.6% of the total. In the case of the municipality of Yarumal, the porcine sub-sector contributes to the 74.15% and the specialized milk sub-sector contributes 25.85% of the total exploitable technical-energy potential, corresponding to 55.08 TJ year^{-1}. San Pedro, Barbosa, Concordia, Angelopolis, Caldas, Jerico, Tamesis, Angostura, Fredonia and Guarne have a total exploitable technical-energy potential from 40.24 TJ year^{-1} to 68.21 TJ year^{-1}, with a predominant contribution from the pig sub-sector, with percentages above 97% with a very low contribution from the specialized dairy sub-sector. Belmira has a total exploitable technical-energy potential of 21.25 TJ year^{-1} with a 38.13% contribution from the porcine subsector. Marinilla, Santa Bárbara, Rionegro, Envigado, Girardota, Bello, Gomez Plata, Amaga, La Ceja, Urrao, Yolombo, El Retiro, Turbo and Arboletes, have a total exploitable technical-energy potential from 15.99 TJ year^{-1} to 36 TJ year^{-1} with a high contribution from the porcine subsector with percentages above 92%.

In the other hand, municipalities such as Carolina del Príncipe, El Carmen de Viboral, Frontino, Sonson, La Union and Abejorral are highly influenced by the contribution of the specialized dairy subsector in percentages ranging from 16.66% to 63.98% (UPME, 2011).

In a study conducted by Contreras et al., 2020, there are 5 types of biomasses prioritized for biogas production in Colombia based on technical, environmental, and socioeconomic criteria (Table 6). Although, these biomasses do not represent a large energy source to fulfill the energy demand compared with other renewable energy sources (i.e., hydropower, fossil fuels), energy generation from them have great potential of development and integration on the national grid, specifically to support energy demands in rural areas nearby, as an energy source for cooking, heating, or local electricity generation at small scale.

Table 6. Biogas energy potential from different biomasses in Colombia

Biomass type	Energy potential (biogas) share (%)
Vinasse from sugar cane	22
Organic Urban Solid Waste (OUSW)	18
Palm oil	21
Pig manure	14
Poultry manure	25
Total biogas energy available	14,670 TJ year^{-1}

Source: Adapted from (Contreras et al., 2020).

As presented in Table 6, utilization of pig manure is an interesting residual biomass option for biogas production. In addition, Contreras et al., 2020 showed that Santander, Antioquia, Valle del Cauca, and Meta are the Departments with the greatest diversity of these biomasses. These results are in accordance with our findings. Pig manure availability in the Department of Antioquia and its bioconversion into biogas showed a great opportunity for energy diversification in rural areas.

Impact of residual biomass on the Colombian energy matrix

Biomethane stands as an important renewable energy for Non-interconnected Electrical Areas (NEA) which impacts 66% of the Colombian territory and 601,486 inhabitants mostly located in areas typically affected by the social conflict and infrastructure restrictions. In that matter, biogas as a non-conventional renewable energy source can offer energy solutions such as fuel gas and/or electricity, allowing the development of more efficient projects with social benefits (CREG, 2016).

Manure produced by the livestock industry (meat, double purpose, and specialized dairy) has a theorical energy potential of 8,566 TJ year^{-1} by anaerobic digestion means. Most of this energy potential depends on the possibility of collection and centralization. In Antioquia, productive systems are based on extensive cattle raising in which dissemination of residual biomass in the pastures of the cattle farms makes it difficult to collect. On the other hand, the specialized dairy subsector has a theoretical energetic potential of 749 TJ year^{-1}. For this farming practice, approximately 25% of the available is collected with an estimated technical-energetic potential of 187 TJ year^{-1}.

There is a technical-energetic potential of 2,084 TJ year^{-1} in Antioquia from the manure produced by the livestock (i.e., specialized dairy) and the porcine subsectors, in which more than 90% of the potential corresponds to the porcine industry.

Strategies such the one presented by Komasilovs et al., 2021 are crucial to enable national and international cooperation between the private sector and public sector with the participation of academic researchers. This will promote the proposal of residual biomass projects based on the technical-energy potential of specialized dairy systems and technified porcine farming.

Reported data on the primary energy supply share in Colombia consists of approximately 75% from non-renewable sources such as oil (39%), gas (27%) and coal (9%). The other 25% stands for hydropower (49%) and bioenergy (51%). By 2020, reported data from the total energy supply reached 1,610,929 TJ, from which 404,426 TJ are generated from renewable sources (International Renewable Energy Agency, 2020). In this research study, it was found an estimated technical-energetic potential from the specialized dairy and porcine subsectors of approximately 2,084 TJ $year^{-1}$ for the department of Antioquia, in which the total primary energy demand was found at approximately 35,298 TJ $year^{-1}$ (UPME, 2021). Technical energetic potential from studied residual biomass represents almost 6% of total energy demand for the department. In addition, it is estimated that there are almost 6,000 rural household without energy coverage in Antioquia, for which the results in this study could represent a sustainable source of energy (Departamento Administrativo de Planeación, 2016).

CONCLUSIONS

Residual biomass available in the Department of Antioquia from the pig and specialized dairy cattle subsectors provides a sustainable energy source that impacts on the economic, social, and environmental dimensions. For the bioconversion of this type of biomass residues, availability, conditioning, collection with efficient transportation mechanisms and centralization is highly recommended to maintain the supply chain for its bioconversion into biofuels.

This research validated the importance of porcine and livestock manure centralization and bioconversion into biogas for energy generation in the Department of Antioquia. Specialized dairy manure and porcine manure contributes with approximately 299,208 tons and 1,223,056 tons per year of technically usable manure respectively.

For the specialized dairy farming industry manure collection is more accessible than for the traditional extensive livestock production practices because livestock is commonly gathered twice a day in cattle housing for milking, where manure can be collected and stored for further treatment. Technified porcine farms based on pig confinement and intensive production systems is the most implemented farming practice in the Department of Antioquia. This practice that allows manure centralization could lead the government, the private sector, and entrepreneurs to invests on renewable projects at medium and large scale. This study approaches data from a technical availability point of view and not from a theoretical perspective and proposes the need to update the current studies available to improve the quality of data.

Although the technical energetic potential from residual biomass in this study represents only 6% of total energy demand for the department of Antioquia, there is an opportunity to provide a sustainable energy solution for approximately 6,000 rural household without energy coverage in Antioquia.

REFERENCES

André, L., Zdanevitch, I., Pineau, C., Lencauchez, J., Damiano, A., Pauss, A. & Ribeiro, T. 2019. Dry anaerobic co-digestion of roadside grass and cattle manure at a 60 L batch pilot scale. *Bioresource Technology* **289**(July), 121737. https://doi.org/10.1016/j.biortech.2019.121737

Arango Osorio, S., Vasco Echeverri, O., López Jiménez, G., González Sanchez, J. & Millán, I.I. 2019. Methodology for the design and economic assessment of anaerobic digestion plants to produce energy and biofertilizer from livestock waste. *Science of the Total Environment* **685**, 1169–1180.

Contreras, M.D., Sequeda Barros, R., Zapata, J., Vanegas Chamorro, M. & Albis Arrieta, A. 2020. A Look to the Biogas Generation from Organic Wastes in Colombia. *International Journal of Energy Economics and Policy* **10**(5), 2146–4553.

CREG. 2016, December 6. *Resolución 240 - Normas aplicables al servicio público domiciliario de gas combustible con biogás y biometano*. 2016. http://apolo.creg.gov.co/Publicac.nsf/1c09d18d2d5ffb5b05256eee00709c02/dafe4d4fc83940e2052580bf005b67d0/$FILE/Creg240-2016.pdf

Departamento Administrativo de Planeación. 2016. *Anuario Estadístico de Antioquia*. Reporte. https://www.antioquiadatos.gov.co/index.php/13-10-4-cobertura-de-energia-en-los-municipios-de-antioquia-ano-2016

Galvis Pinzón, D.P. & Acevedo León, M.L. 2008. *Evaluation of the energy potential of residual biomass from the porcine sector in Colombia*. Universidad Industrial de Santander, 83 pp. (in Spanish).

Herrero Garcia, N., Mattioli, A., Gil, A., Frison, N., Battista, F. & Bolzonella, D. 2019. Evaluation of the methane potential of different agricultural and food processing substrates for improved biogas production in rural areas. *Renewable and Sustainable Energy Reviews* **112**, 1–10.

Hollas, C.E., Bolsan, A.C., Chini, A., Venturin, B., Bonassa, G., Cândido, D., Antes, F.G., Steinmetz, R.L.R., Prado, N.V. & Kunz, A. 2021. Effects of swine manure storage time on solid-liquid separation and biogas production: A life-cycle assessment approach. *Renewable and Sustainable Energy Reviews* **150**, 111472. https://doi.org/10.1016/J.RSER.2021.111472

International Renewable Energy Agency. 2020. Renewable Energy Statistics: Colombian Energy Profile. In *Report*.

Cabeza, I., Thomas, M.T., Vásquez, A.V., Acevedo, P. & Hernández, M., 2016. Anaerobic co-digestion of organic residues from different productive sectors in Colombia: Biomethanation potential assessment. *Chemical Engineering Transactions* **49**, 385–390.

Jiménez Vásquez, A. F. 2021. *Atlas del potencial técnico-energético aprovechable por digestión anaerobia de la biomasa residual pecuaria para los subsectores porcícola y ganadería de leche especializada en el Departamento de Antioquia*. https://repository.udem.edu.co/handle/11407/6604

Kall, K., Roosmaa, Ü. & Viiralt, R. 2016. Assessment of the economic value of cattle slurry and biogas digestate used on grassland | Request PDF. *Agronomy Research* **14**, 54–66. https://www.researchgate.net/publication/303787394_Assessment_of_the_economic_value_of_cattle_slurry_and_biogas_digestate_used_on_grassland

Komasilovs, V., Bumanis, N., Kviesis, A., Anhorn, J. & Zacepins, A. 2021. Development of the digital matchmaking platform for international cooperation in the biogas sector. *Agronomy Research* **19**(Special Issue 1), 809–818. https://doi.org/10.15159/AR.21.018

Krishna Kafle, G. & Chen, L. 2016. Comparison on batch anaerobic digestion of five different livestock manures and prediction of biochemical methane potential (BMP) using different statistical models. *Waste Management* **48**, 492–502. https://doi.org/https://doi.org/10.1016/j.wasman.2015.10.021

Li, J., Jha, A.K. & Bajracharya, T.R. 2014. Dry anaerobic co-digestion of cow dung with pig manure for methane production. *Applied Biochemistry and Biotechnology* **173**(6), 1537–1552. https://doi.org/10.1007/s12010-014-0941-z

Liang, Y. gan, Li, X. juan, Zhang, J., Zhang, L. gan, & Cheng, B. 2017. Effect of microscale ZVI/magnetite on methane production and bioavailability of heavy metals during anaerobic digestion of diluted pig manure. *Environmental Science and Pollution Research* **24**(13), 12328–12337. https://doi.org/10.1007/s11356-017-8832-9

Liang, Y. gan, Xu, L., Bao, J., Firmin, K.A. & Zong, W. 2020. Attapulgite enhances methane production from anaerobic digestion of pig slurry by changing enzyme activities and microbial community. *Renewable Energy* **145**, 222–232. https://doi.org/10.1016/j.renene.2019.06.037

Londoño, A.T., Jaramillo, C.A.P. & Hernández, R.Z. 2017. Evaluation of the methanogenic biochemical potential of the pork porcine precursor in the North of Antioquia. *Journal of Engineering and Technology* **6**(1), 44–54.

Londoño Pineda, A.A., Vélez Rojas (Oscar), O.A., Jonathan, M.P. & Sujitha, S.B. 2019. Evaluation of climate change adaptation in the energy generation sector in Colombia via a composite index – A monitoring tool for government policies and actions. *Journal of Environmental Management*, **250**, 109453. https://doi.org/10.1016/J.JENVMAN.2019.109453

Luna-DelRisco, M., Normak, A. & Orupõld, K. 2011. Biochemical methane potential of different organic wastes and Biochemical methane potential of different organic wastes and energy crops from Estonia energy crops from Estonia. *Agronomy Research* **9**, 331–342.

Marrugo, G., Valdés, C.F. & Chejne, F. 2016. Characterization of Colombian Agroindustrial Biomass Residues as Energy Resources. *Energy and Fuels* **30**(10), 8386–8398. https://doi.org/10.1021/ACS.ENERGYFUELS.6B01596

Martí Herrero, J. 2008. *Design guide and installation manual for family biodigesters.* Publisher: GIZ. https://doi.org/10.13140/RG.2.1.1048.6242 (in Spanish).

McVoitte, W.P.A. & Clark, O.G. 2019. The effects of temperature and duration of thermal pretreatment on the solid-state anaerobic digestion of dairy cow manure. *Heliyon* **5**(7), e02140. https://doi.org/10.1016/j.heliyon.2019.e02140

MinAgricultura. 2018. *Management Report 2018*. Report, 1–171. (in Spanish). In: https://www.minagricultura.gov.co/planeacion-control-gestion/Gestin/PLANEACION/Informe_de_Gesti%C3%B3n_(Metas_Objetivos_Indicadores_Gestion)/INFORME%20DE%20%20GESTION%202018.pdf

Ministerio de Agricultura. 2020. *Agricultural Evaluations - Municipal Agricultural Evaluations and Statistical Yearbook of the Agricultural Sector*. Report, (in Spanish). In: https://www.agronet.gov.co/estadistica/paginas/home.aspx?cod=59

Pham, C.H., Saggar, S., Vu, C.C., Tate, K.R., Tran, T.T.T., Luu, T.T., Ha, H.T., Nguyen, H.L. T. & Sommer, S. G. 2017. Biogas production from steer manures in Vietnam: Effects of feed supplements and tannin contents. *Waste Management* **69**, 492–497. https://doi.org/10.1016/j.wasman.2017.08.002

Pupo-Roncallo, O., Campillo, J., Ingham, D., Hughes, K. & Pourkashanian, M. 2019. Large scale integration of renewable energy sources (RES) in the future Colombian energy system. *Energy* **186**, 115805. https://doi.org/10.1016/j.energy.2019.07.135

Ramirez-Contreras, N.E. & Faaij, A.P.C. 2018. A review of key international biomass and bioenergy sustainability frameworks and certification systems and their application and implications in Colombia. *Renewable and Sustainable Energy Reviews* **96**, 460–478. https://doi.org/10.1016/J.RSER.2018.08.001

Ramírez Balaguera, L.F. & Barrera Ojeda, D.F. 2017. *Potencial energético de la biomasa residual pecuaria del departamento de Cundinamarca – Colombia*. Universidad Distrital Francisco José de Caldas. PhD Thesis. In: https://repository.udistrital.edu.co/handle/11349/5178

Rios, G.P. & Botero, S. 2020. An Integrated Indicator to Analyze Sustainability in Specialized Dairy Farms in Antioquia–Colombia. *Sustainability 2020,* **12**(22), 9595. https://doi.org/10.3390/SU12229595

Sagastume Gutiérrez, A., Cabello Eras, J.J., Hens, L. & Vandecasteele, C. 2020. The energy potential of agriculture, agroindustrial, livestock, and slaughterhouse biomass wastes through direct combustion and anaerobic digestion. The case of Colombia. *Journal of Cleaner Production* **269**, 122317. https://doi.org/10.1016/J.JCLEPRO.2020.122317

UPME, I. 2011. *Atlas del potencial energético de la biomasa residual en Colombia*.

UPME. 2021. June 6. *Proyección Demanda Energía Eléctrica y Gas Natural 2021-2035*. Reporte. https://www1.upme.gov.co/DemandayEficiencia/Documents/UPME_Proyeccion_Demanda_Energia_Junio_2021.pdf

Wang, Y., Li, G., Chi, M., Sun, Y., Zhang, J., Jiang, S. & Cui, Z. 2018. Effects of co-digestion of cucumber residues to corn stover and pig manure ratio on methane production in solid state anaerobic digestion. *Bioresource Technology* **250**(September 2017), 328–336. https://doi.org/10.1016/j.biortech.2017.11.055

Wang, X., Li, Z., Cheng, S., Ji, H., Shi, J. & Yang, H. 2021. Multiple Substrates Anaerobic Co-Digestion: A Farm-Scale Biogas Project and the GHG Emission Reduction Assessment. *Waste and Biomass Valorization* **12**(4), 2049–2057. https://doi.org/10.1007/S12649-020-01166-3/FIGURES/4

Xiao, Y., Yang, H., Yang, H., Wang, H., Zheng, D., Liu, Y., Pu, X. & Deng, L. 2019. Improved biogas production of dry anaerobic digestion of swine manure. *Bioresource Technology* **294**(August), 122188. https://doi.org/10.1016/j.biortech.2019.122188

Yang, J., Wang, D., Luo, Z. & Zeng, W. 2019. Influence of reflux ratio on the anaerobic digestion of pig manure in leach beds coupled with continuous stirred tank reactors. *Waste Management* **97**, 115–122. https://doi.org/10.1016/j.wasman.2019.08.005

Zhang, J., Lu, T., Wang, Z., Wang, Y., Zhong, H., Shen, P. & Wei, Y. 2019. Effects of magnetite on anaerobic digestion of swine manure: Attention to methane production and fate of antibiotic resistance genes. *Bioresource Technology* **291**(121847).

Zhang, W., Lang, Q., Wu, S., Li, W., Bah, H. & Dong, R. 2014. Anaerobic digestion characteristics of pig manures depending on various growth stages and initial substrate concentrations in a scaled pig farm in Southern China. *Bioresource Technology* **156**, 63–69. https://doi.org/10.1016/j.biortech.2014.01.013

Zhao, Y., Sun, F., Yu, J., Cai, Y., Luo, X., Cui, Z., Hu, Y. & Wang, X. 2018. Co-digestion of oat straw and cow manure during anaerobic digestion: Stimulative and inhibitory effects on fermentation. *Bioresource Technology* **269**(July), 143–152. https://doi.org/10.1016/j.biortech.2018.08.040

Agronomy Research **20**(2), 302–309, 2022
https://doi.org/10.15159/AR.22.004

False flax (*Camelina sativa* L.) and oil flax (*Linum usitatissimum* L.) – an important source of deficient omega-3 fatty acids

V. Lykhochvor[1,*], Y. Olifir[2], R. Panasiuk[1] and M. Tyrus[1]

[1]Lviv National Agrarian University, 1 Volodymyra Velykoho Str., UA80381 Dubliany, Lviv region, Ukraine
[2]Institute of Agriculture of the Carpathian region NAAS, 5 Hrushevskoho Str., UA81115 Obroshyne, Pustomyty district, Lviv region, Ukraine
[*]Correspondence: lykhochvor@ukr.net

Received: November 28th, 2021; Accepted: January 30th, 2022; Published: February 2nd, 2022

Abstract. Spring false flax (*Camelina sativa* L.), oil flax *(Linum usitatissimum* L.*)*, spring rape *(Brassica napus oleifera annua Metzd.*), white mustard *(Sinapis alba* L.), and blue mustard *(Brassica juncea Czern*) were studied in order to establish their yield, oil content and quality. It was found that the highest seed yield (2.82 t ha^{-1}) was formed by spring rape. Yields were also high in spring false flax (2.68 t ha^{-1}) and oil flax (2.34 t ha^{-1}). It was found that the highest oil content was in oil flax (52.2%), blue mustard (45.8%) and false flax (45.0%). The highest oil yields were provided by spring rape, false flax and oil flax - 1.21–1.25 t ha^{-1}. It was found that the most physiologically valuable are oil flax and false flax, which have a high content of omega-3(ω-3) fatty acids. It is advisable to use it for therapeutic, prophylactic and dietary purposes. The cultivation of false flax and oil flax is economically feasible and provides an environmental effect due to the reduction of pesticides.

Key words: oil flax, false flax, yield, quality, omega-3 fatty acid.

INTRODUCTION

In the structure of sown areas in Ukraine, the most common are cereals and oilseeds. Sunflower and winter rape occupy a monopoly position in the group of oilseeds. The situation with sunflower in Ukraine forces us to look for promising types of oilseeds (Melnyk et al., 2019). In particular, it is oil flax, spring false flax, mustard species. Due to their biological characteristics and biochemical composition of the oil, they are gaining popularity.

Important crop in Europe for the production of both oil and fibre is an oil flax (*Linum usitatissimum* L.), a member of the family *Linaceae* (Burbulis et al., 2009). However among spring oilseeds, false flax is the most resistant to adverse soil and climatic conditions (Bansal & Durrett, 2016). It grows best in temperate climates, during droughts and high temperatures reduces the duration of the growing season (Liubchenko et al., 2020). False flax sowings are less weeded, which is explained by the release of essential oils by false flax plants', which inhibits the growth of weeds from the stem phase to full maturity of the seeds. It is practically not affected by pests and diseases, so it requires almost no pesticides, which is of great environmental importance (Prakhova, 2013; Shteinyk, 2016). Unlike spring rape, it is also characterized by high resistance of pods to cracking and shedding of seeds.

The restoration of false flax selection occurred mainly due to the high content of omega-3 fatty acids (Chen et al., 2015; Obour et al., 2017). False flax oil contains also other important polyunsaturated fatty acids, has high content of vitamins, is high resistant to oxidation, so it is therapeutic and dietary (Lykhochvor et al., 2016). It should be noted that false flax oil is more resistant to oxidation than usual flax oil. The most common vegetable oils (olive, sunflower, corn) do not contain omega-3, it is also not enough in oils from hemp, rape, soybeans.

The quality of false flax oil is most affected by the high content of alpha-linolenic omega-3 fatty acid, which is in the range of 34.8–41.6%. The second place occupies oleic acid (Maršalkienė et al., 2020). According to other data, the content of omega-3 fatty acids reached 50.2% (Lykhochvor, 2017), and in some varieties - 75% (Drozd, 2011).

For food purposes are used vegetable oils, which contain oleic, alpha-linoleic and linolenic fatty acids. The human body is able to synthesize saturated fatty acids. However, it is not able to synthesize polyunsaturated fatty acids - linoleic (omega-6) and alpha-linolenic (omega-3). Therefore, they must enter the body daily with food. It should be noted that if there are no problems with omega-6 supply (moreover, it is too much), then omega-3 supply is in significant deficit (Mišurcová et al., 2011).

Omega-3 (C 18:3, n3) includes alpha-linolenic (α-linolenic), docosahexaenoic and eicosapentaenoic acids. Their healing properties are extremely valuable for the human body. Omega-6 (C 18:2, n6) include linoleic, arachidonic and gamma-linolenic (γ-linolenic) acids. It has valuable medical properties, but its positive effects are revealed only by the correct ratio between omega-6 and omega-3. Omega-9 (C 18:1, n9) includes oleic acid. It has a number of medical and protective properties. It should be noted that the human body is able to produce omega-9 at the presence of omega-3 and omega-6 fatty acids.

In some countries of the world, false flax is known as gold of pleasure (Košir, 2013). Growing technology affects the productivity of false flax. Thus, the yield of false flax seeds increases and the oil content decreases with increasing nitrogen application rate (Waraich et al., 2013).

In the conditions of climate change it is expedient to grow new crops, in particular *Camelina sativa* L. The highest yield of *Camelina sativa* L. was by the application of N_{90} (Kakabouki et al., 2020).

It appears that spring turnip rape (*Brassica rapa* L. *var. oleifera*) and *Camelina sativa* L. can both be successfully cultivated with different levels of nitrogen and sulphur supply. *Camelina sativa* L. can be an alternative in organic production due to fewer problems with harmful pests, compared with the traditional oilseed crops, rape and turnip rape (Henriksen et al., 2009).

Oil flax has prospects for expanding sown areas (Kiryluk & Kostecka, 2020). Flax oil has the higher content of alpha-linolenic omega-3 fatty acid among oilseeds - 40–57%. Flax seeds and oil are also used as medicines. The oil is used to prepare the drug linetol for the treatment and prevention of atherosclerosis. However, it should be borne in mind that oil flax is more soil demanding than false flax.

The aim of the research was to establish the feasibility of growing oil flax and false flax and to investigate the content of oil and fatty acids in their crops as an alternative to sunflower and rapeseed.

MATERIALS AND METHODS

Research was conducted on the fields of Lviv National Agrarian University on dark gray-podzolic light-loamy soil. The content of humus in the arable layer (according to the method of Tyurin in the modification of Nikitin) - 2.1%, pH of the salt extract - 6.0. The content of easily hydrolysed nitrogen (according to Cornfield) was 105, mobile phosphorus compounds (according to Chirikov) - 140, exchangeable potassium (according to Chirikov) - 120 mg kg^{-1} of soil.

Spring false flax (*Camelina sativa* L.), oil flax *(Linum usitatissimum* L.*),* spring rape (*Brassica napus oleifera annua Metzd.*), white mustard *(Sinapis alba* L.), blue mustard (*Brassica juncea Czern.*) were sown in order to establish their yield, oil content and quality.

The main elements of cultivation technology were as follows. Precursor was winter wheat. Tillage began with stubble peeling, plowing and spring pre-sowing cultivation. Depth of sowing - 2 cm with a seeder SN-16A, rows distance - 15 cm. The terms of sowing depended on the spring time: April 3, 2018, March 20, 2019, April 3, 2020. The rates of fertilizers application were $N_{60}P_{30}K_{60}$. Phosphorus and potassium fertilizers were applied by plowing, nitrogen - by cultivation.

The placement of plots was systematized, repeated three times. The total plot area was 60 m^2, the accounting area - 50 m^2. Yield accounting was performed in the phase of full maturity by the method of sub-section threshing with a Sampo-500 combine and weighing from each accounting area.

The total oil content in the seeds was determined by the mass of dry non-fat residue using a standardized reference method in a Soxhlet apparatus by extraction in a water bath for 8–10 hours. Petroleum ether with a boiling point of 40–65 °C was used as the organic solvent.

Determination of the oil fatty acid composition was performed by a Paisker modified method of gas chromatography of fatty acids' methyl esters on a chromatograph 'Chrom-5' (Czech Republic) with flame-ionization detector in isothermal mode. Chromatography conditions: 3.5 m glass columns with an internal diameter 3 mm, filled with sorbent Chromosorb WAW 100-120 mesh with a mixture of stationary phases SP-2300 2%, SP-2310 3%. Gas flow rate 35 mL min^{-1}, air flow rate - 300 mL min^{-1}, carrier gas - nitrogen. The temperature of the column - 200 °C, the evaporator temperature - 230 °C, the flame ionization detector temperature - 240 °C. Chart ribbon speed 200 mm h^{-1}, scale sensitivity 10-9A, sample volume 5 µl. The fatty acids were identified by peaks on a gas chromatogram, comparing their retention time with the retention time of the peaks of standard pure substances with a known qualitative and quantitative composition. Quantitative estimation of the fatty acid spectrum was performed by the method of the peak areas' normalization of ethylated derivatives and their composition was determined in percent.

Mathematical and statistical processing of research results was carried out by the variance method using Microsoft Excel and Statistica 6.0. The data in the tables and figures are presented as the arithmetic mean value with standard deviation (x ± *SD*).

RESULTS AND DISCUSSION

The most productive among the studied spring oilseeds is spring rape - 2.82 t ha^{-1} (Table 1). The high yield can be explained both by the greater productivity potential of varieties and hybrids of this crop and the existence of more advanced cultivation technologies. The lowest seed yield on average for three years with the same technology was obtained during growing white mustard - 1.82 t ha^{-1} and blue mustard - 1.91 t ha^{-1}. It should be noted that the yield of spring false flax was at the level of rapeseed, it decreased by only 0.14 t ha^{-1}.

Table 1. Seed yield of spring oilseeds, t ha^{-1} (x ± *SD, n* = 6)

Crop	Yield				Increase
	2018	2019	2020	Average	
Spring false flax (*Camelina sativa* L.)	2.83 ± 0.12**	2.60 ± 0.10**	2.61 ± 0.19**	2.68 ± 0.20**	0.14
Oil flax (*Linum usitatissimum* L.)	2.50 ± 0.14**	2.28 ± 0.20**	2.24 ± 0.15**	2.34 ± 0.22**	0.52
Spring rape (*Brassica napus oleifera annua Metzd.*)	2.94 ± 0.20***	2.77 ± 0.17***	2.75 ± 0.18***	2.82 ± 0.23***	1.00
White mustard (*Sinapis alba* L.)	1.94 ± 0.15	1.77 ± 0.12	1,75 ± 0.13	1.82 ± 0.19	-
Blue mustard (*Brassica juncea Czern.*)	2.02 ± 0.18	1.85 ± 0.15	1.86 ± 0.20	1.9 ± 0.21	0.09

Values marked with asterisks are statistically significant compared to White mustard. *$P < 0.05$; **$P < 0.01$; ***$P < 0.001$.

Our research on growing false flax has shown the inexpediency of applying insecticides and fungicides, without which it is almost impossible to grow a high yield of spring rape. In oil flax yields decreased compared to spring rape and false flax, but much higher than in mustard species.

The crops differed in oil content. The highest oil content was found in oil flax seeds - 52.2%, the lowest in white mustard - 40.1%. In false flax, rape and blue mustard the oil content was almost at the same level (Table 2).

Table 2. Oil content in seeds and oil yield per hectare, average for 2018–2020, (x ± *SD*, *n* = 6)

Crop	Oil content, %	Increase, %	Oil yield, t ha^{-1}
Spring false flax (*Camelina sativa* L.)	45.0 ± 1.84*	4.9	1.21**
Oil flax (*Linum usitatissimum* L.)	52.2 ± 1.95***	12.1	1.22**
Spring rape (*Brassica napus oleifera annua Metzd.*)	44.2 ± 1.61*	4.1	1.25***
White mustard (*Sinapis alba* L.)	40.1 ± 1.17	-	0.78
Blue mustard (*Brassica juncea Czern.*)	45.8 ± 1.52**	5.7	0.93*

A clear relationship between crops, oil content and seed yields was not established (Fig. 1). Different types of dependence were revealed. Spring rape has the highest yield and average oil content. White mustard is characterized by low yields and lowest oil content. Blue mustard at low yields has a much higher oil content compared to white mustard. Oil flax combines the highest oil content and average yield. The false flax has a relatively high yield and average oil content.

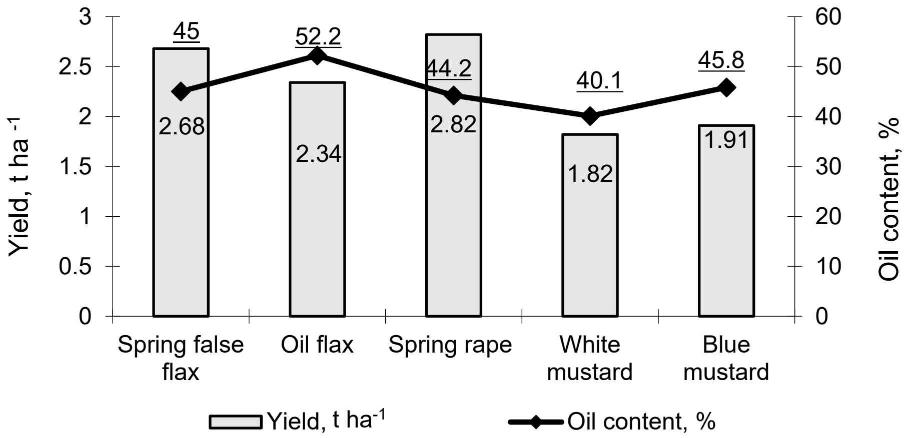

Figure 1. The relationship between yield and oil content in the oilseeds, average for 2018–2020 (x ± *SD*, *n* = 6).

An important integral indicator of crop productivity is the yield of oil per hectare. This indicator is the highest in the most productive crop - spring rape. Mustard species have the lowest oil yield. In false flax it is 1.21 t ha^{-1}, in oil flax - 1.22 t ha^{-1}. Oil flax has a lower yield compared to false flax, but much higher oil content, which provides almost the same oil yield. Given that the price of flax oil and false flax oil is always higher than rapeseed oil and the cost of cultivation is lower, oil flax and false flax provide high economic efficiency. Their cultivation has also a significant environmental effect.

In the last decades, great attention has been given to unsaturated fatty acids because of their beneficial effect on the function of multiple internal organs, protective and antioxidant effects and their potential to replace saturated fats in nutrition (Varga, 2018).

The composition of fatty acids in our studies was characterized by the following indicators. In almost all crops, excepting white mustard, the main fatty acids of the oil were three acids: linolenic, linoleic and oleic (Table 3). In oil flax and spring rape their content was 91.4% and 92.0% respectively. In terms of linolenic acid content, oil flax (56.2%) and false flax (48.8%) prevailed. Blue mustard had a higher content of linoleic acid. Spring rape was characterized by the highest content (60.5%) of oleic acid.

The content of erucic acid, harmful to animals and humans, in the experiment was within acceptable limits (spring false flax - 3.0%, spring rape - 0.2%, oil flax - 0.2%). Exceptions were blue mustard (21.4%) and white mustard (44.5%).

The results of the fatty acids' composition analysis show that the most physiologically valuable are oils from flax and false flax. The composition of the main fatty acids of false flax oil is similar to flaxseed oil. The oil from these crops contains an extremely useful for human health composition of fatty acids.

In research Kolláthová et al. (2019) the analyzed oils (sunflower, soybean, flaxseed and rapessed) 4 oilseeds mainly composed of polyunsaturated fatty acids (PUFA), with the exception of rapeseed oil which primarily contained monounsaturated fatty acids (MUFA). The saturated fatty acid (SFA) content, except for soybean oil, was below 10%.

The most optimal ratio between n-6 and n-3 unsaturated fatty acids (USFA) was found in rapeseed oil (2.22:1).

Table 3. The content of fatty acids in the oil (%) depending on the crop, average for 2018–2020 (x ± *SD, n* = 6)

Crop	omega-3 Linolenic (C 18: 3, n3)	omega-6 Linoleic (C 18:2, n6)	omega-9 Oleic (C 18:1, n9)	Erucic (C 22: 1, n9)
Spring false flax (*Camelina sativa* L.)	48.8 ± 1.21***	17.2 ± 0.62***	18.1 ± 0.84*	3.0 ± 0.22***
Flax oil (*Linum usitatissimum* L.)	56.2 ± 1.30***	19.2 ± 0.74***	16.0 ± 0.95*	0.2 ± 0.03***
Spring rape (*Brassica napus oleifera annua Metzd.*)	11.3 ± 0.95***	20.2 ± 1.05***	60.5 ± 1.42***	0.2 ± 0.02***
White mustard (*Sinapis alba* L.)	22.0 ± 1.00	8.3 ± 0.20	20.5 ± 0.93	44.5 ± 1.20
Blue mustard (*Brassica juncea Czern.*)	21.2 ± 0.86	26.5 ± 1.15***	24.4 ± 1.07*	21.4 ± 0.71***

The study hypothesizes that false flax (Camelina sativa L.), as a high-value biofuel feedstock, could be grown under humid conditions of western Lithuania and that nitrogen fertilisation could influence its seed yield and oil content.Methyl esters of false flax oil have a high iodine value and an especially high content of polyunsaturated linolenic acid: it reached 38.2% in winter false flax oil and 34.3% in summer false flax oil (Karcauskiene et al., 2014).

Omega-6 predominates in the foods that are the basis of our daily diet (pork, butter, sunflower oil, etc.). For a healthy diet, the intake of linoleic (omega-6) and α-linolenic (omega-3) acids with food should be well balanced and the optimal ratio of these acids should be 5:1. In some recommendations it is even found 3:1 and 2:1. In modern food the ratio is far from optimal and reaches 30:1, i.e. there is a significant deficit of omega-3.

To achieve acid balance, you need to use flaxseed or false flax oil, which are high in omega-3. Flaxseeds have nutritional characteristics and are rich source of ω-3 fatty acid: α-linolenic acid (ALA), short chain polyunsaturated fatty acids (PUFA), soluble and insoluble fibers, phytoestrogenic lignans (secoisolariciresinol diglycoside-SDG), proteins and an array of antioxidants (Singh et al., 2011; Goyal et al., 2014).

CONCLUSIONS

Among the studied crops, spring false flax provides a seed yield of 2.68 t ha^{-1}, which is only 0.14 t ha^{-1}less compared with spring rape - the most productive crop.

The most physiologically valuable for the human body are flaxseed oil and false flax oil. The content of omega-3 fatty acid is highest in flax oil (56.2%) and spring false flax (48.8%). The oil yield of these crops is 1.21 t ha^{-1} and 1.22 t ha^{-1}respectively.

REFERENCES

Bansal, S. & Durrett, T.P. 2016. Camelina sativa: An ideal platform for the metabolic engineering and field production of industrial lipids. *Biochimie* **120**, 9–16. https://doi.org/10.1016/j.biochi.2015.06.009

Burbulis, N., Blinstrubienė, A., Kuprienė, R. & Žilėnaitė, L. 2009. Effect of genotype and medium composition on flax (*Linum usitatissimum* L.) anther culture. *Agronomy Research* **7**(Special issue I), 204–209.

Chen, C., Bekkerman, Afshar, R.K. & Neill, K. 2015. Intensification of dryland cropping systems for bio-feedstock production: Evaluation of agronomic and economic benefits of Camelina sativa. *Industrial Crops and Products* **71**, 114–121. https://doi.org/10.1016/j.indcrop.2015.02.065

Drozd, I.F. 2011. Fatty acid composition of oilseed flax in the western region of Ukraine. *Biuleten Instytutu zernovoho hospodarstva* **40**, 72–76 (in Ukrainian).

Henriksen, B.I.F., Lundon, E, Abrahamsen, U. & Eltun, R. 2009. Nutrient supply for organic oilseed crops, and quality of potential organic protein feed for ruminants and poultry. *Agronomy Research* **7**(Special issue II), 592–598.

Goyal, A., Sharma, V., Upadhyay, N., Gill, S. & Sihag, M. 2014. Flax and flaxseed oil: an ancient medicine & modern functional food. *J. Food Sci. Technol.* **51**, 1633–1653. https://doi.org/10.1007/s13197-013-1247-9

Kakabouki, I., Folina, A., Karydogianni, S., Zisi, Ch. & Efthimiadou, A. 2020. The effect of nitrogen fertilization on root characteristics of *Camelina sativa* L. in greenhouse pots. *Agronomy Research* **18**(3), 2060–2068. https://doi.org/10.15159/AR.20.178

Karcauskiene, D., Sendžikienė, E., Makarevičienė, V., Zaleckas, E., Repšienė, R. & Ambrazaitienė, D. 2014. False flax (*Camelina sativa* L.) as an alternative source for biodiesel production. *Zemdirbyste-Agriculture* **101**, 161–168. https://doi.org/10.13080/z-a.2014.101.021

Kiryluk, A. & Kostecka, J. 2020. Pro-Environmental and Health-Promoting Grounds for Restitution of Flax (*Linum usitatissimum* L.) Cultivation. *J. Ecol. Eng.* **21**(7), 99–107. https://doi.org/10.12911/22998993/125443

Kolláthová, R., Varga, B., Ivanišová, E., Gálik, B., Bíro, D., Rolinec, M., Juráček, M., Šimko, M., Hanušovsky, O. & Zábranský, Ľ. 2019. The content of nutrients and fatty acids profile in different oilseeds. *Journal of Central European Agriculture* **20**(4), 1063–1068. https://doi.org//10.5513/JCEA01/20.4.2320

Košir, I.J. 2013. Lucosinulates content in camelina (*Camelina sativa* L.) seeds and oilcakes with regard to production location. *Hmeljarski bilten / Hop Bulletin* **20**, 82–88.

Lykhochvor, A. 2017. Yield and seed quality of spring oilseed crops. *Folia pomeranae universitatis technologiae Stetinensis. Agricultura Alimentaria Piscaria* **336**(43), 75–82. http://dx.doi.org/10.21005/aapz2017.43.3.09

Lykhochvor, V.V., Konyk, H.S. & Lykhochvor, A.M. 2016. False flax is a source of all unsaturated acids. *Ahrobiznes sohodni* **21**, 48–51 (in Ukrainian).

Liubchenko, A., Liubchenko, I., Riabovol, Ia., Riabovol, L., Serzhuk, O., Cherno, O. & Vyshnevska, L. 2020. Analysis of the duration of the vegetation period and phases of development of Somaclonal lines of Camelina sativa. *Ukrainian Journal of Ecology* **10**(3), 1–5. doi: 10.15421/2020_124

Maršalkienė, N., Žilėnaitė, L. & Karpavičienė, B. 2020. Oil content and composition in seeds of Camelina sativa and Crambe abyssinica cultivars. *Journal of Elementology* **25**(4), 1399–1412. doi: 10.5601/jelem.2020.25.3.2023

Melnyk, A., Zherdetska, S., Melnyk, T., Shabir, G. & Ali, S. 2019. Agrobiological features of mustard (*Brassica Juncea* L.) in Ukraine under current climate change conditions. *AGROFOR International Journal* **4**(1), 93–101. https://doi.org/10.7251/AGRENG1901093M
Mišurcová, L., Vávra Ambrožová, J. & Samek, D. 2011. Seaweed lipids as nutraceuticals. *Adv. Food Nutr. Res.* **64**, 339–355. https://doi.org/10.1016/B978-0-12-387669-0.00027-2
Obour, A.K., Obeng, E., Mohammed, Y.A., Ciampitti, I.A. Durrett, T.P., Aznar-Moreno, J.A. & Chen, C. 2017. Camelina seed yield and fatty acids as influenced by genotype and environment. *Agronomy Journal* **109**(3), 947–956. https://doi.org/10.2134/agronj2016.05.0256
Prakhova, T.Ya. 2013. False flax (Camelina sativa (L.) Crantz): monohrafyia. Penza. RYO PHSKhA. 209. (in Russian).
Singh, K.K., Mridula, D., Rehal, J. & Barnwal, P. 2011. Flaxseed- a potential source of food, feed and fiber. *Crit Rev Food Sci Nutr.* **51**, 210–222. https://doi.org/10.1080/10408390903537241
Varga, B. 2018. Available polyunsaturated fatty acids n-6 and n-3 sources in plant oils and utilization suitable in nutrition. PhD. Thesis. Nitra: Slovak University of Agriculuture.
Waraich, E.A., Ahmed, Z., Ahmad, R. & Rengel, Z. 2013. Camelina sativa, a climate proof crop, has high nutritive value and multiple-uses. *Aust. J. Crop Sci*. **7**, 1551–1559.
Shteinyk, R. 2016. False flax is the only crop that does not harm the land and the environment. *APK-inform* **12**, 61–64 (in Russian).

Agronomy Research **20**(2), 310–317, 2022
https://doi.org/10.15159/AR.22.014

Agrochemical methods for reducing the translocation ability of heavy metals in sod-podzolic soil

Yu.A. Mazhayskiy[1], T.M. Guseva[2,*], S.M. Kurchevskiy[3] and V.V. Vcherashnyaya[4]

[1]Meshchersky branch of the all-Russian research Institute of hydraulic engineering and land reclamation n. A.N. Kostyakova, 1A Meshcherskaya Str., RU390021 Ryazan, Russia
[2]Ryazan state medical University n. I.P. Pavlova, 22 Lenina Str., RU390000 Ryazan, Russia
[3]Belarusian National Technical University, 65 Prospekt Nezavisimosti, BE220013 Minsk, Belarus
[4]Belarusian State Order of the October Revolution and the Red Banner of Labor Agricultural Academy, 5 Michurina Str., BE213410 Gorki, Belarus
[*]Correspondence: guseva.tm@yandex.ru

Received: January 25th, 2022; Accepted: March 17th, 2022; Published: April 4th, 2022

Abstract. The impact of technogenesis on the agricultural landscape contributes to the contamination of all its components by heavy metals. The main measure to protect the environment from the input of heavy metals is the prevention of pollution, which is achieved by improving the technology of agricultural production. The development of methods for the agrochemical rehabilitation of technogenically polluted soil, which ensure the receipt of environmentally safe crop products, is an urgent task. The paper presents the results of a lysimetric experiment on the study of the use of fertilizer systems for the purpose of remediation of heavy-metal-contaminated soddy-podzolic soil. It has been experimentally established that the translocation ability of heavy metals and, as a result, the accumulation of toxicants in grain and tilled crops is reduced when using an organomineral fertilizer system. All the studied fertilizer systems reduced the entry of dangerous ecotoxicants - lead and cadmium, into the infiltration water, and also caused the immobilization of Cu and Zn.

Key word: mineral fertilizers, organic fertilizers, soddy-podzolic soil, soil remediation, heavy metals, translocation, chemical reclamation, crop production, environmental safety.

INTRODUCTION

Preservation of soil, improvement of its properties and increase in fertility is one of the main conditions for the existence of mankind. However, at present, on a global scale, there is a systematic decrease in the area of soil in agricultural use. Therefore, it is very important to increase soil fertility, which is achieved through land reclamation measures, favorable for the development of agricultural crops, the mode of use. Soil fertility depends on natural soil formation, agrochemical and agrophysical properties, the influence of cultivating factors in the technology of growing crops and, more recently, on the impact of technogenesis. Heavy metals (HMs) pose a serious threat to the soil cover. All major HM migration cycles in the biosphere begin in the soil, since it is there that metals are mobilized and their migratory forms are formed. A significant reaction surface of mineral matter, the presence of soil solutions and organic matter, saturation with microorganisms, mesofauna, and roots of higher plants create the most complex system of transformation of heavy metal compounds in the soil (Borisochkina & Kaydanova, 2021; Mazhaiskiy & Guseva, 2021). In the process of interaction between soil and metals, they are sorbed by organic matter, iron hydroxides, and clay minerals. Soddy-podzolic sandy soil is the least resistant to the action of technogenesis, since they are poorly provided with nutrients and are permeable. According to many authors, the most acceptable method of rehabilitation and restoration of the fertility of technogenically polluted soil is a rational fertilizer system (Ignatova, 2020; Chernyakova, 2020; Patrikeev & Yanchas, 2020). Organic and phosphate fertilizers are effective as a means of reducing the mobility of heavy metals. Mineral fertilizers improve the trophic indicators of agricultural crops, improving the resistance of plants to adverse environmental influences (Lasmini et al., 2019; Skudra & Ruza, 2019; Burdin et al., 2020; Hlisnikovský et al., 2020; Khajbullin et al., 2020; Murtić et al., 2020; Wiśniewska-Kadżajan & Jankowski, 2020; Kołodziejczyk, 2021; Radchenko et al., 2021). In this regard, the development of scientifically based systems for the use of fertilizers on technogenically modified soddy-podzolic soil is an urgent task. The aim of the research is to evaluate agrochemical methods for reducing the translocation ability of heavy metals in sod-podzolic soil. The results of such studies allow us to offer more effective reclamation recommendations for unproductive soils of light granulometric composition in order to increase their fertility and maintain a positive balance of nutrients due to the normalized application of organic and mineral fertilizers, as well as the conservation and sustainable use of sod-podzolic soils of agricultural landscapes transformed as a result of technogenesis.

MATERIALS AND METHODS

The research was carried out in the conditions of the Meshcherskaya lowland on the territory of the Ryazan region, located in the southeastern part of the central zone of the European part of Russia. For the Ryazan Meshchera, zonal soil is soddy-podzolic soil, which occupies about 70% of the area. It is characterized by a light granulometric composition, low content of organic matter and low fertility (Table 1).

Table 1. Agrochemical characteristics of sod-podzolic soils

Soil layer, cm	Humus, %	$pH_{сол}$	N, %	P_2O_5, mg kg^{-1}	K_2O, mg kg^{-1}
0–10	1.33	5.2	0.032	113	78
10–20	1.29	4.9	0.024	95	66
20–30	1.18	4.8	0.016	76	37
30–40	1,06	4.6	0.010	57	21
0–40	1.22	4.9	0.017	85	51

According to long-term environmental monitoring, this soil is under a significant technogenic load, which has led to the accumulation of zinc, cadmium, lead, copper to levels of medium and high pollution (Mazhaiskiy & Guseva, 2019).

To study the effectiveness of agro-reclamation methods for the rehabilitation and detoxification of soddy-podzolic sandy loamy soil contaminated by heavy metals, a long-term lysimetric experiment (2010–2020) was carried out, the scheme of which is presented in the 2nd Table. A complex soil contamination by HMs, corresponding to the data of monitoring of the technogenic load on soddy-podzolic soil, is modeled in the experiment, taking into account the background content of elements, which amounted to: Cu - 90 mg kg^{-1}, Zn - 110 mg kg^{-1}, Pb - 40 mg kg^{-1}, Cd - 0.6 mg kg^{-1}. The doses of elements per lysimeter were calculated from their content in chemically pure salts ($ZnSO_4 \cdot 7H_2O$ (22.8% Zn), $CuSO_4 \cdot 5H_2O$ (25.5% Cu), $Pb(CH_3COO)_2 \cdot 3H_2O$ (54.6% Pb), $CdSO_4$ (53.9% Cd)).

Table 2. The scheme of the lysimetric experiment

Variant	Fertilizer system
Control	Without fertilizer
1	Cattle manure 40 t ha^{-1}, N90P60K120
2	Cattle manure 40t ha^{-1}, N90P120K120
3	Cattle manure 40t ha^{-1}, N90P240K120
4	Cattle manure 80 t ha^{-1}
5	N90P480K120

For experiments, we used lysimeters designed by the NRIHEM with an area of 1.17 m^2, soil (soddy-podzolic sandy loam) of undisturbed composition. As experimental crops used in crop rotation: potatoes, beets, grain crops (oats, barley). After the end of the experiment in 2020, the content of copper, zinc, lead and cadmium was determined in crop production and lysimetric waters by atomic absorption spectrometry on the AAS–1 spectrophotometer. The mineralization of plant samples was carried out by dry salting, water samples were mineralized by evaporation with concentrated nitric acid (Guidelines for the determination of heavy metals in agricultural soil and crop products, 2021; GOST R 55447–2013). Trial establishment - the introduction of heavy metals and the use of organic-mineral, organic and mineral fertilizer systems took place in 2010. Background liming and manure application was carried out in 2014. Urea (N–46%) or ammonium nitrate (N–34.5%), double superphosphate (P_2O_5–46%), potassium chloride (K_2O–60%), and cattle manure were used in the experiment. Fertilizers were applied before spring tillage. The experiment was carried out in four repetitions, the results were computer statistically processed.

RESULTS AND DISCUSSION

The task of agrochemical means is to create a balanced diet and neutralize the phytotoxic effect for crops in conditions of technogenic soil pollution. A scientifically based fertilizer system is designed to influence a more complete use of nutrients by various crops and prevent the accumulation of heavy metals in crop products (Guseva et al., 2017; Guseva, 2019).

Tables 3–6 present data on the effect of the developed fertilizer systems on the content of pollutants in agricultural crops grown on soddy-podzolic soil contaminated by heavy metals, obtained from the results of a long-term lysimetric experiment.

The content of Pb in potato tubers, fodder beet, grain biomass, as well as in by-products does not exceed the standard values for plant feed. In the main barley production in the variant without the usage of fertilizers, the accumulation of lead was recorded in excess of the maximum allowable concentration (MAC) for food raw materials by 36%.

Table 3. Lead content in crop products, mg kg^{-1}*

Variant		Potato	Barley	Oats	Fodder beet
Control		0.43 ± 0.04 2.95 ± 0.1	0.68 ± 0.04 1.4 ± 0.02	0.75 ± 0.04	0.21 ± 0.01
1	Cattle manure 40 t ha^{-1}, N90P60K120	0.26 ± 0.01 3.12 ± 0.2	0.33 ± 0.01 1.68 ± 0.03	0.84 ± 0.05	0.19 ± 0.01
2	Cattle manure 40 t ha^{-1}, N90P120K120	0.25 ± 0.01 2.92 ± 0.3	0.33 ± 0.01 1.67 ± 0.01	0.83 ± 0.05	0.18 ± 0.02
3	Cattle manure 40 t ha^{-1}, N90P240K120	0.24 ± 0.02 3.39 ± 0.2	0.44 ± 0.02 0.78 ± 0.01	1.34 ± 0.09	0.19 ± 0.01
4	Cattle manure 80 t ha^{-1}	0.42 ± 0.03 2.50 ± 0.1	0.32 ± 0.01 0.96 ± 0.02	1.08 ± 0.08	0.20 ± 0.01
5	N90P480K120	0.27 ± 0.02 2.39 ± 0.2	0.32 ± 0.01 1.03 ± 0.03	0.92 ± 0.07	0.17 ± 0.01
MACp. **		0.5	0.5	–	–
MACf. ***		5.0	5.0	5.0	5.0

*Note: numerator – lead content in main products, denominator - lead content in by-products.

MACp. – maximum allowable concentration of lead in plant products (Temporary maximum allowable level .... 123-4 / 281, 1987).

MACf. – maximum allowable concentration of lead for feed (Maximum allowable concentrations of heavy metals and arsenic in plant raw materials and food products, 1992).

Table 4. Cadmium content in crop products, mg kg^{-1}*

Variant		Potato	Barley	Oats	Fodder beet
Control		0.04 ± 0.003 0.24 ± 0.03	0.21 ± 0.03 0.14 ± 0.01	0.09 ± 0.002	0.02 ± 0.001
1	Cattle manure 40 t ha^{-1}, N90P60K120	0.03 ± 0.001 0.21 ± 0.01	0.07 ± 0.003 0.10 ± 0.01	0.09 ± 0.002	0.02 ± 0.001
2	Cattle manure 40 t ha^{-1}, N90P120K120	0.03 ± 0.001 0.22 ± 0.01	0.10 ± 0.02 0.09 ± 0.004	0.07 ± 0.001	0.02 ± 0.002
3	Cattle manure 40 t ha^{-1}, N90P240K120	0.03 ± 0.002 0.20 ± 0.03	0.07 ± 0.003 0.13 ± 0.02	0.10 ± 0.01	0.02 ± 0.001
4	Cattle manure 80 t ha^{-1}	0.03 ± 0.003 0.23 ± 0.01	0.10 ± 0.02 0.11 ± 0.01	0.10 ± 0.02	0.02 ± 0.002
5	N90P480K120	0.03 ± 0.003 0.23 ± 0.02	0.10 ± 0.01 0.11 ± 0.02	0.09 ± 0.002	0.02 ± 0.001
MACp.**		0.03	0.1	–	–
MACf.***		0.3	0.3	0.3	0.3

*Note: numerator – cadmium content in main products, denominator - cadmium content in by-products.

MACp. – the maximum allowable concentration of cadmium in plant products (Temporary maximum allowable level .... 123-4 / 281, 1987).

MACf. – maximum allowable concentration of cadmium for feed (Maximum allowable concentrations of heavy metals and arsenic in plant raw materials and food products, 1992).

According to the content of cadmium in vegetation in the experiment, the following results were obtained. The content of this element in beets and grain biomass, as well as by-products of potatoes and barley, is within the MAC for plant feed. The accumulation of Cd, in relation to the MAC for food raw materials, occurred in potato tubers in the variant of the experiment without fertilizers, and the accumulation of this element was also observed in the main barley production in the control (the excess was 33% and 110%, respectively).

Table 5. Zinc content in crop products, mg kg^{-1}*

Variant		Potato	Barley	Oats	Fodder beet
Control		10.71 ± 1.2	76.1 ± 6.2	72.3 ± 3.1	11.4 ± 1.2
		103.1 ± 8.9	111.2 ± 10.1		
1	Cattle manure 40 t ha^{-1},	6.62 ± 0.7	48.7 ± 4.1	45.7 ± 4.2	13.1 ± 1.1
	N90P60K120	100.5 ± 10.2	65.2 ± 3.7		
2	Cattle manure 40 t ha^{-1},	6.68 ± 0.9	46.4 ± 4.9	50.1 ± 5.6	16.3 ± 1.5
	N90P120K120	74.8 ± 5.1	59.3 ± 4.9		
3	Cattle manure 40 t ha^{-1},	6.02 ± 0.5	49.2 ± 4.1	50.01 ± 4.8	14.4 ± 1.1
	N90P240K120	67.9 ± 4.9	73.9 ± 5.5		
4	Cattle manure 80 t ha^{-1}	6.10 ± 0.7	37.6 ± 2.2	49.4 ± 4.1	27.3 ± 1.9
		51.7 ± 4.6	72.3 ± 5.2		
5	N90P480K120	9.6 ± 1.1	49.0 ± 4.7	49.7 ± 4.6	21.5 ± 2.2
		99.5 ± 9.9	72.5 ± 6.1		
MACp.**		10	50	–	–
MACf.***		100	50	50	100

*Note: the numerator is the zinc content in the main product, the denominator is the zinc content in the by-products.

MACp. – maximum allowable concentration of zinc in plant products (Temporary maximum allowable level .... 123-4 / 281, 1987).

MACf. – maximum allowable concentration of zinc for feed (Maximum allowable concentrations of heavy metals and arsenic in vegetable raw materials and food products, 1992).

Table 6. Copper content in crop products, mg kg^{-1}*

Variant		Potato	Barley	Oats	Fodder beet
Control		2.06 ± 0.008	6.02 ± 0.8	1.62 ± 0.03	2.26 ± 0.08
		9.06 ± 1.02	8.77± 0.8		
1	Cattle manure 40 t ha^{-1},	1.72 ± 0.07	4.36 ± 0.4	3.67 ± 0.1	1.53 ± 0.02
	N90P60K120	4.72 ± 0.3	2.36 ± 0.08		
2	Cattle manure 40 t ha^{-1},	1.60 ± 0.03	4.00 ± 0.6	2.92 ± 0.07	1.33 ± 0.03
	N90P120K120	8.67± 0.9	5.68 ± 0.5		
3	Cattle manure 40 t ha^{-1},	1.38 ± 0.04	4.75 ± 0.4	3.02 ± 0.2	1.93 ± 0.03
	N90P240K120	6.55 ± 0.8	4.44 ± 0.2		
4	Cattle manure 80 t ha^{-1}	1.86 ± 0.02	3.5 ± 0.1	2.09 ± 0.08	2.79 ± 0.05
		2.67 ± 0.09	4.38 ± 0.3		
5	N90P480K120	1.70 ± 0.04	4.43 ± 0.4	3.36 ± 0.1	2.21 ± 0.04
		10.91 ± 1.1	3.88 ± 0.1		
MACp.**		5	10	–	–
MACf.***		30	30	30	30

*Note: numerator – copper content in the main product, denominator - copper content in by-products.

MACp. – maximum allowable concentration of copper in plant products (Temporary maximum allowable level .... 123-4 / 281, 1987).

MACf. – maximum allowable concentration of copper for feed (Maximum allowable concentrations of heavy metals and arsenic in vegetable raw materials and food products, 1992).

The results of the experiment on the effect of various fertilizer systems on the accumulation of zinc by agricultural plants are as follows. The content of this metal in beets, the main and by-products of potatoes is within the MAC for both plant products and feed. A slight excess of the standards for potatoes and oats was observed in the control variant. The content of Zn in fodder beet did not exceed the standard values in all variants of the experiment. In the biomass of oats, there was an accumulation of zinc in the variant without fertilizers by 45% compared with MAC. In the main and by-products of barley, there was also an excess of the content of this element in the control variant (by 32% and 122%, respectively, compared with the maximum allowable concentrations). Also, an excess of the content of Zn in the by-products of barley was noted in all variants of the experiment, but these values are below the control.

The analysis of the experimental results showed that the Cu content in all test cultures, including by-products, did not exceed the normative values for plant feed and food products.

Thus, the obtained results showed a positive effect of the studied fertilizer system as a factor in the remediation of technogenically polluted soddy-podzolic soil.

The use of organic and mineral fertilizers against the background of liming on soil contaminated by heavy metals causes physicochemical and biological processes in the soil, which lead to the immobilization of HMs, making them not only inaccessible to plants, but also reducing their penetration into soil runoff (Stehlík et al., 2019). The results of the research of lysimetric water are presented in the 7th Table.

Table 7. Content of heavy metals in lysimetric water, mg $L^{-1} \cdot 10^{-3}$

Variant		Cu	Zn	Pb	Cd
Control		2.7 ± 0.1	19.5 ± 1.3	12.0 ± 1.8	3.9 ± 0.4
1	Cattle manure 40 t ha^{-1}, N90P60K120	6.5 ± 0.8	88.5 ± 5.2	3.7 ± 0.5	3.6 ± 0.3
2	Cattle manure 40 t ha^{-1}, N90P120K120	2.6 ± 0.1	44.9 ± 1.7	11.6 ± 1.1	3.7 ± 0.4
3	Cattle manure 40 t ha^{-1}, N90P240K120	6.7 ± 1.1	64.9 ± 9.3	10.6 ± 1.2	3.5 ± 0.2
4	Cattle manure 80 t ha^{-1}	1.8 ± 0.06	10.7 ± 1.3	9.8 ± 0.9	3.2 ± 0.3
5	N90P480K120	3.7 ± 0.3	59.1 ± 1.8	7.2 ± 0.3	2.3 ± 0.1

Copper is able to form many complexes with organic and mineral compounds of various solubility. The ability of a soil to fix Cu is highly dependent on the nature and amount of organic matter. Zinc is a mobile element, practically incapable of complex formation (Medvedev & Derevyagin, 2017). The experiment recorded the removal of these HMs outside the soil profile, but the immobilization of Cu and Zn was noted in the 4th variant of the experiment, the concentration of these elements in lysimetric water decreased by 33% and 45%, respectively, compared with the variant without fertilizers. All studied fertilizer systems reduced the infiltration water of hazardous environmental toxicants - lead and cadmium.

CONCLUSIONS

Agrochemical methods of rehabilitation of technogenically polluted soil must be implemented through the introduction of a scientifically based organo-mineral fertilizer system. In crop rotations, about 40% should be allocated to crops, the roots of which will concentrate a significant part of the HM. After harvesting the above-ground part, crop residues and roots must be plowed to the entire depth of the humus horizon of the contaminated soil. Organic and mineral fertilizers are recommended to be used systematically in crop rotations. A system of periodic (once every four years) application of organic and phosphate fertilizers is proposed. The recommended dose of manure - 40 t ha^{-1} (1 time per four years) is not deficient in the balance of humus, doses of mineral fertilizers, depending on the crop: N - 30–90 kg ha^{-1}, P_2O_5 - 60–120 kg ha^{-1}, K_2O - 60–120 kg ha^{-1} (per year).

REFERENCES

Borisochkina, T.I. & Kaydanova, O.V. 2021. Heavy metals in fractions of different soil dispersion in natural and anthropogenic landscapes: a case study of the Kursk region. *Problems of regional ecology* **4**, 35–42 (in Russian). doi: 10.24412/1728-323X-2021-4-35-42

Burdin, I.A., Arbuzova, E.V., Guseva, T.M., Ilyinsky, A.V. & Kireycheva, L.V. 2020. Justification for the creation of eco-functional biofertilizers based on effluent to restore fertility and increase soil productivity in degraded agricultural lands. *Eurasian Union of Scientists* **8**(77), 52–55 (in Russian).

Chernyakova, G.I., Trotz, N.M. & Kostin, Ya.V. 2020. The effectiveness of the use of an organomineral system for the purpose of inactivation of heavy metals in potato cultivation in the steppe zone of the Samara Volga region. *Proceedings of the Samara State Agricultural Academy* **2**, 27–34 (in Russian). doi: 10.12737/37335

GOST R 55447-2013. Feedstuffs, compound feeds, feed raw materials. Determination of cadmium, lead, arsenic, mercury, chromium, tin by atomic absorption spectroscopy. 2014, 18 pp.

Guidelines for the determination of heavy metals in agricultural soil and crop products. 2021, 62 pp. (in Russian).

Guseva, T.M., Mazhaiskiy, Yu.A. & Ilyinskiy, A.V. 2017. Principles of organizing the production of environmentally friendly crop products and increasing the fertility of technogenically polluted soil. *Bulletin of the Perm State Pharmaceutical Academy* **20**, 251–255 (in Russian).

Guseva, T.M. 2019. *Environmental aspects of the production of high-quality agricultural products on technogenically polluted soil.* In: Collection of articles of the international conference Topical issues in science and practice. Samara, Russia, pp. 23–26 (in Russian).

Hlisnikovský, L., Barlog, P., Kunzová, E., Vach, M. & Menšík, L. 2020. Biomass yield of silage maize, fertilizers efficiency, and soil properties under different soil-climate conditions and fertilizer treatments. *Agronomy Research* **18**(1), 88–99. doi.org/10.15159/AR.20.017

Ignatova, G.A. 2021. The effect of basic tillage and fertilizer systems on the accumulation and mobility of heavy metals in the soil. *Bulletin of Agrarian Science* **2**(83), 15–20 (in Russian). doi: 10.17238/issn2587-666x.2020.2.15

Khajbullin, M., Kadaeva, G., Akhiyarov, B., Valitov, A. & Gajfullin, R. 2020. The quality of spring rape seeds and its dependence on the doses of mineral fertilizers under the conditions of Southern Urals. *Agronomy Research* **18**(2), 450–460, doi.org/10.15159/AR.20.136

Kołodziejczyk, M. 2021. Influence of humic acids, irrigation and fertilization on potato yielding in organic production. *Agronomy Research* **19**(2), 520–530, doi.org/10.15159/AR.21.099

Lasmini, S.A., Wahyudi, I., Rosmini, R., Nasir, B. & Edy, N. 2019. Combined application of mulches and organic fertilizers enhance shallot production in dryland. *Agronomy Research* **17**(1), 165–175. doi.org/10.15159/AR.19.017
Maximum permissible concentrations of heavy metals and arsenic in food raw materials and food products. T.V. Sanitary rules and norms (SanRaN), hygienic standards and a list of guidelines and recommendations on food hygiene. Rarog, Moscow, 1992. 4 pp. (in Russian).
Mazhaiskiy, Yu.A. & Guseva, T.M. 2019. Environmental problems of agricultural landscapes in the Ryazan region. *Biosfera* **3**(11), 156–159 (in Russian).
Mazhaiskiy, Yu.A. & Guseva, T.M. 2021. *Ecological substantiation of detoxification of technogenically polluted lands in the south of the central Non-Chernozem region.* In: International Conference Innovative Technologies in Land Reclamation and Construction. Gorki, Belarus, pp. 68–70 (in Russian).
Medvedev, I.F. & Derevyagin, S.S. 2017. *Heavy metals in ecosystems.* Rakurs, Saratov, 178 pp. (in Russian).
Murtić, S., Čivić, H., Sijahović, E., Koleška, I., Jurković, J. & Tvica, M. 2020. Use of pyrophyllite to reduce heavy metals mobility in a soil environment. *Agronomy Research* **18**(1), 194–205. doi.org/10.15159/AR.20.009
Patrikeev, E.S. & Yanchas, Yu.P. 2020. The effect of humic fertilizers on the mobility of heavy metals in the soil. *International Journal of Humanities and Natural Sciences*, vol. **6**–**1**(45), 6–9 (in Russian). doi: 10.24411/2500-1000-2020-10638
Radchenko, M.V., Trotsenko, V.I., Hlupak, Z.I., Zakharchenko, E.A., Osmachko, O.M., Moisiienko, V.V., Panchyshyn, V.Z. & Stotska, S.V. 2021. Influence of mineral fertilizers on yielding capacity and quality of soft spring wheat grain. *Agronomy Research* **19**(4), 1901–1913, doi.org/10.15159/AR.21.104
Skudra, I. & Ruza, A. 2019. Effect of nitrogen fertilization management on mineral nitrogen content in soil and winter wheat productivity. *Agronomy Research* **17**(3), 822–832. doi.org/10.15159/AR.19.135
Stehlík, M., Czako, A., Mayerová, M. & Madaras, M. 2019. Influence of organic and inorganic fertilization on soil properties and water infiltration. *Agronomy Research* **17**(4), 1769–1778. doi.org/10.15159/AR.19.145
Temporary maximum allowable level (MAL) for the content of certain chemical elements and gossypol in feed for farm animals and feed additives. 123-4/281. 1987, 4 pp. (in Russian).
Wiśniewska-Kadżajan, B. & Jankowski, K. 2020. Effects of the interaction between slurry, soil conditioners, and mineral NPK fertilizers on selected nutritional parameters of Festulolium braunii (K. Richt.) A. Camus. *Agronomy Research* **18**(S2), 1573–1583, doi.org/10.15159/AR.20.125

Agronomy Research **20**(2), 318–325, 2022
https://doi.org/10.15159/AR.22.012

Mapping drainage ditches in agricultural landscapes using LiDAR data

R. Melniks[1,2,*], J. Ivanovs[1], A. Lazdins[1] and K. Makovskis[1]

[1]Latvian State Forest Research Institute 'Silava', Riga street 111, LV-2169 Salaspils, Latvia
[2]University of Latvia, Faculty of Geography and Earth Sciences, Jelgava street 1, LV-1004 Riga, Latvia
[*]Correspondence: raitis.melniks@silava.lv

Received: December 8th, 2021; Accepted: January 30th, 2022; Published: March 22nd, 2022

Abstract. The aim of this study is to develop a method for identification of the drainage ditch network, which can be used for surface runoff modeling and to increase accuracy of estimation of greenhouse gas (GHG) emissions in croplands and grasslands, using remote sensing data. The study area consists of 11 objects throughout Latvia with a total area of 145 km^2. Digital elevation models (DEMs) in two resolutions, which were created using three different interpolation methods, were used for the analysis. Several multi-level data filtering methods were applied to identify ditch network, including flow patterns, which can be used in surface runoff process. The method we developed correctly identified 85–89% of ditches, depending on the DEM used, in comparison to the reference data. Mapped ditches are located within 3 m range of the reference data in 89–93% of cases. The elaborated model is robust and uses openly available source data and can be used for large scale ditch mapping with sufficient accuracy necessary for hydrological modelling and GHG accounting in the national inventories.

Key words: ditch, drainage, LiDAR, cropland, grassland.

INTRODUCTION

Most of the long-term operational infrastructure, including the drainage ditch network, has been developed before compliance with climate change was included in the planning process. Therefore it is essential to obtain accurate data on the location and condition of the ditch network in order to be able to assess its suitability for foreseeable conditions and the need for improvement measures. Ditches reduce the risk of flooding events during spring, as well as after heavy rainfalls, accumulating water and discharging it to downstream water bodies, where the opposite effect - overflow- can occur, if their capacity or runoff is limited. For this reason, ditches and their elements, such as culverts, need to be maintained and functioning (Moussa et al., 2002).

Recently, intensive agriculture, forestry and associated ditching have been identified to pose several complex environmental risks, particularly degradation of wetlands and soil, greenhouse gas emissions (Audet et al., 2017; Peacock et al., 2021), increased nutrient and sediment discharge to water bodies and biodiversity loss (Lidman et al., 2017; Lepistö et al., 2021). Identification of ditches and connections to the rest of the hydrographic network can help in decision making about water management, quality control, as well as risks, and the gathered data can be used to model environmental processes (Roelens et al., 2017).

In lowland agricultural lands of Western Europe, the density of the man-made ditch network has been estimated as 200–300 m ha^{-1}, but in Poland it reaches 150–350 m ha^{-1} (Bryndal & Kroczak 2019). Different research actions were implemented to evaluate and minimize environmental risks and to restore degraded or wet soils in the ditched agricultural and forest landscapes (Ivanovs & Lupikis, 2018; Hasselquist et al., 2018). However, such initiatives are significantly limited by the lack of accurate and site-specific data of ditch networks (Lidberg et al., 2017; Ivanovs & Lupikis 2018; Melniks et al., 2019).

Currently, remote sensing data and high-resolution laser scanning data are becoming increasingly important in environmental research. Therefore, the quality and suitability of a digital terrain model, as well as appropriate methodology are essential for identification of small-scale elements such as a ditch network (Anderson et al., 2006; Vaze at al., 2010).

Various studies have previously been carried out to identify ditches using laser scanning data, but they do not analyze the impact of the DEM interpolation method. Currently, most studies (Sofia et al., 2011; Passalacqua et al., 2012; Cazorzi et al., 2013) identify the ditch network using high-resolution (0.5 and 1 m) digital elevation models, which is considered to be the most widely used approach, because it requires a relatively low density of LiDAR points in comparison to requirements for raw LiDAR point cloud-based approaches. In a study carried out in Belgium (Roelens et al., 2016), classified LiDAR point clouds were used to identify agricultural ditches and their parameters. There are also studies based on different topographic indices, such as Topographic elevation index or Standardized elevation index combined (Passalacqua et al., 2012; Kiss et al., 2015). Most of the studies similar to ours regarding methodologyuse Relative Elevation Attribute or slope analysis, are focused on smaller study areas (up to 150 ha), and use individual laser scanning flight campaigns instead of countrywide assessments (Cazorzi et al., 2013; Rapinel et al., 2015; Roelens et al., 2018b, 2018a).

In our study we developed a method, applicable on large areas, which is based on the logistic approach and analysis of a digital elevation model with a focus on the DEM interpolation method and horizontal resolution.

Study area

The study area (145 km^{-2} in total) consists of 11 regions in Latvia, where agricultural land dominates. The areas have been selected by experts to describe the overall landscape in as general way as possible. Areas are located in different quaternary sediments and are characterized by different types of land management and moisture regimes (Fig. 1).

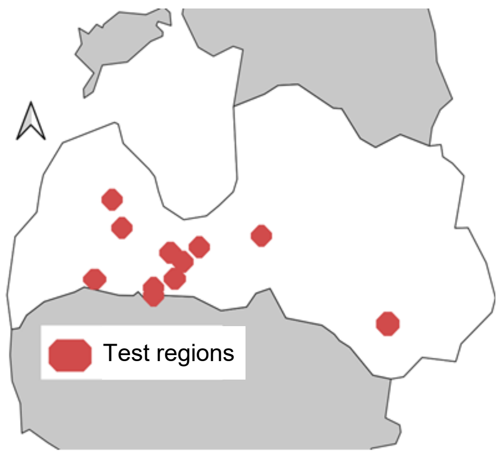

Figure 1. Locations of the digitized test regions, where red points indicate areas with dominating agricultural landscapes.

Reference and airborne LiDAR data

The LiDAR point cloud in LAS format, derived from Latvian Geospatial agencie's National ALS program, was used to create the digital elevation model. The LiDAR data we used, have a vertical accuracy of 0.12 m (2 sigmas with a 95% confidence level against the National Geodetic Network) and a horizontal accuracy of 0.36 m (2 sigmas with a 95% confidence level against the National Geodetic Network). The minimum point density is 4 points m^{-2}, and the average ground point density is 1.5 points m^{-2} (LGIA 2017).

In the study areas manual digitization of the ditch network as vector lines was performed using DEM 0.5 m resolution, which was obtained using the Binning interpolation method. When digitizing, DEM is depicted as a multidirectional hillshade.

MATERIALS AND METHODS

To perform the analysis, DEMs were first generated in horizontal resolutions of 0.5 m and 1 m using three different interpolation methods - Binning, Bilinear and Bicubic, which are implemented in open access GIS, for example GRASS GIS (Fig. 2).

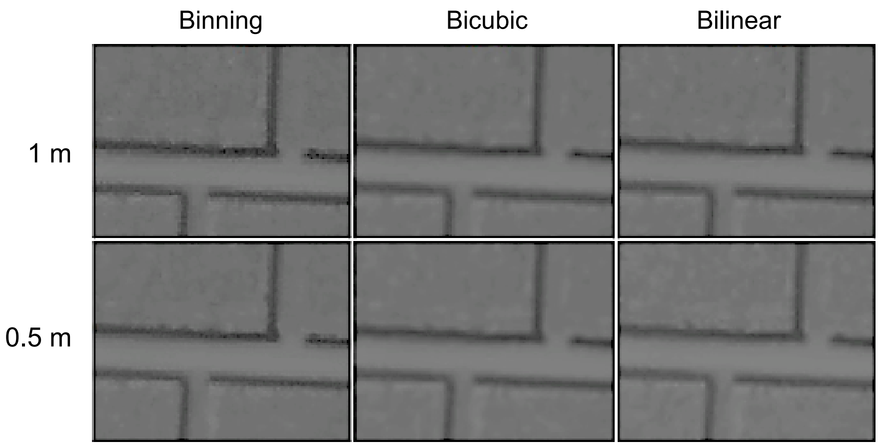

Figure 2. Example of raster images in 0.5 m and 1 m horizontal resolution and different interpolation methods.

To identify the preliminary ditch network using DEM, a logical query based on the identification of local depressions was used, depending on the minimum depth and width of the ditch set by the user (Eq. 1). This type of raster processing has some similarities with Relative Elevation Attribute, which is used in several other studies (Cazorzi et al., 2013; Rapinel et al., 2015; Roelens et al., 2018b). The same analysis was done to all DEM's in both 0.5 m and 1 m resolution. The output of this algorithm is a binary image, where the value of 1 indicates a local reduction corresponding to the set parameters.

$$\text{If ((DEM +X < DEM [-Y,0] \&\& +X < DEM [Y,0]) || (DEM +X < DEM [0, Y] \&\& DEM +X < DEM [0,-Y]) || (DEM +X < DEM [Y,Y] \&\& DEM +X < DEM [-Y,- Y]) || (DEM +X < DEM [-Y,Y] \&\& DEM +X < DEM [Y,-Y]), 1, 0)} \quad (1)$$

where DEM – digital elevation model; X – minimal depth of the ditch; Y – minimal width of the ditch, both in raster cells.

The resulting binary image contains both the ditch network and various supplementary data sets that have met the specified criteria. The higher resolution DEM is used for the analysis and the smaller the minimum depth of the ditch as well as the wider its width, the more we are exposed to pixels that contain ‘noise’. Further processing of the preliminary ditch network was performed using ESRI ArcMap automated vectorization tools.

Multi-level filtering of elements was performed by vectorizing the binary image. First, noise pixel filtering, creation and generalization of linear objects were performed. Vectors are designed considering their length, the distance between the ends, as well as the connection angle for connecting small gaps.

In the next processing step, final filtering was performed. In this step a complex analysis of the ditch network takes place considering the number of its constituent elements, the total length, and the possibility of connectivity in the 15 m buffer zone. In this way elements that do not form a network of ditches consist of objects shorter than 30 m individually or form systems with a total length of less than 100 m are disposed of (Fig. 3).

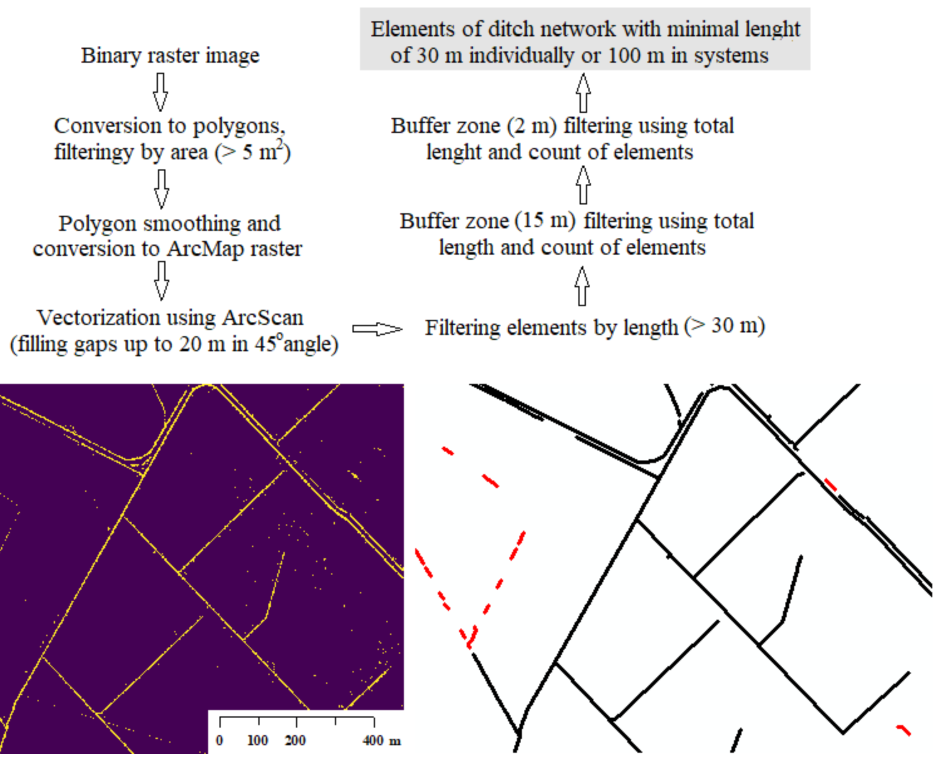

Figure 3. Diagram of data filtering workflow and example of binary image (left), where yellow pixels are representing preliminary ditch data and vectorized data (right) before (red) and after (black) multi-level filtering was performed.

RESULTS

For the analysis we used a minimum ditch depth of 0.3 m and maximum width of 8 m. Only the final data of the model after filtering was used for data analysis. The preliminary ditch data in binary images were not analyzed. Buffer zones of 2 m were created for both reference and modeled data, which were analyzed by converting them to raster format. Accuracy of the modeled ditch data is evaluated by comparison of modeled pixels with reference pixels in the test areas using a confusion matrix (Fig. 4). The confusion matrix is made for each resolution as well as for each interpolation method. Several metrics, such as recall, precision, errors of omission and commission were calculated using the confusion matrix (Tables 1, 2).

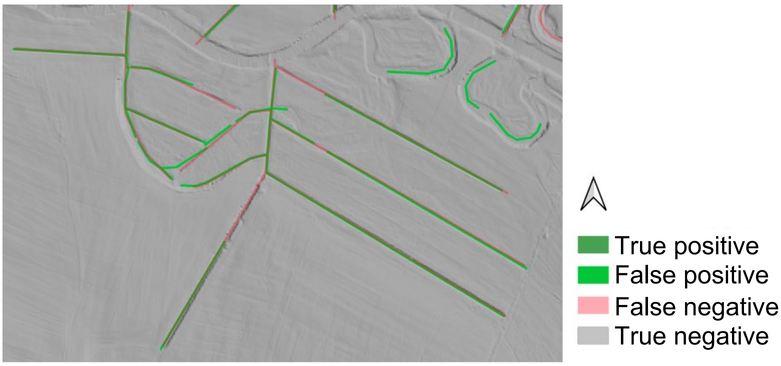

Figure 4. Example of area, where confusion matrix analysis was done.

Given that the confusion matrix is more suitable for raw raster pixel comparison and that our chosen method of analysis should be considered with caution when comparing results with other studies of this type, the Jaccard index was also used to assess the accuracy of the model (Real & Vargas 1996). In this case, 3 m buffer zones are created around the reference ditch vector data and the total length of modeled ditches in the sample areas that overlap with the reference data in the given deviation is determined.

Table 1. Evaluation of the model performance of mapping drainage ditches using DEM in 1 m resolution and 3 different interpolation methods

1 m resolution	Binning	Bicubic	Bilinear
Recall, %	85	86	85
Accuracy, %	98	99	98
Precision	0.77	0.78	0.77
Error of omission, %	15	14	15
Error of commission, %	23	22	23
Jaccard index for overlapping lines in 3 m distance	0.89	0.9	0.89

The results show small but considerable differences in the performance of the model in identifying ditches at both DEM resolutions and the chosen interpolation method. The highest model recall and precision, as well as the smallest errors of omission and commission, using DEM in 1 m horizontal resolution is obtained, when Bicubic interpolation method is applied (Table 1). There is no considerable difference in performance between Binning and Bilinear interpolation methods, where all measures, including Jaccard index, are identical.

When DEM with 0.5 m resolution is used, all metrics have higher accuracy regardless of the interpolation method applied. However, the Bicubic interpolation method shows a significant difference between all parameters in comparison to other methods. The values of the error of omission and error of commission, as well as Jaccard index approves that in Latvia, taking in account the defined drainage ditch morphometric parameters in agricultural lands, this method offers the highest performance from those compared in this study.

Table 2. Evaluation of model performance of mapping drainage ditches using DEM in 0.5 m resolution and 3 different interpolation methods

0.5 m resolution	Binning	Bicubic	Bilinear
Recall, %	88	89	87
Accuracy, %	98	98	98
Precision	0.79	0.81	0.79
Error of omission, %	12	11	13
Error of commission, %	21	19	21
Jaccard index for overlapping lines in 3 m distance	0.91	0.93	0.91

DISCUSSION

The main difference between our study and research results published earlier is the focus area; earlier studies have mainly focused on relatively small and specially selected sample areas (Sofia et al., 2011; Cazorzi et al., 2013; Kiss et al., 2015; Rapinel et al., 2015; Roelens et al., 2018a). To the date we have not found any studies, where national-level LiDAR data sets have been used, covering large areas for automated decryption of the ditch area. The above mentioned studies mostly use laser scanning data from individual missions implemented specially for these studies, which have a higher density of bare ground points. In our case the focus is on the LiDAR data sets acquired within the scope of the National scale program, with relatively low bare ground point density of 1.5–2.0 points m^{-2}, as well as larger and more robust testing area is used. The study implemented in Belgium (Roelens et al., 2018b) used DEM, as well as the point cloud approach, resulting in significantly different results between both methods; however, the error of omission and error of commission in this study are similar those obtained in our study.

The accuracy and consistency of the obtained results comparing with the reference data in our study are significantly higher compared to other studies. It should also be noted that different methods have been applied in the compared studies to assess the performance of the models, so this is not an unambiguous aspect to evaluate.

Performing individual flights with an unmanned aircraft provides an opportunity to obtain a higher density of points, as well as multispectral and RGB images, thus resulting in a wider range of interpretations in the assessment of the overgrowth and technical condition of ditches. This approach provides a wide range of possibilities for classification and monitoring of ditches, as multispectral scenes allow the calculation of different vegetation and moisture indices (Rapinel et al., 2015; Roelens et al 2017).

Acquisition of such data would allow to calculate vegetation and moisture indices. It would be important for the continuation of our study to integrate national scale and local data sets, as they, in combination with LiDAR data, provide a wide range of options for data interpretation. The combination of these data would be valuable within the scope of further studies on the development of a tool for automatic classification of ditches and assessment of their technical condition to be used on a country or local scale analysis.

The assessment of the technical condition of ditches using combined remote sensing data would be very useful, given that the ditch networks have basically unknown, but potentially significant effects on the greenhouse gas (GHG) balance, which EU countries will have to report in the National GHG inventories (Peacock et al., 2021).

CONCLUSIONS

1. The elaborated methodology for identifying drainage ditch network using LiDAR data can be used to map ditches over large areas.
2. In agricultural landscapes the elaborated method demonstrated very high accuracy, similar to the studies, where smaller, individual flight campaign-based sample areas were analyzed.
3. The highest metric parameters were obtained using DEM in 0.5 m resolution, when Bicubic interpolation method was applied.
4. Threshold values should be considered seriously to improve model performance, especially, when mapping is done outside agricultural lands.
5. Further studies with the aim to identify natural stream networks, classify drainage ditch networks and analyze their impact on hydrological regime, and to assess the potential usage for ditch area and volume calculations, which can be used for GHG emission inventory, must be done to extend the field of application of the elaborated method.

ACKNOWLEDGEMENTS. The study is implemented within the scope of the project 'Evaluation of impact of land use soil and climate factors on greenhouse gas (GHG) emission for drainage ditches' (No. LZP-2020/2-0193) funded by the program of 'Fundamental and Applied Research'.

REFERENCES

Anderson, E.S., Thompson, J.A., Crouse, D.A., Austin, R.E. 2006. Horizontal resolution and data density effects on remotely sensed LIDAR-based DEM. *Geoderma*, **132**(3–4), 406–415.

Audet, J., Wallin, M.B., Kyllmar, K., Andersson, S. & Bishop, K. 2017. Nitrous oxide emissions from streams in a Swedish agricultural catchment. *Environmental science, Agriculture Ecosystems. Environment* **236**, 295–303.

Bryndal, T. & Kroczak, R. 2019. Reconstruction and characterization of the surface drainage system functioning during extreme rainfall: the analysis with use of the ALS-LIDAR data - the case study in two small flysch catchments (Outer Carpathian, Poland). *Environmental Earth Sciences* **78**, 215.

Cazorzi, F., Fontana, G.D., Luca, A.D., Sofia, G. & Tarolli, P. 2013. Drainage network detection and assessment of network storage capacity in agrarian landscape. *Hydrology Processes* **27**, 541–553.

Hasselquist, E.M., Lidberg, W., Sponseller, R.A., Ågren, A. & Laudon, H. 2018. Identifying and assessing the potential hydrological function of past artificial forest drainage. *Ambio* **47**, 546–556.

Ivanovs, J. & Lupiķis, A. 2018. Identification of wet areas in forest using remote sensing data. *Agronomy research* **16**(5), 2049–2055.

Kiss, K., Malinen, J. & Tokola, T. 2015. Forest road quality control using ALS data. *Can. J. Forest Research* **45**, 1636–1642.

Latvian Geospatial information agencie (LGIA). 2017. ALS data, and its processing. *Fotogrammetrijas diena 2017*.

Lepistö, A., Räike, A., Sallantaus, T. & Finér, L. 2021. Increases in organic carbon and nitrogen concentrations in boreal forested catchments – Changes driven by climate and deposition. *Science on The Total Environment* **780**, 146627.

Lidberg, W., Nilsson, M., Lundmark, T. & Ågren, A.M. 2017. Evaluating preprocessing methods of digital elevation models for hydrological modelling. *Hydrological Processes* **31**(26), 4660–4668.

Lidman, F., Boily, Å., Laudon, H. & Köhler, S.J. 2017. From soil water to surface water-how the riparian zone controls element transport from a boreal forest to a stream. *Biogeosciences* **14**, 3001–3014.

Melniks, R., Ivanovs, J. & Lazdins, A. 2019. Method for shallow drainage ditch generation using remote sensing data. *Proceedings of the 9th International Scientific Conference Rural Development 2019*, 149–154.

Moussa, R., Voltz, M. & Andrieux, P. 2002. Effects of the spatial organization of agricultural management on the hydrological behaviour of a farmed catchment during flood events. *Hydrological Processes* **16**, 393–412.

Passalacqua, P., Belmont, P. & Foufoula-Georgiou, E. 2012. Automatic geomorphic feature extraction from lidar in flat and engineered landscapes. *Water Resources* **48**, 1–18.

Peacock, M., Audet, J., Bastviken, D., Cook, S., Evans, D., Grinham, A., Holgerson, M.A., Högbom, L., Pickard, A.E., Zieliński, P. & Futter, M.N. 2021. Small artificial waterbodies are widespread and persistent emitters of methane and carbon dioxide. *Global Change Biology* **00**, 1–15.

Rapinel, S., Hubert-Moy, L., Clément, B., Nabucet, J. & Cudennec, C. 2015. Ditch network extraction and hydrogeomorphological characterization using LiDAR-derived DTM in wetlands. *Hydrology Research* **46**, 276.

Real, R., Vargas, J.M., 1996. The Probabilistic Basis of Jaccards's Index of Similarity. *Systematic Biology* **45**(3), 380–385.

Roelens, J., Dondeyne, S., Van Orshoven, J., Diels, J. 2016. Extracting cross sections and water levels of vegetated ditches from LiDAR point clouds. *International Journal of Applied Earth Observation and Geoinformation*. **53**, 64–75.

Roelens, J., Höfle, B., Dondeyne, S., Van Orshoven, J. & Diels, J. 2018a. Drainage ditch extraction from airborne LiDAR point clouds. *ISPRS Journal of Photogrammetry and Remote Sensing* **146**, 409–420.

Roelens, J., Rosier, I., Dondeyne, S., Van Orshoven, J. & Diels, J. 2018b. Extracting drainage networks and thei connectivity using LiDAR data. *Hydrological Processes* **32**(8), 1026–1037.

Roelens, J., Van Orshoven, J., Dondeyne, S. & Diels, J. 2017. Extraction and connection of artificial drainage networks in agricultural areas using LiDAR data. *Communications in agricultural and applied biological sciences* **82**(1). National Symposium on Applied Biological Sciences. Leuven, Belgium, pp. 19–19.

Sofia, G., Tarolli, P., Cazorzi, F., Dalla Fontana, G. 2011. An objective approach for feature extraction: distribution analysis and statistical descriptors for scale choice and channel network identification. *Hydrology and Earth System Sciences* **15**, 1387–1402.

Vaze, J., Teng, J. & Spencer, G. 2010. Impact of DEM accuracy and resolution on topographic indices. *Environmental Modelling & Software* **25**(10), 1086–1098, ISSN 1364-8152.

Agronomy Research **20**(2), 326–340, 2022
https://doi.org/10.15159/AR.22.027

Non-destructive identification of defects and classification of Hass avocado fruits with the use of a hyperspectral image

D.A. Metlenkin[1,*], Y.T. Platov[1], R.A. Platova[1], E.V. Zhirkova[1] and O.T. Teneva[2]

[1]Plekhanov Russian University of Economics, Faculty of Trade Economics and Commodity Science, Department of Commodity Science, Stremyanny lane 36, RU115054 Moscow, Russia
[2]University of Plovdiv 'Paisii Hilendarski', Faculty of chemistry, Department of Chemical Technology, 24 Tsar Assen Str., BL4000 Plovdiv, Bulgaria
[*]Correspondence: Metlenkin.DA@rea.ru

Received: January 15th, 2022; Accepted: April 19th, 2022; Published: May 2nd, 2022

Abstract. Sensory analysis and instrumental analytical methods are used in determining the maturity and quality monitoring of avocado fruits, which are labor-intensive and do not allow the determination of fruit quality in real time. The use of hyperspectral imaging (HSI) methods in the range of 400–1,000 nm and of the multivariate analysis was demonstrated for a non-destructive grading of Hass avocado fruits into quality classes according to the number of hidden defects. Using the sensory analysis, avocado fruits were separated into quality classes according to the number of defects after being stored for 10 days. Development of a classification model included several steps: image recording and analysis using the ANOVA and PCA method, image segmentation (selection of ROI), pre-processing (SNV-correction, centering), selection of a multivariate classification method (PLS-DA, SIMCA) and a spectral range, model verification. The analysis of hyperspectral images of avocado fruits has detected spectral regions with the maximal variance responsible for the change of the content of pigments and moisture within the avocado fruit exocarp. Comparison of PLS-DA and SIMCA models on the basis of best accuracy and test-validation results was carried out. Comparison of models showed SIMCA model as the most efficient model for fruit classification into quality classes depending on the number of hidden defects. The implementation of the developed approach as a digital avocado fruit sorting system at different stages of the product life cycle is proposed.

Key words: HSI, sensory analysis, chlorophyll, multivariate analysis, PCA, PLS-DA, SIMCA.

INTRODUCTION

Fresh avocado fruits from the evergreen tropical plant (*Persea americana Mill.*) are persistently in high demand by consumers due to their high nutritional qualities and the ability to be consumed fresh (Ferreira da Vinha et al., 2013; Hurtado-Fernandez, 2018). Post-harvest losses in the supply chain of fresh avocado fruits are between 25% and 50% of the total yield and affect economic indicators of suppliers and sales organizations

(Bustos & Moors, 2018). In this connection, the control of avocado fruit quality is one of the most important challenges in improving the economic distribution efficiency.

The development and ripening stages of avocado fruits are important in determining the minimum quality requirements that allow continuing the ripening process and achieving the consumer maturity (UNECE, 2019). The quality control of avocado fruits including maturity testing is done both by a sensory analysis (ISO 6658:2005 2017), for example by determining a skin (exocarp) color and by instrumental methods: fruit hardness measurement with the use of a penetrometer (Ochoa-Ascencio et al., 2009), measurement of moisture, MS%, and dry matter, DM%, determining lipid content in pulp (mesocarp) (Donetti & Terry, 2014).

In addition to the labor intensity and the destructive character one of the defects of said instrumental methods is the increased risk of marketing substandard fruits and the increased losses in the distribution chain because of the fruit quality heterogeneity in a large batch. In recent years attempts are made to use a non-destructive technology for fruit quality control, in particular imaging methods such as: spectral analysis methods (Raman imaging, multi- and hyperspectral imaging, fluorescent visualization and laser light backscatter imaging), nuclear magnetic methods (magnetic resonance imaging and soft X-ray imaging) and other methods including thermal, infra-red thermography and microwave imaging (Hussain, 2018; Avotins et al., 2020; Starý et al., 2020).

The HSI method (Lohumi et al., 2015; Abdulridha et al., 2019) is considered as the advanced non-destructive instrumental method of fruit and vegetable control. As opposed to the other spectroscopy methods, the HSI technology permits: first, scanning the whole sample and thereby considering the heterogeneity of samples and segmenting the image into the regions of interest (ROIs); second, hyperspectral images also generate a set of information both in VIS- and in NIR-ranges while presenting both spatial and spectral information of the objects (Elmasry et al., 2012; Manley, 2014). Most HSI-cameras are intended for recording the information in VIS-/NIR-spectral ranges. The HSI and the multivariate analysis allow monitoring and controlling the product quality within the PAT concept (Process Analytical Technology - PAT) (Rodionova & Pomerantsev, 2006). For analyzing hyperspectral images multivariate analysis methods: classification and quantification are used (Granato et al., 2018; Ferraz et al., 2019).

Due to the integration of the principal functions of imaging and spectroscopy the HSI method is used both for monitoring the ripeness (Pinto et al., 2019) and for forecasting the values of physical and chemical properties of avocado fruits (Pu et al., 2015; Vega Díaz et al., 2021). The HSI for avocado quality control was used for assessing the dry matter content as shown in (Vega Díaz et al., 2021). With the use of the HSI in the range of 400–1,000 nm and a support vector machine regression the authors achieved a significant accuracy ($R^2 = 0.9$) in the prediction of dry matter content of Hass avocado fruits. The classification of avocado fruits according to the ripening stage is possible with the use of the HSI in the range of 300–900 nm and of different ripeness indices (Pinto et al., 2019).

The principal cause of the decline of avocado fruit quality indices is superficial and hidden defects that appear and are manifested at different stages of the product life cycle. The problem in identifying superficial and hidden defects of Hass avocado fruits is related to the peculiarities of exocarp color, which is characterized by a darker shade by contrast with other avocado varieties and depends on a quantitative ratio of pigments at different ripeness stages. So, there is a need in the development of a procedure of identification of hidden avocado fruit defects with the use of a real-time HSI-technology.

The identification of defects is one of the complicated tasks of the control of fruit quality indices because of the diversity of defect types (Bhargava & Bansal, 2021). The review (Bhargava & Bansal, 2021) provides the studies on the identification of defects of fruits and vegetables: apples, pears, bananas, potatoes, cucumbers etc. The article (Patel et al., 2019) presents the study involving the identification of superficial defects of mango with the use of spectroscopy methods and the HSI-technology.

The studies show that a hyperspectral image of an apple and mango skin (Elmasry et al., 2009; Rivera et al., 2014) can be used not only for predicting the ripening stage but also for determining internal damages and hidden defects. The fruits characterized by a leathery dark skin like avocado are not used for developing non-destructive quality monitoring technologies (Magwaza & Tesfay, 2015; Arendse et al., 2018). Therefore, the development of a non-destructive method of monitoring the quality and detecting hidden defects of Hass avocado fruits with the use of a sensory analysis of the condition of exo- and mesocarp is topical and is intended to decrease the loss at all stages of the product life cycle.

It is evident that the identification of defects in individual fruits in a large batch with the use of the HSI-technology would allow grading them in real-time into groups of uniform quality and hence to decrease the amount of waste.

The goal of the study consists in the development of a non-destructive method of identifying (detecting) defects of avocado fruits and their classification according to the number of defects into quality classes with the use of the HSI methods and the multivariate analysis.

MATERIALS AND METHODS

Objects of the study were taken from the commercial batch avocado fruits, in which defects were determined by organoleptic method. The objects of the study involved the samples of premium Hass avocado fruits (n = 10) (country of origin: Tanzania; yield of 2021) which were selected from one batch and used for developing a chemometric classification model into quality classes according to the number of defects.

The avocado fruits were stored for 10 days (the storage life established by the supplier is 14 days) in a refrigerator at t = 4 °C. The samples of avocado fruits were distributed after the storage among quality classes by the number of defects in accordance with the provisions of the standard (UNECE, 2019).

The sensory analysis of avocado fruit exocarp was performed before the storage, after 10 days of storage at t = 4 °C exo- and mesocarp of the samples were investigated. Hass avocado fruits had specific external characters: oval shape, leathery and bosselated exocarp. The fruits were closely sized, healthy, clean, at the stage of consumer maturity, not overrippen, without significant mechanical damages, without excessive external humidity, with a carefully cut off fruit stem. In two samples of Hass avocado fruits (No 4 and 5) minor superficial defects were detected as wrinkles and corking on the skin, respectively.

According to the sensory analysis the avocado fruits were separated into three classes (Table 1) in accordance with (UNECE, 2019): critical defects - 'crit'; slight superficial defects - 'slight'; healthy fruits, no defects - good quality 'good'). According to the standard (UNECE, 2019), avocados are classified into three classes: 'Extra' Class, Class I, Class II, which classes are generally distinguished by a number of minor superficial defects. So, for Class I the area of mesocarp defects shall not exceed 4 cm^2 and for Class II - 6 cm^2. So, following the sensory analysis, the avocado fruits having intolerable defects were placed into an individual category Crit.

Modelling of avocado fruit grading into quality classes according to the number of defects with the use of the HSI-technology includes several steps: image recording and analysis using the ANOVA and PCA method, image segmentation (selection of ROI), pre-processing (SNV-correction, centering), selection of a multivariate classification method and a spectral range, model verification.

Hyperspectral images were obtained with the hyperspectral camera Specim IQ (Spectral Imaging Ltd, Finland) in the range of 400–1,000 nm (204 bands). For obtaining the images the image illuminated region with a halogen lamp QL 500BW Falcon Eyes. The illumination angle was 30° to achieve an even illumination of the samples. The hyperspectral camera was placed in the top part of the illuminated region with the lamp at a distance of 30 cm from the samples. The following hyperspectral images were obtained: 2 images of each side of all ten fruits (with the half turn). A similar building of a hyperspectral image database is provided in the study (Wedding et al., 2011). The obtained hyperspectral images were imported to a PC for a subsequent processing.

During the analysis of hyperspectral images and the development of models of avocado fruit classification into quality classes according to the number of defects the following multivariate methods have been used: variance analysis (ANOVA) and principal component analysis (PCA), partial least squares discriminant analysis (PLS-DA), soft independent modelling of class analogies (SIMCA), in Albedo 4.0.23 (MFTI, Russia) (Strakhov et al., 2013) and Prediktera Breeze ver. 2021.1.0 (Prediktera AB, Sweden) software applications. Data obtained by ANOVA and PCA was used as pseudocolors to build an RGB-image for estimating the fruit condition and confirming wavelengths that are significantly responsible for the total variance of hyperspectral images. The PLS-DA is a generic chemometric method for multivariate discrimination and classification of data (Zontov et al., 2020) based on the use of PLS2 regression for the correlation between the **X** predictor matrix / the **Y** response matrix and dummy variables. SIMCA in its turn is also a method for data classification based on the analysis of samples from each class by PCA.

The classification modeling included the segmentation of hyperspectral images with the use of ROI selection (the whole fruit, ellipses), preprocessing of spectral data: Standard Normal Variate (SNV-correction) and centering. Centering is the subtraction of the mean value from each variable to analyze the variance about the mean. The SNV-correction is a transformation that separates light scattering effects from spectral data by centering and scaling individual spectra. During the chemometric modelling the SNV-correction (Barnes et al., 1989) was used to reduce the effects of multicollinearity and background shift in a hyperspectral image.

The model verification was performed using the accuracy index (%) and during the test-validation using the test-validation accuracy index, %. During test-validation of classification models 30% of HSI data (different ROI's of 3 avocado fruits) was used as a test set of samples.

RESULTS AND DISCUSSION

Sensory analysis

The results of the sensory analysis of avocado fruit condition before and after storage are presented in Table 1.

Table 1. Condition of avocado fruit exocarp before and after storage

Sample number	Description of avocado fruit condition from the sensory evaluation	
	Before storage	After storage / quality class
1	No defects	Anthracnose / crit
2	No defects	Anthracnose / crit
3	No defects	Damages resulting from a low temperature / slight
4	Skin defect (wrinkles)	Skin defect (wrinkles) / slight
5	Skin defect (corking)	Skin defect (corking) / slight
6	No defects	No defects / good
7	No defects	Skin defect (wrinkles) / slight
8	No defects	No defects / good
9	No defects	Skin defect (wrinkles) / slight
10	No defects	No defects / good

The sensory analysis of the condition of exo- and mesocarp performed after the storage of avocado fruit has detected the following:

- Avocado fruit sample No. 5 (Fig. 1, a) was characterized by an exocarp corking however no changes in the mesocarp consistency were detected. The defect is related to tolerable ones, for it does not lead to critical changes of the fruit pulp;
- Avocado fruit sample No. 3 (Fig. 1, b) was characterized by a local mesocarp darkening and softening. The detected defect was supposedly due to the exposure of the fruit to a low temperature but was tolerable, as the area of the damaged pulp did not exceed 6 cm2. Specific signs of chilling do not appear at once but 12–48 hours later, so this defect can be related to hidden ones;
- Samples No. 4, 7 and 9 (Fig. 1, c) were characterized by a skin defect as wrinkles. The study of the mesocarp has detected a minor pulp softening but the change was not of a progressive pattern, what allows relating it to tolerable defects;
- Two avocado fruit samples (No. 1 and 2) developed critical defects (Fig. 1, d) within the storage period. Rounded brownish black depressed spots were recorded on the surface of the avocado fruits and the pulp under the affected skin area became dark and softened. Said signs correspond to the fungal disease - the anthracnose crown rot (ACR) induced by *Colletotrichum gloeosporioides* (Lu et al., 2017). Microorganisms and fungi present in air and on the fruit surface can penetrate into fruit tissues via various microdamages of the exocarp when the fruits are harvested, packed and transported. As the fungal disease is quickly transmitted to healthy fruits, it is important to detect these critical defects at an early stage to remove the damaged fruits from the bulk of the batch;
- Avocado fruit samples No. 6, 8 and 10 were characterized by the absence of defects of exo- and mesocarp. The development of tolerable and critical defects of the fruits was not recorded. The sensory analysis of the avocado fruits allowed observing the enhancement of the ripening stage characterized by the skin browning and the decreased mesocarp density.

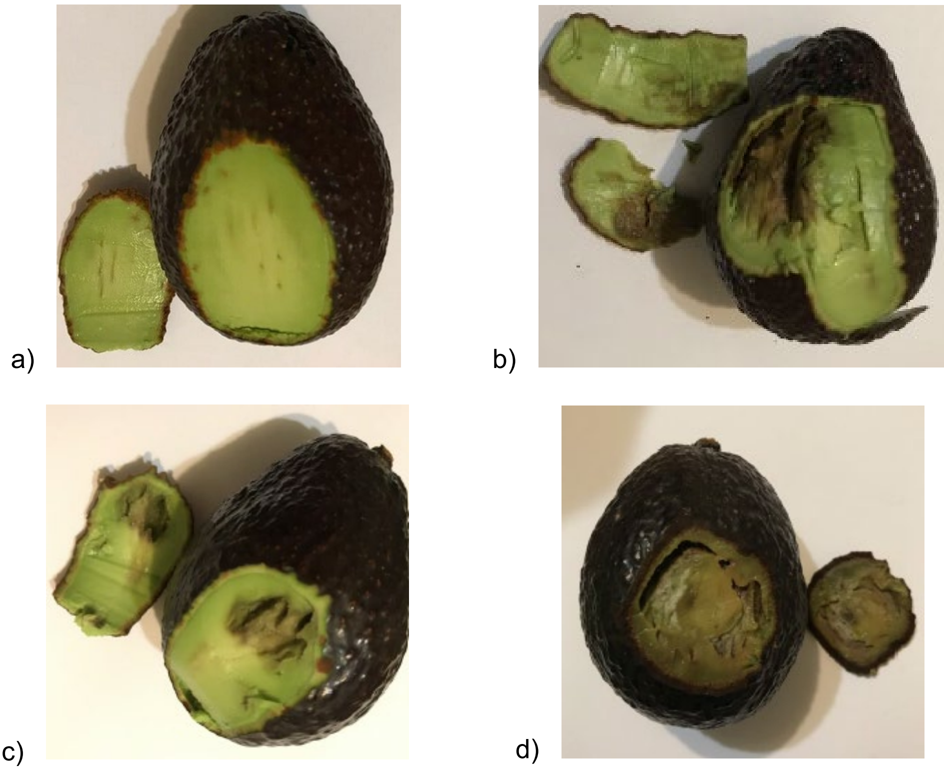

Figure 1. Mesocarp of avocado fruit samples with different superficial skin defects: a) No. 5 with corking – without mesocarp changes; b) No. 3 with the defects resulting from the low temperature exposure – local browning and change in mesocarp density; c) No. 4 with wrinkles – insignificant loss of mesocarp density; d) No. 2 with the signs of a disease (anthracnose) – significant darkening and loss of the pulp density.

During the storage of avocado fruits in the presence of oxygen a number of natural oxidative processes are promoted followed among other by the activation of enzymes. The modification of avocado mesocarp density is related to the transformation of protopectin to pectin, it is enhanced as the maturation progresses and is accompanied by the disintegration of the pulp plant tissue and the increased moisture (Obenland et al., 2012). At the same time a significant reduction of the fruit pulp density relative to the exocarp results in the formation of voids under the skin and in a more active exposure of avocado fruit pulp to oxygen, what accelerates the oxidation. According to the performed studies (Lyu, 2019) in overripe avocado fruits the oxidation leads to critical defects (significant darkening of the pulp, deterioration of consumer properties). A late detection of avocado fruit hidden defects that are rapidly developed during the after-ripening can result in the decrease of quality indices of the whole batch of avocado fruits and in the increase of storage losses. The specification of the classes established by the standard (UNECE, 2019) was used to generate a reliable and accurate classification model, which will allow determining fruits with hidden and intolerable defects quickly and taking a decision on the optimal shelf life and period of sale of avocado fruits.

An average response of the spectral signatures of avocado fruits of the three classes (see Sensory analysis) is shown in Fig. 2. Spectral signatures was selected after assigning category for each avocado fruit using whole fruit ROI from four hyperspectral images.

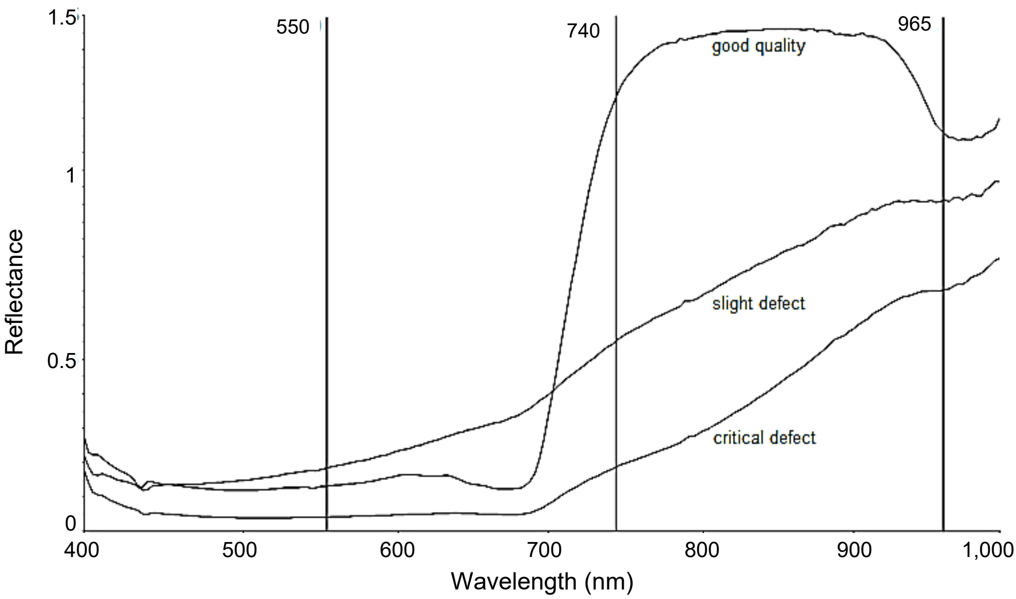

Figure 2. Average response of the spectral signatures of avocado fruits classified into 3 classes: Good, Slight and Crit.

So for increasing the efficiency of grading of a large batch of avocado fruits the use of the HSI-technology is proposed to detect superficial and hidden (internal) defects.

Hyperspectral image analysis by the ANOVA method. According to the variance estimation of hyperspectral image data, spectral wavelengths with the maximal variance at 550, 740 and 965 nm were selected. Principal distinctions in spectral signatures of avocado fruits were analyzed within spectral wavelengths with the maximal variance at 550, 740 and 965 nm:

- The reflection band at 550 nm corresponds to chlorophyll reflection (Matsuda et al., 2012). During the sensory analysis of avocado fruits having anthracnose signs a significant darkening of the exocarp was recorded. It is related to the degradation of chlorophyll *a* to pheophytin *a* (Milenković et al., 2012) which is enhanced during the bacteriological damage of fruits and is accompanied among others with the mesocarp darkening. The comparison of absorption spectral signatures showed the shift of the chlorophyll *a* absorption band from 666 nm to 672 nm for avocado fruit samples with anthracnose signs.
- The red-edge spectral region including the wavelength range from 690 to 750 nm (Croft & Chen, 2017) correlates with the physiological condition of plants. According to (Curran et al., 1990) the red-edge region is susceptible to the changes in chlorophyll content and the maximal slope in the red-edge region is indicative of the fruit ripeness stage. The study (Lyu, 2019) also notes that the reflection in the red-edge region is reduced progressively as the avocado fruits are ripening and notably

over-ripening. As shown in Fig. 1 the red-edge spectral region is closely related to the number of defects in avocado fruits: the maximal slope for the samples with the mold damage of exocarp and the minimal slope for the fruits without defects. For fruits with defects from the slight and crit quality classes the NIR-spectrum in the range of 700–970 nm has lower reflection values than for undamaged fruits from the 'good' class.

- The spectral region of 900 to 965 nm is corresponding to the first overtone of the OH stretch frequency (Ollinger, 2011; Joe & Gopal, 2017). Avocado fruit ripening is accompanied by the reduction of water mass fraction with the increase of lipid and dry matter mass fraction, pit darkening and the development on the fruits of the exocarp color characteristic of the variety (Clark et al., 2003). Possibly, the differences in the reflection intensity at 965 nm are due to chlorophyll modification processes and a subsequent change in refractive properties of cells manifested in the near-infrared range (Croft & Chen, 2017).

The wavelengths with the maximal variance were assigned to pseudocolors and were used to build an RGB-image (Fig. 3, a): 550 nm - green, 740 nm - red, 965 nm - blue. According to the RGB- image (Fig. 3, a) avocado fruits are graded into quality classes by the number of defects: fruits of slight and crit quality classes have a blue pseudocolor (965 nm), the anthracnose fruits have a higher blue color over the whole surface; fruits of the good quality class have a green pseudocolor (550 nm), what is connected with the absence of chlorophyll degradation processes. A RGB-image with the use of pseudocolors allows estimating the fruit condition and confirming wavelengths that are significantly responsible for the total variance of a hyperspectral image selected by the ANOVA variance analysis.

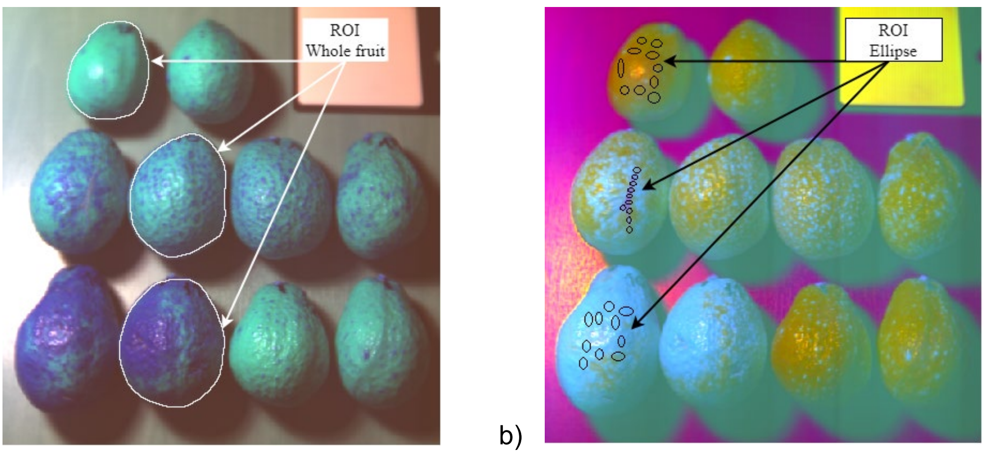

a) b)

Figure 3. RGB-image of avocado fruits with the use as colors of a) spectrum wavelengths; b) principal components. The figure a) shows the segmentation of a hyperspectral image by selecting a whole fruit as ROI, the figure b) – ROI are ellipses.

The analysis of a hyperspectral image of avocado fruit samples was performed by the principal component analysis method. Following the analysis four principal components (PC) were determined: the first, the second, the third and the fourth PC in a combination account for 99.9% of the total variance (81.6%, 15.5%, 1.8% and 0.9%, respectively).

Test coefficients showing the correlation of reflection coefficients at the wavelengths for 1–4 PCs are provided in Fig. 4. The data were used to interpret the PCs.

The first PC accounting for 81.6% of the total variance is related to all reflection coefficients of the spectrum wavelengths, is presented with the sign (+) over the whole spectral range and possibly is responsible for the total variance and correlation between the pixels (including the pixels of avocado samples) of the hyperspectral image (Fig. 4).

For the 2nd PC according to the sign (+/–) and the wavelength test coefficients the spectrum is divided into two ranges: the sign (+) is related to test coefficients of the spectrum wavelengths corresponding to the VIS-range, the sign (–) is related to the NIR-range (Fig. 4). By analogy with the test coefficients according the 1st PC, the 2nd PC is related to all reflection coefficients of the spectrum wavelengths but separates the range of values by the sign (+/–).

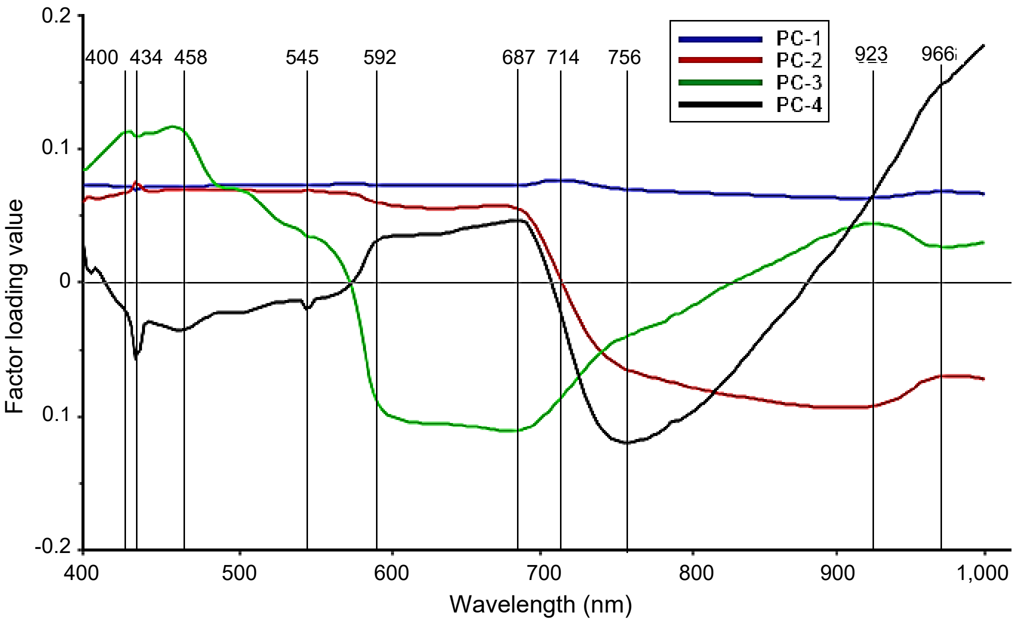

Figure 4. Line loadings plot of PCA.

For the 3rd PC crests of bands were detected that are attributed to carotenoid pigments (429, 434 and 458 nm) (Hooijschuur et al., 2015) and to the 1st overtone of OH (923 nm) with the sign (+), to chlorophyll *a* (687 nm) and chlorophyll *b* (592 nm and 603 nm) (Croft & Chen, 2017) with the sign (–). The test coefficients at 592 and 687 nm are related to a decrease of chlorophyll content in avocado fruits. The reduction of chlorophyll concentration during storage increases the content of carotenoid pigments in the exocarp of avocado fruits. The increase of lutein (a yellow pigment related to the class of carotenoid pigments) content in the skin and pulp of an avocado fruit during ripening is supported by the studies (Ashton et al., 2006). So, the interpretation of the 3rd PC is connected with the change of reflection in the band range of chlorophyll and lutein during storage within the exocarp of avocado fruits without hidden defects, the ripening stage of the fruits being not critical.

For the 4th PC crests of bands were detected that are attributed to anthocyans (545 nm) (Merzlyak et al., 2003), carotenoids (434 and 458 nm), the red-edge crest (756 nm) with the sign (–) against the 1st overtone of OH (923 and 966 nm), chlorophyll *a* (687 nm) and chlorophyll *b* (592 nm) with the sign (+). As shown in the study (Ashton et al., 2006) anthocyan content in avocado fruit exocarp is increased as Hass avocado fruits are over-ripening. At the same time the reflection band at 545 nm with the sign (–) corresponding to the reflection of anthocyans acts as an indicator of the critical ripening state of avocado fruits and as an indirect indicator of the fruit bacterial damage (Ashton et al., 2006). Such avocado fruits have to be quickly sorted and removed from the bulk of the batch to reduce storage losses. It its turn the maximal value of the test coefficients for the 4th PC with the sign (–) at 750 nm corresponds to the red-edge spectral region, what correlates to the physiological condition of the plants. In view of the foregoing, it is determined that the 4th PC is responsible for the fruit degradation process considering the test coefficient extrema with the sign (–) at 545 and 750 nm.

According to the interpretation of the PCs and their contribution to the total variance three PCs were selected which were assigned to pseudocolors (1st PC - red, 3rd PC - green, 4th PC - blue) and the following RGB-image (Fig. 3, b) was developed. According to the figure (Fig. 3, b) the 4th PC detects defective avocado fruits which are presented by a blue pseudocolor.

The RGB-images (Fig. 3) with the use of pseudocolors were used for the HSI segmentation and the development of a classification model. Based on the obtained RGB-images different regions of interest (ROI's) of avocado fruit surface were selected: whole fruit, ellipses as circles about a place of defect.

During the selection of ROIs, the shape and the intensity of spectral signatures of avocado fruits from three quality classes (Fig. 3) were considered. The ROI selection was carried out manually by the segmentation of a whole avocado fruit and by the selection of 10 spectral signatures as ellipses from each fruit. During the selection of ellipse ROIs a hyperspectral image was magnified to define exactly the boundaries of a healthy skin surface of avocado fruits and a defect one. Once being segmented each ROI was assigned to classification variables - quality classes according to the number of defects. Each ROI both of a whole fruit and of an ellipse represents an average response of the spectral signature of an avocado fruit from one of the three quality classes.

The classification of avocado fruits into quality classes according to the number of defects by multivariate analysis methods was performed with the use of different multivariate classification methods (Torres & Amigo, 2020), regions of interest and spectral ranges (Jia et al., 2020). For increasing the accuracy of the final models the calibration was performed with the selection of regions of interest - ellipses (n = 10) on avocado fruits from different quality classes. The advantage of the selection of such regions of interest is in that for each class determined according to the number of defects it is possible to select more variables, to increase respectively the prediction reproducibility and adequacy. The SNV (Standard Normal Variate) - correction and centering were used as a pre-processing of hyperspectral image data. At the pre-modelling stage data smoothing by Savitzky-Golay method was also used but the obtained results in the model accuracy were not satisfactory (not shown in the Table).

Whole fruits (n = 5) over the total area were selected as the regions of interest for the prediction, what is required for a correct quality monitoring after the development of a model. Modelling results are presented in Table 2.

Table 2. Multivariate models of Hass avocado classification according to the defects

Method	Region of interest (ROI)	Average spectrum		
		Spectral range, nm	Training Accuracy, %	Test-validation Accuracy, %
PLS-DA	Whole fruit	400–1,000	0	0
	Whole fruit	500–990	100.0	40.0
	Ellipse	400–1,000	100.0	60.0
	Ellipse	500–990	100.0	80.0
SIMCA	Whole fruit	400–1,000	36.4	20.0
	Whole fruit	500–990	36.4	20.0
	Ellipse	400–1,000	93.3	80.0
	Ellipse	500–990	**100.0**	**100.0**

The grading of avocado fruits into quality classes is supported by the sensory analysis including the sensory analysis of a mesocarp condition after hyperspectral images are recorded. For developing a classification model three classes were used according to the sensory analysis of quality classes: 1) Crit - fruits with the marked skin anthracnose (critical defects); Slight - fruits with damages resulting from a low temperature, an excessive external moisture, skin corking and skin wrinkles (minor superficial defects); Good - fruits without defects.

When modelling, a low accuracy of the models with the use of whole fruits as the ROIs was recorded, it is related to data sets that are not sufficient for classification: with the use of whole fruit ROIs the number of variables for calibration was 10, while with the use of ellipse ROIs the number was 100 (10 ellipses from 10 fruits). Among others a low accuracy of the models with the use of whole fruit ROIs is determined by the incorporation in the ROIs of spectral signatures of shadows and reflections caused by a high illumination of the samples with a halogen lamp. The increased accuracy of classification models depending on the selection of a spectral range is also recorded: excluding the region of 400–500 nm (weak signal with a low reflection intensity or the absence of a signal), excluding the region of 990–1,000 nm (significant noises). So, the number of predicting variables and the selection of a spectral range has a direct effect on the accuracy of classification models.

According to the results of modelling and test-validation the SIMCA model with the use of ellipses as the ROI's in the range of 500–990 nm was selected as the most representative one. During modelling critical distances (Dcrit) between the classes were selected. The SIMCA Cooman's model diagram within the model coordinates Good (X-axis) and Crit (Y-axis) is presented in Fig. 5. A higher accuracy and efficiency of the SIMCA model as compared to the PLS-DA model is related to the structure of the used data (Pomerantsev & Rodionova, 2018): the class Good is used as a target one and the classes Crit and Slight can be considered as one class including defects of various degree. With this data structure one class is implied to be located in the middle and the remained classes occupy the periphery (Pomerantsev & Rodionova, 2018). According to (Oliveri & Downey, 2012; Pomerantsev & Rodionova, 2014) SIMCA is a classifier of one class, so in the case of classification of avocado fruits according to the number of defects it is a more efficient algorithm as opposed to PLS-DA.

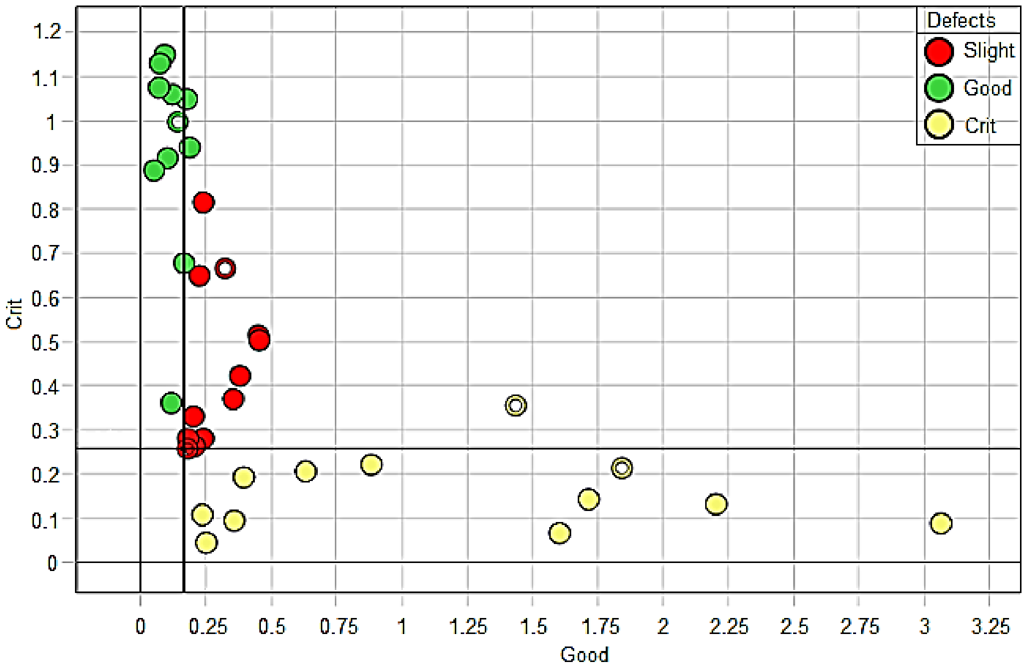

Figure 5. Coomans plot of SIMCA model.

Upon the completion of the records of hyperspectral images a SIMCA multivariate model was built to classify avocado fruits into quality classes according to the number of defects. The quality and accuracy of the obtained model are supported by the test-validation with the accuracy of 100% (Table 2).

However, the developed SIMCA model is not suitable for sorting other avocado varieties, due to differences in exocarp color characteristics of other avocado varieties such as Fuerte or Pinkerton. Comparing the results with similar approaches, it should be noted that deep learning algorithms are structurally different from traditional machine learning or multivariate methods and have dramatically more parameters (Hu et al., 2021). Thus, implementing deep learning algorithms to build an effective classification model of avocado fruits might be a challenging task both for a developer and an operator. Proposed approach provides diagnostic tools, intuitive modelling and rapid predictions (Vikström, 2021) that can be applied *on-line* with performance comparable to modern deep learning algorithms.

CONCLUSIONS

The potential of using a hyperspectral image in a visual-near infrared range and the multivariate analysis has been shown for the non-destructive identification of hidden defects of avocado fruits. The analysis of a hyperspectral image of avocado fruits by ANOVA and PCA algorithms has detected spectral regions responsible for the presence within avocado fruits of pigments and moisture and correlating to physiological condition of the fruits and the number of hidden defects. RGB-image based on data obtained by ANOVA and PCA as pseudocolors was used for estimating the fruit condition and selection of different ROI's of avocado fruit surface. For grading avocado fruits into quality classes (the number of hidden defects) different regions of interest of hyperspectral images and multivariate analysis method - PLS-DA, SIMCA were used. The SIMCA method allowed building a classification model of avocado fruits with the accuracy of 100%. The use of the proposed approach permits grading avocado fruits into quality classes without using destructive methods. The current study could form the basis for future R&D projects and implementation of digital avocado fruit sorting systems in retail quality control laboratories.

REFERENCES

Abdulridha, J., Batuman, O. & Ampatzidis, Y. 2019. UAV-based remote sensing technique to detect citrus canker disease utilizing hyperspectral imaging and machine learning. *Remote Sensing* **11**(11), 1373.

Arendse, E., Fawole, O. A., Magwaza, L. S. & Opara, U. L. 2018. Non-destructive prediction of internal and external quality attributes of fruit with thick rind: A review. *Journal of Food Engineering* **217**, 11–23.

Ashton, O.B., Wong, M., McGhie, T.K., Vather, R., Wang, Y., Requejo-Jackman, C. & Woolf, A. B. 2006. Pigments in avocado tissue and oil. *Journal of Agricultural and Food Chemistry* **54**(26), 10151–10158.

Avotins, A., Kviesis, K., Bicans, J., Alsina, I. & Dubova, L. 2020. Experimental Analysis of IoT Based Camera SI-NDVI Values for Tomato Plant Health Monitoring Application. *Agronomy Research* **18**(S2), 1138–1146.

Barnes, R.J., Dhanoa, M.S. & Lister, S.J. 1989. Standard normal variate transformation and Detrending of near – infrared duffuse reflectance spectra, *Journal of Applied Spectroscopy* **43**(5), 772–777.

Bhargava, A. & Bansal, A. 2021. Fruits and vegetables quality evaluation using computer vision: A review. *Journal of King Saud University-Computer and Information Sciences* **33**(3), 243–257.

Bustos, C.A. & Moors, E.H. 2018. Reducing post-harvest food losses through innovative collaboration: Insights from the Colombian and Mexican avocado supply chains. *Journal of Cleaner Production* **199**, 1020–1034.

Clark, C.J., McGlone, V.A., Requejo, C., White, A. & Woolf, A.B. 2003. Dry matter determination in 'Hass' avocado by NIR spectroscopy. *Postharvest Biology and Technology* **29**(3), 301–308.

Croft, H. & Chen, J.M. 2017. Leaf pigment content, comprehensive remote sensing. doi:10.1016/B978-0-12-409548-9.10547-0

Curran, P.J., Dungan, J.L. & Gholz, H.L. 1990. Exploring the relationship between reflectance red edge and chlorophyll content in slash pine. *Tree physiology* **7**(1–2–3–4), 33–48.

Donetti, M. & Terry, L.A. 2014. Biochemical markers defining growing area and ripening stage of imported avocado fruit cv. Hass. *Journal of Food Composition and Analysis* **34**(1), 90–98.

ElMasry, G., Wang, N. & Vigneault, C. 2009. Detecting chilling injury in Red Delicious apple using hyperspectral imaging and neural networks. *Postharvest biology and technology* **52**(1), 1–8.

Elmasry, G., Kamruzzaman, M., Sun, D.W. & Allen, P. 2012. Principles and applications of hyperspectral imaging in quality evaluation of agro-food products: a review. *Critical reviews in food science and nutrition* **52**(11), 999–1023.

Ferraz, G.A.S., Ferraz, P.F.P., Martins, F.B., Silva, F.M., Damasceno, F.A. & Barbari, M. 2019. Principal components in the study of soil and plant properties in precision coffee farming. *Agronomy Research* **17**(2), 418–429.

Ferreira da Vinha, A., Moreira, J. & Barreira, S. 2013. Physicochemical parameters, phytochemical composition and antioxidant activity of the algarvian avocado (Persea americana Mill.). *Journal of Agricultural Science* **5**(12), 100–109.

Granato, D., Putnik, P., Kovačević, D.B., Santos, J.S., Calado, V., Rocha, R.S. & Pomerantsev, A. 2018. Trends in chemometrics: Food authentication, microbiology, and effects of processing. *Comprehensive Reviews in Food Science and Food Safety* **17**(3), 663–677.

Hooijschuur, J.H., Verkaaik, M.F., Davies, G.R. & Ariese, F. 2015. Raman spectroscopy for future planetary exploration: photodegradation, self-absorption and quantification of carotenoids in microorganisms and mineral matrices. *Journal of Raman Spectroscopy* **46**(10), 856–862.

Hu, X., Chu, L., Pei, J., Liu, W. & Bian, J. 2021. Model complexity of deep learning: A survey. *Knowledge and Information Systems* **63**(10), 2585–2619.

Hurtado-Fernandez, E., Fernandez-Gutierrez, A. & Carrasco-Pancorbo, A.E. 2018. Exotic Fruits. Avocado fruit–Persea americana. In: *Exotic Fruits*, F. Federal University of Ceará, Ed. Ceará, Brazil: Elsevier, 37–48.

Hussain, A., Pu, H. & Sun, D.W. 2018. Innovative nondestructive imaging techniques for ripening and maturity of fruits–a review of recent applications. *Trends in Food Science & Technology* **72**, 144–152.

Jia, B., Wang, W., Ni, X., Lawrence, K.C., Zhuang, H., Yoon, S.C. & Gao, Z. 2020. Essential processing methods of hyperspectral images of agricultural and food products. *Chemometrics and Intelligent Laboratory Systems* **198**, 103936.

Joe, A.A.F. & Gopal, A. 2017. Identification of spectral regions of the key components in the near infrared spectrum of wheat grain. In *2017 International Conference on Circuit, Power and Computing Technologies (ICCPCT)* (pp. 1–5). IEEE.

Lohumi, S., Lee, S., Lee, H. & Cho, B.K. 2015. A review of vibrational spectroscopic techniques for the detection of food authenticity and adulteration. *Trends in Food Science & Technology* **46**(1), 85–98.

Lu, J., Ehsani, R., Shi, Y., Abdulridha, J., de Castro, A.I. & Xu, Y. 2017. Field detection of anthracnose crown rot in strawberry using spectroscopy technology. *computers and electronics in agriculture* **135**, 289–299.

Lyu, Y. 2019. *Identify the ripening stage of avocado by multispectral camera using semi-supervised learning on small dataset*. PhD Theses. Hong Kong University of Science and Technology. https://repository.ust.hk/ir/Record/1783.1-102308

Magwaza, L.S. & Tesfay, S.Z. 2015. A review of destructive and non-destructive methods for determining avocado fruit maturity. *Food and bioprocess technology* **8**(10), 1995–2011.

Manley, M. 2014. Near-infrared spectroscopy and hyperspectral imaging: non-destructive analysis of biological materials. *Chemical Society Reviews* **43**(24), 8200–8214.

Matsuda, O., Tanaka, A., Fujita, T. & Iba, K. 2012. Hyperspectral imaging techniques for rapid identification of Arabidopsis mutants with altered leaf pigment status. *Plant and Cell Physiology* **53**(6), 1154–1170.

Merzlyak, M.N., Solovchenko, A.E. & Gitelson, A.A. 2003. Reflectance spectral features and non-destructive estimation of chlorophyll, carotenoid and anthocyanin content in apple fruit. *Postharvest biology and technology* **27**(2), 197–211.

Milenković, S.M., Zvezdanović, J.B., Anđelković, T.D. & Marković, D.Z. 2012. The identification of chlorophyll and its derivatives in the pigment mixtures: HPLC-chromatography, visible and mass spectroscopy studies. *Adv. Technol.* **1**(1), 16–24.

Obenland, D., Collin, S., Sievert, J., Negm, F. & Arpaia, M.L. 2012. Influence of maturity and ripening on aroma volatiles and flavor in 'Hass' avocado. *Postharvest biology and technology* **71**, 41–50.

Ochoa-Ascencio, S., Hertog, M.L. & Nicolaï, B.M. 2009. Modelling the transient effect of 1-MCP on ‘Hass’ avocado softening: A Mexican comparative study. *Postharvest Biology and Technology* **51**(1), 62–72. doi: 10.1016/j.postharvbio.2008.06.002

Oliveri, P. & Downey, G. 2012. Multivariate class modeling for the verification of food-authenticity claims. *TrAC Trends in Analytical Chemistry* **35**, 74–86.

Ollinger, S.V. 2011. Sources of variability in canopy reflectance and the convergent properties of plants. *New Phytologist* **189**(2), 375–394.

Patel, K.K., Kar, A. & Khan, M.A. 2019. Potential of reflected UV imaging technique for detection of defects on the surface area of mango. *Journal of food science and technology* **56**(3), 1295–1301.

Pinto, J., Rueda-Chacón, H. & Arguello, H. 2019. Classification of Hass avocado (persea americana mill) in terms of its ripening via hyperspectral images. *TecnoLógicas* **22**(45), 111–130. doi: 10.22430/22565337.1232

Pomerantsev, A.L. & Rodionova, O.Y. 2018. Multiclass partial least squares discriminant analysis: Taking the right way – A critical tutorial. *Journal of Chemometrics* **32**(8), e3030.

Pomerantsev, A.L. & Rodionova, O.Y. 2014. Concept and role of extreme objects in PCA/SIMCA. *Journal of Chemometrics* **28**(5), 429–438.

Pu, Y.Y., Feng, Y.Z. & Sun, D.W. 2015. Recent progress of hyperspectral imaging on quality and safety inspection of fruits and vegetables: a review. *Comprehensive Reviews in Food Science and Food Safety* **14**(2), 176–188.

Rivera, N.V., Gómez-Sanchis, J., Chanona-Pérez, J., Carrasco, J.J., Millán-Giraldo, M., Lorente, D. & Blasco, J. 2014. Early detection of mechanical damage in mango using NIR hyperspectral images and machine learning. *Biosystems Engineering* **122**, 91–98.

Rodionova, O.E. & Pomerantsev, A.L. 2006. Chemometrics: achievements and prospects. *Advances in chemistry* **75**(4), 302–321 (in Russian).

Starý, K., Jelínek, Z., Kumhálová, J., Chyba, J. & Balážová, K. 2020. Comparing RGB - based vegetation indices from UAV imageries to estimate hops canopy area. *Agronomy Research* **18**(4), 2592–2601.

Strakhov, P.V., Nikolenko, A.A., Chaban, L.N., Shurygin, B.M. 2013. Software for processing hyperspectral images ‘Albedo’ // *Proc. of the 56th Scientific Conference of MIPT*: All-Russian Scientific Conference ‘Actual Problems of Fundamental and Applied Sciences in the Modern Information Society’, All-Russian Youth Scientific Innovation Conference ‘Physical and Mathematical Sciences: Current Problems and Their Solutions’), Dolgoprudny, 25– 30 November 2013, Moscow: MFTI, 1, 89–91 (in Russian).

Torres, I. & Amigo, J.M. 2020. An overview of regression methods in hyperspectral and multispectral imaging. *Data Handling in Science and Technology* **32**, 205–230.

UNECE STANDARD FFV-42. 2019. ‘Concerning the marketing and commercial quality control of Avocados’. Agricultural Quality Standards, Geneva, Switzerland.

Vega Díaz, J.J., Sandoval Aldana, A.P. & Reina Zuluaga, D.V. 2021. Prediction of dry matter content of recently harvested ‘Hass’ avocado fruits using hyperspectral imaging. *Journal of the Science of Food and Agriculture* **101**(3), 897–906. doi: 10.1002/jsfa.10697

Vikström, A. 2021. A comparison of different machine learning algorithms applied to hyperspectral data analysis.

Wedding, B.B., White, R.D., Grauf, S., Wright, C., Tilse, B., Hofman, P. & Gadek, P.A. 2011. Non-destructive prediction of ‘Hass’ avocado dry matter via FT-NIR spectroscopy. *Journal of the Science of Food and Agriculture* **91**(2), 233–238.

Zontov, Y.V., Rodionova, O.Y., Kucheryavskiy, S.V. & Pomerantsev, A.L. 2020. PLS-DA–A MATLAB GUI tool for hard and soft approaches to partial least squares discriminant analysis. *Chemometrics and Intelligent Laboratory Systems* **203**, 104064.

Agronomy Research **20**(2), 341–356, 2022
https://doi.org/10.15159/AR.22.023

Morphological and anatomical characterization of *Actinidia kolomikta* (Rupr. & Maxim.) Maxim. (C3) and *Amaranthus tricolor* L. (C4) leaves

S. Motyleva[1,*], E. Vlasova[1], N. Kozak[1], M. Gins[2] and V. Gins[2]

[1]Federal Horticultural Research Center for Breeding, Agrotechnology and Nursery, 4 Zagorevskaj Str., RU115598 Moscow, Russia
[2]Federal Scientific Center of Vegetable Growing, 14 Selectnaya Str., Moscow region, Odintsovsky urban district, RU143080 VNIISSOK village, Russia
[*]Correspondence: motyleva_svetlana@mail.ru

Received: February 1st, 2022; Accepted: March 27th, 2022; Published: April 27th, 2022

Abstract. Morphological and anatomical features of new cultivars with photosynthesis of C3 (*Actinidia kolomikta* (Rupr. & Maxim.) Maxim. cv. 'Narodnaya') and C4 (*Amaranthus tricolor* L. cv. 'Valentina') were established by light and scanning electron microscopy, as well as energy-dispersive analysis. The leaf lamina of *Actinidia kolomikta* cv. 'Narodnaya' has a dorsoventral anatomical structure, anomocytic stomata on the abaxial epidermis and two types of trichomes: multicellular, uniseriate hairs and multicellular bristle-like protrusions, containing raphids. The needle-like raphides are located in subepidermal layers along the veins. A vascular system of petiole consists of two upper concentric bundles and the crescentic vascular strand. A starch sheat is present. Raphides (needle-shaped and rectangular) are located in phloem and cortical parenchyma cells, contain Ca, K, Mg, P and Si. The leaf lamina of *Amaranthus tricolor* cv. 'Valentina' have the kranz-anatomy, dorsiventral mesophyll and contain druses. Betacyanins are concentrated in the epidermis and mesophyll, but are not present in the bundle sheath. The number of vascular bundles in petioles is odd-numbered and variable (from 5 to 13). Trichomes are multicellular, uniseriate, ending in a large oval cell. Cells with betacyanins are present in the epidermis cortex, and, rarely, the collenchyma and phloem of the petiole. Cells with betaxanthins are absent. A starch sheat is brightly pigmented with betacyanins. The crystall sand is deposited in the parenchyma cells of the cortex and pith of the petiole and contains Ca (mainly) and K oxalates. Druses in the leaf lamina additionally contain Mg and P.

Key words: *Actinidia kolomikta* (Rupr. & Maxim.) Maxim., *Amaranthus tricolor* L., leaf, mineral inclusions, morphology, betacyanins, light microscopy, scanning electron microscopy, energy dispersive analysis.

INTRODUCTION

An anatomical and morphological survey in plant breeding is carried out for identify signs of authenticity of new varieties, markers of adaptability, as well as limits of intraspecific variability (Lotova, 2011; Crivellaro & Schweingruber, 2015; Durnova et al., 2021).

The accumulation of calcium oxalate crystals is a normal activity closely integrated with metabolism of the photosynthetic organisms. It has been suggested that crystals play a significant role in maintaining the ion balance of the cell, in plant protection, in mechanical support of tissues, in detoxification, in light harvesting and reflection (Franceschi & Horner, 1980; Semenova & Romanova, 2011). However, the causes of the crystal formation and their physiological role remain insufficiently established (McConn & Nakata, 2002).

Another controversial issue is the physiological role of betalains and anthocyanins in the vegetative organs of plants. These substances, which have antioxidant properties, are thought to increase the photostability of leaves and stems, to protect against increased levels of UV radiation, and to defense against pathogenic fungal infection (Close & Beadle, 2003; Solovchenko & Merzlyak, 2008; Flexas et al., 2012).

The life-forms of the *Actinidiaceae* Gilg & Werderm. are represented by perennial woody vines and shrubs with climbing shoots. These plants use C3 photosynthesis. The anatomical structure of the stem of *Actinidia kolomikta* (Rupr. & Maxim.) Maxim is typical for dicotyledonous plants. Collateral vascular tissues without separate bundles are arranged in a ring around the core (Condon, 1992; Clearwater & Clark, 2003; Roy et al., 2020). There are raphides and mucilage in shoots and leaves (Ferguson, 2011). White and pink areas appear on the green leaves during the budding - flowering phase. The bleaching areas of leaves turn pink if they are in direct sunlight. The pink color of the leaves is associated with anthocyanins synthesis (Kolbasina et al., 2007; Wang et al., 2015).

The genus *Amaranthus* L. differs from typical dicotyledonous plants by many physiological and anatomical characteristics. Amaranth is characterized by high drought, thermal and salt resistance thanks to C4 photosynthesis. Leaves are characterized by Kranz anatomy, where mesophyll cells are grouped around the cells of the bundle-membrane in a ring-like manner. This structure contributes to a faster outflow of photosynthetic products compared to C3 species (Chirkova, 1999; Zhigila et al., 2014). Amaranth leaf mesophyll contains calcium oxalate crystals (Tooulakou et al., 2016). Leaves of *Amaranthus tricolor* L. have many colors, often variegated. The purple-red color is associated with the presence of betacyanins in the vacuoles of cells, which are represented by amaranthin and isomaranthin. The presence of yellow shades is associated with the presence of betanin, iso-betanin (betaxanthins). The *Amaranthus tricolor* L. leaves also contain abundant amounts of photosynthetic and non-photosynthetic carotenoids and chlorophylls (Cai et al., 1998, 2005; Sarker & Oba, 2020a). *Amaranthus* L. species with red color of vegetative organs (*A. tricolor* L., *A. gangeticus* L.) as a rule surpasses green-leaved species (*A. dibius* K. Krause, *A. lividus* L., *A. hypochondriacus* L.) in terms of the antioxidant capacity, the total content of phenolic compounds, flavonoids, carotenoids and betalains. A high thermal and salt tolerance of *Amaranthus tricolor* L. is associated with these substances (Shu et al., 2009; Khanam & Oba, 2013; Hoang et al., 2019; Sarker & Oba, 2019a, 2019b; 2020d). In particular, an increase in the content of phenolic acids, ascorbic acid, rutin, isoquercetin, nonenzymatic antioxidants (ascorbate, carotenoids), antioxidant enzymes (superoxide dismutase (SOD) and AsA peroxidase (APX), etc.) under salt stress was found (Sarker & Oba, 2018a, 2018b, 2020c, 2020e). At the same time the leaves nutritional qualities in the content of protein, ash, energy, dietary fiber, minerals, β–carotene, vitamin C and antioxidants are increases. For this reason, *Amaranthus* *tricolor* L. is considered a promising vegetables crop for farmers in areas prone to salinization (Sarker & Oba, 2018d; Sarker et al., 2018; Sarker & Oba, 2020c). It leaves in raw form can be ingredients of salads, soups and sauces, enriching them with biologically active substances, giving them an original taste and color (White & Brown, 2010). *Amaranthus tricolor* L. is used as raw material for the production of food coloring (Gins et al., 2002).

There is an increasing interest among breeders in non–traditional crops such as *Amaranthus* L. (Svirskis, 2003; Sarker et al., 2020; Sarker & Oba, 2020b) and *Actinidia kolomikta* (Rupr. & Maxim.) Maxim (Česonienė & Daubaras, 2007) in recent years. Growing of *Amaranthus tricolor* L. cultivars is commercially and economically profitable in the Moscow region of Russia both in field and in a greenhouse (Pivovarov et al., 2019). The Federal Scientific Center of Vegetable Breeding has selected the *Amaranthus tricolor* cv. 'Valentina'. All vegetative and reproductive organs have a purple–red color of varying intensity. According to the content of amaranthin, they are arranged in the following order: inflorescences (2.2 mg g^{-1}) > leaves (1.4 mg g^{-1}) > stems (0.8 mg g^{-1}) > roots (0.15 mg g^{-1}). As the size increases, the leaf blades change color from red-purple to red-green. (Gins et al., 2002; Kononkov et al., 2018; Platonova et al., 2018).

Many countries grow actinidia species for commercial purposes (Williams et al., 2003). The high nutritional value of actinidia fruits is formed by a complex of biologically active phytochemical (organic and inorganic) components, such as ascorbic acid, phenolic compounds, amino acids, carbohydrates, fiber and minerals (Motyleva et al., 2018). *Actinidia kolomikta* (Rupr. & Maxim.) Maxim is suitable for cultivation in most regions of Russia due to high winter hardiness, early ripening of fruits and a short growing season (Kolbasina et al., 2007). The Federal Scientific Center of Breeding, Agrotechnologies and Nursery has created the *Actinidia kolomikta* cv. 'Narodnaya'.

Both cultivars cv. 'Valentina' (*Amaranthus tricolor* L.) and cv. 'Narodnaya' (*Actinidia kolomikta* (Rupr. & Maxim.) Maxim.) are successfully grown in the Central region of Russia. In previous years, these cultivars were used as models of C3 and C4 plants for comparative evaluation of the leaves physiological and biochemical properties (Motyleva et al., 2021). Knowledge of the leaves anatomical structure, and, in particular, tissue localization of non-photosynthetic pigments and crystals is necessary for further comprehensive and objective assessment of their functional properties. Therefore, we investigated leaves of *Amaranthus tricolor* cv. 'Valentina' and *Actinidia kolomikta* cv. 'Narodnaya' the plants of which which differ significantly in life–forms, anatomical structure and physiological properties.

MATERIALS AND METHODS

A vegetation experiment with amaranth and actinidia plants was conducted during 2020–2021. The plants of both species were grown in natural conditions with artificial protection from precipitation. The experimental site was located at an altitude of 168 m above sea level. Geographical coordinates 55° 7′ 27″ north latitude, 37° 56′ 55″ east longitude. The climate is temperate continental.

Seeds of *Amaranthus tricolor* L. cv. 'Valentina' were sown in boxes. The seedlings were transplanted one by one into plastic pots (with a diameter and height of 250 and 175 mm, respectively). Two-year-old plants *Actinidia kolomikta* (Rupr. & Maxim.) Maxim. cv. 'Narodnaya' were also individually planted into plastic pots (300 and 230 mm in diameter and height, respectively). In total, 20 pots with amaranth and actinidia plants were planted (Fig. 1).

a) b)

Figure 1. General view of the plants of *Actinidia kolomikta* (Rupr. & Maxim.) Maxim. cv. 'Narodnaya' (a) and *Amaranthus tricolor* L. cv. 'Valentina' (b).

The pots were filled with a mixture of peat and sand (5:1) and had a drainage layer at the bottom. In the pots with the control samples, the substrate moisture was kept at the level of 45–50% for amaranth and 54–60% for actinidia. The soil moisture was determined using the SOIL moisture meter MC–7828 SOIL. Average environmental indicators of the experimental period: day/night temperatures 17.2 °C / 11.7 °C, relative moisture 64%, daytime length 17 h.

The leaves of the middle part were used for all analyzes.

Light microscopy. There were 20 plants taken for every cytological examination. Anatomical analyses were carried out on native material at different stages of ontogenesis without stains and fixatives. Longitudinal and cross sections of fresh matter were cut by hand and microtom (Microm HM 430). Sections were placed in a drop of water, looked and photographed through a 10x or 40x objective of a Zeiss (Jena, Germany) Axiostar plus light microscope equipped with a Digital Camera Canon Power Shot A640 (zoom from 4.0 to 16.0).

Scanning Electron Microscopy. To visualize the microstructure of the adaxial and abaxial surfaces of the leaves, as well as to fulfill the mineral composition of the inclusions, an analytical scanning electron microscope (REM) JEOL JSM–6010 LA (JEOL Ltd, Japan) was used. The die-cuts of 5 mm × 5 mm were taken to the left and right of the central veins from at least 10 leaves and placed on carbon tape mounted on the microscope stage. The cross-sections of the leaves with a thickness of 0.5–1 mm were fixed perpendicular to the surface of the table. The leaves were not pre-treated, as microscopy was carried out under low vacuum conditions (60 Pa) and the deformation of the cross–sections was negligible.

Energy dispersive analysis. The mineral composition was determined by energy dispersion spectrometry (EDS) along with a scanning electron microscope in accordance with the technique of Motyleva (2018) and Motyleva et al. (2021). EDS was used for qualitative and quantitative analysis of available elements in X-ray spectra obtained by scanning the observed image with an electron beam. X-ray microanalysis data were obtained in accordance with standard protocols and included an image of the microstructure of the sample under study, a table of data in weight and atomic percentages, spectra and histograms. An example of spectral data is shown on Fig. 2. Ten measurements were taken for each sample. The local analytical area was 3 mm and the scanning area was at least 12 µm. The mean quadratic deviation did not exceed 1.2–6.9%.

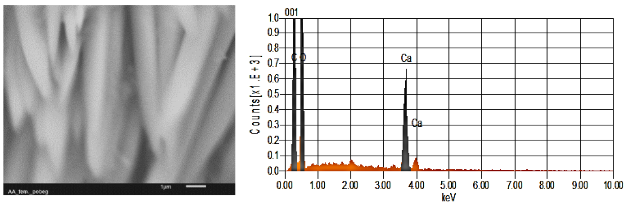

Chemical	Mass, %	Atom, %	Sigma
C	45.47	55.81	0.04
O	43.57	40.15	0.15
Ca	10.96	4.04	0.13
Total	100	100	

Figure 2. The scanned area, the spectrogram and the table of results in the EDS analysis interface.

RESULTS AND DISCUSSION

Actinidia kolomikta (Rupr. & Maxim.) Maxim. cv. 'Narodnaya'

The epidermis cells on both sides of the leaf lamina of *Actinidia kolomikta* (Rupr. & Maxim.) Maxim. cv. 'Narodnaya' have the same irregular, elongated, rarely oval shape (Fig. 3).

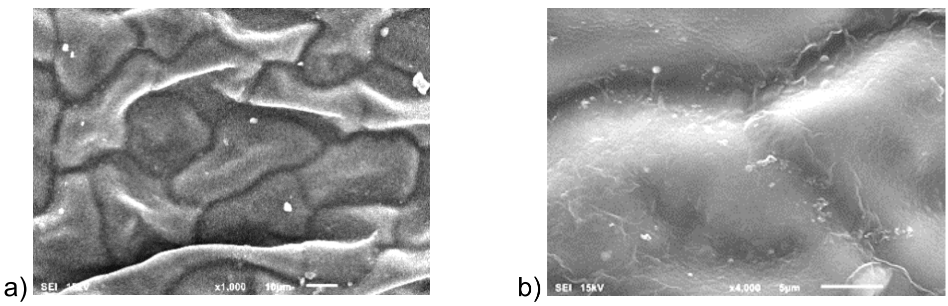

Figure 3. Microstructures of the adaxial surface of *Actinidia kolomikta* (Rupr. & Maxim.) Maxim. cv. 'Narodnaya' leaves under 1,000× (a) and 4,000× (b) magnification.

The abaxial surface is more folded than adaxial. Anomocytic stomata are present only on the abaxial surface. They are located evenly at the level of the leaf surface or slightly buried. There are stomatal characteristics: the length from 12.07 to 16.96 µm, elongated shape, pronounced rings. The wax layer evenly covers the epidermis on both sides of the leaf lamina (Fig. 4). It has smooth or slightly bumpy structure, what is clearly visible at 4,000 x magnification (Figs 3–4).

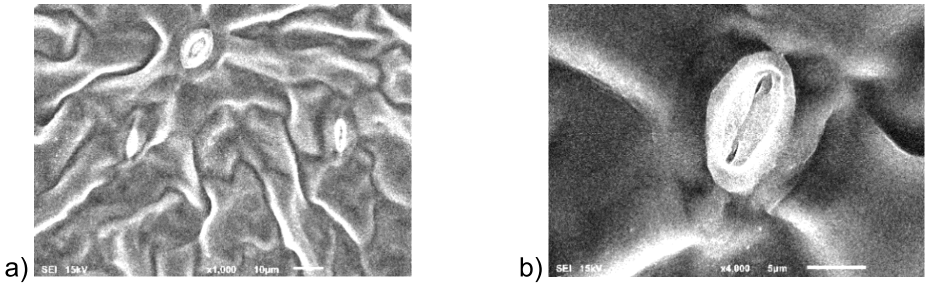

Figure 4. Microstructures of the abaxial surface of *Actinidia kolomikta* (Rupr. & Maxim.) Maxim. cv. 'Narodnaya' leaves under 1,000× (a) and 4,000× (b) magnification.

There are long, multicellular, uniseriate trichomes with an average length of 243.4–375.8 µm on the midrib vein on both sides of the leaf lamina. In addition, rare uniseriate hairs consisting of 2–3 segments are located along secondary veins on the abaxial surface (Fig. 5).

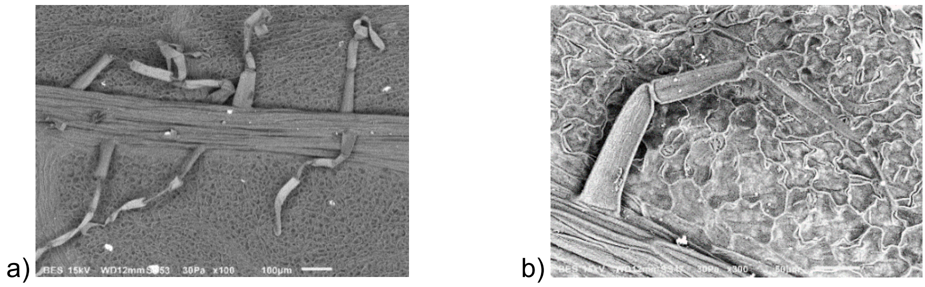

Figure 5. Trichomes of the abaxial surfaces of *Actinidia kolomikta* (Rupr. & Maxim.) Maxim. cv. 'Narodnaya' leaves under 100× (a) and 300× (b) magnification.

Multicellular bristle - like protrusions above a thin vascular bundle are also rarely found there. There are raphids inside these protrusions (Fig. 6).

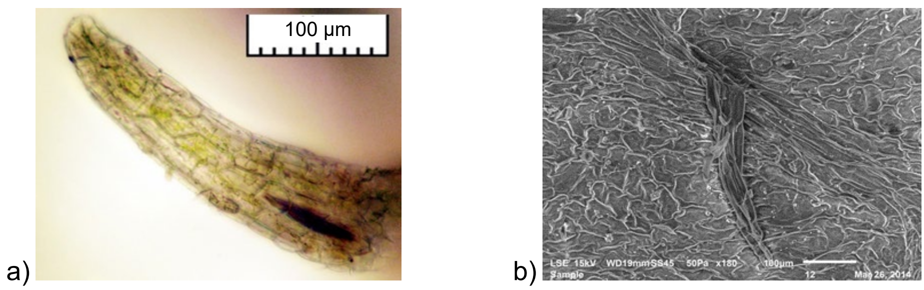

Figure 6. Multicellular bristle - like protrusions of the adaxial surface of *Actinidia kolomikta* (Rupr. & Maxim.) Maxim. cv. 'Narodnaya' leaves.

The leaf blade on the cross sections has a dorsoventral structure. However, the cells of the palisade tissue are tortuous and do not have a clear prismatic shape (Fig. 7, a).

The cross sections show that raphides are deposited in the mesophyll under the epidermis of both sides of the leaf lamina (Fig. 7, b). The plan shows that the raphides are laid mainly along the veins (Fig. 7, c).

Figure 7. Leaf lamina cross sections (a, b) and a plan of the raphids deposition on the abaxial side (c) of leaves of *Actinidia kolomikta* (Rupr. & Maxim.) Maxim. cv. ‘Narodnaya’.

Reddish areas may appear on the green leaf under unfavourable conditions. The synthesis of anthocyanins is noted in the epidermis and is often accompanied by trichomes red pigmentation (Fig. 8, a). Anthocyanin cells are also found in the palisade layer (Fig. 8, b).

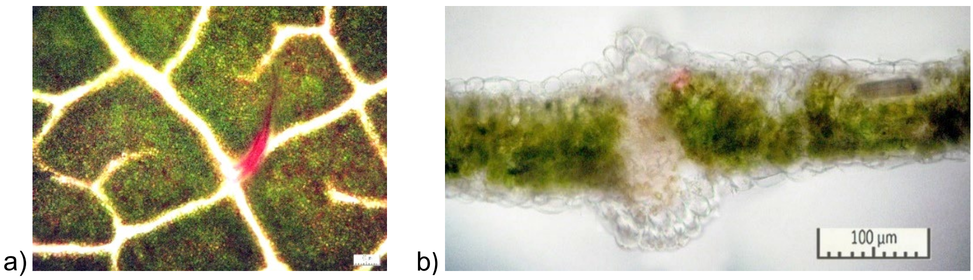

Figure 8. Plan of the adaxial surface (a) and cross section (b) of *Actinidia kolomikta* (Rupr. & Maxim.) Maxim. cv. ‘Narodnaya’ leaves containing anthocyanins.

The leaf petiole is oval and grooved in cross section (Fig. 9, a). The vascular system of petiole consists of three parts: two upper concentric bundles with an inner xylem and the crescentic vascular strand. In the middle vein of the leaf, separate bundles break off from the crescent (Fig. 9, b).

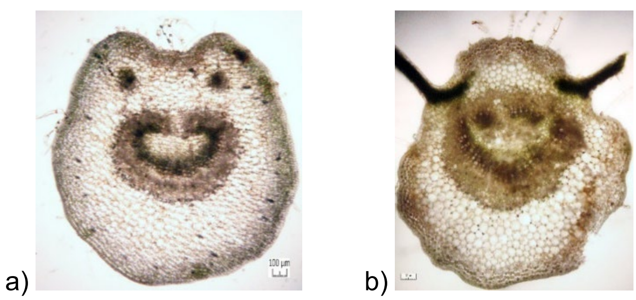

Figure 9. Cross section of the petiole (a) and the midvein (b) of *Actinidia kolomikta* (Rupr. & Maxim.) Maxim. cv. ‘Narodnaya’ leaves.

The phloem of vascular strand contains raphides. From the outside, the phloem is covered by the single-row starch sheat (endodermis). The cortical parenchyma is collenchymatous.

Raphides are packed together lengthwise in ideoblast cells of cortical parenchyma. Two types of crystals have been found. The first type is represented by needle-shaped crystals with a length of 20–25 µm and a width of 0.4–0.6 µm. The second type is in the form of a rectangular prism with a width of 5.6–6.5 µm (Fig. 10).

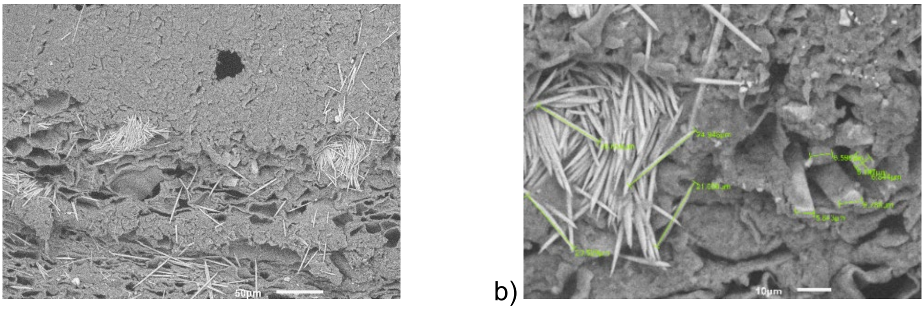

a) b)

Figure 10. Mineral inclusions on the cross section of the petiole of *Actinidia kolomikta* (Rupr. & Maxim.) Maxim. cv. 'Narodnaya' leaves: needle-shaped crystals (a) and idioblasts (raphides) with needle-shaped crystals (on the left) and rectangular crystals (on the right) (b).

In general, the presented data on the leaf morphological anatomical structure of cv. 'Narodnaya' consistent with the diagnostic characteristics of the *Actinidia kolomikta* (Rupr. & Maxim.) Maxim. (Ferguson, 2011, Motyleva et al., 2017). Of all the wide diversity of trichomes described for *Actinidiaceae* Gilg & Werderm (Watson & Dallwitz, 1992) we observed two types: multicellular, uniseriate hairs and multicellular bristle-like protrusions, containing raphids. The presented description of tissue composition of the petiole cv. 'Narodnaya' generally coincided with that of *Actinidia kolomikta* stem (Roy et al., 2020). Therefore, the presence of a starch sheat in the petioles of cv. 'Narodnaya' is quite logically, since, according to Ferguson (2011), the presence of identical layer in the stem of *Actinidia kolomikta* is a species trait. We believe that the presence of a starch sheat contributes to the high frost resistance of shoots of the *Actinidia kolomikta* compared to other *Actinidia* Lindl. species (Kolbasina et al., 2007). We have noted the appearance of anthocyanin staining of adaxial epidermis cells, trichomes and palisade mesophyll cells in connection with adaptive responses of plants to stress. This pigmentation is not associated with variegated foliage, which is noted during the flowering period (Wang et al., 2015) and may have other chemical profile (Kovinich et al., 2014, 2015).

***Amaranthus tricolor* L. cv. 'Valentina'**

The adaxial surface of leaves of *Amaranthus tricolor* L. cv. 'Valentina' has chaotically arranged segmented trichomes 80–100 µm long and small stomata (8.51 µm). The shape of epidermal cells is irregularly polygonal (Fig. 11).

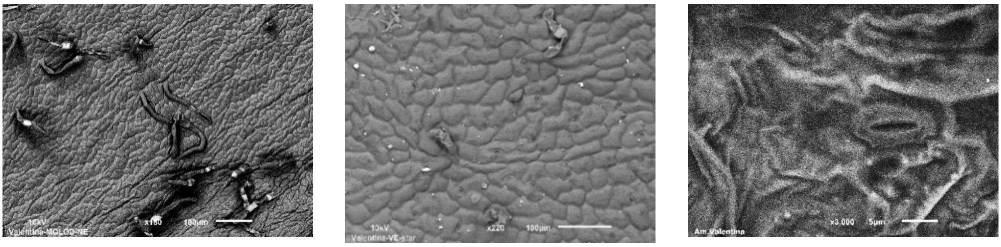

Figure 11. Microstructures of the adaxial surface of *Amaranthus tricolor* L. cv. 'Valentina' leaves under 150×, 220× and 3,500× magnification.

The abaxial surface of leaves of cv. 'Valentina' has small stomata (12.31 µm). Shape of epidermal cells is irregularly polygonal, too (Fig. 12, a, b). Some epidermal cells contain betacyanins predominantly adjacent to the stomata. Cells of abaxial epidermis are most intensively stained than adaxial one (Fig. 12, c).

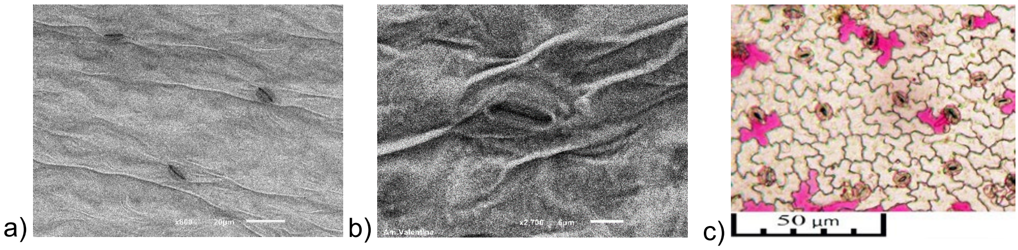

Figure 12. Microstructures of the adaxial surface of *Amaranthus tricolor* L. cv. 'Valentina' leaves under SEM, 100× (a) and 2,700× (b) magnification, and by light microscopy (c).

Leaf lamina on the cross-sections demonstrate the Kranz-type leaf anatomy inherent in C4 plants. All vascular bundles surrounded by a layer of bundles heath cells with centripetally arranged chloroplasts. In addition, there are single-row layers of mesophyll cells under the adaxial and abaxial epidermis. The leaf lamina is characterized by dorsoventral structure, since the adaxial mesophyll cells have a palisade structure and the abaxial one are spongy. Part of the mesophyll cells on both sides of the leaf lamina contain betacyanins. Their presence in the cells vacuoles does not exclude the existence of chloroplasts in the cytoplasm. There are no betacyanins in the bundles heath cells. (Fig. 13).

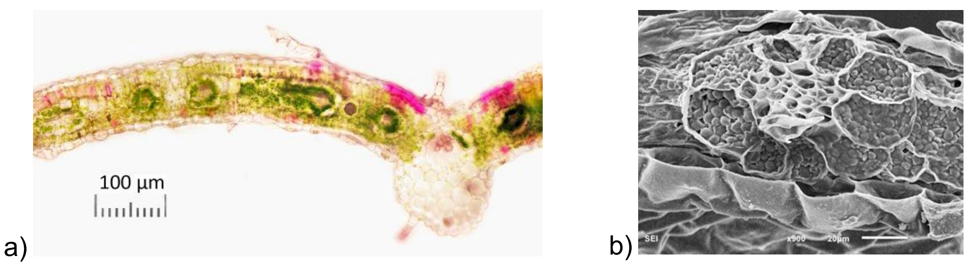

Figure 13. Cross sections of *Amaranthus tricolor* L. cv. 'Valentina' leaves under light microscopy (a). Kranz-structure: vascular bundles surrounded by a layer of bundle sheath cells. SEM, 900× magnification (b).

Large druses up to 40 microns in diameter are located between the vascular bundles (Fig. 14, a, c). The druse is an aggregate mass of small crystals (Fig.14, c). The SEM image of a cross section of the leaf shows regularly arranged druses. The average distance between the druses is 243.3 μm.

a) b) c)

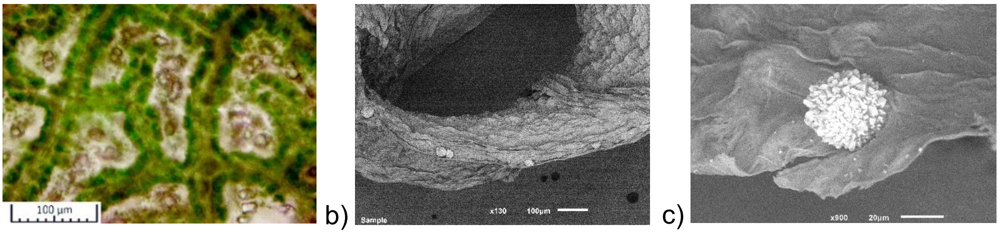

Figure 14. *Amaranthus tricolor* L. cv. 'Valentina' leaves: the plan of druses deposition under light microscopy (a), the cross sections and the druse under SEM, 130× and 900× magnification (b, c).

The petiole is fluted and winged from the middle. On the cross-section the circumference of the petiole on the adaxial side breaks by a deep groove covered with trichomes (Fig. 15, a). Under the epidermis of the petiole is a two- or three-row collenchyma. The collenchyma covers the cortical parenchyma and is interrupted in the area of small furrows where stomata are located. The vascular bundles are scattered in a semicircle around the pith. Outside, they are surrounded by a single-row endodermis brightly pigmented with betacyanins. In addition to the endodermis, cells with betacyanins are found in cortical parenchyma and in the epidermis. They are scattered randomly and condense in areas under the furrows in the cortical parenchyma. Occasionally, the presence of pink pigments in the cells of collenchyma and phloem was noted. The number of vascular bundles at the base of petioles is odd-numbered and variable. We observed from 5 to 13. The petiole passes into the midrib, gradually decreasing in diameter. At the same time, the number of vascular bundles decreases sequentially from the petiole base to the distal tip of the midvein. Collenchyma and endodermis are also gradually disappearing (Fig. 15, b).

a) b)

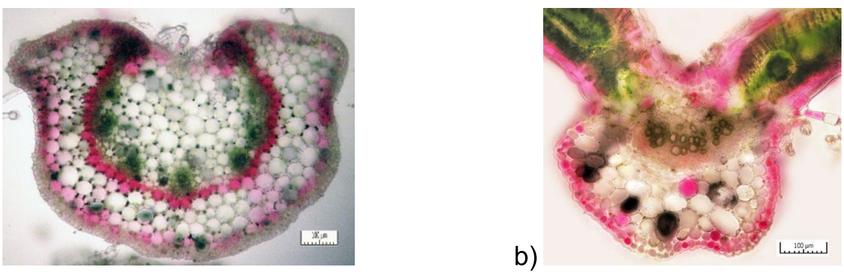

Figure 15. Cross sections of petiole (a) and midvein (b) of *Amaranthus tricolor* L. cv. 'Valentina' leaves (light microscopy).

Trichomes are multicellular, uniseriate, ending in a large oval cell in the distal tip and becoming multiseriate at the base. The hairs often contain betacyanins (Fig. 16).

According to the results of a morphological and anatomical study, we were found that the leaves of *Amaranthus tricolor* L. cv. ‘Valentina’ have a typical for C2 kranz-type of leaf anatomy. We have clarified the leaves anatomical characteristics of *Amaranthus tricolor* L. made on other samples by Arya et al. (2017), El–Ghamery et al. (2017), Hussain et al. (2018). Our data on the dorsoventral structure of the leaf lamina are coincides with description of Tsutsumi et al. (2017). We have established the variability of the number of vascular bundles at the base of petioles. Similar data were obtained on successive sections of other amaranth species (Timonin, 1984, 2011).

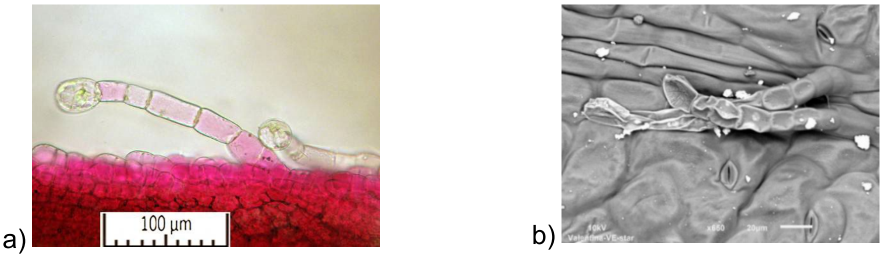

Figure 16. Trihomes of *Amaranthus tricolor* L. cv. ‘Valentina’ leaves under light microscopy (a) and SEM (b), 650× magnification.

The cortical and pith parenchyma contain idioblasts with crystal sand (Fig. 17).

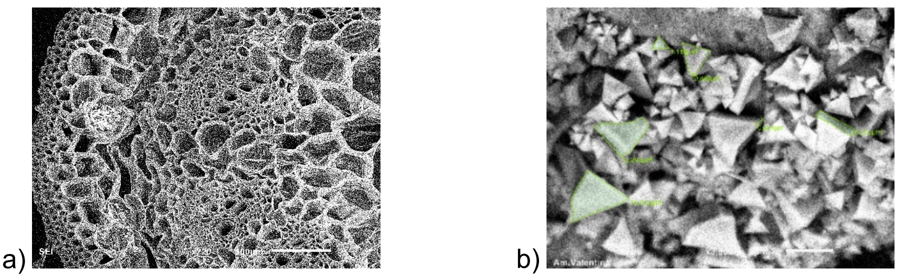

Figure 17. The crystal sand in idioblast among parenchyma cortical cells of the petiole on the cross–section of *Amaranthus tricolor* L. cv. ‘Valentina’ leaves.

For the first time betacyanins localization in leves of *Amaranthus tricolor* L. has been described. In the leaf lamina they are concentrated in the epidermis and in the mesophyll subepidermal cells. And in the leaf petiole, they are present mainly in endodermis, cortical parenchyma and epidermis. Such betacyanins localization significantly and positively affects the adaptive properties of plants according to the data presented in the introduction.

Visual appearance of plants and anatomical sections of leaves demonstrate that cv. ‘Valentina’ does not contain betaxanthins. We came to this conclusion due to the fact that we did not observe cells with yellow or orange vacuoles. The results of chemical analysis confirm the data of microscopic studies (Gins et al., 2002; Kononkov et al., 2018; Platonova et al., 2018).

The chemical composition of crystals was studied by the EDS method. According to the results of the analysis, it was found that Ca is the main element of all mineral inclusions in the leaves of both actinidia and amaranth. The highest concentration of Ca in druses and crystal sand have the leaves of amaranth (38.59 and 26.33 mass %, respectively). Druses from the leaf lamina also contain Mg, P and K. Crystall sand from petiole is a typical oxalate, consisting of Ca and K. Actinidia leaf crystals contain Mg, P, Ca, K and Si. Large rectangular crystals contain more Si (3.5 times), Mg (2 times), Ca and K (1.4 times) compared to needle-shaped crystals. But needle-shaped crystals contain P 1.8 times more than rectangular ones. (Table 1).

Table 1. Chemical composition of mineral inclusions of actinidia and amaranth leaves, mass %

Elements	Type of mineral inclusions in leaves of:			
	Amaranthus tricolor L. cv. 'Valentina'		*Actinidia kolomikta* (Rupr. & Maxim.) Maxim. cv. 'Narodnaya'	
	Druses	Crystal sand	Needle-shaped crystal	Rectangular crystal
C	29.61 ± 1.11	28.24 ± 0.87	39.30 ± 1.31	36.23 ± 1.21
O	30.91 ± 0.98	42.65 ± 1.15	45.92 ± 1.43	44.12 ± 1.34
Mg	0.25 ± 0.01	–	0.02 ± 0.005	0.04 ± 0.01
P	0.48 ± 0.04	–	0.11 ± 0.008	0.06 ± 0.01
Ca	38.59 ± 1.14	26.33 ± 1.02	13.67 ± 0.21	18.74 ± 0.22
K	0.16 ± 0.02	2.72 ± 0.04	0.81 ± 0.04	1.12 ± 0.04
Si	–	–	0.02 ± 0.008	0.07 ± 0.01

Notes: – element not detected.

Current studies have shown that Ca^{2+} is a key element in signaling pathways and is mobilized in stressful situations. And the ability to accumulate this element increases the survival and adaptability of cultivars to adverse environmental factors. (Sanders et al., 2002; Reddy & Reddy, 2004; White, 2004).

CONCLUSIONS

So, we have established the features of the anatomical structure of the leaves of C3 and C4 plants on the example of *Actinidia kolomikta* (Rupr. & Maxim.) Maxim. (cv. 'Narodnaya') and *Amaranthus tricolor* L. (cv. 'Valentina'), respectively. The noted features of the leaf petiole tissues in both varieties generally coincide with anatomical characteristics of the stem and leaf petiole of these species according to other authors, and, therefore, are species-specific.

It has been shown that amaranth leaves contain trichomes of one type, but actinidia has two types. Betalains / anthocyanins can accumulate in the leaves trichomes of both species.

The endodermis in the leaf petioles is clearly expressed due to the presence of amyloplasts (in actinidia and amaranth) and betacyanins (in amaranth). The presence of amyloplasts indicates a high adaptability of cultivars, since these inclusions in the endodermis cells are responsible for storing glucose by polymerization and starch reutilization, and also play the role of statolites - georeceptor structures (Fleurat-Lessard, 1981).

Betalains in the leaves of the cv. 'Valentina' (*Amaranthus tricolor* L.) are represented only by betacyanins. Betaxanthins are absent. Betacyanins in leaf blades are deposited in the epidermal and subepidermal layers, but are not present in the bundle sheath. We assume that the established feature of betacyanins localization is due to the fact that the cells of the bundle sheath and mesophyll differentially express many genes (Bowman et al., 2013). Betacyanins accumulate in the parenchyma and collenchyma cells of leaf petioles. The abundance of betacyanin cells in cortex under stomata can affect transpiration and gas exchange.

It was found that mineral inclusions in the amaranth petioles are present in the form of crystal sand, and are connected into the mineral aggregates - druses in the leaf lamina. The crystall sand contains oxalates of Ca (mainly) and K. There are Mg and P additionally present in the mineral composition of druses.

It should be noted, that cells with raphides in actinidia leaves are mainly located close to or inside the vascular bundles. Raphides with needle-shaped crystals are deposited in the subepidermal layers of the mesophyll along the vascular bundles in leaf lamina and are located in the phloem of petioles. Raphides with needle-shaped and rectangular crystals having an identical elements composition are also deposited in the cortex of leaf petioles. Raphides contain Ca, K, Mg and P, just like amaranth druses, but differ in the presence of Si.

ACKNOWLEDGEMENTS. The reported study was funded by RFBR and BRFBR, project number 20–516–00012\21.

REFERENCES

Bowman, S.M., Patel, M., Yerramsetty, P., Mure, C.M., Zielinski, A.M., Bruenn J.A. & Berry J.O. 2013 A novel RNA binding protein affects rbcL gene expression and is specific to bundle sheath chloroplasts in C4 plants. *BMC Plant Biol*. **13**(138), 24 p. doi: 10.1186/1471–2229–13–138

Arya, S. Rajesh, K.T. & Santhoshkumar, R. 2017. Comparative studies on morphology and anatomy of selected species of the genus *Amaranthus* L. in Kerala. *Indian Journal of Plant Sciences*, **6**(2), 99–105.

Cai, Y.–Z., Sun, M., Wu, H.X., Huang, R.H. & Corke, H. 1998. Characterization and quantification of betacyanin pigments from diverse *Amaranthus* species. *Journal of Agricultural and Food Chemistry* **46**, 2063–2070. doi: 10.1021/JF9709966

Cai, Y.–Z., Sun, M. & Corke, H. 2005 HPLC Characterization of Betalains from Plants in the Amaranthaceae. *Journal of chromatographic science* **43**(9), 454–460 doi: 10.1093/CHROMSCI/43.9.454

Česonienė, L. & Daubaras, R. 2007. Determining of genetic diversity and genetic relationships among Lithuanian selections of *Actinidia kolomikta*. *Agronomy Research* **5**(1), 13–20.

Chirkova, T.V.1999. Amaranth – the culture of the XXI century. *Soros educational journal* **10**, 22–27 (in Russian).

Clearwater, M.J. & Clark, C.J. 2003. In vivo magnetic resonance imaging of xylem vessel contents in woody lianas. *Plant, Cell and Environment* **26**, 1205–1214. doi: 10.1046/J.1365–3040.2003.01042.X

Close, D.C. & Beadle C.L. 2003. The ecophysiology of foliar anthocyanin. *The Botanical Review* **69**(2), 149–161. doi: 10.1663/0006–8101(2003)069[0149:TEOFA]2.0.CO;2

Condon, J.M. 1992. Aspects of kiwifruit stem structure in relation to transport ISHS. *Acta Horticulturae* **297**, II International Symposium on Kiwifruit: 419–426. doi: 10.17660/ACTAHORTIC.1992.297.55

Crivellaro, A. & Schweingruber F.H. 2015. *Stem Anatomical Features of Dicotyledons. Xylem, phloem, cortex and periderm characteristics for ecological and taxonomical analysis.* Publisher: Kessel Publishing House. 159 pp. ISBN: 978–3–945941–08–9 Corpus ID: 90687506

Durnova, N., Simakova M, Isaev D., I. Simakova I. & Simakov A. 2021. Morphology of *Camellia sinensis* L. leaves as marker of white tea authenticity. *Agronomy Research* **19**(3), 1436–1445. doi: 10.15159/ar.21.126

El–Ghamery, A.A., Sadek, A.M. & Abdelbar, O.H. 2017. Comparative anatomical studies on some species of the genus Amaranthus (Family: Amaranthaceae) for the development of an identification guide. *Annals of Agricultural Sciences* **62**(1), 9 p. doi: 10.1016/j.aoas.2016.11.001

Ferguson, A.R. 2011. Kiwifruit: A Botanical Review. In book: *Horticultural Reviews*, Volume **6**, 1–64. doi: 10.1002/9781118060797.ch1

Flexas, J., Loreto, F. & Medrano, H. 2012. *Terrestrial Photosynthesis in a Changing Environment: A Molecular, Physiological, and Ecological Approach*. Cambridge University Press, 728 pp. doi: 10.1017/CBO9781139051477.002

Franceschi, V.R. & Horner, H.T. 1980. Calcium oxalate crystals in plants. *Bot. Rev.* **46**, 361–427. doi: 10.1007/BF02860532

Fleurat–Lessard, P. 1981. Ultrastructural features of the starch sheath cells of the primary pulvinus after gravistimulation of the sensitive plant (Mimosa pudica L.). *Protoplasma* **105**, 177–184. doi: 10.1007/BF01279216

Gins, M.S., Gins, V.K. & Kononkov, P.F. 2002. Change in the biochemical composition of amaranth leaves during selection for increased amaranthine content. *Applied Biochemistry and Microbiology* **38**(5), 474–479. doi: 10.1023/A:1019980821313

Hoang, L.H., De Guzman, C.C., Cadiz, N.M. & Tran, D.H. 2019. Physiological and phytochemical responses of red amaranth (*Amaranthus tricolor* L.) and green amaranth (*Amaranthus dubius* L.) to different salinity levels. *Legume Research. An International Journal* **470**, 1–6. doi: 10.18805/LR–470

Hussain, A.N., Zafar, M., Ahmad, M., Khan, R., Yaseen, G., Khan, M.S., Nazir, A., Khan, A.M. & Shaheen, S. 2018. Comparative SEM and LM foliar epidermal and palyno-morphological studies of *Amaranthaceae* and its taxonomic implications. *Microsc Res Tech.* **81**(5), 474–485. doi: 10.1002/jemt.23001

Khanam, U.K.S. & Oba, S. 2013. Bioactive substances in leaves of two amaranth species, *Amaranthus tricolor* and *A. hypochondriacus*. *Canadian J. Plant Sci.* **93**, 47–58. doi: 10.4141/CJPS2012–117

Kolbasina, E.I., Solovyova, L.V., Tulnova, N.N., Kozak, N.V., Skripchenko, N.V., Moroz, P.A., Korchemnaya, N.A. & Gvosdezkaya, A.I. 2007. *Cultured Flora of Russia: Actinidia. Schisandra.* Moscow. Rosselhozakademia, pp. 327 (in Russian). ISBN 978-5-85941-258-7

Kononkov, P.F., Gins, M.S. & Gins, V.K. 2018. *Amaranth. Introduction in Russia.* Moscow. Scientific and Publishing Center 'Luch'. 319 pp.

Kovinich, N., Kayanja, G., Chanoca, A., Otegui, M.S. & Grotewold, E. 2015. Abiotic stresses induce different localizations of anthocyanins in *Arabidopsis*. *Plant Signaling & Behavior*, **10**(7), e1027850. doi: 10.1080/15592324.2015.1027850

Kovinich, N., Kayanja, G., Chanoca, A., Riedl, K., Otegui, M.S. & Grotewold, E. 2014. Not all anthocyanins are born equal: distinct patterns induced by stress in *Arabidopsis*. *Planta* **240**, 931–940. doi: 10.1007/s00425–014–2079–1

Lotova, L.I. 2011. *Morphology and anatomy of higher plant*s. Editorial URSS, 528 pp. (in Russian). ISBN 5–8360–0140–5

McConn, M.M. & Nakata, P.A. 2002. Calcium oxalate crystal morphology mutants from *Medicago truncatula. Planta* **215**, 380–386. doi: 10.1007/s00425–002–0759–8

Motyleva, S.M., Gins, M.S., Kabashnikova, L.F., Kozak, N.V., Tetyannikov, N.V., Mertvischeva, M.E., Domanskaya, I.N. & Pilipovich, T.S. 2021. Drought effects on the physiological and biochemical parameters of *Amaranth* (C–3) and *Actinidia* (C–4) plants. *SABRAO Journal of Breeding and Genetics* **53**(2), 248–262.

Motyleva, S., Kozak, N., Kulikov, I., Medvedev, I. & Imamkulova, Z. 2017. The peculiarities of *Actinidia* species leaves micromorphology. *Agrobiodiversity*, 342–346. doi: 10.15414/agrobiodiversity.2017.2585–8246.342–346

Motyleva, S.M., Kozak, N.V. & Kulikov, I.M. 2018. The low molecular weight metabolites in the water extract of fruits of *Actinidia* Lindl. *Problems Biol. Med. Pharm. Chem.* **10**(21), 91–97. doi: 10.29296/25877313–2018–10–18

Pivovarov, V.F., Gins, M.S. & Gins, V.K. 2019. Economic efficiency of the raw materials production for obtaining a natural food dye from amaranth. *IOP Conference Series Earth and Environmental Science* **395**(1), 012085. doi: 10.1088/1755–1315/395/1/012085

Platonova, S.Y., Peliy, A.F., Gins, E.M. Sobolev, R.V., Vvedenskiy, V.V. 2018. The study of morphological and biochemical parametres of *Amaranthus tricolor* L. Valentina variety. *RUDN Journal of Agronomy and Animal Industries* **13**(1), 7–13. doi: 10.22363/2312–797x–2018–13–1–7–13 (in Russian).

Reddy, V.S. & Reddy, A.S. 2004. Proteomocs of calcium–signalling components in plants. *Phytochem*. **65**, 1745–1776. doi: 10.1016/J.PHYTOCHEM.2004.04.033

Roy, Y.F., Boyko, V.I. & Remen, K.S. 2020. The anatomical structure of the stem of *Actinidia kolomikta* Maxim. in the conditions of south–west Belarus. *Actual problems of the forest complex* **5**, 140–143 (in Russian).

Sanders, D., Pellow, J., Brownlee, C. & Herper, J.F. 2002. Calcium at the crossroads of signaling. *Plant Cell* **1,** 101–417. doi: 10.1105/tpc.002899

Sarker, U. & Oba, S. 2018a. Augmentation of leaf color parameters, pigments, vitamins, phenolic acids, flavonoids and antioxidant activity in selected *Amaranthus tricolor* under salinity stress. *Sci. Rep.* **8**, 12349. doi: 10.1038/s41598–018–30897–6

Sarker, U. & Oba, S. 2018b. Catalase, superoxide dismutase and ascorbate–glutathione cycle enzymes confer drought tolerance of *Amaranthus tricolor*. *Scientific Reports* **8**, 16496. doi: 10.1038/s41598–018–34944–0

Sarker, U. & Oba, S. 2018c. Drought stress effects on growth, ROS markers, compatible Solutes, phenolics, flavonoids, and antioxidant activity in *Amaranthus tricolor*. *Appl. Biochem. Biotechnol.* **186**, 999–1016. doi: 10.1007/ s12010–018–2784–5

Sarker, U. & Oba, S. 2018d. Drought stress enhances nutritional and bioactive compounds, phenolic acids and antioxidant capacity of *Amaranthus* leafy vegetable. *BMC Plant Biol*. **18**, 258. doi: 10.1186/s12870–018–1484–1

Sarker, U. & Oba, S. 2019a. Antioxidant constituents of three selected red and green color *Amaranthus* leafy vegetable. *Scientific Reports.* **9**, 18233. doi: 10.1038/s41598-019-52033-8

Sarker, U. & Oba, S. 2019b. Salinity stress enhances color parameters, bioactive leaf pigments, vitamins, polyphenols, flavonoids and antioxidant activity in selected *Amaranthus* leafy vegetables. *J. Sci. Food Agric.* **99**, 2275–2284. doi: 10.1002/jsfa.9423

Sarker, U. & Oba, S. 2020a. Leaf pigmentation, its profiles and radical scavenging activity in selected *Amaranthus tricolor* leafy vegetables. *Sci. Rep.* **10**, 18617. doi: 10.1038/s41598-020-66376-0

Sarker, U. & Oba, S. 2020b. Nutraceuticals, phytochemicals, and radical quenching ability of selected drought-tolerant advance lines of vegetable amaranth. *BMC Plant Biol.* **20**, 564. doi: 10.1186/s12870-020-02780-y

Sarker, U. & Oba, S. 2020c. Phenolic profiles and antioxidant activities in selected drought-tolerant leafy vegetable amaranth. *Sci. Rep.* **10**, 18287. doi: 10.1038/s41598-020-71727-y

Sarker, U. & Oba, S. 2020d. Polyphenol and flavonoid profiles and radical scavenging activity in leafy vegetable *Amaranthus gangeticus*. *BMC Plant Biol.* **20**, 499. doi: 10.1186/s12870-020-02700-0

Sarker, U. & Oba, S. 2020e. The response of salinity stress–induced *A. tricolor* to growth, anatomy, physiology, non–enzymatic and enzymatic antioxidants. *Front. Plant Sci.* **11**, 559876. doi: 10.3389/fpls.2020.559876

Sarker, U., Hossain, M.N., Iqbal, M.A. & Oba, S. 2020. Bioactive Components and Radical Scavenging Activity in Selected Advance Lines of Salt–Tolerant Vegetable Amaranth. *Front. Nutr.* **7**, 587257. doi: 10.3389/fnut.2020.587257

Sarker, U., Islam, M.T. & Oba, S. 2018. Salinity stress accelerates nutrients, dietary fiber, minerals, phytochemicals and antioxidant activity in *Amaranthus tricolor* leaves. *PLoS ONE* **13**(11), e0206388. doi: 10.1371/journal.pone.0206388

Semenova, G.A. & Romanova, A.K. 2011. Crystals in sugar beet (*Beta vulgaris* L.) leaves. *Cell and Tissue Biology* **53**(1), 74–80 (in Russian). doi: 10.1134/S1990519X11010147

Shu, Z., Shao, L., Huang, H.–Y., Zeng X.–Q., Lin Z.–F., Chen G.–Y. & Peng C.–L. 2009. Comparison of thermostability of PSII between the chromatic and green leaf cultivars of *Amaranthus tricolor* L. *Photosynthetica* **47**, 548–558. doi: 10.1007/s11099–009–0080–x

Solovchenko, A.E. & Merzliak, M.N. 2008. Screening of visible and UV radiation as a photoprotective mechanism in plants. *Russian Journal of Plant Physiology* **55**, 719–737. doi: 10.1134/S1021443708060010

Svirskis, A. 2003. Investigation of amaranth cultivation and utilisation in Lithuania. *Agronomy Research* **1**(2), 253–26.

Timonin, A.K. 1984. Anatomy of the vegetative leaves in some species of the genus Amaranthus L. 2. The leaf blade, petiole and vascular system of the foliar axis. *Byulleten' Moskovskogo Obshchestva Ispytatelei Prirody. Otdel Biologicheskii* **89**(6), 119–127 (in Russian).

Timonin, A.K. 2011. *Anomalous secondary thickening of centrosperms: specificity of morphofunctional evolution of plants*. Association of Scientific Publications KMK. 355 pp. (in Russian).

Tooulakou, G., Giannopoulos, A., Nikolopoulos, D., Bresta, P., Dotsika, E., Orkoula, M.G., Kontoyannis, C.G., Fasseas, C., Liakopoulos, G., Klapa, M.I. & Karabourniotis, G. 2016. Alarm Photosynthesis: Calcium Oxalate Crystals as an Internal CO2 Source in Plants *Plant Physiology* **171**, 2577–2585. doi: 10.1104/pp.16.00111

Tsutsumi, N., Tohya, M., Nakashima, T. & Ueno O. 2017. Variations in structural, biochemical, and physiological traits of photosynthesis and resource use efficiency in Amaranthus species (NAD–ME–type C4). *Plant Production Science* **20**(3), 300–312. doi: 10.1080/1343943X.2017.1320948

Wang, Z.–X., Fan, S.–T., Chen, L., Zhao, Y., Yang, Y.–M., Ai, J., Li, X.–Y., Liu, Y.–X. & Qin, H.–Y. 2015. *Actinidia kolomikta* leaf colour and optical characteristics. *Biologia plantarum* **59**(4), 767–772. doi: 10.1007/s10535–015–0544–8

Watson, L. & Dallwitz, M.J., 1992 onwards. *The families of flowering plants: descriptions, illustrations, identification, and information retrieval*. Version: 20th October 2021. delta–intkey.com.

White, P.J. 2004. Calcium signals in root cells: the roles of plasma membrane calcium channels. *Biologia* **59**(S3), 77–83.

White, P.J. & Brown, P.H. 2010. Plant nutrition for sustainable development and global health. *Ann. Bot.* **105**(7), 1073–1080. doi: 10.1093/aob/mcq085

Williams, M.H., Boyd, L.M., McNeilage, M.A., MacRae, E.A., Ferguson, A.R., Beatson, R.A. & Martin, P.J. 2003. Development and commercialization of 'Baby Kiwi' (*Actinidia arguta* Planch.). *Acta Hort*. **610**, 81–86. doi: 10.17660/ACTAHORTIC.2003.610.8

Zhigila, D., Yuguda, U., Akawu, J. & Oladele, F. 2014. Palynomorphs and floral bloom as taxonomic characters in some species of the genus *Amaranthus* L. (*Amaranthaceae*). *Bayero Journal of Pure and Applied Sciences* **7**, 164–168. doi: 10.4314/BAJOPAS.V7I2.29

Agronomy Research **20**(2), 357–370, 2022
https://doi.org/10.15159/AR.22.019

Indemnities to Russian farmers for losses due to extreme weather event losses: the challenges and opportunities

V.V. Nosov[1,7,*], D.A. Vorob'eva[2], E.E. Udovik[3], V.N. Zhenzhebir[4], D.E. Morkovkin[5] and A.A. Gibadullin[6]

[1]Peoples' Friendship University of Russia (RUDN University), Agrarian Technological Institute, 6 Miklukho-Maklaya Str., RU117198 Moscow, Russia
[2]Saratov State Vavilov Agrarian University, Department of project management and foreign economic activity in the agro-industrial complex, 1 Teatralnaya square, RU410012 Saratov, Russia
[3]Kuban State Technological University, Department of Economics and Finance, 2 Moskovskaya Str., RU350072 Krasnodar, Russia
[4]Plekhanov Russian University of Economics, Specialized Department of Commercial Policy, 36 Stremyanny lane, RU117997 Moscow, Russia
[5]Financial University under the Government of the Russian Federation, Department of Economic Theory, 49 Leningradsky avenue, RU125167 Moscow, Russia
[6]State University of Management, Department of economics and management, 99 Ryazansky Prospekt, RU109542 Moscow, Russian
[7]Kutafin Moscow State Law University, Department of Management and Economics, 9 Sadovaya-Kudrinskaya Str., RU125993 Moscow, Russia
[*]Correspondence: novla@list.ru

Received: February 15th, 022; Accepted: April 19th, 2022; Published: April 25th, 2022

Abstract. The paper aims to examine indemnity payments to Russian farmers for weather-related loss. Indemnity payments can be made as crop insurance payments or direct payments from budget. The manuscript presents the official data on damage caused by extreme weather and the amount of insurance payments and direct payments to farmers for the years 2005–2021. To process the results of our research, we performed correlation and regression analysis using STATISTICA package. We presented the results of the research in tabular and graphical forms. The research revealed that the average proportion of insurance payments for crop losses in indemnity payments to farmers is 22.1%, and direct payments from budgets of various levels amount to 25.7%. Indicatively, 52.2% of damage remains uncompensated. According to findings, RUB 1 billion in premium subsidies raises insured area by 0.14% under a steady trend, while other factors result in reduction by 1.1%. The paper reviews the barriers that hinder the development of subsidized crop insurance. We propose a series of measures that can promptly improve the current situation, such as the stabilization of the legal framework, a tighter control over insurance rates and the need for authorities to stem corruption. We also note that in setting insurance rates, it is important to consider the farming techniques, selective breeding potential, and adoption of index insurance.

Key words: budget, crop cultivation, crop insurance, indemnity, loss, risk.

INTRODUCTION

Despite all the achievements of modern science and technology, agricultural production in Russia still implies a high risk caused by climatic and biological factors that have a negative impact on yields, which reflects in the low economic performance of farms and the whole agri-food system.

According to the Hydrometeorology and Environmental Monitoring Agency, over the last century, the temperature has increased by about 0.8 °C (Hydrometeorology, 2021). The temperature increase in Russia was 1.5 times higher than the global temperature over the same period and led to a 20% decrease in precipitation. By the end of the 21st century, the global temperature may rise by an additional 1.4 to 5.8 °C (Intergovernmental Panel on Climate Change (IPCC), 2001).

Climate change has contributed to droughts, which have negative effects on agricultural production. Drought is not the only natural hazard linked to global climate change. The increase in average annual temperatures may also lead to a spread of pests and pathogens, as they would not be killed by cold temperatures. However, climate change has led to a decline in insect populations; this process is taking place all over the world (Kingsolver et al., 2011; Boggs, 2016; Kellermann & van Heerwaarden, 2019; Wagner, 2020). Many insects are pollinators of crops and perennial plants and, therefore, are critical for crop production.

A decrease in precipitation along with a 1 °C increase in the annual average temperature creates conditions that dramatically elevate the risk and severity of fires.

On the other hand, some territories of the Russian Federation experience more rainfall, which causes freshets and floods, changes in atmospheric circulation and therefore hurricanes and storms.

Flooding affects agricultural lands, causing waterlogging that results in low yields. A lack of hydraulic structures compounds the problem - their number is just two-thirds of the required number, and the wear rate of three-quarters of these structures is over 80%.

According to Muenchener Rueckversicherungs-Gesellschaft AG, in 2021, global economic losses from natural disasters reached $280 billion, which is $210 billion and 33% more than that of the previous year and 67% more than in 2019 (Sims & Hübner, 2022).

In July 2021, Germany, the UK, the Netherlands, Belgium and Luxemburg saw much above average precipitation, with devastating floods affecting agricultural lands and pastures, gardens and vineyards. The flood destroyed grain storage, caused a loss of livestock and damaged the agricultural infrastructure. In Germany alone, the damage amounted to more than EUR 9.3 billion. The natural anomaly aggravated the crisis caused by the pandemic.

Climate change has already affected crop yields in some countries, and these effects are expected to continue (Mourtzinis et al., 2019).

The agricultural production practice has developed a whole range of measures that can mitigate or prevent environmental negative output impact: crop diversification, selection, technology, irrigation, etc. (Nosov, 2019). However, these instruments cannot always be used effectively to protect farmers against loss of revenue successfully.

Crop insurance has a long history (Hardaker et al., 2004) and is a crucially important source of farmers' financial protection: farmers use crop insurance payments to recover from adverse events covered by the insurance policy (Goodwin, 2001).

In 1922, the U.S. Senate laid the foundation of the crop insurance system. In 1938, the Federal Crop Insurance Corporation (FCIC) was established within the U.S. Department of Agriculture, and the next year, the first crop insurance program was introduced (Kramer, 1983).

Many researches by Barnett (2000), Glauber (2004), Miranda & Glauber (1997) provide the information that in U.S. crop insurance with premium subsidies has been practiced since the adoption of the Federal Crop Insurance Act in 1980 (P.L. 96–365), with further amendments and completions, which resulted in the drafting of the Federal Crop Insurance Reform Act of 1994 (P.L. 103–354), and the Agricultural Risk Protection Act (ARPA) of 2000 (P.L. 106–224).

Glauber et al. (2002) state that the principal form of crop loss assistance in the United States has been provided through the Federal Crop Insurance Program.

The Agricultural Act of 2014 (P.L. 113–79) solidified insurance as the cornerstone of U.S. agricultural policy. According to Ker et al. (2016), the Congressional Budget Office (2014) estimates that this act will increase spending on agricultural insurance programs by $5.7 billion to $89.8 billion over the next decade. On December 20, 2018, the 2018 Farm Bill (P.L. 115–334) was signed into law, that affected the development of agricultural insurance to 2023, the Agriculture Risk Coverage (ARC) and Price Loss Coverage (PLC) programs and the Noninsured Crop Disaster Assistance Program (NAP). The average cost of the program is projected to be nearly $8 billion per year for FY2021-FY2025 and to remain at around that level in FY2026-FY2030 (Rosch, 2021).

The Common Agricultural Policy (CAP) of the European Union describes insurance as an important risk management tool in agriculture.

The main feature of the modern agricultural insurance system is the availability of a wide range of insurance plans (Fig. 1).

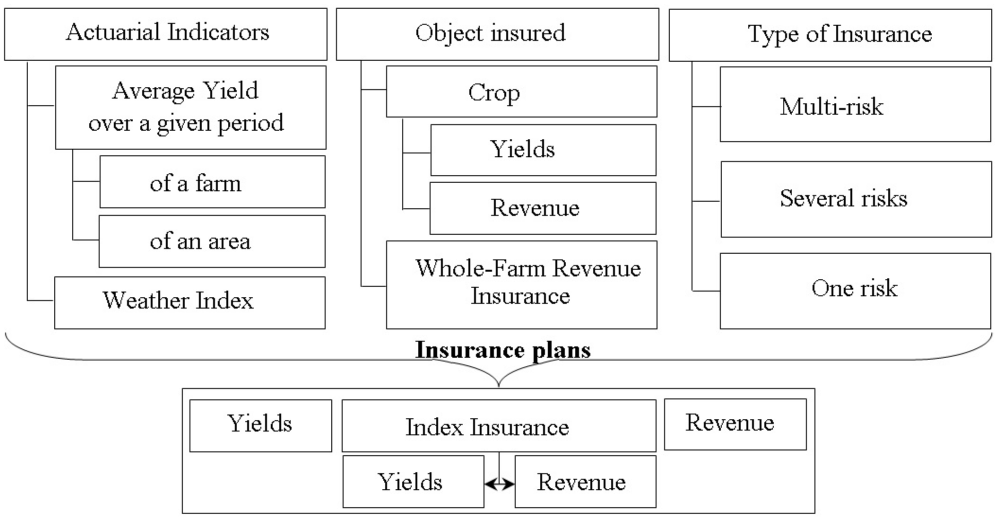

Figure 1. Insurance plans[1].
[1]Created by authors.

Actuarial practices that are used to calculate insurance rates and insurance payments are based on average crop yields, weather index and average zonal yield.

A further distinction of insurance programs is the subject matter of insurance, therefore, there are yield protection, crop revenue protection, and household revenue protection policies.

There are three major types of crop insurance:

- Multi-peril crop insurance that covers crop losses caused by various natural events (drought, hail, fire, flooding);
- Several-peril crop insurance;
- Single-peril crop insurance.

It is important to note that the crop insurance system differs across countries in several ways: available policies, the role of the government (subsidies), and the voluntary or compulsory basis of insurance. For instance, in some European Union countries, insurance only covers one risk of low yields (hail, frost). The most common agriculture insurance policy in Spain, Italy and France is the multi-risk damage. Unlike most European countries, in Germany, there is no developed agricultural insurance program. In Greece and Cyprus, insurance is public and mandatory. We would like to point out that without adequate government subsidies, crop insurance would not be an effective instrument of farmers' protection (Miranda & Glauber, 1997).

Premium subsidies enable agricultural producers to participate in agricultural insurance programs, reduce the financial burden of insurance policy and support farmers' income. The state-supported system of agricultural insurance enables social interconnection and stability of rural areas (Hardaker, 1999; Vávrová, 2005; Chen & Liang, 2021).

Thus, insurance is essential for the sustainable development of agriculture in the context of climate change, as it makes the agricultural sector more attractive to investors and prevents the outflow of resources in the long term. Agricultural insurance is a reaction of business to serious production risk.

According to the Agreement on Agriculture, another instrument of farmers' protection is direct payments made to agricultural producers for relief from natural disasters (Agreement on Agriculture, 1995).

In Russia, insurance payments and direct payments are made to agricultural producers in the event of extreme weather events and natural disasters. However, state supported agricultural insurance that should serve as the main farmers' protection instrument is not effective as it has many flaws. It was therefore necessary to conduct this study. This research aims to examine the practice of indemnification of Russian farmers for losses due to extreme weather events in the form of direct payments from budget or insurance payments, and to identify the key issues and propose possible solutions.

MATERIALS AND METHODS

The official data on damage caused by extreme weather and the amount of insurance payments and direct payments to farmers for 2005–2021 is available on the websites of the Ministry of Agriculture of the Russian Federation and the Federal Agency for State Support of the Agro-Industrial Complex.

Since this is time series data, there is a possibility that a trend can create spurious correlation between indicators that can result in wrong statistical inference (Davidson & MacKinnon, 1993). When there is a trend, there is an autocorrelation of time series levels that can be measured using the linear correlation coefficient (1).

$$r_1 = \frac{\sum_{t=2}^{n}(y_t - \overline{y}_1)\cdot(y_{t-1} - \overline{y}_2)}{\sqrt{\sum_{t=2}^{n}(y_t - \overline{y}_1)^2 \cdot \sum_{t=2}^{n}(y_{t-1} - \overline{y}_2)^2}} \quad (1)$$

In building the regression equation, to remove linear trend from two time series, we propose to include time as an independent variable (2).

$$y_t = a + bx + ct + \varepsilon_t \quad (2)$$

Autocorrelation coefficients and regression parameters were calculated using the STATISTICA package.

The results of the research are presented in tabular and graphical forms.

RESULTS AND DISCUSSION

During the research period, Russian agriculture suffered a loss of about RUB 193.97 billion or $5.71 billion caused by extreme weather. Fig. 2 presents the annual loss in agriculture from extreme weather events that amounts to RUB 11.4 billion or $0.3 billion on average.

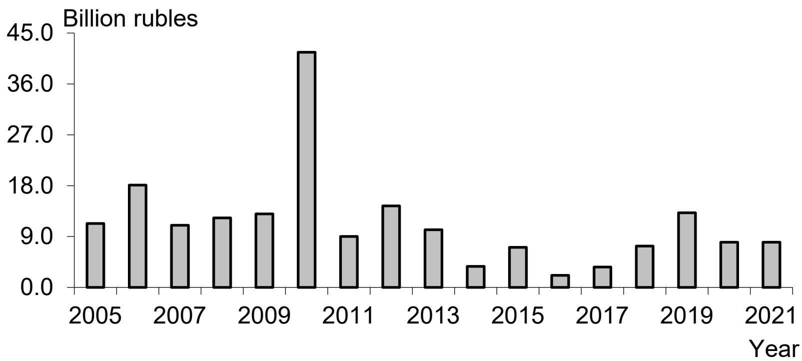

Figure 2. Agricultural losses from natural disasters[1].

[1]Created by authors.

As mentioned above, in Russia, farmers can either enter into an insurance contract and get loss payments or get direct payments from budgets of all levels. Fig. 3 presents the structure of indemnities paid to farmers.

In the reporting period, the proportion of loss compensation to farmers is 22.1%, and the proportion of direct payments is 25.7%. Thus, 52.2% of farmers' losses (which is about RUB 97.03 billion or $3.0 billion in absolute terms) were never compensated. Annually, agricultural producers were losing about RUB 6.1 billion or $0.2 billion.

In 2018, the Russian government made a change to the legislation which affected entitlement to direct payments from budgets of various levels. According to this change, only those farmers who have not bought an insurance policy against crop failure could get compensation for only 50% of documented actual damage. In 2020, only agricultural producers who purchased state-supported crop insurance for crop failure could get compensation for financial losses from shortfall. In 2021, direct payments were not provided at all.

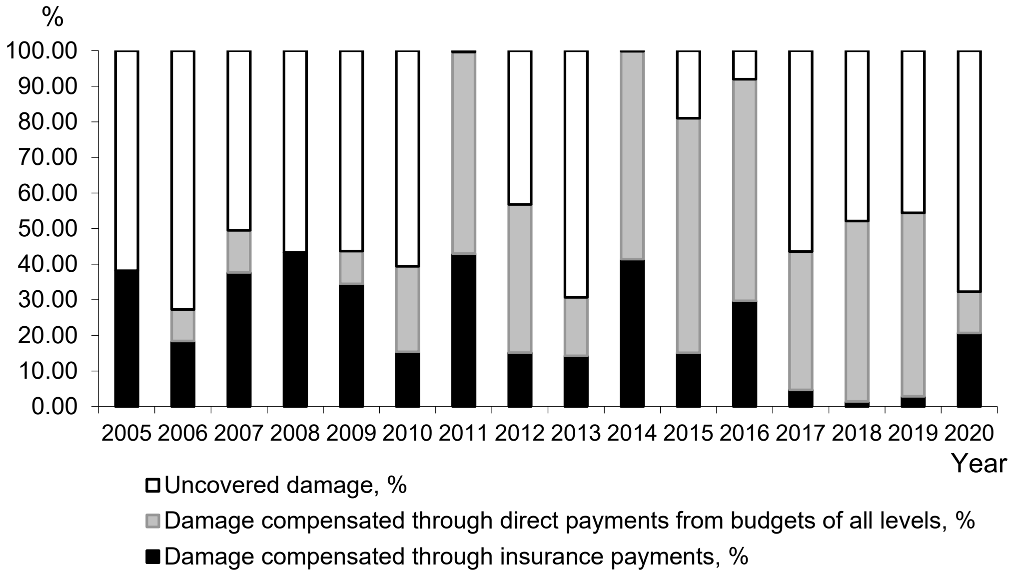

Figure 3. Structure of indemnities paid to farmers[1].
[1]Created by authors.

The Government expected that refusal to compensate farmers with direct payments from the federal budget with the requirement of an insurance policy to qualify for a subsidy in farming would stimulate farmers to insure plantings. Concurrently, the state would partially bear the costs of premiums. Despite adopted decrees, concepts and programs, insurance is unpopular among farmers. Therefore, the proportion of insured crop area is quite small - only 6.3% in 2021 (Fig. 4).

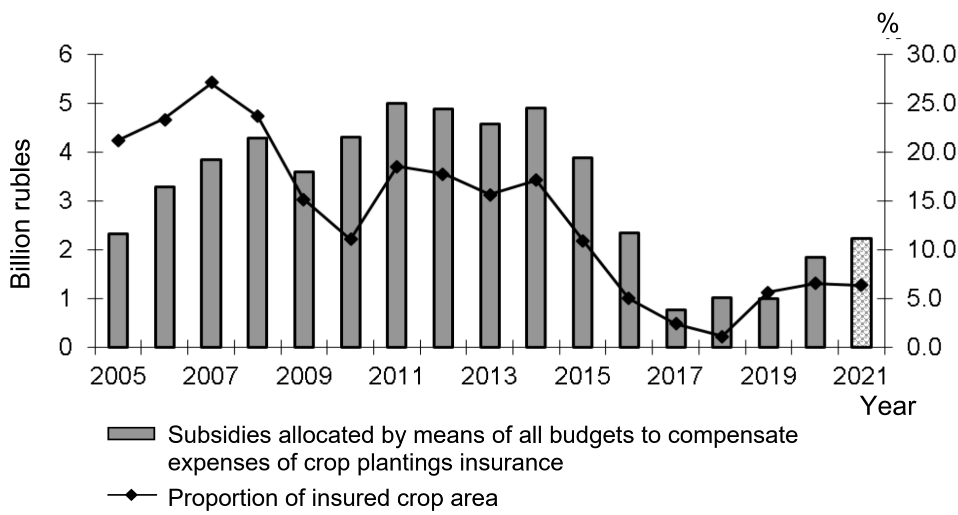

Figure 4. Proportion of insured crop area and subsidized crop insurance[1].
[1]Created by authors.

In absolute terms, this proportion is estimated to be 4.9 million hectares, which is less than in the previous year.

According to the Ministry of Agriculture, National Crop Insurers Alliance and several agricultural scientists (Inshakova et al., 2018; Namirova et al., 2021), a downward trend in the proportion of insured crop area is determined by the low insurance culture of agricultural producers, the global financial crises of 2008 and 2014, the EU and US sanctions against Russia and the recession of the national economy that had a negative effect on the subsidized crop insurance.

The above statement is superficial and does not describe the issues properly. Therefore, we shall assess the effect of subsidies from budget on the amount of insured crops. According to Formula 1, coefficients of autocorrelation, between subsequent levels of time series of allocated subsidies x_t and x_{t-1}, and amount of insured crop y_t and y_{t-1}, for the period from 2005 to 2021 are $r_x^1 = 0.831$ and $r_y^1 = 0.809$, respectively, which shows a close relationship between every next and previous level and, therefore, a linear trend in series. To remove the trend and spurious correlation caused by it from each time series, we introduce time as an independent variable to the regression model (Formula 2; Table 1).

Table 1. Parameters of regression equation*

Regression equation coefficient	Coefficient value	Standard deviation of regression coefficient	*t*-test	*p*-value
a	17.66	3.613	4.888	0.0002
b	0.14	0.052	2.607	0.0207
c	-1.1	0.204	-5.394	0.0001

Note: $R^2 = 0.835$; F(2.14) = 35.512; $p = 0.0000$; dw = 1.73; *Calculated by authors using the STATISTICA package.

The *b* parameter shows that allocation of subsidies of RUB 1 billion from budgets of various levels for partial compensations of premiums to agricultural producers leads to a quite insignificant 0.14% increase in the proportion of insured crop area in the existence of a steady trend. To reach the target of 11.3% set for the agriculture development program by 2025, RUB 11.65 billion or $0.15 billion in subsidies should be provided by budgets of various levels. In view of existing conditions, the Government cannot afford the amount of funding needed.

The *c* parameter shows that the impact of all factors on the indicator except for the amount of subsidies results in a 1.1% decrease in the proportion of insured crop area.

One of the main reasons behind the current situation in agriculture is the low level of indemnity payments. The reasons for such a low level of indemnity payments were described by Nosov et al., 2014; Nosov, 2019. This includes shady schemes when insurance companies and farmers, with help from executive bodies, agree on indemnities in specific proportions of the premium if farmers insure their future harvest. Moreover, many entities of the Russian Federation do not monitor the reliability of information in insurance contracts. At the same time, negligence appears on the part of the authorized executive bodies of the constituent entities of the Russian Federation, which is manifested in the absence of acts of verification of the concluded insurance contracts between the insurer and the insured.

As a result, we can see budget overrun, insured farming area reduction, and insurers keeping budget money.

Overstating the insurance value in insurance contracts is evidence of a corruption component of these contracts. The higher the insurance value, the greater will be the amount of insurance premiums paid by the insured, and the greater will be the budget expenditures. Naturally, insurers, insurants and local bodies will not strive for an adequate and objective assessment of the insurance value of the crop.

According to paragraph 1 of Article 951 of the Civil Code of the Russian Federation: 'if the insured amount specified in the property insurance contract or entrepreneurial risk exceeds the insured value, the contract is insignificant in that portion of the insured amount that exceeds the insured value. The excess insurance premium paid in this case is not returnable'.

That is, if the insurance value is inflated, and insurance premiums are determined, according to this value, they will also be overstated, and the budget will incur unnecessary expenses. In this case, the insurance company will not pay the amount claimed in the contract, and insurance compensation, in any case, will be paid, starting from the market value of the property, moreover, overpaid insurance premiums will not be returned.

Embezzlement of funds allocated to subsidize the insurance on an especially large scale took place in Moscow, Saratov, Bryansk, Nizhny Novgorod regions, in the Republic of Bashkortostan. This list can be continued further. It is important to note that these subjects of the Russian Federation make up a part of the second cluster. The participants of criminal groups accused of crimes under part 4 of Article 174.1, part 4 of Article 159, part 4 of Article 158, parts 1, 2, 3 of Article 210 of the Criminal Code of the Russian Federation, issued documents on behalf of agricultural producers and provided them to the executive authorities in order to create fictitious grounds for the subsequent transfer of subsidies, and also concluded fictitious crop insurance contracts.

At the same time, those farmers who do not participate in shade schemes face rejection from insurance companies to pay indemnities. In such case, insurance companies are taking advantage of economic, financial and legal incompetency of farmers in performance of contract. Another reason for rejection of indemnities appeared on January 1st, 2012, after the enactment of Law No. 260: excess and deductibles provided as clauses in an insurance policy. This reason accounted for 33% of rejections. The higher the deductible franchise is, the lower the insurance rate is. Those agricultural producers who choose low insurance rates when concluding the insurance policy, can sometimes not obtain insurance compensation as it will be equal to zero, even in case of reduction in yields by 50% given certain conditions of insurance.

According to data presented in Table 2, the state directed a large amount of subsidies to insurance premiums instead of direct payments. However, direct payments proved to be much more efficient than insurance payments.

In the 2012–2017 period, the sum of insurance premiums amounted to RUB 48.5 billion, including RUB 21.3 billion paid from public funds. The sum of indemnities was RUB 7.1 billion.

RUB 17.7 billion were allocated from the federal budget for direct disaster relief payments, 20% less than that for insurance subsidies, while farmers got 2.5 times the sum of indemnities. Over the 2018–2020 period, the sum of insurance premiums amounted to RUB 7.6 billion, including RUB 3.8 billion paid from public funds. The sum of indemnities was RUB 2.1 billion. This time, the allocation for direct disaster relief payments was 3 times the amount of insurance subsidies, and farmers got 5.4 times the sum of indemnities.

Table 2. Parameters of regression equation*

Indicator	2012–2017	2018–2020
Sum of insurance premiums, RUB billion (USD billion)	48.5 (1.2)	7.6 (0.11)
incl. from public funds (USD billion)	21.3 (0.52)	3.8 (0.055)
Sum of indemnities, RUB billion (USD billion)	7.1 (0.18)	2.1 (0.03)
Direct reimbursement, RUB billion (USD billion)	17.7 (0.44)	11.4 (0.17)
Indemnity to premium ratio, %	14.5	27.6
Direct reimbursement to insurance premium compensation paid from public funds ratio, times	0.8	3.0
Direct reimbursement to the sum of indemnities ratio, times	2.5	5.4

*Calculated by authors.

The Ministry of Agriculture has proven to be incompetent in introducing regulations on agriculture. In 2007, a State Program for Development of Agriculture and Regulation of the Agricultural Commodity Markets in 2008–2013 was established, which determined that federal funding would be available only if not less than 10% of premium expenses will be allocated from provincial budget. Later on, a Decree No. 1091 of December 31st, 2008 was issued on limitations on taking out insurance policies, that were further invalidated by the decision of the Russian Supreme Court No. GKPI 09-819 of September 1st, 2009. At the same time, the Ministry of Agriculture was distributing subsidies among the subjects of the Russian Federation in accordance with the above-mentioned Decree: proportionally to the sum of paid premiums and within the limits of budgetary commitments and funding for these needs. Thus, the state suggests that farmers shall pay a 100% premium and reserves the right to reduce its involvement in compensation, which is exactly what had happened.

In 2010, the government raised insurance premiums by 30% to 10%, which was not actuarially sound.

In 2012, the above-mentioned Law No. 260 was enacted, which, according to the Government and agricultural scientists, was supposed to modernize the system of agricultural insurance with state support. Nowadays, we can observe the changes this modernization has led to.

Secondary legislation regarding crop insurance changes every year. Most changes are lobbied by the National Crop Insurers Alliance but never registered. Meanwhile, every year the Ministry of Agriculture develops a crop insurance plan for the year with a three-month delay, which results in subjects and farmers not being able to plan their expenses for insurance and not contributing to an increase in insured area.

In 2017, budget expenditures on crop insurance were included in the unified subsidy and were supposed to be RUB 2 billion or $0.03 billion. In fact, only RUB 0.7 billion or $1 million were allocated.

This situation can be explained by regional government bodies in agriculture having the right to decide on the allocation of subsidies between the farmers and to redistribute them to areas of support inside the subsidy using the priority coefficients. The priority of crop insurance in most subjects equaled to zero because of the failure of the protection mechanism. Before, regional government bodies did not have such rights.

The Ministry of Agriculture admitted the problem with integrating subsidies for insurance premiums into the unified subsidy. From 2020, support to agricultural producers was reformed; the unified subsidy was replaced with individual subsidies targeted at insurance premiums.

Besides, 1st March 2019, Federal Act No 563 On the amendments to Federal Act No 260 came into force and eliminated loss of crops and perennial crops thresholds, i.e. non-deductible franchise alongside with obligatory deductible franchise, which could not be less than 10% and more that 50% of the insurance coverage.

In 2021, the National Crop Insurers Alliance lobbied for more changes to Federal Act No. 260. According to the Ministry of Agriculture, these changes should stimulate farmers, especially smallholders, to purchase crop insurance. Since July 1, 2021, a subsidy of 80% of insurance premium is available to farmers. It will be available to smallholders for 2 years, and as of July 1, 2023, it will be reduced to 70%, from July 1, 2024 - to 60%, from July 1, 2025 - to 50%. For other farmers, the subsidy will be reduced every year: from July 1, 2022 - to 70%, from July 1, 2023 - to 60%, from July 1, 2024, 50%.

Moreover, farmers can choose one or several risks when taking out an insurance policy and get a lower insurance rate. Insured events include natural disasters that have led to the declaration of a state of emergency by federal or regional government.

Nevertheless, according to the Ministry of Agriculture and National Crop Insurers Alliance, the occurred changes have not resulted in a sharp increase of insured acreage. According to the preliminary data, in 2021, the insured area was 4.9 million hectares, which is even less than in the previous year (Fig. 4). The above changes came into effect on July 1st, 2021. However, farmers insured winter crops planted on 29 million hectares, or 38% of the area of Russia.

According to Goodwin & Smith (1995), Just, Calvin & Quiggin (1999), Makki & Somwaru (2001), Russo et al. (2022), taking out an insurance policy is related to natural risks on farmer's territory and measures of risk aversion (Puelz & Snow, 1994). We agree with Miranda (1991), that farmers will buy insurance only if expected indemnities exceed premiums paid. This is exactly what we do not see in Russia now.

These statements correspond with two problems of crop insurance: use of innovative technologies in crop production and use of new varieties cultivated for a specific territory. Innovative technologies and new varieties of crops significantly reduce the risk of major crop loss compared to traditional farming methods (Arshadi et al., 2018, Horváth et al., 2021). According to current regulations, insurance rates are the same for conventional and innovative technologies. This issue was extensively described by Woodard et al. (2021), the authors claimed existing rules disincentivize the adoption of skip-row patterns of crop planting in the Central Great Plains. We agree that poorly thought out crop insurance system can cause elimination of any progressive crop growing technique and a need for new insurance solutions.

According to Zhichkin et al. (2021), volume 1 of the State Register of Selection Achievements Authorized for Use for Production Purposes contains constraints to adoption of new improved varieties. In the paper, the authors describe the development of a new information system of crop varieties adaptive to a specific territory. Such an approach allows a reduction of insurance coefficients for a single variety and a reduction in insurance policy costs for farmers growing these varieties.

As stated by the Ministry of Agriculture and the National Crop Insurers Alliance, one of the solutions to the problems with crop insurance, with state support, is index insurance. However, it does not go any further than words because of the transparency of approach, which makes money embezzlement difficult for bureaucrats.

The essence of index insurance is that payouts are based on a predetermined index and not on actual losses incurred. This approach was extensively described by Carter et al. (2016), Clarke (2016), Jensen & Barrett (2017), Goodwin et al. (2000). Note that different types of index-based insurance are a good alternative to traditional multi-risk insurance and have considerable advantages:

- no moral hazard and adverse selection;
- standardized and transparent structure;
- low administrative expenses, availability, etc.

Just as with every insurance product, index insurance has its weaknesses. One of the most commonly cited impediments to this uptake is basis risk that arises when the index measurements that reflect changes in the yield curve do not match farmer's actual loss. This can result in a loss of the indemnity payment because the yield exceeds the index. Sometimes index-based insurance provides with indemnities, farmers that did not experience any loss. Therefore, index insurance in agricultural insurance with state support should be supervised and developed to meet the needs of farmers and encourage the adoption of crop insurance in Russia.

CONCLUSIONS

Up to 2021, compensation for damage caused by extreme weather was paid to farmers as insurance payments and direct payments. The proportion of insurance payments to farmers is 22.1%, the proportion of direct payments is 25.7%. Thus, 52.2% of farmers' losses were never compensated. Annually, agricultural producers were losing about RUB 6.1 billion or $0.2 billion. Since 2021, direct payments were cancelled, which, from our point of view, strained the financial situation of farmers and made crop insurance the only source of farmers' financial protection from extreme weather events. The proportion of insured crop area remains quite small – only 6.3% in 2021. Allocation of RUB 1 billion in premium subsidies from budgets of various levels raises insured area by 0.14% under a steady trend. Other factors result in reduction by 1.1%. The main reasons behind the current situation in agriculture are:

- low level of indemnity payments;
- corruption and incompetency of those responsible for crop insurance;
- equal insurance coverage for conventionally grown crops and crops grown using innovative technologies;
- limitations associated with the ability to insure only specific crop varieties recommended for cultivation on the territory under volume 1 of the State Register of Selection Achievements Authorized for Use for Production Purposes;
- availability of only multi-risk insurance plans;
- actuarially unfair insurance rates offered by plans.

To reach the target of 11.3% set for the agriculture development program by 2025, RUB 11.65 billion or $0.15 billion in subsidies should be provided by budgets of various levels. In view of existing conditions, the Government cannot afford that. To improve the current situation with crop insurance with state support as the only source of farmers' financial protection from extreme weather events and reach the target of insured area, we propose the following set of measures:

- to stop annual changes to secondary legislation and methodology of crop insurance;
- to monitor decisions taken by the Ministry of Agriculture;
- to tighten control over actions of officials responsible for verification of information in state insurance policies in the subjects of the Russian 464 Federation;
- if any overestimation of insured value of yield has been identified, it is important to solve an issue of insurance companies refunding budget funds in case of their excessive transferring to the notified bodies of the constituent entities of the Russian Federation;
- agricultural insurance with state support (given expenses for management of insurance) should be used by insurers only for paying insurance benefits to agricultural producers in subsequent years, if there are not enough payments in the current year;
- to set actuarially sound rates and make their calculation available on the website of the Federal Agency for State Support of the Agro-Industrial Complex for social control;
- to consider cultivation techniques and selective breeding potential of crops when taking out an insurance policy;
- adoption of index insurance.

Only this way, agricultural producers may show some interest in concluding agricultural insurance policies.

FUNDING. This paper has been supported by the RUDN University Strategic Academic Leadership Program.

REFERENCES

A report on climate features on the territory of the Russian Federation in 2020. Moscow, 2021. P. 6. https://www.meteorf.ru/upload/pdf_download/doklad_klimat2020.pdf

Agreement on Agriculture. Annex 2: Domestic Support – The Basis for Exemption from The Reduction Commitments. *https://www.wto.org/english/docs_e/legal_e/14-ag_02_e.htm#annII*. Accessed 08.04.2022.

Arshadi, A., Karami, E., Sartip, A., Zare, M. & Rezabakhsh, P. 2018. Genotypes performance in relation to drought tolerance in barley using multi-environment trials. *Agronomy Research* **16**(1), 5–21. doi:10.15159/AR.18.004

Barnett, B. 2000. The U.S. Federal Crop Insurance Program. *Canadian Journal of Agricultural Economics* **48**(4), 539–551.

Boggs, C.L. 2016. The fingerprints of global climate change on insect populations. *Current Opinion in Insect Science* **17**, 69–73.

Carter, M.R., Cheng, L. & Sarris, A. 2016. Where and how index insurance can boost the adoption of improved agricultural technologies. *Journal of Development Economics* **118**, 59–71. doi:10.1016/j.jdeveco.2015.08.008

Chen, Z. & Liang, H. 2021. Effectiveness improvement of financial poverty alleviation in zhanjiang. *ACM International Conference Proceeding Series*, 649–651. doi:10.1145/3452446.3452604

Clarke, D.J. 2016. A theory of rational demand for index insurance. *American Economic Journal Microeconomics* **8**(1), 283–306. doi:10.1257/mic.20140103

Davidson, R. & MacKinnon, J. 1993. *Estimation and Inference in Econometrics*. Oxford University Press, New-York, 896 pp.

Federal Agency for State Support of the Agro-Industrial Complex. State of the agricultural insurance market. Available at http://www.fagps.ru/docs1/ (in Russian).

Glauber, J. 2004. Crop Insurance Reconsidered. *American Journal of Agricultural Economics* **86**(5), 1179–1195.

Glauber, J., Collins, K. & Barry, P. 2002. Crop Insurance, Disaster Assistance, and the Role of the Federal Government in Providing Catastrophic Risk Protection. *Agricultural Finance Review* **62**(2), 81–102.

Goodwin, B. 2001. Problems with Market Insurance in Agriculture. *American Journal of Agricultural Economics* **83**(3), 643–649.

Goodwin, B.K. & Smith, V.H. 1995. *The Economics of Crop Insurance and Disaster Aid.* American Enterprise Institute Press, Washington, D.C., 64 pp.

Goodwin, B.K., Roberts, M.C. & Coble, K.H. 2000. Measurement of price risk in revenue insurance: Implications of distributional assumptions. *Journal of Agricultural and Resource Economics* **25**, 195–214.

Hardaker, J. 1999. Income insurance in European agriculture. *EC Reports and studies* **1**, 95.

Hardaker, J., Huirne, R. & Anderson, J. 2004. *Coping with Risk in Agriculture. (2nd edition).* Wallingford: CABI Publishing, 345 pp.

Horváth, É., Gombos, B. & Széles, A. 2021. Evaluation phenology, yield and quality of maize genotypes in drought stress and non-stress environments. *Agronomy Research* **19**(2), 408–422. doi:10.15159/AR.21.073

Inshakova, A.O., Uskova, M.S., Dolinskaya, V.V. & Frolova, E.E. 2018. Dynamics of the legislative development of public-private partnership in the sphere of agricultural insurance in Russia and the US. *Espacios* **39**(28).

Intergovernmental Panel on Climate Change (IPCC). 2001. *Climate Change 2001: Impacts, Adaptation, and Vulnerability; Contribution of Working Group II to the Third Assessment Report of the Intergovernmental Panel on Climate Change*. Cambridge University Press: Cambridge, UK, 1042 pp.

Jensen, N. & Barrett, C. 2017. Agricultural index insurance for development. *Applied Economic Perspectives and Policy* **39**(2), 199–219. doi:10.1093/aepp/ppw022

Just, R.E., Calvin, L. & Quiggin, J. 1999. Adverse Selection in Crop Insurance: Actuarial and Asymmetric Information Incentives. *American Journal of Agricultural Economics* **81**, 834–849.

Kellermann, V. & van Heerwaarden, B. 2019. Terrestrial insects and climate change: Adaptive responses in key traits. *Physiological Entomology* **44**, 99–115.

Ker, A., Tolhurst, T. & Liu, Y. 2016. Bayesian estimation of possibly similar yield densities: implications for rating crop insurance contracts. *American Journal of Agricultural Economics* **98**(2), 360–382.

Kingsolver, J., Woods, H., Buckley, L, Potter, K, Maclean, H. & Higgins, J. 2011. Complex life cycles and the responses of insects to climate change. *Integrative and Comparative Biology* **51**, 719–732.

Kramer, R.A. 1983. Federal Crop Insurance: 1938–82. *Agricultural History* **57**, 181–200.

Makki, S.S. & Somwaru, A.L. 2001. Asymmetric Information in the Market for Yield and Revenue Insurance Products. *Economic Research Service, U.S. Department of Agriculture, Technical Bulletin*, 1892.

Miranda, M. & Glauber, J. 1997. Systemic Risk, Reinsurance, and the Failure of Crop Insurance Markets. *American Journal of Agricultural Economics* **79**(1), 206–215.

Miranda, M. 1991. Area-yield Crop Insurance Reconsidered. *American Journal of Agricultural Economics* **73**, 233–242.

Mourtzinis, S., Specht, J. & Conley, S. 2019. Defining Optimal Soybean Sowing Dates across the US. *Scientific Reports* **9**(1), 1–7.

Naminova, K.A., Makaeva, K.I., Uchurova, E.O., Boldyreva, E.S. & Godzhaeva, E.S. 2021. Risk insurance of agricultural organizations in Russia: Trends, problems, directions of development. In: *IOP Conference Series: Earth and Environmental Science* **848**(1). doi:10.1088/1755-1315/848/1/012192

Nosov, V. 2019. Insurance Premium Subsidies in Crop Farming: Challenges and Opportunities. In: *Proceedings of the 33rd International Business Information Management Association Conference, IBIMA 2019: Education Excellence and Innovation Management through Vision 2020*, 7594–7600.

Nosov, V., Kotar, O., Kosheleva, M., Alajkina, L. & Novikova, N. 2014. Assessing effectiveness of insurance premium subsidy in agricultural insurance. *Ecology, Environment and Conservation* **20**(4), 1857–1863.

Overview of CAP Reform 2014–2020, Agricultural Policy Perspective Brief No. 5. Brussel: European Commission.

Puelz, R. & Snow, A. 1994. Evidence on Adverse Selection: Equilibrium Signaling and Cross-Subsidization in the Insurance Market. *Journal of Political Economy* **102**, 236–257.

Risk Management Agency. *http://www3.rma usda.gov/apps/sob/*. Accessed 01.04.2019.

Rosch, S. 2021. Federal Crop Insurance: A Primer. Congressional Research Service. https://sgp.fas.org/crs/misc/R46686.pdf.

Sims, T. & Hübner, A. 2022. Natural disasters cost insurers $120 billion in 2021, Munich Re says. https://finance.yahoo.com/news/natural-disasters-cost-insurers-120-101801359.html. Accessed 08.04.2022.

STATISTICA Package. Statsoft. http://statsoft.ru/products/trial/. Accessed 08.04.2022.

Statistic data on crop and perennial plantings insurance with state support. *http://www.fagps.ru.* Accessed 01.04.2022.

The Ministry of Agriculture of the Russian Federation. Available at https://mcx.gov.ru/ (in Russian).

Vávrová, E. 2005. The Czech agricultural insurance market and a prediction of its development in the context of the European Union. *Agricultural Economics (Zemědělská ekonomika)* **51**, 531–538.

Wagner, D.L. 2020. Insect declines in the Anthropocene. *Annual Review of Entomology* **65**, 457–480.

Woodard, J.D., Pavlista, A.D., Schnitkey, G.D., Burgener, P.A. & Ward, K.A. 2012. Government insurance program design, incentive effects, and technology adoption: The case of skip-row crop insurance. *American Journal of Agricultural Economics* **94**(4), 823–837. doi:10.1093/ajae/aas018

Zhichkin, K., Nosov, V., Zhichkina, L., Łakomiak, A., Pakhomova, T. & Terekhova, A. 2021. Biological bases of crop insurance with state support. In: *IOP Conference Series: Earth and Environmental Science* **677**(2), 0198.

Agronomy Research **20**(2), 371–388, 2022
https://doi.org/10.15159/AR.21.162

A mathematical model of the rear-trailed top harvester and an evaluation of its motion stability

J. Olt[1,*], V. Bulgakov[2], H. Beloev[3], V. Nadykto[4], Ye. Ihnatiev[4], O. Dubrovina[2]
M. Arak[1], M. Bondar[2] and A. Kutsenko[2]

[1]Estonian University of Life Sciences, Institute of Technology, 56 Kreutzwaldi Str., EE 51006 Tartu, Estonia
[2]National University of Life and Environmental Sciences of Ukraine, 15 Heroiv Oborony Str., UA03041 Kyiv, Ukraine
[3]University of Ruse “Angel Kanchev”, 5 Studentska Str., BG7017 Ruse, Bulgaria
[4]Dmytro Motornyi Tavria State Agrotechnological University, 18B Khmelnytsky Ave, UA72310 Melitopol, Zaporozhye Region, Ukraine
[*]Correspondence: jyri.olt@emu.ee

Received: October 7th, 2021; Accepted: December 10th, 2021; Published: December 10th, 2021

Abstract. Improving the quality of sugar beet harvesting to a great extent depends on the first operation in the process, which involves cutting and harvesting sugar beet tops. This technological process is performed with the use of either the haulm harvesting modules of beet harvesters or top harvesting machines as separate agricultural implements, which are aggregated with a tractor. At the same time, front-mounted harvesters are as widely used as trailed asymmetric implements, in which case the aggregating tractor moves on the already harvested area of the field. The purpose of this work is to determine the optimal design and kinematic parameters that would improve the stability in the performance of the technological process of harvesting sugar beet tops by means of developing the basic theory of the plane-parallel motion performed by the rear-trailed asymmetric top harvester. As a result of the analytical study, an equivalent scheme has been composed, on the basis of which a new computational mathematical model has been developed for the plane-parallel motion of the asymmetric top harvester in the horizontal plane on the assumption that the connection between the wheeled tractor and the rear-trailed top harvester is made in the form of a cylindrical hinge joint. Using the results of mathematical modelling, the system of linear second-order differential equations that determines the transverse movement of the centre of mass of the aggregating wheeled tractor and the rotation of its longitudinal symmetry axis by a certain angle about the said centre of mass as well as the angle of deviation of the rear-trailed asymmetric top harvester from the longitudinal symmetry axis of the tractor at an arbitrary instant of time has been obtained. The solving of the obtained system of differential equations provides for determining the stability and controllability of the motion performed by the asymmetric machine-tractor unit, when it performs the technological process of harvesting sugar beet tops.

Key words: harvesting machine, plane-parallel motion, stability of movement, sugar beet tops.

INTRODUCTION

One of the current problems in the beet industry is the high-quality harvesting of the tops (Gruber, 2005; Sarec et al., 2009; Boson et al., 2019), which implies cutting and harvesting the green mass, which is used later, as completely as possible and cutting the root crowns without causing damage to or loss of root bodies (loss of sugar-bearing mass in case of sugar beets). This applies almost equally to the harvesting of sugar beets and fodder beets, carrots and other root crops, the parts of which are harvested separately - first the tops are cut from the roots, then the roots are lifted from the soil (Bulgakov et al., 2017a). The technological process of haulm harvesting is carried out by either the harvesting modules of beet harvesters or top harvesting machines as separate agricultural implements aggregated with tractors, mostly row-crop tractors. Throughout the world, both front-mounted topping implements and trailed asymmetric top gathering machines are widely used, in the latter case the aggregating tractor moving on the already harvested section of the field. Such asymmetric units are especially widely used, when harvesting fodder beet tops Pogorely & Tatyanko, 2004).

It should be noted that today trailed asymmetric agricultural machines are produced in the agricultural industries of many countries in the world and such asymmetric units are successfully used. This primarily applies to the units with trailed asymmetrically positioned harvesting machines, such as the mentioned machines for harvesting sugar and fodder beet tops, rotary windrowers, rotary mowers, trailed forage harvesters and the like (Boson et al., 2019).

While there is an acute need to perform the above-mentioned processes using the described design and it is necessary to ensure their high quality, asymmetric trailed harvesters have one significant disadvantage associated with the resulting unstable movement in the transverse-horizontal plane, which must be overcome in some way. The conditions of unstable movement of the aggregating tractor and the asymmetric harvester installed behind that arise in this case are due to the action of the turning moment produced by the external forces acting on the wheels and implements, when performing the given process (Bulgakov et al., 2020a).

The numerous scientific studies and subsequent engineering developments (Wang & Zhang, 2013; Wu et al., 2013; Zhang et al., 2013; Gu et al., 2014) have made it possible to overcome this disadvantage by using various technical methods. Among the known ways to solve this problem there are two most widely used variants of aggregating asymmetric agricultural machines with aggregating tractors, which are able to provide the relatively stable movement of the unit. The first of them involves a rigid connection between the asymmetric machine and the aggregating tractor during their operation in the technological process. While this alternative provides, in general, the conditions for the stable movement of the asymmetric machine, the existing turning moment creates such conditions, under which the steer wheels of the aggregating tractor must constantly turn to the side opposite to the direction of the side slip. In this case, the controllability of such an asymmetric machine-tractor unit becomes much worse, which not only complicates the conditions of its operation, but can reduce the quality of the specified process overall (Vasilenko, 1996). The first option is most suitable for the operation of simple and light asymmetric machines, such as mowers with small working widths, with tractors of considerable weights.

In the second case, the connection between the rear-trailed asymmetric agricultural machine and the aggregating tractor, when performing the technological process, is provided by a cylindrical hinge, i.e. the conditions for the movement of the tractor and the machine relative to each other are created. Under these conditions, the controllability of the machine-tractor unit under consideration is significantly improved, but additional provisions are required to ensure that the aggregated asymmetric machine does not deviate in the horizontal plane in the process of its operational travelling under the action of the arising turning moment. That is, this method of aggregation is more effective, but it sets a problem of somehow reducing the generated turning-around moment or creating the conditions for its compensation by the 'moment of counteraction'.

Thus, there is an urgent need to find conditions for increasing the stability of motion of any asymmetric machine-tractor unit, and one of the ways is the theoretical research into its movement in the transverse-horizontal plane, i.e. its plane-parallel motion.

When conducting such theoretical research, it is necessary to remember that the stable movement and high-quality functioning of one or another asymmetric agricultural machine-tractor unit should be considered as its response to the input controlling and disturbing actions. In this case, the response of the machine-tractor unit to the controlling actions characterizes its controllability and the response to the disturbing actions - the stability of movement.

The authors have developed a new rotor-type top harvester, which can be used in the form of a front-mounted or rear-trailed aggregated machine. The design and process scheme of using the top harvesting machine hitched behind the aggregating wheeled tractor is presented in Fig. 1. Thus, the presented machine-tractor unit, in which harvesting machine (II) with a working width of 3 rows is asymmetrically attached to the aggregating wheeled tractor (I), is asymmetric.

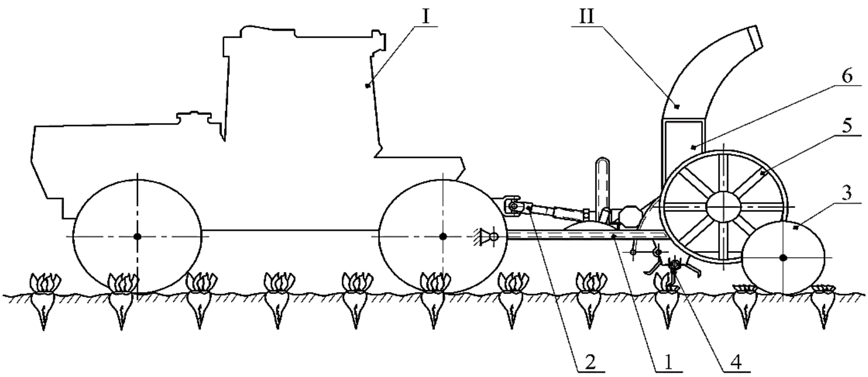

Figure 1. Design and process scheme of asymmetric top harvesting unit in longitudinal-vertical plane: I – wheeled tractor; II – trailed asymmetric harvesting machine; 1 – frame; 2 – universal-joint drive; 3 – pneumatic support-and-finder wheel; 4 – rotary haulm cutting device; 5 – conveying device; 6 – loading device.

In this case, the technological process of cutting the tops is carried out with the use of a rotary topping device (4), which performs the continuous cutting of the entire mass within the working width. In the process of work, the cutting device (4) is positioned relative to the crowns of root crops by means of two pneumatic support-and-finder wheels (3), which move in the inter-row spacing. The cut-off green mass of the haulm is loaded with the use of an arc-shaped loading device (6) into the body of the vehicle moving on the harvested area of the beet field next to the harvester.

Thus, the search for the conditions that ensure the stable movement of this asymmetric top harvesting unit is an urgent and difficult task, the solution of which will significantly improve its technical and operational properties.

Many published works (Hac et al., 2008; Szakács, 2010; Yildiz, S. 2010; Demšar et al., 2012; Li et al., 2016; Anche & Subramanian, 2018; Bulgakov et al., 2020a, 2020b) have been concerned with the research into the stability of the movement performed by trailed asymmetric agricultural machines as parts of various machine-tractor units, based on the generation of their analytical mathematical models. Most of these studies use the basic provisions from the classical theory of the stability of agricultural machine-tractor units in perturbed and unperturbed motion, which is analysed with the use of generated systems of differential equations of motion (Bulgakov et al., 2017b). In this case, the behavior of different machine-tractor units is considered, as a rule, in their plane-parallel motion together with the rear-trailed agricultural machine. Most of the above-mentioned known works are concerned with the research into the machine-tractor units that comprise a wheeled aggregating tractor and a rear-trailed rotary windrower.

Analytical studies on the asymmetric machine-tractor units that consist of a wheeled tractor and a rear-trailed top harvester have not been published until now. It should be noted that in such research it is necessary to take into account the properties of the elastically damping pneumatic tires on the aggregating tractor wheels and the forces arising at the points of contact between these wheels and the ground, which is deformed, as well as the design features of the trailed machine, its size and the external forces acting on the supporting wheels and tools of the machine, the generated traction resistance, the way the machine is attached to the rear hitch of the aggregating tractor, and so on.

The aim of the study was to determine the optimal kinematic and design parameters that will increase the stability of the technological process of harvesting sugar beet tops, basing on the development of the fundamentals for the theory of the plane-parallel motion performed by the rear-trailed asymmetric top harvester.

MATERIALS AND METHODS

The main provisions of the theory of plane-parallel motion performed by the asymmetric top harvesting machine-tractor unit will be considered by the example of an aggregating wheeled tractor, behind which a top harvesting machine is attached. The aggregating tractor moves along the harvested part of the sugar beet plantation, while the haulm harvesting machine, which is positioned to the right of the tractor, moves along the sugar beet crop area and cuts and collects the green mass of the haulm and loads it, through the loading device, into the body of the vehicle that moves next to the tractor (or scatters it on the field). The connection between the wheeled aggregating tractor and the specified haulm topper during the operation of this machine-tractor unit is provided by the vertical cylindrical hinge joint in the rear hitch device of the tractor.

Thus, this harvesting machine-tractor unit is asymmetric, because the top harvester trailed behind the aggregating tractor is offset to the right from its longitudinal axis.

For the analytical study of this machine-tractor unit, it is first necessary to generate its equivalent schematic model, considering the motion of all its points only in a plane parallel to the plane of the field surface. First of all, it should be noted at once that this asymmetric top harvesting machine-tractor unit is a complex dynamic system and due to its asymmetry its movement in the horizontal plane will certainly be unstable.

In addition, to study this movement, it is necessary to formalize some properties of such a machine-tractor unit and on the basis of that make some assumptions. These assumptions will not misrepresent the real process in any way, but will greatly simplify the analytical research. Namely, the main assumptions are as follows:

1. The surface of the field, on which this top harvesting unit moves, is horizontal, and therefore the heel and trim of this machine-tractor unit are neglected.
2. Wheeled aggregating tractor is presented in the form of a solid body having a longitudinal plane of symmetry, which passes through its centre of mass.
3. The oscillations of the traction resistance of the trailed top harvester do not have a significant effect on the speed of translational movement of this unit, as a result of which it is assumed in the first approximation to have a constant value.
4. Interaction between the pneumatic tires on the running wheels of the aggregating tractor and the support-and-finder wheels of the trailed top harvesting machine, on the one hand, and the soil surface, on the other hand, especially in lateral directions, completely corresponds to the so-called hypothesis of side slip applied to the pneumatic tires on the wheels.
5. As only small values of the gyroscopic and stabilizing moments acting on the pneumatic tires on the running wheels of the aggregating tractor and the support-and-finder wheels of the top harvester as well as the moments of their twisting about the vertical axes are observed during the movement of the given unit, they will be left out of consideration.
6. The slip angles of the pneumatic tires on the running wheels of the aggregating tractor, which are located on the same geometric axis, as well as the lateral forces acting on them, are assumed to be quite small.
7. The turn angles of the left and right steer wheels of the aggregating tractor are assumed to be small and equal to each other, because it is reasonable to consider the main movement of this top harvesting machine-tractor unit, when it performs the technological process of harvesting sugar beet tops, to be straight.

Theory and modelling

Taking into account the above-mentioned assumptions, the aggregating wheeled tractor in the equivalent scheme can be presented in an arbitrary position. In this case, its main points are selected and designated with the corresponding letters: the tractor's centre of mass - point S; the centre of the steer wheel axle - point A; the centre of the driving wheel axle - point B; the hitching point of the aggregated top harvester is designated by the point C. At the same time, the stub axles of the steer wheels of the aggregating tractor are included, because of their small size, in the total length of the front wheel axle.

Further, the systems of coordinate axes have to be chosen for this dynamic system and shown in the equivalent diagram with an aim of analysing its movements relative to these systems. First of all, the fixed Cartesian coordinate system $XOYZ$ is rigidly connected to the surface of the beet field, which acts as the plane (the axis Z is not shown), in which the plane-parallel motion of the machine-tractor unit takes place. The separate spatial system of coordinate axes $X_TSY_TZ_T$ has its origin at the centre of mass of the aggregating tractor (point S). Its axis SY_T coincides with the longitudinal axis of the tractor, the axis SX_T is directed normally to the right with respect to the direction of the tractor's movement, and axis SZ_T is directed vertically upwards. For the direction of motion of the tractor's front steer wheels, the movable coordinate system X_AAY_A with its centre located at the point A is assigned. The axis AY_A always coincides with the direction of motion of the tractor's front steer wheels (parallel to the planes of these wheels), while the axis AX_A is directed perpendicular to the axis AY_A and to the right with respect to the course of motion of the tractor.

It is also assumed, taking into account the previously made assumptions, that the aggregating wheeled tractor on its working run performs translational and uniform motion with the speed V_o relative to the stationary coordinate system XOY. However, in the process of performing the work movement, under the influence of external random factors, the aggregating wheeled tractor deviates from its original position, receives an additional speed and begins its relative motion in the plane XOY. In this case, the plane Y_TSX_T associated with the centre of mass of the tractor rotates in the plane XOY around the vertical axis SZ_T that passes through the point S. The angle φ formed by the longitudinal axis of symmetry of the wheeled tractor and the axis OY is the characteristic of this rotation.

During the relative motion of the tractor, its centre of mass moves along the axis OX, which is represented by the change in coordinate X_S (Fig. 2).

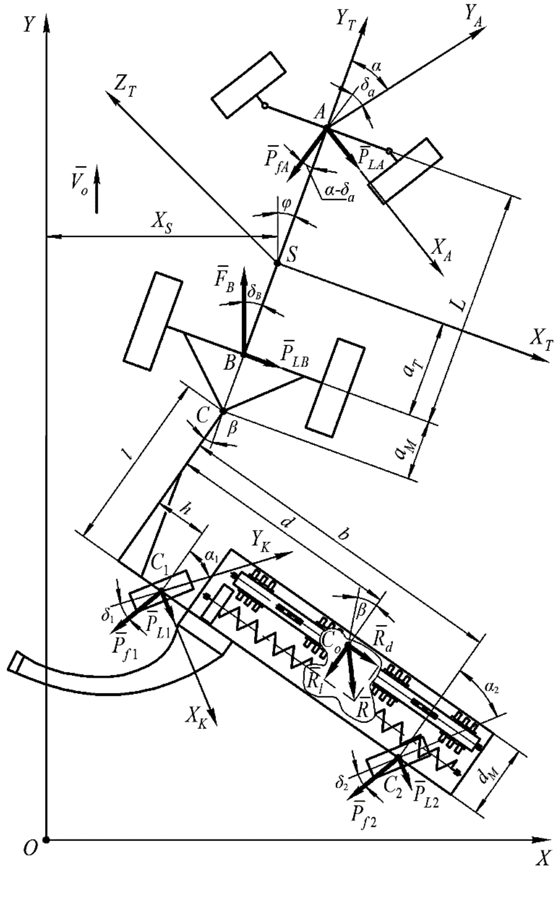

Figure 2. Equivalent scheme of asymmetric top harvesting machine-tractor unit.

Thus, the wheeled aggregating tractor has two degrees of freedom relative to the plane XOY, namely: linear coordinate X_S and angular coordinate φ, which are further used as the generalized coordinates.

The next step is to show on the equivalent diagram the external forces acting on the wheeled aggregating tractor during its plane-parallel motion and determine their physical attributes. These forces are as follows. First of all, it is the driving force $\bar{F}_B$, which is generated by the rear two driving wheels of the tractor and can be applied at the point B.

The driving force $\bar{F}_B$ forms the slip angle δ_B with the longitudinal axis of symmetry of the aggregating tractor. The tractor is also affected by the rolling resistance force $\bar{P}_{fA}$ generated by the two front steer wheels, applied at the point of intersection between their axis and the longitudinal axis SY_T (point A) and deflected from the direction of movement of the tractor's running gear through the slip angle δ_A. There are also lateral forces acting on the tractor from the two axles: $\bar{P}_{LA}$ and $\bar{P}_{LB}$ and applied respectively at points A and B. Finally, the draught resistance force $\bar{P}_{KR}$ is applied to the wheeled aggregating tractor by the top harvester at the point C and deflected from the longitudinal axis of the tractor, that is, from the axis SY_T, through the angle β.

It should be noted at once that the main moment (i. e. the turning moment M_t relative to the point C) of all the external forces acting on the rear-trailed top harvester is not transferred to the aggregating tractor due to the hinge connection of the aggregated asymmetric machine at the point C.

As a result, the influence of the trailed asymmetric machine on the aggregating wheeled tractor is represented only by its traction resistance $\bar{P}_{KR}$ and the angle β of turn (deviation) in the horizontal plane.

Following the above considerations, there is the complete basis for generating the differential equations of the plane-parallel motion performed by the wheeled aggregating tractor. For that purpose, the original Lagrange equations of the second kind of the following form can be used (Dreizler & Lüdde, 2010):

$$\frac{d}{dt}\left(\frac{\partial T_T}{\partial \dot{q}_i}\right)-\frac{\partial T_T}{\partial q_i}=Q_i\,, \tag{1}$$

where T_T – kinetic energy of a wheeled aggregate tractor; q_i – generalized coordinates; Q_i – generalized forces, according to the corresponding generalized coordinates q_i.

The kinetic energy T_T of the aggregate wheeled tractor relative to the horizontal plane XOY is defined as:

$$T_T=\frac{M_T\cdot V_S^2+J_S\cdot \omega_T^2}{2}, \tag{2}$$

where M_T – mass of the aggregate tractor; V_S – linear velocity of the center of mass of the tractor in the plane XOY; J_s – the moment of inertia of the tractor relative to the vertical axis SZ_T; ω_T – angular speed of rotation of the tractor around the axis SZ_T.

If we express linear V_S and angular ω_T velocity through generalized coordinates X_S and φ, we obtain:

$$V_S=\dot{X}_S\,, \tag{3}$$

$$\omega_T=\dot{\varphi}. \tag{4}$$

Taking into account expressions (3) and (4), the kinetic energy T_T of the wheeled aggregate tractor can be determined as follows:

$$T_T=\frac{M_T\cdot \dot{X}_S^2+J_S\cdot \dot{\varphi}^2}{2}. \tag{5}$$

Since the kinetic energy T_T of the tractor due to expression (5) depends only on velocities $\dot{X}_S$ and $\dot{\varphi}$ and does not depend on the most generalized coordinates q_i, the partial derivative will be:

$$\frac{\partial T_T}{\partial q_i} = 0. \tag{6}$$

At the same time, the partial derivatives of the velocities $\dot{X}_S$ and $\dot{\varphi}$ the corresponding generalized coordinates $\dot{X}_S$ and φ will be equal to:

$$\frac{\partial T_T}{\partial \dot{X}_S} = M_T \cdot \dot{X}_S, \tag{7}$$

$$\frac{\partial T_T}{\partial \dot{\varphi}} = J_S \cdot \dot{\varphi}. \tag{8}$$

The time derivatives of expressions (7) and (8) are determined by the following expressions:

$$\frac{d}{dt}\left(\frac{\partial T_T}{\partial \dot{X}_S}\right) = M_T \cdot \ddot{X}_S, \tag{9}$$

$$\frac{d}{dt}\left(\frac{\partial T_T}{\partial \dot{\varphi}}\right) = J_S \cdot \ddot{\varphi} \tag{10}$$

Using the values obtained from expressions (9) and (10), taking into account expression (6) for the two generalized coordinates X_S and φ and substituting them into expression (1), we obtain the following system of differential equations for the plane-parallel motion of the aggregate wheeled tractor in this form:

$$\left.\begin{aligned} M_T \cdot \ddot{X}_S &= Q_{X_S}, \\ J_S \cdot \ddot{\varphi} &= Q_{\varphi}. \end{aligned}\right\} \tag{11}$$

The next step is to determine the right-hand sides of the differential equations of system (11), i.e., the generalized forces: Q_{X_S} and Q_{φ}.

First, the value of the generalized force Q_{X_S} with reference to the generalized coordinate X_S has to be determined. For that purpose, the dynamical system under consideration is imparted a virtual displacement and the expression is generated for the elementary work of the forces on the virtual displacement δX_S. The result is as follows:

$$\begin{gathered} \delta A_{X_S} = P_{LA} \cdot \cos(\varphi + \alpha) \cdot \delta X_S - P_{fA} \cdot \sin(\varphi + \alpha - \delta_A) \cdot \delta X_S + \\ + P_{LB} \cdot \cos\varphi \cdot \delta X_S - F_B \sin(\delta_B - \varphi) \cdot \delta X_S - P_{KR} \cdot \sin(\varphi + \beta) \cdot \delta X_S, \end{gathered} \tag{12}$$

where α – the angle of rotation of the steered wheels of the tractor.

From expression (12) we obtain that the generalized force Q_{X_S} on the generalized coordinate X_S will be:

$$\begin{gathered} Q_{X_S} = \frac{\delta A_{X_S}}{\delta X_S} = P_{LA} \cdot \cos(\varphi + \alpha) - P_{fA} \cdot \sin(\varphi + \alpha - \delta_A) + \\ + P_{LB} \cdot \cos\varphi - F_B \sin(\delta_B - \varphi) - P_{KR} \cdot \sin(\varphi + \beta). \end{gathered} \tag{13}$$

Thus, this generalized force Q_{X_S} is equal to the sum of the projections of all active external forces applied to the wheeled tractor on the axis *OX*.

In order to determine the generalized force Q_{φ} with reference to the generalized coordinate φ, again, a virtual displacement of the given dynamical system is assumed, but this time an angular one, and the expression is generated for the elementary work of the forces on the virtual displacement $\delta\varphi$. The following is obtained:

$$\begin{aligned}\delta A_{\varphi} &= P_{LA}\cdot\left(L-a_T\right)\cos\alpha\cdot\delta\varphi - P_{fA}\cdot\left(L-a_T\right)\sin\left(\alpha-\delta_A\right)\cdot\delta\varphi - \\ &-P_{LB}\cdot a_T\cdot\delta\varphi + F_B\cdot a_T\sin\delta_B\cdot\delta\varphi + P_{KR}\cdot\left(a_T+a_M\right)\sin\beta\cdot\delta\varphi.\end{aligned}\tag{14}$$

From expression (14), it is derived that the generalized force Q_{φ} with reference to the generalized angular coordinate φ will be:

$$\begin{aligned}Q_{\varphi} &= \frac{\delta A_{\varphi}}{\delta\varphi} = P_{LA}\cdot\left(L-a_T\right)\cos\alpha - P_{fA}\cdot\left(L-a_T\right)\sin\left(\alpha-\delta_A\right) - \\ &-P_{LB}\cdot a_T + F_B\cdot a_T\sin\delta_B + P_{KR}\cdot\left(a_T+a_M\right)\sin\beta.\end{aligned}\tag{15}$$

That is, the generalized force Q_{φ} on the generalized coordinate φ is equal to the algebraic sum of the moments of all external forces relative to the point *S*.

Let us further analyze obtained expressions (13) and (15) for generalized forces Q_{X_S} and Q_{φ} and find possibilities for their simplification. These expressions can be simplified because for small angles the value of cosines can be approximately considered as equal to unities, and the value of sines can be considered as equal to the most angles.

Therefore, expression (13) can be represented as follows:

$$Q_{X_S} = P_{LA} - P_{fA}\left(\varphi+\alpha-\delta_A\right) + P_{LB} - F_B\left(\delta_B-\varphi\right) - P_{KR}\left(\varphi+\beta\right),\tag{16}$$

or

$$Q_{X_S} = P_{LA} + P_{LB} - P_{fA}\alpha + P_{fA}\delta_A - F_B\delta_B + \left(F_B - P_{fA} - P_{KR}\right)\varphi - P_{KR}\beta\cdot\tag{17}$$

Given that $F_B - F_{fA} - P_{KR} = 0$, then in the final form we obtain an expression for determining the generalized force Q_{X_S} of the following form:

$$Q_{X_S} = P_{LA} + P_{LB} - P_{fA}\alpha + P_{fA}\delta_A - F_B\delta_B - P_{KR}\beta\cdot\tag{18}$$

Let us perform similar transformations for expression (15), taking into account small values of angles α and β. Finally, we obtain an expression for the generalized force Q_{φ} of the following form:

$$\begin{aligned}Q_{\varphi} &= P_{LA}\left(L-a_T\right) - P_{fA}\cdot\alpha\left(L-a_T\right) - P_{LB}\cdot a_T + P_{fA}\cdot\delta_A\left(L-a_T\right) + \\ &+ F_B\cdot\delta_B\cdot a_T + P_{KR}\cdot\beta\left(a_T+a_M\right).\end{aligned}\tag{19}$$

Forces P_{LA} and P_{LB}, which are included in dependencies (18) and (19), can be replaced by expressions formed on the basis of the so-called hypothesis of 'lateral input' of pneumatic wheel tires (Macmillan, 2002; Kutkov, 2014; Abyzov & Berezin, 2018) of this form:

$$P_{LA} = k_A\cdot\delta_A,\tag{20}$$

$$P_{LB} = k_B\cdot\delta_B,\tag{21}$$

where k_A, k_B – coefficients of lateral input of pneumatic tires of running wheels of the aggregating wheeled tractor.

In expressions (20) and (21) it is necessary to substitute the values of the input angles δ_A and δ_B, which are determined on the basis of the construction of velocity plans of points *A* and *B*, that is, the middle of the front (controlled) and rear (traction) axles of the aggregate tractor at their plane and parallel motion in the horizontal plane *XOY*.

Using the technique outlined in (Hwang et al., 2021), we constructed the above velocity plans, allowed us to graphically find the values of velocities V_A and V_B, then through their projections on the axes *X* and *Y*, as well as the corresponding tangents of angles and based on the neglect of small quantities, find the angles themselves δ_A and δ_B. As a result, the final expressions for the lateral forces P_{LA} and P_{LB} of this type:

$$P_{LA} = k_A \cdot \left[\frac{-\dot{X}_S - (L - a_T)\dot{\varphi}}{V_o} + \varphi + \alpha \right], \tag{22}$$

$$P_{LB} = k_B \cdot \left[-\frac{\dot{X}_S - a_T \cdot \dot{\varphi}}{V_o} + \varphi \right]. \tag{23}$$

To determine the position of the supporting copying wheels of the topper at an arbitrary moment of time, consider its diagram separately and show on it a movable coordinate system $Y_K C_1 X_K$, rigidly connected with the left supporting copying wheel of the topper (Fig. 3). The axis $C_1 Y_K$ is always parallel to the plane $C_1 X_K$ of the support wheel, but perpendicular to it and pointing to the right in the direction of the mower harvester's movement. These directions of movement for the right support wheels of the hitch machine in the first approximation can be considered similar. However, the moving coordinate system is not shown here.

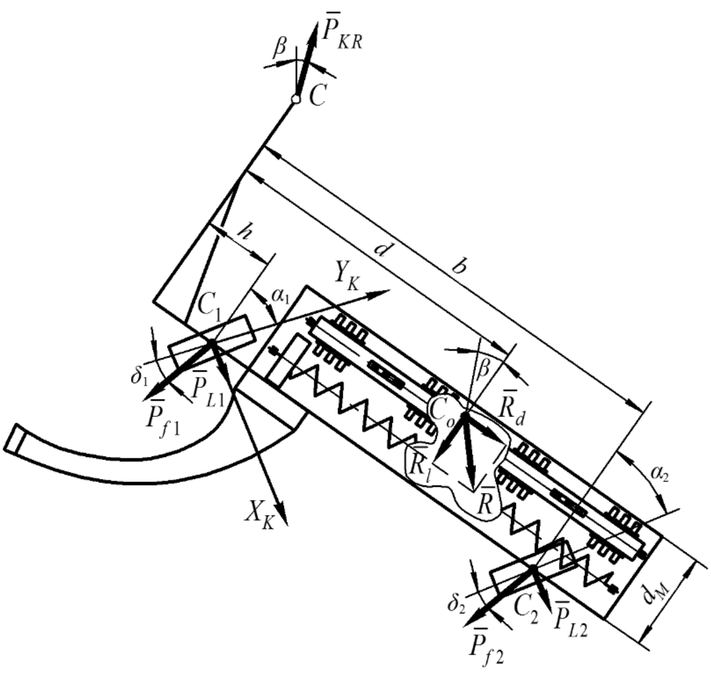

Figure 3. Equivalent diagram of an aggregated harvester.

As presented, the trailed harvester as a dynamic system can be regarded as a physical pendulum with only one degree of freedom - the angle β of rotation in the horizontal plane. This angle β of rotation will be the generalized coordinate in the subsequent differential equations in the form of the original Lagrange equations of dynamics of the form (1).

Let us define in this case the components necessary for expression (1). Thus, the kinetic energy T_H of the aggregated harvesting machine will be:

$$T_H = \frac{J_C \cdot \dot{\beta}^2}{2}, \tag{24}$$

where J_C – the moment of inertia of the hitch harvester relative to the vertical axis passing through the point C; $\dot{\beta}$ – the angular velocity of rotation of the harvesting machine around the point C.

In this case, the necessary partial derivatives included in the original Lagrange equations of the second kind (1) are from the following expressions:

$$\frac{\partial T_H}{\partial \dot{\beta}} = J_C \cdot \dot{\beta}, \tag{25}$$

$$\frac{\partial T_H}{\partial \beta} = 0, \tag{26}$$

$$\frac{d}{dt}\left(\frac{\partial T_H}{\partial \dot{\beta}}\right) = J_C \cdot \ddot{\beta}. \tag{27}$$

Given expressions (22) and (23), the differential equation of motion of a trailed harvester will look like this:

$$J_C \cdot \ddot{\beta} = Q_\beta. \tag{28}$$

To determine the generalized force Q_β, included in expression (28), let us denote the external forces acting on the trailed harvester. External forces acting on the harvester during its technological process include longitudinal $\bar{R}_l$ and transverse $\bar{R}_d$' components of the resistance force $\bar{R}$ of the harvested haulm array, which are applied to the machine at a point C_o; $\bar{P}_{f1}$ rolling resistance force of the left copying wheel of the harvester, applied at a point C_1 and deflected from the wheel plane at the entry angle δ_1; $\bar{P}_{f2}$ - rolling resistance force of the right copying wheel of the tillage machine applied at the point C_2 and deflected from the wheel plane by the entry angle δ_2; lateral forces $\bar{P}_{L1}$ and $\bar{P}_{L2}$, applied according to the left and right copying wheels of the tillage machine at the points C_1 and C_2.

To determine the generalized force Q_β by coordinate β let us use the expression for the elementary work of forces on a possible displacement $\delta\beta$. Then:

$$\begin{aligned} \delta A_\beta = {} & R_l \cdot d \cdot \delta\beta - R_d\left(l - d_M\right)\cdot\delta\beta + P_{f1}\cos\left(\alpha_1 - \delta_1\right)\cdot h \cdot \delta\beta + \\ & + P_{f2}\cdot\cos\left(\alpha_2 - \delta_2\right)\cdot b \cdot \delta\beta + P_{f1}\sin\left(\alpha_1 - \delta_1\right)\cdot l \cdot \delta\beta + \\ & + P_{f2}\cdot\sin\left(\alpha_2 - \delta_2\right)\cdot l \cdot \delta\beta - P_{L1}\cdot\cos\alpha_1 \cdot l \cdot \delta\beta - \\ & - P_{L2}\cdot\cos\alpha_2 \cdot l \cdot \delta\beta + P_{L1}\cdot\sin\alpha_1 \cdot h \cdot \delta\beta + P_{L2}\cdot\sin\alpha_2 \cdot b \cdot \delta\beta, \end{aligned} \tag{29}$$

where d, l, d_M, h and b – construction parameters of the harvesting machine (Fig. 3); a_1 and a_2 – the angles of the left and right gauge wheels of the harvester respectively.

From expression (29) we obtain that the generalized force Q_β on the generalized angular coordinate β will be equal to:

$$Q_\beta = \frac{\delta A_\beta}{\delta\beta} = R_l \cdot d - R_d\left(l - d_M\right) + P_{f1}\cos\left(\alpha_1 - \delta_1\right)\cdot h +$$
$$+ P_{f2}\cdot\cos\left(\alpha_2 - \delta_2\right)\cdot b + P_{f1}\sin\left(\alpha_1 - \delta_1\right)\cdot l +$$
$$+ P_{f2}\cdot\sin\left(\alpha_2 - \delta_2\right)\cdot l - P_{L1}\cdot\cos\alpha_1\cdot l -$$
$$- P_{L2}\cdot\cos\alpha_2\cdot l + P_{L1}\cdot\sin\alpha_1\cdot h + P_{L2}\cdot\sin\alpha_2\cdot b. \quad (30)$$

Analysing the obtained expression (30). As in the previous case, the cosines of small angles can be replaced by units, and the sines by the angles themselves. Moreover, if we take into account the small values of angles a_1 and a_2, then expression (30) can be presented in the following form:

$$Q_\beta = R_l \cdot d - R_d\left(l - d_M\right) + P_{f1}\cdot h + P_{f2}\cdot b + P_{f1}\cdot l\left(\alpha_1 - \delta_1\right) +$$
$$+ P_{f2}\cdot l\left(\alpha_2 - \delta_2\right) - P_{L1}\cdot l - P_{L2}\cdot l + P_{L1}\cdot\alpha_1\cdot h + P_{L2}\cdot\alpha_2\cdot b. \quad (31)$$

Moreover, from Fig. 3 it is clear that $R_d = R_l \cdot \tan\beta$. And since the value of the angle β is small $\tan\beta \approx \beta$, and therefore:

$$R_d = R_l \cdot \beta. \quad (32)$$

As in the case of an aggregate wheeled tractor, the lateral forces P_{L1} and P_{L2}, acting on the supporting copying wheels of the tiller can be replaced by expressions formed on the basis of the hypothesis of ‘lateral input’ of its pneumatic wheel tires. Namely:

$$P_{L1} = k_1 \cdot \delta_1, \quad (33)$$

$$P_{L2} = k_2 \cdot \delta_2, \quad (34)$$

where k_1, k_2 – coefficients of lateral input of pneumatic tires of basic copying wheels of the harvesting machine; δ_1, δ_2 – angles of input of pneumatic basic copying wheels of the harvesting machine.

As in the previous case, to determine the lateral forces P_{L1} and P_{L2} need to find the input angles δ_1, δ_2 respectively the left and right supporting coping wheels of the harvester. For this purpose, we constructed velocity plans for finding the velocities of points C_1 and C_2, their projections on the axes X and Y taking into account the tangents of the angles and neglecting the small values. As a result, we found the final expressions for these input angles of this form:

$$\delta_1 = \frac{-\dot{X}_S + \dot{\varphi}\left(a_T + a_M\right) + \dot{\beta}\left(l^2 + h^2\right)^{\frac{1}{2}}}{V_o} + \varphi + \beta + \alpha_1, \quad (35)$$

$$\delta_2 = \frac{-\dot{X}_S + \dot{\varphi}\left(a_T + a_M\right) + \dot{\beta}\left(l^2 + b^2\right)^{\frac{1}{2}}}{V_o} + \varphi + \beta + \alpha_2. \quad (36)$$

If we substitute the values of expressions (35) and (36) in expressions (33) and (34), it is possible to obtain the value of lateral forces P_{L1} and P_{L2}, taking into account the input angles δ_1 and δ_2, which can then be used to find the generalized force Q_β.

Now, given expressions (33), (34), which are transformed with expressions (35) and (36), the generalized force Q_β, due to expression (31) can be represented by the following expression:

$$Q_\beta = R_l \cdot d - R_d\left(l - d_M\right)\beta + P_{f1} \cdot h + P_{f2} \cdot b + P_{f1} \cdot l\left(\alpha_1 - \delta_1\right) + \\ + P_{f2} \cdot l\left(\alpha_2 - \delta_2\right) - k_1 \cdot \delta_1 \cdot l - k_2 \cdot \delta_2 \cdot l + k_1 \cdot \delta_1 \cdot \alpha_1 \cdot h + k_2 \cdot \delta_2 \cdot \alpha_2 \cdot b. \quad (37)$$

If we consider that the product of two small quantities is even smaller, the sum of the last two terms $(k_1 \cdot \delta_1 \cdot \alpha_1 \cdot h) + (k_2 \cdot \delta_2 \cdot \alpha_2 \cdot b)$ in expression (37) can be neglected. In this case we have:

$$Q_\beta = R_l\left[d - \left(l - d_M\right)\beta\right] + P_{f1}\left[h + \left(\alpha_1 - \delta_1\right) \cdot l\right] + \\ + P_{f2}\left[b + \left(\alpha_2 - \delta_2\right) \cdot l\right] - k_1 \cdot \delta_1 \cdot l - k_2 \cdot \delta_2 \cdot l. \quad (38)$$

If we now take into account all of the last expressions, we get the final value for the generalized force Q_β of the trailed harvester in the following form:

$$\begin{aligned} Q_\beta &= R_l\left[d - \left(l - d_M\right)\beta\right] + \\ &+ P_{f1}\left\{h + \left(\alpha_1 - \left[\frac{-\dot{X}_S + \dot{\varphi}\left(a_T + a_M\right) + \dot{\beta}\left(l^2 + h^2\right)^{\frac{1}{2}}}{V_o} + \varphi + \beta + \alpha_1\right]\right) \cdot l\right\} + \\ &+ P_{f2}\left\{b + \left(\alpha_2 - \left[\frac{-\dot{X}_S + \dot{\varphi}\left(a_T + a_M\right) + \dot{\beta}\left(l^2 + b^2\right)^{\frac{1}{2}}}{V_o} + \varphi + \beta + \alpha_2\right]\right) \cdot l\right\} - \\ &- k_1 \cdot l\left[\frac{-\dot{X}_S + \dot{\varphi}\left(a_T + a_M\right) + \dot{\beta}\left(l^2 + h^2\right)^{\frac{1}{2}}}{V_o} + \varphi + \beta + \alpha_1\right] - \\ &- k_2 \cdot l\left[\frac{-\dot{X}_S + \dot{\varphi}\left(a_T + a_M\right) + \dot{\beta}\left(l^2 + b^2\right)^{\frac{1}{2}}}{V_o} + \varphi + \beta + \alpha_2\right]. \end{aligned} \quad (39)$$

Substituting expressions (18), (19) and (39) for generalized forces Q_{X_S}, Q_φ and Q_β taking into account expressions (22) and (23), which should be substituted into expressions (11) and (28) respectively, and discarding terms of higher order of smallness, after a number of transformations we obtain a system of second order linear differential equations describing the motion of an asymmetric machine-tractor unit in the horizontal plane:

$$\left.\begin{aligned} &A_{11} \cdot \ddot{X}_S + A_{12} \cdot \dot{X}_S + A_{13} \cdot \dot{\varphi} + A_{14} \cdot \varphi + A_{15} \cdot \beta = f_{11} \cdot \alpha, \\ &A_{21} \cdot \ddot{\varphi} + A_{22} \cdot \dot{\varphi} + A_{23} \cdot \varphi + A_{24} \cdot \dot{X}_S + A_{25} \cdot \beta = f_{21} \cdot \alpha, \\ &A_{31} \cdot \ddot{\beta} + A_{32} \cdot \dot{\beta} + A_{33} \cdot \beta + A_{34} \cdot \dot{\varphi} + A_{35} \cdot \varphi + A_{36} \cdot \dot{X}_S = f_{31}, \end{aligned}\right\} \quad (40)$$

where $A_{11} = M_T$;

$A_{12} = \dfrac{k_A + k_B + P_{fA} - F_B}{V_o}$;

$A_{13} = \dfrac{\left(k_A + P_{fA}\right) \cdot (L - \alpha_T) + (F_B - k_B) \cdot \alpha_T}{V_o}$;

$A_{14} = F_B - k_A - k_B - P_{fA}$;

$A_{15} = P_{KR}$;

$A_{21} = J_S$;

$$A_{22} = \frac{(k_A + P_{fA}) \cdot (L - \alpha_T)^2 + (k_B - F_B) \cdot \alpha_T^2}{V_o};$$
$$A_{23} = -A_{13} \cdot V_o;$$
$$A_{24} = A_{13};$$
$$A_{25} = P_{KR}(\alpha_T + \alpha_M);$$
$$A_{31} = J_c;$$
$$A_{32} = \frac{l \cdot \left[(k_1 + P_{f1}) \cdot (l^2 + h^2)^{\frac{1}{2}} + (k_2 + P_{f2}) \cdot (l^2 + b^2)^{\frac{1}{2}}\right]}{V_o};$$
$$A_{33} = R_l(l - d_M) + l(k_1 + k_2 + P_{f1} + P_{f2});$$
$$A_{34} = \frac{l \cdot (\alpha_T + \alpha_M) \cdot (k_1 + k_2 + P_{f1} + P_{f2})}{V_o};$$
$$A_{35} = l(k_1 + k_2 + P_{f1} + P_{f2});$$
$$A_{36} = \frac{A_{35}}{V_o};$$
$$f_{11} = k_A;$$
$$f_{21} = (L - \alpha_T) \cdot k_A;$$
$$f_{31} = R_l \cdot d + P_{f1} \cdot h + P_{f2} \cdot b - \alpha_1 \cdot l \cdot k_1 - \alpha_2 \cdot l \cdot k_2.$$

RESULTS AND DISCUSSION

The obtained mathematical model (40) is the basis for studying the influence of the rotation angle β of the trailed tillage machine on the oscillations of the course angle φ of the tractor, by constructing the amplitude-frequency and phase-frequency characteristics. It is known (David et al., 2009) that the amplitude-frequency response should be as small as possible when the dynamic system works out any perturbation. Ideally, it should be equal to zero. At the same time, the phase-frequency shift (i. e., the delay of the response of the dynamic system to the disturbing influence) should be as large as possible. As a result, the desired amplitude-frequency characteristics should be equal to 0, while the phase-frequency characteristics, on the contrary, should tend to 0 when the dynamic system is working out the perturbation ∞.

Those parameters and modes of operation of the investigated asymmetric machine-tractor unit, which in the working range of oscillations of controlling and disturbing input influences maximally approximate the actual amplitude-frequency and phase-frequency characteristics to the desired ones - will therefore be considered optimal.

To perform numerical calculations of differential equations (40) on the computer, a program was developed. Methodology of practical use of obtained mathematical model (40) is considered on example of analysis of stability of motion in horizontal plane of asymmetric machine-tractor unit developed by us with the following construction parameters: M_T = 4,250 kg, J_S = 4.6 kN m s^2, P_{KR} = 7.3 kN, P_{FA} = 1.7 kN, L = 2.45 m, α_T = 0.98 m; α_M = 1.20 m; k_A = 80 kN rad^{-1}, k_B = 120 kN rad^{-1}.

It should be noted at once that we used for aggregation of the asymmetric mower harvester the power tool of the integral scheme, in which about 60% of the weight is on the front axle, and the rest (40%) - on the rear axle. The driving wheels of both axles in this case, as a rule, are active-primitive and equipped with pneumatic tires of the same size. In this case, the wheels of the front and rear axles of the aggregate tractor are equipped with the same pneumatic tires of size 16.9R30. At air pressure in pneumatic tires equal to 130 kPa coefficient k_A of input resistance of front wheels is 120 kN rad^{-1}. The air pressure in the pneumatic tires of the rear engines is 100 kPa, which corresponds to the value of a similar coefficient k_B, equal to 90 kN rad^{-1}.

As a result of these numerical calculations on the PC of the obtained mathematical model, we plotted the amplitude and phase frequency characteristics, which allow us to estimate the stability of the working motion of the asymmetric machine-tractor unit (Fig. 4 and Fig 5).

On the basis of the obtained graphical dependencies, we will analyze how some construction and technological factors of the given harvester machine affect the amplitude and phase frequency characteristics of oscillations of the course angle φ of the wheel tractor when changing the frequency of oscillations of the angle β of deviation of the trailed harvester in the horizontal plane.

First, we consider the influence of the translational velocity V_o of a given harvesting machine. The analysis of the obtained amplitude-frequency characteristics testifies to the following. First, as the frequency of the disturbing oscillations (i.e., the angle β) increases, the amplification factor of the considered dynamic system of this input effect at each speed mode of motion of the harvesting machine gradually decreases (Fig. 4).

There is every reason to believe that this result is logical, since the greater the frequency of oscillations of perturbation ω, the greater the stabilizing role played by the inertial properties of the dynamic system, which is considered.

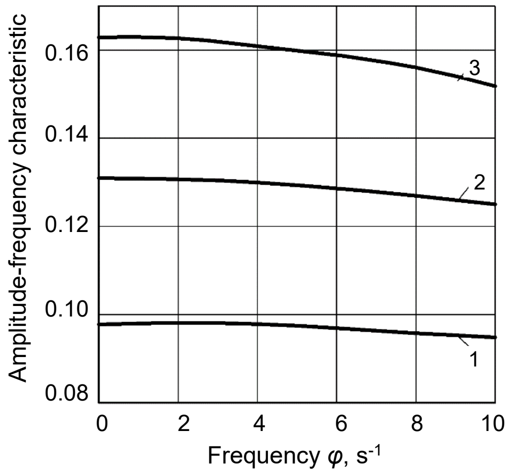

Figure 4. Amplitude-frequency characteristic of the course angle φ of the tractor of the integral configuration when it works out disturbances in the form of oscillations of the turn angle β of the mower harvester at different speeds of the machine: 1) V_o = 1.5 m s^{-1}; 2) V_o = 2.0 m s^{-1}; 3) V_o = 2.5 m s^{-1}.

Secondly, with the increase of speed V_o of the harvesting machine movement, it becomes more sensitive to perturbing influences. For example, at frequency of oscillations of the angle β at a level $\omega = 4$ s^{-1} and speed of machine movement 1.5 m s^{-1} its amplitude-frequency characteristic makes 0.09 (curve 1, Fig. 4). In simplified to understand form, this means that for the vibration amplitude of the perturbation (angle β) at 5° (and this is palpable) the vibration amplitude of the course angle φ of the aggregate tractor is only 0.5°, which is almost imperceptible.

At a speed V_o of movement of the harvesting machine at the level of 2.5 m s^{-1} and the same frequency of vibration perturbation $\omega = 4$ s^{-1} the amplitude-frequency characteristic of the dynamic system increases to a mark 0.15 (curve 3, Fig. 4). Compared with the previous velocity mode (when the amplitude-frequency response is equal to 0.09) this is almost 1.5 times greater. However, by the same amplitude of oscillations of the angle $\beta = 5°$ the amplitude of oscillations of the course angle of the tractor φ does not exceed 0.7°.

Thus, at a speed of 2.5 m s^{-1} in a range of vibration frequency of disturbing influences (angle β fluctuations) $\omega = 0–10$ s^{-1} the amplitude-frequency characteristic of the given machine-tractor at application of the integral aggregate tractor changes already in a range 0.163–0.152 (curve 3, Fig. 4).

As we see, in qualitative terms, an increase in the speed V_o of the machine-tractor unit under consideration leads to an undesirable increase in the amplitude-frequency response when it reproduces the external disturbing influence in the form of oscillations of the angle β of rotation of the harvester. In quantitative terms, this influence is such that it cannot worsen the practical stability of motion of the given harvesting machine.

Now, as for the delayed response of the considered dynamic system to the disturbing influence. Under the condition of increasing its frequency, the phase-frequency response at each speed mode of the machine-tractor unit movement increases (Fig. 5).

That is, the greater the value of the perturbation frequency ω, the more influential are the inertial properties of the unit and the greater is its delay (in this case, the phase shift) to the action of perturbing influences. The same inertial properties of the tillage machine are also responsible for the fact that its reaction time to disturbances increases as its speed V_o increases. So, if at $V_o = 1.5$ m s^{-1} and $\omega = 10$ s^{-1} the phase shift of dynamic system (i.e. phase-frequency characteristic) makes - 15° (curve 1, Fig. 5), then already at speed $V_o = 2.5$ m s^{-1} and at the same frequency ω this parameter increases to a mark - 25° (curve 3, Fig. 5). The phase shift difference in this case is 10° or 0.17 rad.

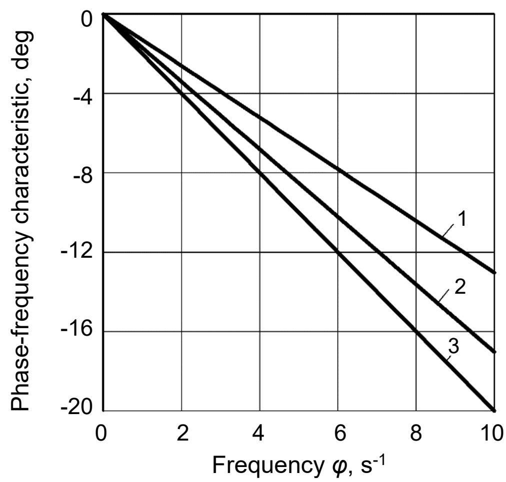

Figure 5. Phase-frequency characteristic of the course angle φ of the tractor of the integral configuration when it works out disturbances in the form of oscillations of the tiller turning angle β at different speeds of the machine: 1) $V_o = 1.5$ m s^{-1}; 2) $V_o = 2.0$ m s^{-1}; 3) $V_o = 2.5$ m s^{-1}.

CONCLUSIONS

1. Using the developed equivalent scheme (Fig. 2) of motion of an asymmetric harvesting machine-tractor unit, a new calculated mathematical model of its plane-parallel motion in the horizontal plane is constructed.

2. A new system of linear differential equations (40) of the second order is obtained, which describes the dynamics of the transverse displacement of the center of mass of the aggregate wheeled tractor, its course angle, and the angle of deviation of the trailed hitch from the longitudinal axis of the tractor at any time.

3. The obtained system of differential equations (40) after its solution on the PC made it possible to establish the stability and controllability of the movement of the asymmetric harvesting machine-tractor unit when performing the technological process of harvesting sugar beet tops.

REFERENCES

Abyzov, A.A. & Berezin, I.Ya. 2018. Calculating curvilinear motion of transport vehicles based on a finite element modeling of track-ground interaction. *Buletin of the South Ural University. Series: Mechanical Ingineering Industry* **18**(4). doi: 10.14529/engin180408

Anche, M. & Subramanian, C., 2018. Model Based Compensator Design for Pitch Plane Stability of a Farm Tractor with Implement. *IFAC-PapersOnLine* **51**, 208–213. https://doi.org/10.1016/j.ifacol.2018.05.043

Boson, E.S., Verniaev, O.V., Smirnov, I.I. & Sultan-Shach, E.G. 2019. *Theory, Construction and Calculation of Agricultural Machines*. 2nd Ed., Scientific Publisher, 810 pp. ISBN: 9789388399838

Bulgakov, V., Adamchuk, V., Arak, M. & Olt, J. 2017a. A theoretical study of haulm loss resulting from rotor topper oscillation. *Chemical Engineering Transactions* **58**, 223−228. doi: 10.3303/CET1758038.

Bulgakov, V., Adamchuk, V., Nadykto, V., Kistechok, O. & Olt, J. 2017b. Theoretical research into the stability of motion of the ploughing tractor-implement unit operating on the 'push-pull' principle. *Agronomy Research* **15**(4), 1517−1529. doi: 10.15159/AR.17.069

Bulgakov, V., Holovach, I., Nadykto, V., Parakhin, O., Kaletnik, N., Shymko, L. & Olt, J. 2020 a. Motion stability estimation for modular traction vehicle-based combined unit. *Agronomy Research* **18**(4), 2340−2352. doi: 10.15159/AR.20.183

Bulgakov, V., Kuvachov, V. & Olt, J. 2020b. Theory of smoothness of movement of multiple-axle agricultural combined tractor-implement units, Proceedings of the 31st DAAAM International Symposium, pp. 0056−0065, B. Katalinic (Ed.), Published by DAAAM International, ISBN 978-3-902734-29-7, ISSN 1726-9679, Vienna, Austria. doi: 10.2507/31st.daaam.proceedings.008

Demšar, I., Bernik, R. & Duhovnik, J., 2012. A Mathematical Model and Numerical Simulation of the Static Stability of a Tractor. *Agric. Conspec. Sci*. **77**, 143–150.

Dreizler, R.M. & Lüdde, C.S. 2010. *Theoretical Mechanics*. Springer, 402 pp. doi: 10.1007/978-3-642-11138-9

Gruber, W. 2005. Trends in sugar beet harvesting. *Landtechnik* **60**(6), 320–321.

Gu F., Hu Z., Wu H., Peng B., Gao X. & Wang S. 2014. Development and experiment of 4LT-A staggered-dig sugar beet combine. *Nongye Gongcheng uebao/Transactions of the Chinese Society of Agricultural Engineering* **30**(23), 1–9.

David, M.-F., Voicu, G., David, L. & Rusanescu, C.-O. 2009. Experimental analysis considered the dynamics of mobiles agricultural aggregates. *Bulletin UASVM Agriculture* **66**(1), 51–58. doi: 10.15835/buasvmcn-agr:3727

Hac, A., Fulk, D. & Chen, H., 2008. Stability and Control Considerations of Vehicle-Trailer Combination. SAE *Int. J. Passeng. Cars - Mech. Syst.* **1**, 925–937. https://doi.org/10.4271/2008-01-1228

Hwang, S-J, Jang, M-K. & Nam, J.-S. 2021. Application of Lateral Overturning and Backward Rollover Analysis in a Multi-Purpose Agricultural Machine Developed in South Korea. *Agronomy* **11**(2), 297. https://doi.org/10.3390/agronomy11020297

Kutkov, G.M. 2014. *Tractors and Automobiles: the theory and the technological properties*, Moscow, Kolos, 506 pp. (in Russian).

Li, Z., Mitsuoka, M., Inoue, E., Okayasu, T., Hirai, Y. & Zhu, Z., 2016. Parameter sensitivity for tractor lateral stability against Phase I overturn on random road surfaces. *Biosystems Engineering* **150**, 10–23. https://doi.org/10.1016/j.biosystemseng.2016.07.004

Macmillan, R.H., 2002. *The Mechanics of Tractor - Implement Performance*. University of Melbourne, 165 pp. http://eprints.unimelb.edu.au.

Pogorely, L.V. & Tatyanko, N.V. 2004. *Beet-harvesting machines: History, Construction, Theory, Prognosis*, Feniks, Kyiv, 232 pp. (in Ukrainian).

Sarec, P., Sarec, O., Przybyl, J. & Srb, K. 2009. Comparison of sugar beet harvesters. *Listy cukrovarnicke a reparske* **125**(7–8), 212–216 (in Czech).

Szakács, T., 2010. Developing stability control theories for agricultural transport systems. *Acta Polytechnica Hungarica* **7**(2), 25–37.

Vasilenko, P.M. 1996. *Introduction to agricultural mechanics*. Agricultural Education, Kiev, 252 pp. (in Russian).

Yildiz, S. 2010. *Improving high speed lateral stability of longer and heavier vehicles by active steering*. Master´s Thesis, Eindhoven University og Technology, 78 pp. http://mate.tue.nl/mate/pdfs/12270.pdf.

Wang, F. & Zhang, D. 2013. Design and experiment of disc-dig sugar beet combine. *Nongye Gongcheng Xuebao/Transactions of the Chinese Society of Agricultural Engineering* **29**(13), 7–14.

Wu, H., Hu, Z., Peng, B., Wang, H. & Wang, B. 2013. Development of auto-follow row system employed in pull-type beet combine harvester. *Nongye Gongcheng Xuebao/Transactions of the Chinese Society of Agricultural Engineering* **29**(12), 17–24.

Zhang, G., Xu, W. & Fan, S. 2013. Analysis and parameter optimization of adjustable beet top cutting mechanism. *Nongye Gongcheng Xuebao/Transactions of the Chinese Society of Agricultural Engineering* **29**(18), 26–33.

Agronomy Research **20**(2), 389–403, 2022
https://doi.org/10.15159/AR.21.159

Development of an algorithm for assessing canopy volumes with terrestrial LiDAR to implement precision spraying in vineyards

A. Pagliai[1,*], D. Sarri[1], R. Lisci[1], S. Lombardo[1], M. Vieri[1], C. Perna[1], G. Cencini[1], V. De Pascale[1] and G. Araújo E Silva Ferraz[2]

[1]University of Florence, Department of Agriculture, Food, Environment and Forestry (DAGRI), Piazzale delle Cascine 15, IT50144 Florence, Italy
[2]Federal University of Lavras (UFLA), Department of Agricultural Engineering, Campus Universitário, PO Box 3037, CEP 37200-000 Lavras, Minas Gerais, Brazil
[*]Correspondence: andrea.pagliai@unifi.it

Received: February 13th, 2021; Accepted: November 28th, 2021; Published: December 3rd, 2021

Abstract. Precision spraying is one of the techniques for the reduction of pesticides use and it can help achieve the new European Green Deal standards. The aim of such technique is to apply the right amount of pesticides according to the target characteristics. The precision spraying implementation requires target volume assessment, which can be carried out by LiDAR sensors. Such technique requires complex and time-consuming procedures of canopy characteristics computing through post-processing points cloud reconstruction. The present work aimed to develop and test an algorithm through the use of a tractor-coupled with terrestrial LiDAR and GNSS technology in order to simplify the process. With the aim to evaluate the algorithm the LiDAR-based volume was correlated with two manual measurements of canopy volume (Tree Row Volume and Point Net Cloud). The results showed good correlations between manual and LiDAR measures both for total canopy volumes ($R^2 = 0.67$ and 0.56) and for partial canopy volume ($R^2 = 0.74$). In conclusion, although the LiDAR-based algorithm works in automatic mode, the canopy volumes approximation seems acceptable to estimate the canopy volumes, with the advantages of a swifter procedure and less laborious post-processing computations.

Key words: canopy management technique, canopy measurements, site-specific data, variable rate technique, viticulture.

INTRODUCTION

In the last few decades, the public authorities focused their attention on reducing pesticide use and/or improving the efficiency of spraying operation (European Parliament, 2009; MIPAAF, 2014). The European Commission has recently declared that it is essential to introduce coherent strategies to halve the use of chemical pesticides by the year 2030 (ECP, 2020). Variable rate applications (VRA), telemetry of crop protection stages, integrated pest management (IPM) and decision support systems (DSS) can be effective strategies to achieve the European goals. VRA consists of variable-rate spraying according to the characteristics of the canopy (height, width, volume, leaf area, leaf density) or vigour index (Miranda-Fuentes et al., 2016; Tsoulias et al., 2019; Cheraïet et al., 2020; Román et al., 2020). A 20–30% reduction in pesticide use has been achieved by detecting tree size and architecture, (EPRS, 2016). Other improvements have been reached by using auxiliary telemetry tools for crop protection phases (Sarri et al., 2020). In addition, the adoption of Integrated Pest Management (IPM) was able to reduce a sprayed area by approximately 50–80% (EPRS, 2017).

The variable-rate application technique consists in obtaining similar plant protection products (PPP) deposits according to canopy characteristics (Gil et al., 2013). To fulfil the variable-rate applications, canopy dimensions have to be measured. Originally, canopy measurement was carried out manually and the corresponding canopy indicators were created (Tree Row Volume, Leaf Area Index, Leaf Wall Area, Unit Canopy Row, Ellipsoid Volume Method) (Pergher & Petris, 2008; Miranda-Fuentes et al., 2015). Obtaining these manual indicators was time-consuming. Gradually, thanks to technological development, faster and more efficient measurement methods have been developed (Rosell & Sanz, 2012; Comba et al., 2019). Several studies have used ultrasonic sensors to improve variable-rate application (Llorens et al., 2010; Llorens et al., 2011, Gil et al., 2013). These sensors operate with ultrasonic waves, and provide a precise assessment of canopy width in small portions of vegetation. Improvements of canopy detections were provided by LiDAR (Light Detection and Ranging) sensors. The LiDAR technology works with laser beams, and it provides canopy point cloud, at various angular resolution and various aperture angle (Rosell & Sanz, 2012). Thus, the entire vertical profile of the canopy can be reconstructed. Many studies were carried out for implementing the LiDAR-based canopy measurements (Palacín et al., 2007; Rosell et al., 2009a; Llorens et al., 2011; Sanz et al., 2013; Miranda-Fuentes et al., 2015; Tsoulias et al., 2019). Some works obtained canopy characteristics with complicated and laborious steps that required a great amount of post-processing operations. In other works it was necessary to carry out point cloud reconstruction and data filtering to obtain a correct and precise canopy characterization. Only after these operations it was possible to run the canopy parameters computing. Although they are valid methods for research domains, these procedures do not coincide with the implementation of variable-rate operations during work operations. The data extract must be well suited with the tractor speed during spray operations to implement VRA. Therefore, for data processing, few milliseconds are usable. Moreover, the accuracy of canopy measurements, reached by post-processing operations is often too high for practical purposes. Very few studies were focused on practical and operative tools for assessing canopy volumes in real time (Zhang et al., 2018). It is thus evident that a functional LiDAR-based tool is needed to optimise the variable-rate application of pesticides in viticulture. A procedure for automating the LiDAR-based canopy volume computing in real-time was developed to reach this target.

Therefore, this paper focuses on the development and testing of a LiDAR-based algorithm and software for the automatic calculation of canopy volume using a tractor-coupled with terrestrial 2D LiDAR and GNSS receiver.

In order to check algorithm and software, a number of comparison tests were carried out between two different manual canopy volume measurements and LiDAR canopy volume measurements. The experimental tests were carried out in two vineyards, with different row spacing and plant density parameters. Finally, the canopy volumes of four vine-rows, which were completely travelled, were analysed in two work sessions to check the software functioning during the different growth stages.

MATERIALS AND METHODS

Instrumentations:

The 2D LiDAR Sick TIM561 was used (Fig. 1, a) to perform the study. The main sensor features were an angular resolution of 0.33°, an aperture angle of 270°, a working range from 0.05 m to 10 m, a laser emission wavelength of 850 nm and a scanning frequency of 15 Hz (TIM561 Sick). Thanks to these characteristics, 12,150 points were captured each second.

Moreover, to obtain geo-referenced data, the 2D LiDAR was coupled with Ag Leader GPS6500 GNSS receiver (Fig. 1, b). This GNSS receiver provides differential correction with a horizontal position accuracy of 0.4 m, a velocity accuracy of 0.03 m s^{-1} and a maximum data rate of 50 Hz (GPS 6500, Ag Leader).

The LiDAR sensor and GNSS receiver were connected together through a Panasonic Tough Pad FG-Z1, where the algorithm and software for calculating the canopy volume were installed (Fig. 1, c).

Figure 1. Instruments assembled during a field test session with details of the individual tools used (a) GNSS receiver; b) LiDAR sensor; c) Panasonic computer).

During field tests, all these instrumentations were mounted on a Kubota B2420 tractor. On the one hand, the Panasonic computer and the GNSS receiver were assembled near the steering station. On the other hand, the 2D LiDAR was positioned in the rear of the tractor in a vertical position to correctly scan the vertical profiles of the canopy, thanks to 270° opening angle.

Algorithm and Software:

The calculation of the canopy volume was made using an algorithm for extracting the canopy contours, integrated into software for real-time visualisation of the canopy volumes and its main characteristics. In addition, the software creates a comma-separated values (CSV) file-data where the volumes of canopies, associated with their global position (EPSG:4326-WGS 84), and working parameters of the tractor (speed, distance between $scan_i$–$scan_{i+1}$) were recorded.

It is worth noting that before starting the data acquisition, the GNSS acquisition frequency can be changed from 0.1 to 15 Hz in the software interface page.

Its frequency rate controlled the entire exchange of data. Specifically, each time the GNSS string arrived, it was processed by software that sent a data request to the LiDAR. Instantly, a LiDAR scan was run, processed and recorded (with an angular resolution of 0.33° and a scan range of 270°). This process was reiterated until the data acquisition end. For the transfer of LiDAR data, an ethernet connection was used. Instead, an RS232 serial port was used for GNSS data transfer.

First of all, row data provided by LiDAR sensor were transformed from polar to cartesian coordinates. The transformation was made for all points individuated by LiDAR sensor in a single scan (angular resolution: 0.33°; aperture angle: 270°;

maximum point for single scan: 810) and for all scan frequency (scan frequency: 15 Hz = 15 scan s^{-1}), using the following formula:

$$C\_xy_{ij} = \begin{cases} X = DV_{ij} * \cos\alpha_{ij} \\ Y = H_{Li} + DV_{ij} * \sin\alpha_{ij} \end{cases} \quad (1)$$

where C_xy_{ij} – detected canopy point in cartesian coordinates; DV_{ij} – distance between LiDAR and canopy at determined angular position j and the moment i; α_{ij} – angle subtended by DV_{ij}; H_{Li} – LiDAR average height from ground-level. Graphically representation is shown in Fig. 2.

Then, if X coordinates of the canopy points (C_xy_{ij}), that corresponded to the distance between LiDAR and canopy in the cartesian system, were equal or bigger than semi row spacing ($D_{rs}/2$), they were considered in the calculation of canopy volume as values 0, because these points did not belong to the canopies near the tractor. In comparison, laser beams that did not encounter any obstacles were not counted. Moreover, another condition had to be respected. The Y coordinates of the canopy points (C_xy_{ij}) must be bigger than H_{co} (average cordon height). In this way, the points detected in the ground-level or other interferences, as grass or vine trunk, were not considered. Thanks to LiDAR characteristics (TIM561 Sick), particularly the aperture angle of 270°, it was possible to detect two sides of vine-rows for each working route. Therefore, the conversion formula and the conditions previously exposed were viable for both sides of vine-rows (Fig. 2, left side).

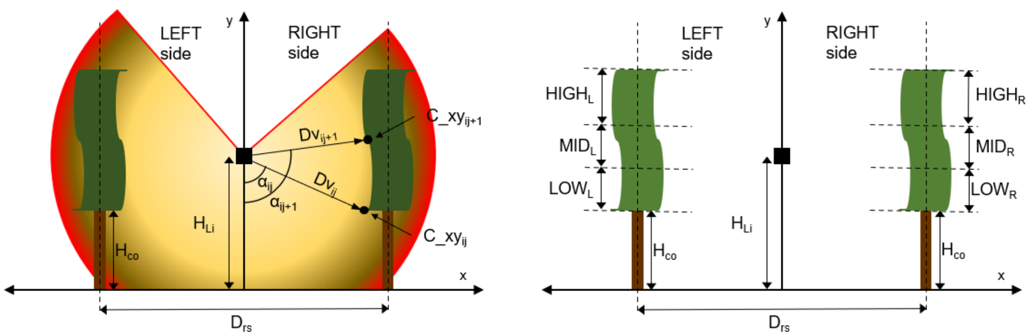

Figure 2. In the left side of the figure, the LiDAR and algorithm working principles were represented. In the other side, the subdivisions in three bands were shown.

A subdivision of total canopy volume in three bands according to the height from cordon was carried out. Specifically the low band was between the cordon (H_{co}) up to 0.30 m in vertical height (H_{co+30}), the middle band was between the end of the previous one up to 0.60 m apart the cordon (H_{co+60}) and the high band was between the end of the previous one up to the last canopy detected point (*ymax*) (Fig. 2, right side). The subdivision in three bands was necessary to discriminate how the canopy arranges on the vertical profile. Without these partitions, only the total canopy volume would have been measured and it would not have been possible to show the differences in the vertical profile of the canopy.

Then the algorithm, according to different canopy bands, computed total and partial means of the x-values of canopy points (C_xy_{ij}). To differentiate the three bands, the y-values of canopy points (C_xy_{ij}) were used. These average values ($\overline{X_{tot}}$; $\overline{X_{high}}$; $\overline{X_{mid}}$; $\overline{X_{low}}$) correspond to distance between LiDAR and canopy in a different portion of canopy profile. The subtraction between semi row spacing ($D_{rs}/2$) and average values were done to obtain both total average canopy width and partial average canopy widths (low, mid and high canopy bands). Finally, the entire and partial areas of canopy sections were obtained by the multiplication between their widths and heights. In such a manner, the canopy areas (m^2 scan^{-1}) of vertical LiDAR scan were obtained, both for left and right sides. The equations below showed the procedure aforementioned (2) (3) (4) (5).

$$\overline{X_{tot}} = \frac{\sum_{y=H_{co}}^{ymax} x_i}{n_t} \rightarrow A_{tot} = \left(\frac{D_{rs}}{2} - \overline{X_{tot}}\right) * (ymax - H_{co}) \quad (2)$$

$$\overline{X_{high}} = \frac{\sum_{y=H_{co+60}}^{ymax} x_i}{n_h} \rightarrow A_{high} = \left(\frac{D_{rs}}{2} - \overline{X_{high}}\right) * (ymax - H_{co+60}) \quad (3)$$

$$\overline{X_{mid}} = \frac{\sum_{y=H_{co+30}}^{H_{co+60}} x_i}{n_m} \rightarrow A_{mid} = \left(\frac{D_{rs}}{2} - \overline{X_{mid}}\right) * (H_{co+60} - H_{co+30}) \quad (4)$$

$$\overline{X_{low}} = \frac{\sum_{y=H_{co}}^{H_{co+30}} x_i}{n_l} \rightarrow A_{low} = \left(\frac{D_{rs}}{2} - \overline{X_{low}}\right) * (H_{co+30} - H_{co}) \quad (5)$$

where $\overline{X_{tot}}$, $\overline{X_{high}}$, $\overline{X_{mid}}$, $\overline{X_{low}}$ – average values of x coordinates, respectively for total canopy, high canopy band, mid canopy band and low band; H_{co} – cordon height; H_{co+30} – cordon height plus 0.30 m; H_{co+60} – cordon height plus 0.60 m; $ymax$ – the y coordinate of last canopy point detected by LiDAR; x_i – x coordinate in C_xy_{ij}; n_t, n_h, n_m, n_l – number of canopy points included respectively in total, high, mid and low canopy band; A_{tot}, A_{high}, A_{mid}, A_{low} – respectively total section area of the canopy and partial sections area (high, mid, low); ($D_{rs}/2$) – semi row spacing.

The first version of the algorithm had not division into three canopy bands. Nevertheless, during the early tests, it became necessary to highlight how the canopy arranges in the vertical profile. It has been essential for showing how the total canopy volume and the proportion of partial canopy volume, in the vertical profile, changed during the growing season.

The final algorithm step consisted in calculating the canopy volumes through the multiplication between the canopy area and travelled distance by tractor during a detection session. The travelled distance was obtained by GNSS receiver. The final output was a CSV file with canopy volumes (total and partial) linked with their global positions, provided by GNSS receiver. The volumes of canopy can be obtained referring to the distance travelled (Eqs 6, 7, 8, 9) or to the linear meter of row (Eqs 10, 11, 12, 13).

$$V_{tot} = A_{tot} * D_t, \ \ m^3 {D_t}^{-1} \quad (6)$$

$$V_{high} = A_{high} * D_t, \ \ m^3 {D_t}^{-1} \quad (7)$$

$$V_{mid} = A_{mid} * D_t, \ \ m^3 {D_t}^{-1} \quad (8)$$

$$V_{low} = A_{low} * D_t, \ \ m^3 {D_t}^{-1} \quad (9)$$

$$V_{tot} = (A_{tot} * D_t) * \frac{1}{D_t},\ m^3m^{-1}$$

$$V_{tot} = (A_{tot} * D_t) * \frac{1}{D_t},\ m^3m^{-1} \quad (10)$$

$$V_{high} = \left(A_{high} * D_t\right) * \frac{1}{D_t},\ m^3m^{-1} \quad (11)$$

$$V_{mid} = (A_{mid} * D_t) * \frac{1}{D_t},\ m^3m^{-1} \quad (12)$$

$$V_{low} = (A_{low} * D_t) * \frac{1}{D_t},\ m^3m^{-1} \quad (13)$$

where V_{tot} – total canopy volume; V_{high} – high band canopy volume; V_{mid} – mid band canopy volume; V_{low} – low band canopy volume; D_t – distance travelled.

The algorithm carried out all calculations, both for left and right side of vine-rows, during a working session.

The algorithm was integrated into a software, designed to process LiDAR data automatically and in real-time. This software was implemented in Visual Studio with C# programming language. The software has an interface page, where parameters can be changed according to vineyards characteristics, and a working page, where canopy volumes and heights, positions and errors codes (about LiDAR) can be seen. On the first page, it was possible to change parameters such as row spacing, LiDAR height and cordon height from ground level. This allowed the setting into other vineyards (with different characteristics) or potentially into other crops for instance orchards. In the second window, the recording of the work session can be activated and, at the end of it, a CSV file is created. This output contains the main working parameters such as time, GNSS position and tractor speed, and canopy characteristics such as total canopy volumes, high band, mid band and low band canopy volumes for both the right and left side.

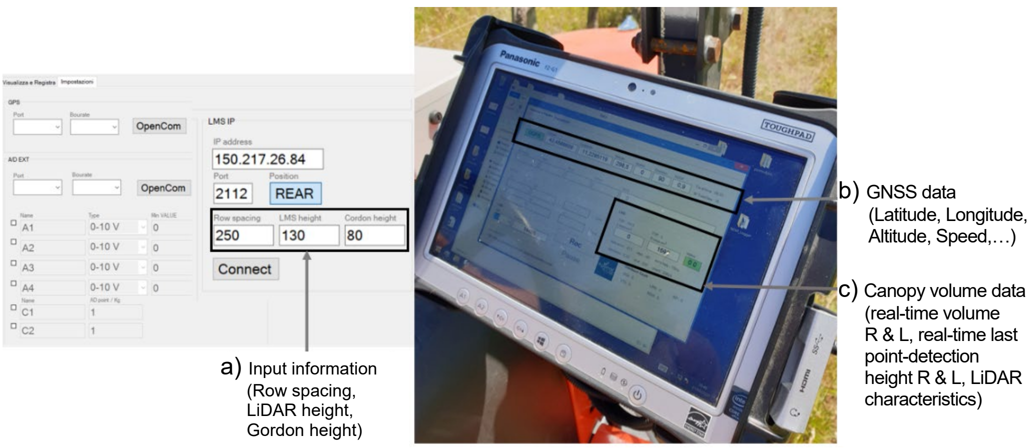

Figure 3. Software interface for computing, in real-time, canopy volumes. On the left, the interface window, that allows to set parameters about LiDAR position and vineyard characteristics was shown. On the right, there is the working window, where canopy volumes (right and left side) and canopy heights were shown in real-time.

Field tests:

The field tests were carried out in two different vineyards in Chianti Classico region. The first one was located in Gretole (43°27'23.0" N; 11°13'51.9" E), Castellina in Chianti, Siena, Italy and the other located in San Felice (43° 23' 24.8" N; 11° 27' 26.5" E), Castelnuovo Berardenga, Siena, Italy.

At the moment of tests, the vineyard in Gretole was 11 years old, was cordon trained, with a row spacing of 2.5 m and an average distance between vines of 0.8 m. With a plant density of ~5,000 vine ha^{-1}. San Felice's vineyard was cordon trained, it was 15 years old, and the plant density was higher than the first one (~9,000 vine ha^{-1}). It is due to a smaller row spacing (~1.4 m). Both vineyards were mainly composed of *Vitis vinifera* L. cv. 'Sangiovese'. During the 2020 vegetative season (May-July), three test sessions were carried out in three different phenological phases (BBCH 57, BBCH 71, BBCH 81), for a total of 26 vines sampled for each measurement technique. This was done to test whether the algorithm could work at very different inter-row distances, distinguish canopy growth during sprout's development, and differentiate canopy volume according to different vigour zones.

To check the algorithm two different types of manual non-destructive canopy measurements were carried out. The first manual measurements was the Tree Row Volume (TRV) which was measured for each single vines involved in the experiments. The TRV technique involved in this experiment was partially revised from conventional TRV to provide the volume of the canopy of each vine (m^3 $plant^{-1}$) (Scapin et al., 2015). This was achieved by computing the average canopy height (m), the average canopy width (m) and the average canopy length (m) of a single vine with the following Eq. (14).

$$TRV = \overline{H} * \overline{W} * \overline{L}, \quad (m^3\ pl^{-1}) \qquad (14)$$

where $\overline{H}$ – was the average canopy height; $\overline{W}$ – was the average canopy width; $\overline{L}$ – was the average canopy length; m^3 pl^{-1} – unit of measure.

The other manual measurements adopted was the Point Net Canopy (PNC). It consisted in measuring the canopy width for each mesh of the net, positioned in parallel to vineyard row and in front of the canopy surface (Fig. 4). The PNC provides more detailed canopy volume than TRV because several canopy width for each vine sampled were measured. To calculate the PNC, a net, with a mesh of 0.15 m × 0.15 m, was located to a distance of 0.5 m from vertical canopy axis. Then, the distance (d_i) between canopy external surface and net was manually measured for each mesh of the net. In addition, the value d_i was subtracted by the distance between the net and vertical canopy axis (0.5 m) in order to obtain canopy widths for each mesh of the net. This value was multiplied by the area of the mesh (A_i = 0.0225 m^2) to obtain the volumes of the canopy subtended by single meshes. Finally, they were added up to obtain the total volume of the canopy of a single vine, as follows in the Eq. (15).

$$PNC = \sum_{i=1}^{n} [A_i * (0.5\,m - d_i)], \quad (m^3\ pl^{-1}) \qquad (15)$$

where d_i – distance between canopy external surface and net; A_i – mesh area; $0.5\,m$ – the distance between net and canopy vertical axis; i – number of meshes contained the sampled vine canopy.

PNC provides detailed information on the spatial distribution of canopy volume. In particular, canopy volumes for different vegetation bands (0–0.3 m; 0.30–0.60 m; and > 0.60 m; distance from cordon) can be extracted from this manual measurements. This was essential to correlate with the canopy volume bands provided by LiDAR algorithm.

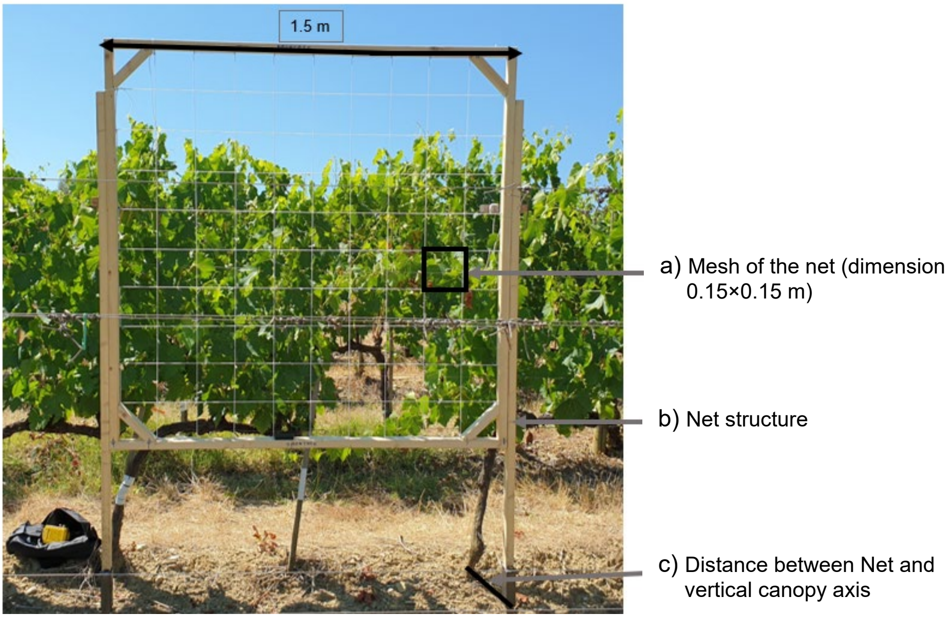

Figure 4. Net positioned for a manual measurement session. (a) Net mesh dimension; b) Net structure; c) Distance Net structure–Vertical canopy axis.

Finally, TRV and PNC measurements were compared with LiDAR measurements to validate the performance of the algorithm. The LiDAR measurements were carried out throughout vine-rows, containing the sampled vines, at an average speed of 1 m s^{-1}. The acquisition frequency was set up at 10 Hz, to obtain a scan each about 0.1 m. From these data, the LiDAR canopy volumes, corresponding to sampled vines manually, were extracted thanks to GNSS receiver and a digital marker that highlights sampled vines in the file output. The vine-rows, including the sampled vines, were travelled in their entirety in order to get the full characterisation of the canopy.

RESULTS AND DISCUSSION

Manually and LiDAR measurements on single vines:

As far as the canopy volumes of sampled vines, the minimum, average and maximum values for the three measurement techniques (TRV, PNC and LiDAR) were summarised in Table 1. In this table, canopy volume values, in different work sessions (May and July), were simultaneously shown to highlight how LiDAR measurements have detected the increasing of canopy volumes during the growing phase (from BBCH 57 to BBCH 81). The increase in canopy volumes was also identified by the other manual measurements. This suggest that the algorithm and software work well enough.

Table 1. Minimum, mean and maximum values of manuals and LiDAR measurements in the same plants at different growth stages (BBCH 57–BBCH 81)

	TRV		PNC		LIDAR	
	BBCH 57	BBCH 81	BBCH 57	BBCH 81	BBCH 57	BBCH 81
Min.	0.118	0.326	0.086	0.115	0.096	0.219
Mean	0.229	0.368	0.150	0.253	0.193	0.288
Max.	0.307	0.472	0.210	0.360	0.290	0.403

Two comparisons of total canopy volumes between instrumental and manually measurements to validate the LiDAR measurements were analysed. Linear regressions provide more evidence of the algorithm good functioning. This analysis highlights good correlations between TRV and LiDAR measurements ($R^2 = 0.67$) and PNC and LiDAR measurements ($R^2 = 0.56$), how it is shown in Fig. 5. The obtained linear regression (TRV *vs* LiDAR) has slightly lower coefficients of determination than other similar comparisons presented in some papers (Rosell et al., 2009b; Tsoulias et al., 2019). Indeed, Tsoulias et al. (2019) found a better coefficient of determination ($R^2 = 0.77$), under similar conditions and with the same experimental parameters, but this result was obtained with a significantly lower tractor speed. Instead, Rosell et al. (2009b) reported a better coefficient of determination ($R^2 = 0.97$), but this was obtained with a small sample size and in an apple orchard.

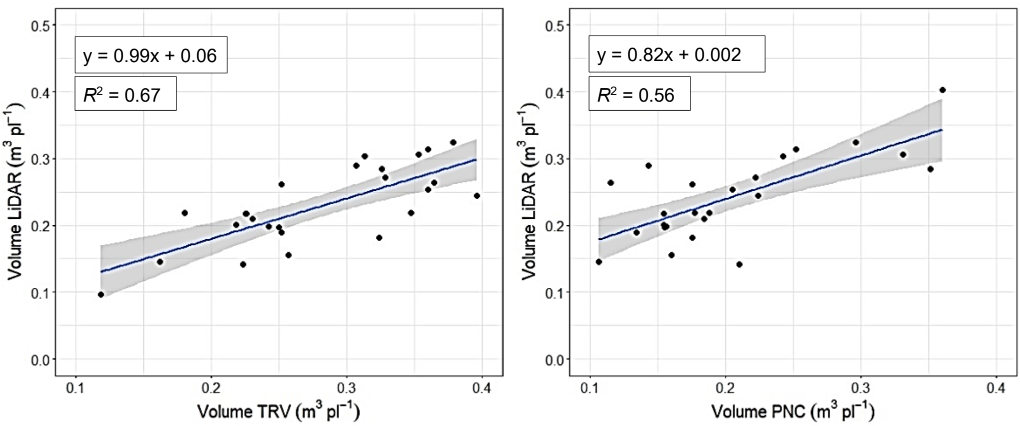

Figure 5. The linear regression of TRV (x) versus LiDAR (y) volume measurements is shown on the left graph. The linear regression of PNC (x) versus LiDAR (y) volume measurements is represented on the right chart.

This study wanted to test the automated assessment algorithm of canopy volume in operational working conditions, hence this could be the reason for obtaining smaller coefficients of determination. However, this approximation is justified because the tractor speed was set to the average speed for future software implementation in canopy management operations and variable-rate spraying applications.

With regard to canopy volumes divided into three bands, linear regressions between LiDAR and PNC measurements were obtained. The TRV measurements were not considered because the TRV method does not provide specific canopy information as vertical distribution of canopy volumes. LiDAR and PNC correlations for low and mid bands reported similar determination coefficients, respectively 0.498 and 0.491 (Fig. 6). Instead, the coefficient of determination for the high band, i.e. the portion of the canopy between a distance of 0.60 m from cordon height and the last canopy point detected by LiDAR, is 0.736, as shown in Fig. 6. The differences in coefficient of determination between the canopy bands are probably due to the dimension of bands. In fact, the high band includes a portion of canopy bigger than other bands. So, this brings about the values of the canopy of high band (m3 pl-1) being bigger than those of the mid and low band. Therefore, slight deviations between PNC and LIDAR measurements in the high band cause a minor deterioration of the coefficient of determination compared to what happens in low and mid bands, where the values of the canopy are smaller.

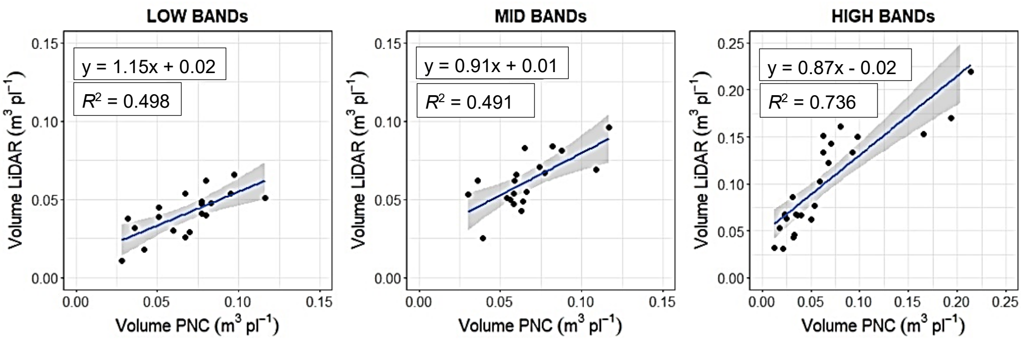

Figure 6. The linear regressions of PNC (x) *versus* LiDAR (y) volume measurements are shown with the detail of the three canopy bands (on the left: Low Band; in the middle: Mid Band; on the right: High Band).

However, this value highlights a good approximation provided by the algorithm for automated canopy volumes computing. This information is essential in future developments of precision spraying. In fact, the total canopy volume based on LiDAR is an excellent index to assess the spatial variability in terms of canopy quantity in vineyards. Thanks to the total canopy volume, the pesticides spray volume can vary according to site-specific information. Moreover, the spray volume can be targeted according to the vertical canopy variability, due to the division of the canopy into bands.

The significant correlation obtained in the high canopy bands is another interesting aspect to be evaluated more carefully. Indeed, the computation of canopy high bands could potentially be affected by less accuracy due to slight lateral inclinations of vineyards or tractor roll motion. Nevertheless, they do not seem to be problematic in the canopy volume approximation. Therefore, the algorithm gives a good approximation of the total canopy volume and provides helpful information about the vertical distribution of canopy volumes.

LiDAR measurements of entire vineyards

The canopy volumes detected by LiDAR software during two working sessions (May and July) were showed. The data represent the canopy volumes (m^3m^{-1}) of four vine-rows completely travelled at a constant tractor speed of 1 ms^{-1}. This situation simulated the usual working conditions of canopy management.

The absolute frequency of total canopy volumes partitioned in breaks of 0.01 $m^3 m^{-1}$ during the evolution of total canopy volumes from BBCH 57 stage to BBCH 81 was showed in Fig. 7.

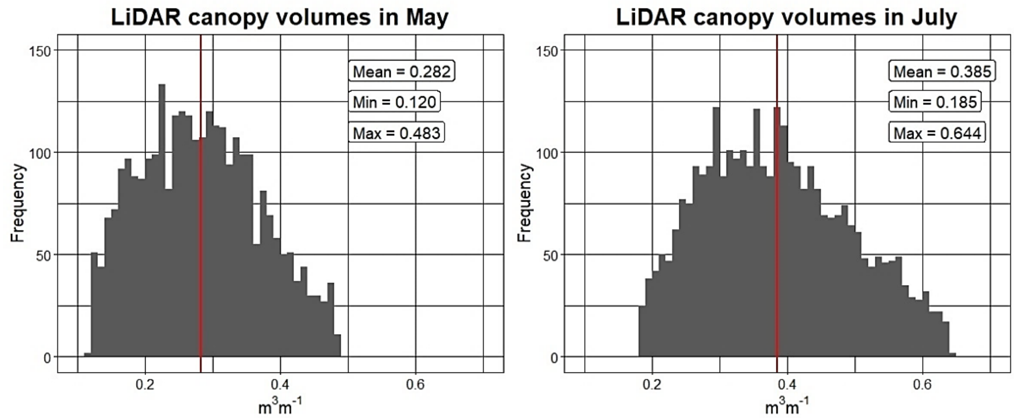

Figure 7. Absolut frequencies of LiDAR measurements with a interval of 0.01 ($m^3 m^{-1}$). Such measurements were part of the software output (CSV file) where tractor, coupled with LiDAR, travelled completely four vine-rows. The red line corresponds to the mean value.

In BBCH 57 stage, an average canopy volume of 0.282 m^3 per linear meter of vine-row was detected, with a minimum value of 0.120 $m^3 m^{-1}$ and a maximum of 0.483 $m^3 m^{-1}$. Instead, in BBCH 81 stage, an average canopy volume of 0.385 $m^3 m^{-1}$ was measured, with a minimum of 0.185 $m^3 m^{-1}$ and a maximum of 0.644 $m^3 m^{-1}$.

The increase in canopy volume (from 0.282 to 0.385 $m^3 m^{-1}$) between the two phases was 37% reflecting thenatural growth phase of the vineyard, as shown in Table 2. This increase was also detected by the two manual canopy measurements (Table 1). Therefore, the algorithm for the automatic calculation of canopy volumes was able to detect the different canopy volumes during the growth phase of the vineyard.

Table 2. Means of canopy volumes of LiDAR measurements, percentage of canopy distribution between bands and rate of volume increase between different growth stages (BBCH 57 – BBCH 81)

	BBCH 57		BBCH 81		BBCH 57 – BBCH 81
	Mean	%	Mean	%	%
Tot	0.282		0.385		37%
High	0.1565	61%	0.205	60%	31%
Mid	0.0598	23%	0.0834	24%	39%
Low	0.0417	16%	0.0549	16%	32%

In addition, the canopy volumes data were analysed according to the differentiation of the three bands (low, mid and high band). In this case, the absolute frequency of partial canopy volumes was partitioned in intervals of 0.001 $m^3 m^{-1}$ because of the lower canopy volume detected for single bands. Fig. 8 showed the data obtained in two different work sessions, corresponding to the BBCH 57 and BBCH 81 growth stage, and differentiated for single bands. The lower band is situated on the bottom of Fig. 8, and the others are above according to an increasing levels layout.

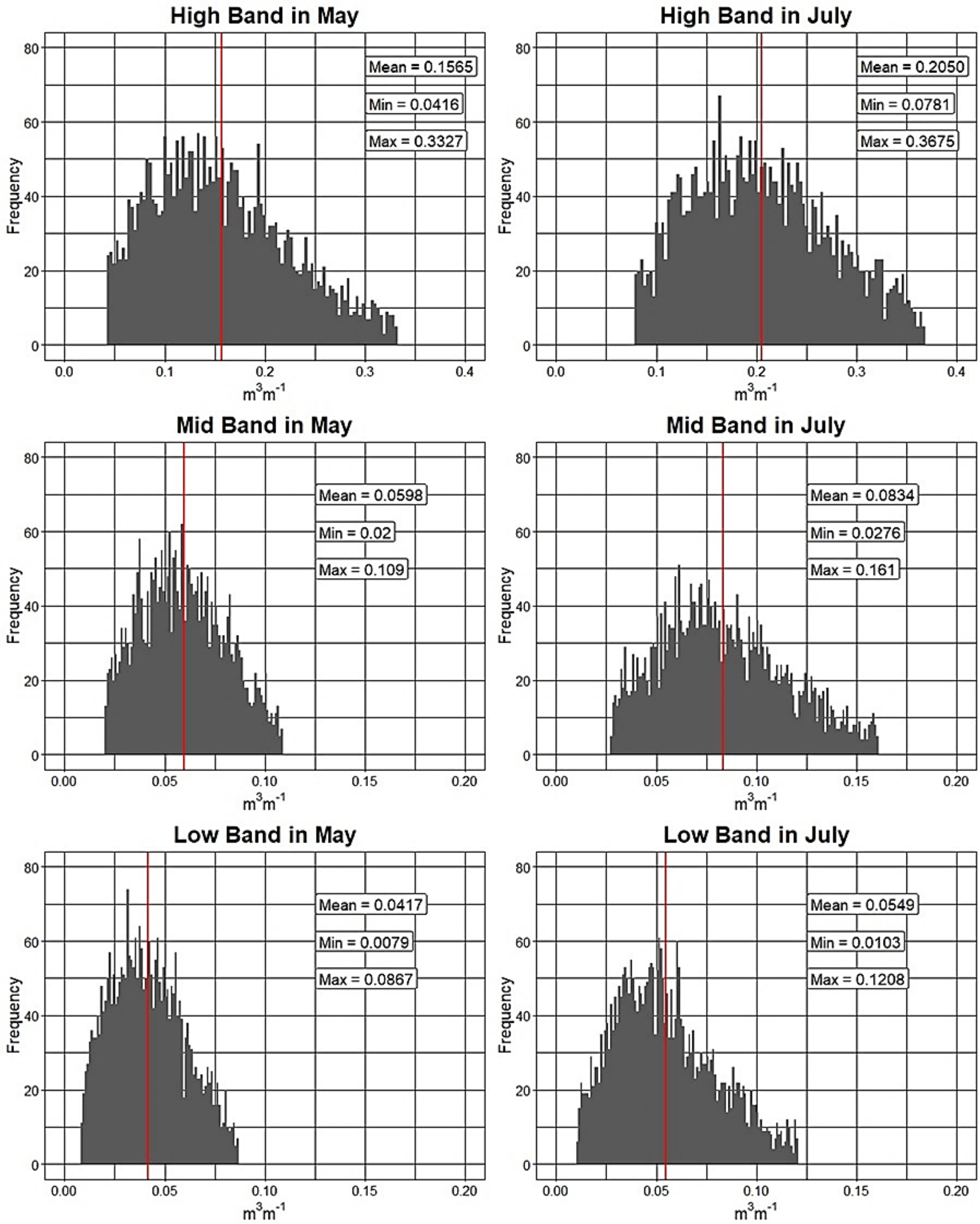

Figure 8. Absolut frequencies of LiDAR measurements of the three bands (Low, Mid, High) with an interval of 0.01 (m^3 m^{-1}). These measurements are part of software output (CSV file) where tractor, coupled with LiDAR, travelled completely four vine-rows. The red line corresponds to the mean value.

The graphs of low band canopy volumes showed that the average value of canopy volumes ranges from 0.042 m^3 m^{-1} to 0.055 m^3 m^{-1} during the growth stage (May–July), increasing 32%. A similar trend was highlighted for the other bands. The mid band ranges from 0.059 m^3 m^{-1} to 0.083 m^3 m^{-1}, with a volume increase of 39%, and the high band goes from 0.156 m^3 m^{-1} to 0.205 m^3 m^{-1}, with a rise of 31% (Table 2) These increases prove that the software could also detect the growth of canopy volumes into the three bands between different moments of detections. The proportion of canopy distribution between bands seems not to change in the two different data collections.

CONCLUSIONS

The LiDAR-based algorithm and software for automated canopy volume calculation described in this work, can be a valid alternative to the complex and laborious procedures of canopy characteristics computing through post-processing points cloud reconstruction. The good correlations obtained between manual and LiDAR-based measurements (R^2 = 0.67, R^2 = 0.74) suggest that the simplified computing system can be a valuable tool for measuring canopy characteristics, such as tree row volume, and distinguishing the spatial canopy distribution.

The LiDAR-based algorithm showed good working adaptability on different vineyards vertical training systems, such as cordon training or Guyot, with different plant density. With inputs that can be set (row spacing, cordon height and LiDAR height) according to crop characteristics, the software for automatic canopy volume calculation can potentially be used in orchards.

The working conditions under which the software was tested are an indication that the LiDAR-based system can work at speeds similar to the on-farm management and spraying operations. Further tests will need to be carried out to fully investigate the best scanning frequency to achieve more accurate canopy volumes without compromising tractor working speed and efficiency. In addition, another interesting suggestion to evaluate further is the relation between canopy evaluation shown in this paper and canopy extraction in post-processing.

The results achieved in correlations between manual and LiDAR measurements take the work to the next stage of development. Firstly, it is necessary to check for bugs or other instrumental problems through a large number and lengthy field tests. Moreover, it will be about understanding how to best interact the data obtained from this system with the spraying equipment and spray volume.

In conclusion, the system (LiDAR, GNNS receiver, algorithm and software) has the potential to be implemented in precision viticulture both in on go variable-rate equipment and int on-board terminals based on prescription maps.

ACKNOWLEDGEMENTS. Tuscany Region's public funding supported this work through the ‘Kattivo’ Project (PSR 2014-2020-PIF 43/2015). The authors are grateful to the wine-farm Tenuta Gretole, Ruffino (Castellina in Chianti) and Società Agricola San Felice (Castelnuovo Berardenga) for the technical support during the field tests.

REFERENCES

Cheraïet, A., Naud, O., Carra, M., Codis, S., Lebeau, F. & Taylor, J. 2020. An algorithm to automate the filtering and classifying of 2D LiDAR data for site-specific estimations of canopy height and width in vineyards. *Biosystems Engineering* **200**, 450–465. doi: 10.1016/j.biosystemseng.2020.10.016

Comba, L., Biglia, A., Aimonino, D.R., Barge, P., Tortia, C. & Gay, P. 2019. 2D and 3D data fusion for crop monitoring in precision agriculture. In: *Proceedings of 2019 IEEE International Workshop on Metrology for Agriculture and Forestry (MetroAgriFor)*. Portici, Italy, pp. 62–67. doi: 10.1109/MetroAgriFor.2019.8909219

Communication from the commission to the European Parliament, the Council, the European Economics and Social Committee and the Committee of the Regions. A Farm to Fork Stratsegy for a fair, healthy and environmentally-friendly food system. 2020. **COM/2020/381 final**, pp 19.

Directive 2009/128/EC of the European Parliament and the Council of 21 October 2009 establishing a framework for Community action to achieve the sustainable use of pesticides. 2009. *Official Journal of the European Union,* **L309**, 71–86.

EPRS (European Parliamentary Research Service). 2016. Precision agriculture and the future of farming in Europe. *European Parliamentary Research Service*, **PE 581.892**, pp. 40. https://ec.europa.eu/knowledge4policy/publication /precision-agriculture-future-farming-europe_en%0Ahttps://euagenda.eu/upload/publications/untitled-63196-ea.pdf

EPRS (European Parliamentary Research Service). 2017. Precision agriculture in Europe: Legal, social and ethical considerations. *European Parliamentary Research Service*, **PE 603.207**, pp. 80. http://www.europarl.europa.eu/RegData/etudes/STUD/2017/603207/EPRS_STU(2017)603207_EN.pdf

Gil, E., Llorens, J., Llop, J., Fàbregas, X., Escolà, A. & Rosell, J.R. 2013. Variable rate sprayer. Part 2 - Vineyard prototype: Design, implementation, and validation. *Computers and Electronics in Agriculture*, **95**, 136–150. doi: 10.1016/j.compag.2013.02.010

Llorens, J., Gil, E., Llop, J. & Escolà, A. 2010. Variable rate dosing in precision viticulture: Use of electronic devices to improve application efficiency. *Crop Protection* **29**(3), 239–248. doi: 10.1016/j.cropro.2009.12.022

Llorens, Jordi, Gil, E., Llop, J. & Escolà, A. 2011. Ultrasonic and LIDAR sensors for electronic canopy characterization in vineyards: Advances to improve pesticide application methods. *Sensors* **11**(2), 2177–2194. doi: 10.3390/s110202177

MIPAAF (Ministry of Agricultural, Food and Forestry Policies). 2014. National action plan for sustainable use of plant protection products. pp 83 (in Italian). https://www.mite.gov.it/sites/default/files/archivio/normativa/dim_22_01_2014.pdf

Miranda-Fuentes, A., Llorens, J., Rodríguez-Lizana, A., Cuenca, A., Gil, E., Blanco-Roldán, G.L. & Gil-Ribes, J.A. 2016. Assessing the optimal liquid volume to be sprayed on isolated olive trees according to their canopy volumes. *Science of the Total Environment* **568**, 296–305. doi: 10.1016/j.scitotenv.2016.06.013

Miranda-Fuentes, Antonio, Llorens, J., Gamarra-Diezma, J.L., Gil-Ribes, J.A. & Gil, E. 2015. Towards an optimized method of olive tree crown volume measurement. *Sensors* **15**(2), 3672–3687. doi: 10.3390/s150203671

Palacín, J., Pallejà, T., Tresanchez, M., Sanz, R., Llorens, J., Ribes-Dasi, M., Masip, J., Arnó, J., Escolà, A. & Rosell, J.R. 2007. Real-time tree-foliage surface estimation using a ground laser scanner. *IEEE Transactions on Instrumentation and Measurement* **56**(4), 1377–1383. doi: 10.1109/TIM.2007.900126

Pergher, G. & Petris, R. 2008. Pesticide dose adjustment to the canopy parameters for treatments to the tree crops. In: *Proceedings of Phytophatology Days*, pp. 317–322 (in Italian).

Román, C., Llorens, J., Uribeetxebarria, A., Sanz, R., Planas, S. & Arnó, J. 2020. Spatially variable pesticide application in vineyards: Part II, field comparison of uniform and map-based variable dose treatments. *Biosystems Engineering* **195**, 42–53. doi: 10.1016/j.biosystemseng.2020.04.013

Rosell, J.R. & Sanz, R. 2012. A review of methods and applications of the geometric characterization of tree crops in agricultural activities. *Computers and Electronics in Agriculture* **81**, 124–141. doi: 10.1016/j.compag.2011.09.007

Rosell, J.R., Llorens, J., Sanz, R., Arnó, J., Ribes-Dasi, M., Masip, J., Escolà, A., Camp, F., Solanelles, F., Gràcia, F., Gil, E., Val, L., Planas, S. & Palacín, J. 2009a. Obtaining the three-dimensional structure of tree orchards from remote 2D terrestrial LIDAR scanning. *Agricultural and Forest Meteorology* **149**(9), 1505–1515. doi: 10.1016/j.agrformet.2009.04.008

Rosell, J.R., Sanz, R., Llorens, J., Arnó, J., Escolà, A., Ribes-Dasi, M., Masip, J., Camp, F., Gràcia, F., Solanelles, F., Pallejà, T., Val, L., Planas, S., Gil, E. & Palacín, J. 2009b. A tractor-mounted scanning LIDAR for the non-destructive measurement of vegetative volume and surface area of tree-row plantations: A comparison with conventional destructive measurements. *Biosystems Engineering* **102**(2), 128–134. doi: 10.1016/j.biosystemseng.2008.10.009

Sanz, R., Rosell, J.R., Llorens, J., Gil, E. & Planas, S. 2013. Relationship between tree row LIDAR-volume and leaf area density for fruit orchards and vineyards obtained with a LIDAR 3D Dynamic Measurement System. *Agricultural and Forest Meteorology* **171–172**, 153–162. doi: 10.1016/j.agrformet.2012.11.013

Sarri, D., Lombardo, S., Pagliai, A., Zammarchi, L., Lisci, R. & Vieri, M. 2020. A technical-economic analysis of telemetry as a monitoring tool for crop protection in viticulture. *Journal of Agricultural Engineering* **51**(2), 91–99. doi: 10.4081/jae.2020.1029

Scapin, M.D.S., Behlau, F., Scandelai, L.H.M., Fernandes, R.S., Silva Junior, G.J. & Ramos, H. H. 2015. Tree-row-volume-based sprays of copper bactericide for control of citrus canker. *Crop Protection* **77**, 119–126. doi: 10.1016/j.cropro.2015.07.007

Tsoulias, N., Paraforos, D.S., Fountas, S. & Zude-Sasse, M. 2019. Estimating canopy parameters based on the stem position in apple trees using a 2D lidar. *Agronomy* **9**(11), 740. doi:10.3390/agronomy9110740

Zhang, Z., Wang, X., Lai, Q. & Zhang, Z. 2018. Review of Variable-Rate Sprayer Applications Based on Real-Time Sensor Technologies. In (book) *Automation in Agriculture - Securing Food Supplies for Future Generations* **i**(4), 53–79 doi: 10.5772/intechopen.73622

Agronomy Research **20**(2), 404–413, 2022
https://doi.org/10.15159/AR.22.028

Adaptation of various maize hybrids when grown for biomass

M.V. Radchenko[1,*], V.I. Trotsenko[1], A.O. Butenko[1], I.M. Masyk[1], Z.I. Hlupak[1], O.I. Pshychenko[1], N.O. Terokhina[2], V.M. Rozhko[3] and O.Y. Karpenko[3]

[1]Sumy National Agrarian University, Faculty of Agrotechnology and Nature Management, Department of Agrotechnologies and Soil Science, 160 G Kondratieva Str., UA40021 Sumy, Ukraine
[2]Sumy National Agrarian University, Department of Foreign Languages, 160 D Kondratieva Str., UA40021 Sumy, Ukraine
[3]National University of Life and Environmental Sciences of Ukraine, Agrobiological faculty, Department of Agricultural and Herbology, 15 Heroiv Oborony Str., UA03041 Kyiv, Ukraine
[*]Correspondence: radchenkonikolay@ukr.net

Received: January 10th, 2022; Accepted: May 1st, 2022; Published: May 10th, 2022

Abstract. The aim of this research is to optimize growth and development of maize for biomass by selecting maize hybrids to fulfill their productivity potential. The following maize hybrids were the subject of research: Forteza, DM Native, DM Skarb. The greatest height of plants was formed in the interphase period of milk-wax maturity of grain in hybrid Forteza - 286.4 cm. In hybrid DM Native the height of plants was - 271.2 cm, hybrid DM Skarb - 263.6 cm. Weight of one plant of hybrids studied during the maize growing season ranged from 442 g to 760 g. Thus, the largest mass of maize plants was recorded in the milk-wax maturity stage. It was the largest at the hybrid Forteza and amounted to 760 g, that is more than at the hybrid DM Native for 3.4% (26 g) and at the hybrid DM Skarb for 6.6% (50 g). The average crop yield of the hybrid Forteza for the period of research was 55.1 t ha^{-1}. Hybrids DM Native and DM Skarb provided this indicator at the level of 50.6 and 45.7 t ha^{-1} respectively. Hybrid Forteza provided a maximum crop yield 55.1 t ha^{-1} with plant height 286.4 cm, assimilation surface of one plant and a crop 0.59 m^2; 42.8 thousand m^2 ha^{-1} and plant weight 760 g.

Key words: hybrid, leaf surface, plant, cob, crop yield.

INTRODUCTION

Among the high-yielding spring crops, maize occupies a leading position as unsurpassed in terms of potential yield of grain and silage. It is one of the main sources of forage and energy resources. In many regions of the world of the temperate climate, maize is the main forage crop. The area of maize cultivation for silage has shifted significantly to the north. Today, this subtropical plant is widely used in the main agroclimatic zones of Ukraine (Knyazyuk, 2018).

Over the past few years, maize cultivation areas in Ukraine have grown several times and now amount to 4.3–4.7 million hectares. This is due to the comprehensive use of maize as forage, food and industrial crops (Palamarchuk, 2018). At the present stage, agricultural producers in Ukraine are faced with the task of significant increasing the productivity of maize for needs of the national economy. This problem can be solved by using highly productive hybrids, advanced energy-saving technologies, high-quality seeds, etc. are used (Bagan, 2015).

On the basis of many years of research, the scientific developments and practical experience in growing maize using intensive energy-saving technology have been generalized. Much attention has been paid to improving the basic elements of technology for growing maize used for grain, silage, green fodder, as well as for food purposes and promising directions for increasing maize production in Ukraine (Chandiposha & Chivende, 2014; Haddadi & Mohseni, 2016).

The increase in the area under maize became possible thanks to creation of new hybrids with a shorter maturity period. It made possible to increase the area under this crop in the northern regions. The fundamental direction of increasing the yield of maize is the introduction of intensive type hybrids of different maturite groups. Not all hybrids respond equally to specific agroecological and technological conditions of cultivation, therefore, their potential productivity is different. Highly productive hybrids take a large amount of nutrients from soil, consume a lot of water, so they require appropriate agricultural technology. If such conditions are not created, then a potentially more productive hybrid may yield its position in harvesting capacity to another less productive, but also less demanding hybrid (Lavrynenko et al., 2018; Butenko et al., 2019; Kadyrov & Kharitonov, 2019).

The continuous work of crop breeders on improving the architectonics of a maize plant focuses on the components that determine the formation of productivity and resistance to stress factors - the size and angle of inclination of the leaves, the architectonics of the root system and more. Maize genotypes vary in their response to the full range of possible temperatures by not always clear signs (Lynch, 2007; Kolisnyk et al., 2019). Therefore, we need a differentiated approach to the selection of hybrids of the corresponding group of maturity and purpose. To increase the level of realization of the yield potential of modern hybrids and protect crops from negative abiotic and biotic environmental factors, in addition to agrotechnical measures, the development of morphological and heterosis models and selection of hybrids on this basis with specific adaptability to agroecological factors is important (Troyer, 2014; Horváth et al., 2021).

First-grade maize silage should contain 40–50% of maizecobs in green mass and 25–35% of dry matter, which is provided during harvesting plants in wax maturity phase (Lipovy et al., 2003).

In the period of wax maturity, maize also has negative qualities relating to silage: the lower parts of maizestalks and cut cobs get coarse; only 15–18% of the grain reach physiological or technical maturity. At the same time, in full maturity of maize, the stalks turn yellow and coarse and contain practically no carotene. The yield of dry matter and its nutrition are reduced by 5–6% due to an increase in the amount of fiber and cobs.

Taking in consideration the above, the duration of the wax maturity phase of maize must be prolonged in order to have time to harvest the mass for silage. It is problematic to suspend or slow down the physiological processes that take place in a maize plant during the grain filling period. Therefore, to obtain the maximum productive yield of maize in the wax maturity phase, it is necessary to extend the cropping period by sowing hybrids of different prematureness. This way it becomes possible to create an appropriate feed conveyor for harvesting silage with a total harvesting period of 20–30 days (Yamkova, 2014; Babkov & Zhelobkova, 2019).

To obtain high and stable maize yields in each farm, it is necessary to have a range of hybrids with a different type of reaction to the variability of environmental conditions, including the intensive type (to obtain maximum yields on a high agricultural background), medium plastic hybrids, which have a wide adaptive potential (to obtain relatively stable yields in fields with an unstable agricultural background), and highly stable (for a guaranteed yield under conditions of variable meteorological factors on poorly nutrient soils). The ability to economically and efficiently use life-giving factors is a property of highly adaptive genotypes (Kitayova et al., 2013).

For maize, it is important that the seeds are sown evenly both across the length and width of the row. The uniformity of their distribution creates favorable conditions for the emergence of even and proper sprouts, high evenness of plants in height and development, simultaneous maturation, the same density and quality of grain in the corncob (Sun et al., 2009; Weidong & Matthijs, 2009; Li et al., 2012).

Taking into account the above, it is necessary to analyze the seeding machinery and sowing units produced by the industry, with due regard for the technological properties of the machine, the agrobiological characteristics of the crop and soil and climatic conditions (Ipsilandis & Vafias, 2005; Farsiani et al., 2011; Saberi et al., 2012).

The purpose of research is to optimize the growth and development of silage maize by selecting maize hybrids to realize their productivity potential.

MATERIALS AND METHODS

The researches for study of varietal features of maize for silage were conducted during 2017–2021 in the Educational, Scientific and Production Complex of Sumy National Agrarian University. The researches were conducted according to research methods of Dospehov (1985), Pidoprygora & Pysarenko (2003).

The following corn hybrids were the subject of the research: Forteza, DM Native, DM Skarb. The receding crop was winter wheat. Sowing was carried out after beginning of physical soil maturity at the temperature of 10–12 °C at the depth 10 cm by wide-row sowing with row spacing 70 cm and sowing rate 85 thousand of seeds per ha^{-1}.

In modern agricultural industry, the main method of maize sowing is a single-grain one with 70 cm spacing, which ensures maximum productivity of machines with minimal labor, costs and energy expenditures during sowing and care of crops (Amanullah et al., 2009; Tang et al., 2013).

The sown area of the plot was 50 m^2. Variants of the research were placed in triplicate. The alternation of variants was consistent. Before sowing maize, mineral fertilizers were applied: nitroammophoska 150 kg ha^{-1} and carbamide 200 kg ha^{-1}. Nitroammophoska is a triple physiologically neutral fertilizer - concentrated, nitrogen-phosphorus-potassium, granular with the content and ratio of mineral nutrients N:P:K = 16:16:16. Carbamide is a concentrated amide fertilizer. Mass fraction of nitrogen (N) is 46.2%. Form of fertilizer - granular.

During the phenological observations, the beginning of the developmental stage of maize plants was assumed when it was present in at least 10% of plants, and the complete developmental stage in 75%. The average height was determined from 25 plants in two non-adjacent rows of the plot by measuring with a rail from the ground to the longest of the upper leaves. To determine the growth of aboveground part of the plant, samples were taken from each plot of 20 plants and were weighed in laboratory in the raw state. The structure of crops (length and cob diameter, the number of rows and grains in a row, the number of grains from a cob) was determined by selected samples. The leaf area was determined by calculation. The calculation method is based on determining the area of a separate leaf by multiplying the length by the width and the verified coefficient, which for cereals with linear (oblong) leaf shape is 0.67. The yield of biomass maize was calculated by total harvesting and weighing from each plot. Processing and generalization of research results were carried out according to Dospehov (1985) using Microsoft Excel.

The soil of experimental field is a typical powerful heavy-loamy and medium humus black soil, which is characterized by the following indices: humus content in arable layer (according to I.V. Tiuryn) - 4.0%, reaction of soil solution is close to neutral (pH 6.5), the content of easily hydrolyzed nitrogen (according to I.V. Tiuryn) 9.0 mg, movable phosphorus and exchangeable potassium (according to Ph. Chyrikov), accordingly, 14 mg and 6.7 mg per 100 g of soil.

Table 1. Weather conditions of vegetative seasons for 2017–2021

Year	Average daily air temperature, °C		Amount of precipitation, mm	
	annual air temperature, °C	± to the long-tern indicator, (7.4 °C)	for the reporting year, mm	± to the long-term norm, (593.0 mm)
2017	8.1	+ 0.7	449.0	– 144.0
2018	9.4	+ 2.0	539.0	– 54.0
2019	9.6	+ 2.2	409.0	– 184.0
2020	10.2	+2.8	466.0	– 127.0
2021	9.4	+ 2.0	453.0	– 140.0

Weather conditions in 2018 and 2020 are more favorable for formation of maximum yields. The climatic conditions of 2017, 2019 and 2021 are extreme for growing crops due to low precipitation and significant deviations in air temperature during the growing season.

RESULTS AND DISCUSSION

To obtain high yields of quality products, it is important to timely obtain and maintain even and proper sprouts of optimal density. Maize requires increased moisture supply and adequate soil temperature for seed germination. Therefore, under adverse weather conditions, maize seeds have a longer germination period. This usually results in a significant decrease in field germination and crop productivity. Cold resistance is the ability of seeds to sprout at a positively low (threshold) temperature of 6–8 °C, and sprouts - actively photosynthesize at low temperatures. This trait is genetically determined and manifests at all levels of biological organization - cellular, population. High level of cold resistance ensures sprouts and development of young hybrid plants in early sowing of maize in overmoistened soil at a positively low temperature (Wijewardana et al., 2016).

The highest field germination of seeds was observed in Forteza hybrid - 92.3%, and the lowest in DM Skarb hybrid - 85.5%. Depending on the hybrid, a plant density on average ranged from 7.27 to 7.85 pcs m^2. The highest index of a plant density was observed in Forteza hybrid - 7.85 pcs m^2 (Table 2).

Table 2. Degree of maize density depending on the variety characteristics (average for 2017–2021)

Cultivar (hybrid)	Ground germination capacity, %	Degree of plant density, pcs m^2	Preservation of the plants during the vegetation season	
			pcs m^2	%
DM Native	89.6	7.62	6.90	90.6
Forteza	92.3	7.85	7.25	92.4
DM Skarb	85.5	7.27	6.44	88.6
LSD_{05}	0.99	0.078	0.12	1.69

The highest plant safety in Forteza hybrid was 7.25 pcs m^2 (92.4%), the lowest in DM Skarb hybrid - 6.44 pcs m^2 (88.6%).

Morphometric indicators and their ratios become important for development of the optimal morphotype of maize hybrid plants (Cherchel et al, 2014).

Maize plants, like other non-perennial crops, have their limited height, that is, at the time of maturation, they stop their linear growth in any combination of agrotechnical and meteorological conditions. Fluctuations of daily gain of plants in height in the interstage periods and in general during the vegetation season can aid in determination of the influence of various factors on the productional processes of plants (Mazur et al, 2018).

Hybrids have been found to significantly affect the linear growth of maize. At the beginning of the development stage of maize (7–8 leaves), the highest plant height was observed in the hybrid Forteza - 77.3 cm, in DM Native hybrid this indicator was 72.0 cm, and in DM Skarb hybrid - 69.1 cm.

The obtained experimental data indicate that the increase in the linear height of plants occurs before the ear emergence phase, and their maximum value was observed in the interstage period of milky-wax maturity of the grain. The greatest height of plants was formed in the interphase period of milk-wax maturity of grain in hybrid Forteza - 286.4 cm. In hybrid DM Native the height of plants was - 271.2 cm, hybrid DM Skarb - 263.6 cm (Table 3).

Table 3. Dynamics of maize plant height depending on the variety characteristics (average for 2017–2021), cm

Cultivar (hybrid)	Phenological phases		
	7–8 leaves	Ear emergence	Milk-wax maturity
DM Native	72.0	198.5	271.2
Forteza	77.3	208.3	286.4
DM Skarb	69.1	188.0	263.6
LSD_{05}	2.09	4.18	3.81

Physical and physiological processes that transform solar energy into organic matter in the atmosphere - leaf - plant - agrocenosis system have an important influence on quantitative and qualitative indicators of crop yielding capacity formation. The intensity of this process depends greatly on the characteristics and spectral composition of sunshine, energy balance between energy absorbed and costs of photosynthesis, transpiration, thermal and moisture circulation, the availability of nutrients and readily available moisture, etc. To optimize production processes and form the maximum possible maize yield, the size of a plant leaf apparatus is important that accumulates solar radiation during photosynthesis and provides the creation of organic matter (Andriyenko, 2003).

Thanks to the type C4 photosynthesis, which leads to rapid accumulation of organic matter in plants, maize has the highest dry matter yield per 1 ha of crop area (Ruile et al., 2015).

The researches allowed to investigate the response of maize plants to varietal characteristics by determining their indicators of photosynthetic activity. The area of leaf surface of the sowing is quite variable and depends both on weather conditions during the years of research and on the factors studied (Table 4).

Table 4. Dynamics of leaf area growth depending on the variety characteristics (average for 2017–2021)

Cultivar (hybrid)	Leaf-area duration, m^2					
	7–8 leaves		Ear emergence		Milk-wax maturity	
	on the plant	thousand m^2 ha^{-1}	on the plant	thousand m^2 ha^{-1}	on the plant	thousand m^2 ha^{-1}
DM Native	0.038	2.6	0.51	35.2	0.54	37.3
Forteza	0.045	3.1	0.55	39.8	0.59	42.8
DM Skarb	0.039	2.5	0.48	31.0	0.50	32.2
LSD_{05}	0.0026	-	0.031	-	0.030	-

At the beginning of vegetation season (7–8 leaves), on average over the years of research, the area of the leaf apparatus fluctuated within 2.5–3.1 thousand m^2 ha^{-1} in all plots. In the ear emergence phase, the largest area of the assimilation area of one plant and the crop was in Forteza hybrid (0.55 m^2; 39.8 thousand m^2 ha^{-1}), slightly smaller - in DM Native hybrid (0.51 m^2; 35.2 thousand m^2 ha^{-1}), in the variant with DM Skarb hybrid - 0.48 m^2; 31.0 thousand m^2 ha^{-1}, accordingly. In the milky-waxy maturity phase, the largest area of the assimilation area of one plant and the crop was in Forteza hybrid (0.59 m^2; 42.8 thousand m^2 ha^{-1}), slightly smaller - in DM Native hybrid (0.54 m^2; 37.3 thousand m^2 ha^{-1}), in DM Skarb hybrid - 0.50 m^2; 32.2 thousand m^2 ha^{-1}, accordingly.

Analyzing the data in Table 5, it is fair to say that the weight of one plant in the hybrids studied during the maize growing period ranged between 442 and 760 g. Thus, the largest mass of maize plants was recorded in the milk-wax maturity phase. In Forteza hybrid, it was the largest and amounted to 760 g. In the DM Native hybrid - 734 g, DM Skarb hybrid 710 g.

Table 5. Influence of variety characteristics on the weight of one maize plant (average for 2017–2021), g

Cultivar (hybrid)	Phenological phases		
	7–8 leaves	Ear emergence	Milk-wax mturity
DM Native	447.0	653.0	734.0
Forteza	471.0	686.0	760.0
DM Skarb	442.0	641.0	710.0
LSD_{05}	4.90	8.63	14.31

An important characteristic of the productivity of maize hybrid plants is the biometric characteristics of maizecobs such as number of rows, number of grains in the row, number of grains per corncob, length and diameter of the cob. Providing maize plants with favorable conditions for growth and development led to an increase in the biometric indicators of maizecobs.

The highest values of maizecob length and diameter were obtained using Forteza hybrid and were 16.2 cm and 4.5 cm, respectively (Table 6).

The number of rows in the maizecob and the grains in the row tend to increase depending on the variety characteristics. Thus, according to the variants of the experiment, the number of rows ranged between 14.0 and 16.0 pieces. The number of grains in the row ranged between 31.4 and 34.2 pcs (LSD_{05} = 0.55). The researches have shown that the impact of different maize hybrids on the number of rows and the number of grains in a row was insignificant The highest of those indicators were observed on the plots with Forteza hybrid - 16.0, 34.2 pcs, accordingly. The lowest of those indicators were observed on the plots with DM Skarb hybrid - 14.0, 31.4 pcs, accordingly.

Table 6. Maizecob biometrics depending on the variety characteristics (average for 2017–2021)

Cultivar (hybrid)	Length, cm	Diameter, cm	No. of rows, pcs	No. of grains in the row, pcs
DM Native	15.7	4.1	16.0	33.5
Forteza	16.2	4.5	16.0	34.2
DM Skarb	14.7	3.9	14.0	31.4
LSD_{05}	0.56	0.26	2.30	0.55

The obtained data indicate that the maximum number of grains from one maizecob have been obtained in the variants with Forteza hybrid - 540.4 pcs. (Fig. 1).

So, the hybrids increased the values on average from 34.5 to 85.1 pcs. of grains from one maizecob or by 6.4–15.7% (LSD_{05} = 19.5).

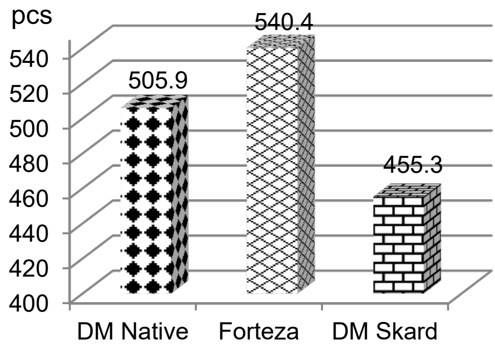

Figure 1. Number of grains from one maizecob depending on the variety characteristics (average for 2017–2021), pcs.

The main indicators of the productivity of crops are their yield, which in terms of production characterizes the amount of the produce. The ultimate goal of maize cultivation for biomass is to get the highest yield with high quality. The crop formation and the accumulation of its economic value is an important result of complex biochemical and physiological processes. The plant best reveals its potential under optimal environmental conditions, which depend on specific soil and climatic conditions of the year and varietal specificity.

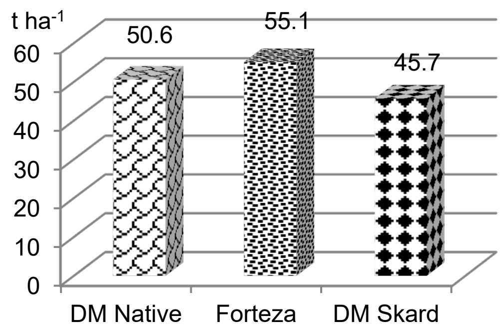

Figure 2. Maize biomass yield depending on the variety characteristics (average for 2017–2021) t ha^{-1}.

For modern cultivation of stable crops of maize such biological properties of modern hybrids as plasticity and stability acquire great importance and characterize the adaptive properties of the organism, reveal the dynamics of changes in the genotype response to variations in environmental conditions, allow for their functions to stay relatively constant (Taran et al., 2018; Hlisnikovský et al., 2020). The data obtained by us, which characterize the magnitude of maize biomass, fully confirm the above point (Fig. 2).

The graph data indicate that the yield of hybrids of different maturity averaged between 45.7 and 55.1 t ha^{-1} (LSD_{05} = 3.85). The maximum yield, on average, during the researches period was formed by Forteza hybrid of 55.1 t ha^{-1}. DM Native and DM Skarb hybrids provided 50.6 and 45.7 t ha^{-1}, accordingly, for that indicator (Fig. 2).

CONCLUSIONS

The obtained experimental data of researches testify that the best indicators of productivity of maize for biomass are received at sowing of the hybrid Forteza. This hybrid provided the maximum height of a plant - 286.4 cm with assimilation surface of one plant and sowing 0.59 m^2; 42.8 thousand m^2 ha^{-1} and plant weight 760 g. The number of rows in a cob is 16.0 pcs and of grains in a row is 34.2 pcs. The average crop yield of the hybrid Forteza for the period of research was 55.1 t ha^{-1}. Hybrids DM Native and DM Skarb provided this indicator at the level of 50.6 and 45.7 t ha^{-1} respectively.

REFERENCES

Amanullah, Riaz A., Khattak & Shad K. Khalil. 2009. Plant Density and Nitrogen Effects on Maize Phenology and Grain Yield. *Journal of Plant Nutrition* **32**(2), 246–260. https://doi:org/10.1080/01904160802592714

Andriyenko, A.L. 2003. Photosynthetic activity and productivity of new hybrids of corn depending on the density of plants standing. *Bulletin of the Institute of Grain Farming of UAAN* **20**, 36–38 (in Ukrainian).

Babkov, A.V. & Zhelobkova, M.V. 2019. Research of agrotechnologicall characteristics of grain of certain corn hybrids. *Scientific Works* **82**(2), 106–115 (in Ukrainian). https://doi.org/10.15673/swonaft.v82i2.1274

Bagan, A.V. 2015. Formation of productivity and quality of grain of corn hybrid depending on predecessor. *Bulletin of Poltava State Agrarian Academy* **4**, 32–35 (in Ukrainian). https://doi.org/10.31210/visnyk2015.04.07

Butenko, A.O., Sobko, M.G., Ilchenko, V.O., Radchenko, M.V., Hlupak, Z.I., Danylchenko, L.M. & Tykhonova, O.M. 2019. Agrobiological and ecological bases of productivity increase and genetic potential implementation of new buckwheat cultivars in the conditions of the Northeastern Forest-Steppe of Ukraine. *Ukrainian Journal of Ecology* **9**(1), 162–168. https://www.ujecology.com/articles/agrobiological-and-ecological-bases-of-productivity-increase-and-genetic-potential-implementation-of-new-buckwheat-culti.pdf

Chandiposha, M. & Chivende, F. 2014. Effect of ethephon and planting density on lodged plant percentage and crop yield in maize (Zea mays L.). *African Journal of Plant Science* **8**(2), 113–117. https://doi: org/10.5897/ajps2013.1135

Cherchel, V.Yu., Marochko, V.A. & Tagantsova, M.M. 2014. Index validation for ratio of maize hybrids upper ear attachment to plant height thereof (Zea mays L.). *Plant Varieties Studying and Protection* **2**(23), 40–44. https://doi.org/10.21498/2518-1017.2(23).2014.56127

Dospehov, B.A. 1985. *Methods of field experience*. Kolos, Moscow, 351 pp.

Farsiani, A., Ghobadi, M. & Jalali-Honarmand, S. 2011. The effect of water deficit and sowing date on yield components and seed sugar contents of sweet corn (Zea mays L.). *African Journal of Agricultural Research* **6**(26), 5769–5774. https://doi:org/10.5897/ajar11.1242

Haddadi, M.H. & Mohseni, M. 2016. Plant Density Effect on Silage Yield of Maize Cultivars. *Journal of Agricultural Science* **8**(4), 186–191. https://doi:org/10.5539/jas.v8n4p186

Horváth, É., Gombos, B. & Széles, A. 2021. Evaluation phenology, yield and quality of maize genotypes in drought stress and non-stress environments. *Agronomy Research* **19**(2), 408–422. https://doi.org/10.15159/AR.21.073

Hlisnikovský, L., Barlog, P., Kunzová, E., Vach, M. & Menšík, L. 2020. Biomass yield of silage maize, fertilizers efficiency, and soil properties under different soil-climate conditions and fertilizer treatments. *Agronomy Research* **18**(1), 88–99. https://doi.org/10.15159/AR.20.017

Ipsilandis, C.G. & Vafias, B.N. 2005. Plant Density Effects on Grain Yield per Plant in Maize: Breeding Implications. *Asian Journal of Plant Sciences* **4**(1), 31–39. https://doi:org/10.3923/ajps.2005.31.39

Kadyrov, S. & Kharitonov, M. 2019. Productivity of corn hybrids in relation to the seeding rate. *Agronomy Research* **17**(1), 123–132. https://doi.org/10.15159/AR.19.013

Kitayova, S.S., Ponurenko, S.G., Chernobai, L.M. & Derkach, I.B. 2013. Rate of moisture-lossing of maize grain during maturation for hybrids which belong to different maturity groups. *Plant Breeding and Seed Production* **104**, 66–74 (in Ukrainian). https://doi: org / 10.30835 / 2413-7510.2013.42021

Knyazyuk, O.V. 2018. *Agroecological features and techniques of corn cultivation technology: monograph*. Nilan LTD, Vinnytsia, 114 pp.

Kolisnyk, O.M., Kolisnyk, O.O., Vatamaniuk, O.V., Butenko, A.O., Onychko, V.I., Onychko, T.O., Dubovyk, V.I., Radchenko, M.V., Ihnatieva, O.L. & Cherkasova, T.A. 2019. Analysis of strategies for combining productivity with disease and pest resistance in the genotype of base breeding lines of maize in the system of diallel crosses. *Modern Phytomorphology* **14**, 49–55. https://doi.org/10.5281/zenodo.190112

Lavrynenko, Y.O., Marchenko, T.Y. & Zabara, P.P. 2018. Breeding properties and their role in stabilization of corn grain production in Ukraine. *Irrigated agriculture* **72**, 91–100 (in Ukrainian). https://doi.org/10.32848/0135-2369.2019.72.21

Li, Chun-Qi, Wang, Ting-Liang, Cheng, Xiang-Wen, Cao, Ruo-Yao, Li, Yun, Lu, Peng & Li, Chao-Hai. 2012. Effects of Plant Density on Anatomical Structure of Ear Leaf in Summer Maize. *Acta Agronomica Sinica* **37**(11), 2099–2105. https://doi:org/10.3724/sp.j.1006.2011.02099

Lipovy, V.G., Lechman, P.V. & Rozbitska, N.V. 2003. Corn of different groups of ripeness in the silage conveyor of the central forest-steppe of Ukraine. *Feed and feed production* **50**, 22–24 (in Ukrainian).

Lynch, J.P. 2007. Roots of the second green revolution. *Australian Journal of Botany* **55**(5), 493–512. https://doi:org/10.1071/bt06118

Mazur, V.A., Tsyganska, O.I. & Shevchenko, N.V. 2018. The height of maize plants depending on technological methods of cultivation. *Agriculture and forestry* **8**, 5–13 (in Ukrainian).

Palamarchuk, V.D. 2018. Influence of the covering depth and the seed fr action on the content of starch in corn grain and bioethanol output. *Bulletin of Poltava State Agrarian Academy* **2**, 55–65 (in Ukrainian). https://doi: 10.31210

Pidoprygora, V.S. & Pisarenko, P.V. 2003. *Workshop on the basics of scientific research in agronomy*. InterGrafika, Poltava, 138 pp.

Ruile, S., Schmitz, S. Mönch-Tegeder, M. & Oechsner, H. 2015. Degradation efficiency of agricultural biogas plants – a full-scale study. *Bioresource Technology* **178**, 341–349. https://doi: 10.1016/j.bior-tech.2014.10.053

Saberi, A.R., Kiani, A.R., Mosavat, S.A. & Halim, R.A. 2012. The effect of different sowing patterns and deficit irrigation management on yield and agronomic characteristics of sweet corn. *African Journal of Biotechnology* **11**(74), 13882–13887. https://doi:org/10.5897/ajb10.2695

Sun, Rui, Zhu, Ping, Wang, Zhi-Min, Cong, Yan-Xia, Gou, Ling & Zhao, Ming. 2009. Effect of Plant Density on Dynamic Characteristics of Leaf Area Index in Deve-lopment of Spring Maize. *Acta Agronomica Sinica* **35**(6), 1097–1105. https://doi:org/10.3724/sp.j.1006.2009.01097

Tang, Li-Yuan, Li, Cong-Feng, Ma, Wei, Zhao, Ming, Li, Xiang-Ling & Li, Lian-Lu. 2013. Characteristics of Plant Morphological Parameters and Its Correlation Analysis in Maize under Planting with Gradually Increased Density. *Acta Agronomica Sinica* **38**(8), 1529–1537. https://doi:org/10.3724/sp.j.1006.2012.01529

Taran, V.G., Kalenska, S.M., Novytska, N.V. & Danyliv, P.A. 2018. Stability and plasticity of corn hybrids in depending on fertilizing system and density of plant stand in the right-bank forest-steppe of Ukraine. *Biological Resources and Nature Management* **10**(3–4), 147–156. https://doi.org/10.31548/bio2018.03.019

Troyer, A.F. 2014. Background of U. S. Hybrid Corn. *Crop Science* **44**(2), 370–380. https://doi: 10.2135/cropsci2004.3700

Weidong, L. & Matthijs, T. 2009. Response of Yield Heterosis to Increasing Plant Density in Maize. *Crop Science* **49**(5), 1807–1816. https://doi:org/10.2135/cropsci2008.07.0422

Wijewardana, Ch., Henry, W.B., Hock, M.W. & Reddy, K.R. 2016. Growth and physiological trait variation among corn hybrids for cold tolerance. *Canadian Journal of Plant Science* **96**(4), 639–656. https://doi:org/10.1139/cjps-2015-0286

Yamkova, V. 2014. Features of growing corn for silage. *Proposal* **5**, 56–58 (in Ukrainian).

Agronomy Research **20**(2), 414–423, 2022
https://doi.org/10.15159/AR.21.160

Winter wheat leaf blotches development depending on fungicide treatment and nitrogen level in two contrasting years

A. Švarta*, G. Bimšteine, Z. Gaile, J. Kaņeps and I. Plūduma-Pauniņa

Latvia University of Life Sciences and Technologies, Lielā iela 2, LV-3001 Jelgava, Latvia
*Correspondence: agrita.svarta@llu.lv

Received: January 31st, 2021; Accepted: December 1st, 2021; Published: December 4th, 2021

Abstract. Tan spot (caused by *Pyrenophora tritici-repentis*) and Septoria tritici blotch (caused by *Zymoseptoria tritici*) are the most widespread winter wheat leaf diseases in Latvia. The aim of the present research was to clarify the development of leaf blotches on winter wheat depending on fungicide treatment schemes under four nitrogen rates. A two-factorial trial was conducted at the Research and Study farm "Pēterlauki" (Latvia) of Latvia University of Life Sciences and Technologies. For this study, data from the 2018/2019 and 2019/2020 growing seasons was used. Four schemes of fungicide application and an untreated variant, as well as four nitrogen rates (N120, N150, N180, and N210 kg ha^{-1}) were used. The total disease impact during the vegetation period was estimated by calculating the area under the disease progress curve (AUDPC). The severity of leaf blotches in winter wheat leaves differed significantly during both vegetation seasons. Tan spot was the dominant disease in 2019 (18.7% in untreated variant). The development of tan spot was reduced by fungicide treatment; however, only in 2019, the influence of fungicide was significant. Septoria tritici blotch was the dominant disease in 2020 (11.4% in untreated variant), and its development was decreased by fungicides. Nitrogen fertilizer rate had no significant effect on the development of Septoria tritici blotches. Yield harvested in 2020 were significantly higher than those in 2019 (on average 5.23 t ha^{-1} in 2019, 8.40 t ha^{-1} in 2020). The using of fungicides provided significant increase of yield but there were no significant differences among fungicide treatment schemes.

Key words: winter wheat, *Pyrenophora tritici-repentis, Zymoseptoria tritici*, values of AUDPC, control.

INTRODUCTION

Wheat is an economically important cereal crop throughout the world, including Latvia. In 2019, the total sown area of winter wheat was 381.5 thousand ha (30.9% from total area of sowings) with the average yield of 5.28 t ha^{-1} (Central Statistical Bureau of Latvia, 2019).

The occurrence of leaf blotches is one of the factors affecting winter wheat grain yields. Septoria tritici blotch (caused by *Zymoseptoria tritici*) and tan spot (caused by *Pyrenophora tritici-repentis*) are the most important winter wheat leaf diseases in Europe (Willocquet et al., 2021), but the severity of both diseases vary significantly among the years (Bankina et al., 2018; Švarta et al., 2020; Willocquet et al., 2021). In

Latvia, tan spot was first identified only in the first half of the 1990s, but in recent years, the disease has become dominant. The severity of Septoria tritici blotch has been significantly lower and has exceeded the severity of tan spot only in a few years (Bankina et al., 2018).

The main source of tan spot infection is wheat straw debris, where pseudothecia with ascospores develop (Cotuna et al., 2015). The spread of disease significantly increased in continuous wheat sowings and in fields under minimum tillage (El Jarroudi et al., 2013; Bankina et al., 2018). The time of the appearance of the first tan spot symptoms and the further development of disease depend on meteorological conditions (Bankina et al., 2018; Schierenbeck et al., 2019; Willocquet et al., 2021) and susceptibility of variety (Kremneva et al., 2021). In years with high humidity and high average air temperatures, the susceptibility response to the disease was observed in more varieties than in years with dry conditions (Kremneva et al., 2021).

In contrast, the development of Septoria tritici bloch mainly depends on meteorological conditions, and agronomic practice is less important (Kuzdralinsky et al., 2015; Bankina et al., 2018). Optimal conditions for the development of Septoria leaf blotch are: minimum temperatures of 8 °C and maximum temperatures between 15 °C and 25 °C, relative humidity higher than 80%, and long periods of leaf wetness.

Wheat diseases management in Europe is mainly based on the use of fungicides and resistant varieties (Willocquet et al., 2021). In general, one to three applications are used, depending on the severity of diseases, susceptibility of variety, and yield potential (Willocquet et al., 2021), but in Ireland - even four applications are used (Creissen et al., 2018). The results of five-year (2013–2017) field experiments in six European countries revealed that disease levels were affected by the level of fungicide use, by cultivar resistance, and by meteorological conditions (Willocquet et al., 2021). In most cases, multiple disease intensities were lower when fungicide use was determined according to local recommendations (for example, one fungicide application in Norway and Sweden, two applications in Belgium), compared to no or limited protection (Willocquet et al., 2021). Gomes et al. (2016) found that susceptible varieties (with high levels of infection coefficient) need two fungicide applications (at GS 34 and GS 47). In moderate resistant varieties (with low levels of infection coefficient), preventive fungicide treatment at GS 34 proves to be beneficial, but resistant varieties do not need a disease control. In turn, Willocquet et al. (2021) confirmed that differences between cultivars reduce as the level of fungicide protection increases.

Nitrogen application significantly increases the grain yields, but nitrogen fertilization may also influence the development of foliar disease due to larger canopies that provide more favourable conditions for pathogens infection and development. Castro et al. (2018) found that severities of Septoria tritici blotch and tan spot significantly decreased with the increase in N rate. In contrast, Jensen & Jørgensen (2016) established that higher N rates was probably a major reason for the increased severity of Septoria tritici blotch in sowings with high densities.

The aim of the present research was to clarify the development of leaf blotches on winter wheat depending on fungicide treatment schemes under four nitrogen rates.

MATERIALS AND METHODS

Two-factor field experiments were carried out at the Study and Research farm "Pēterlauki" of Latvia University of Life Sciences and Technologies (56º 30.658′ N and 23º 41.580′ E). For this study, data from the 2018/2019 and 2019/2020 growing seasons was used. One of the most popular cultivars in Latvia 'Skagen' was used in the trial.

Four schemes of fungicide application and an untreated variant (Table 1), as well as four nitrogen rates (N120 (80+40), N150 (80+70), N180 (80+70+30), and N210 (80+80+50) kg ha^{-1}) were used. In total, 20 variants were arranged using a split plot design in four replications, more detailed information was given in previous publication (Švarta et al., 2020).

The intensity of fungicide treatment was demonstrated by treatment frequency index (TFI) (Nistrup Jørgensen, 2008).

Table 1. Fungicide treatment schemes

Variants	Treatment timing-growth stage (GS) according to BBCH*	Active ingredients of fungicides	Dose, L ha^{-1}	Treatment frequency index
F0 (untreated variant)	Without fungicides	-	-	-
F1 (one treatment)	55–59	Protioconazole 130 g L^{-1}; bixafen 65 g L^{-1}; fluopyram 65 g L^{-1}	0.750	0.5
F2 (one treatment)	55–59	Protioconazole 130 g L^{-1}; bixafen 65 g L^{-1}; fluopyram 65 g L^{-1}	1.500	1.0
F3 (two treatments)	32–33	Protioconazole 160 g L^{-1}; spiroxamin 300 g L^{-1}	0.625	1.0
	55–59	Protioconazole 130 g L^{-1}; bixafen 65 g L^{-1}; fluopyram 65 g L^{-1}	0.750	
F4 (three treatments)	32–33	Protioconazole 160 g L^{-1}; spiroxamin 300 g L^{-1}	0.625	2.0
	55–59	Protioconazole 130 g L^{-1}; bixafen 65 g L^{-1}; fluopyram 65 g L^{-1}	0.750	
	63–65	Metconazole 90 g L^{-1}	1.000	

* BBCH – phenological growth stages of cereals according to the 'BiologisceBundesanstalt, Bundessortenamt und Chemische Industrie' (BBCH) scale.

Soil at the site was loam, sod-calcareos soil. Soil is characterized by the following indicators depending on the year: pH_{KCl} = 6.4–7.0, organic matter content 29–40 g kg^{-1}, P_2O_5 content 118–167 mg kg^{-1} and K_2O content 262–244 mg kg^{-1} of the soil.

The rate of nitrogen fertilizer was divided into two applications for variants N120 and N150, and into three applications - for variants N180 and N210. Before sowing, fertilizer was applied N - 11–25 kg ha^{-1}, P_2O_5 - 33–65 kg ha^{-1} and K_2O - 65 kg ha^{-1}.In spring, after resumption of vegetative growth, ammonium nitrate (NH_4NO_3; N 34.4%) was used for all variants. The second top-dressing consisting of ammonium sulphate ($(NH_4)_2SO_4$; N21, S 24%) at the rate of 100 kg ha^{-1} was done in winter wheat at

GS 29–31, and the remaining amount of needed nitrogen was added using ammonium nitrate. The final application was done at GS 47–51 with ammonium nitrate.

Weeds were controlled using foliar commercial herbicides: in 2019, tritosulfuron (714 g kg^{-1}) + florasulam (54 g kg^{-1}) 70 g kg^{-1} and adjuvant Dash 0.5 L ha^{-1}, in 2020, florasulam 9100 g kg^{-1}) + halauxifen-methyl (104.2 g kg^{-1}) 0.04 kg ha^{-1} and MCPA (750 g L^{-1}) 1.5 L ha^{-1} were used.

The severity of leaf blotches was assessed: for the whole plant - at GS 31–32, for three upper leaves - at GS 37 and GS 63–65, and for two upper leaves - at GS 73 and GS 75–79. Growth stages were noted according to BBCH scale. In the first assessment, 25 plants were evaluated. In further assessments, 50 leaves were evaluated from every plot, proportionally taking flag leaves, first leaves and second leaves from each plot. The severity was expressed in percentages.

The total disease impact during vegetation period was estimated by calculating the area under the disease progress curve (AUDPC) using the formula (1) (Simko & Piepho, 2012):

$$A_k = \sum_{i=1}^{N_{i-1}} \frac{(y_i + y_{i+1})}{2} (t_{i+1} - t_i) \qquad (1)$$

where n – data-set extent; a_i – variable at the i index of a data-set, N.

The yield was harvested at GS 89–90, and yield data was adjusted to 14% moisture. Mathematical data processing was done by using R-studio, multi-way Anova analysis, and correlation analysis. Bonferroni test was used for the comparison of means; the differences were considered statistically significant when $p < 0.05$.

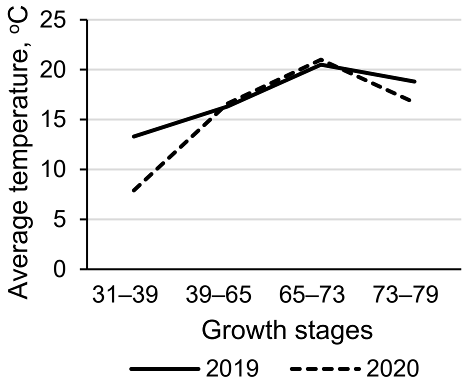

Figure 1. Average temperatures in 2019–2020 (data from the Study and Research farm "Pēterlauki" meteorological station).

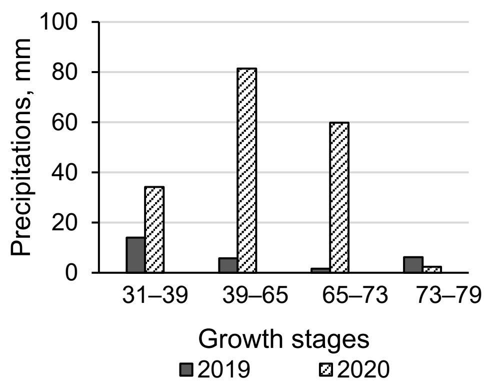

Figure 2. Amounts of precipitation in 2019–2020 (data from the Study and Research farm "Pēterlauki" meteorological station).

The meteorological data (average temperature (°C) and the amount of precipitation (mm)) were summarised according to growth stages of winter wheat when the evaluation of leaf blotches was done (Figs 1, 2). The meteorological conditions were significantly different in both research years. Overall, the air temperatures in the vegetation period were higher than long-term observations in both trial years - in some decades the increase of average air temperature reached even +5.0 °C (in 2019: - 3rd decade of June; in 2020 - 3rd decade of April, 2nd decade of May, 3rd decade of June.

There was a significant difference between the amounts of precipitation during the research years. In 2019, the amount of precipitation was low (for most decades only 20–30% from long-term observations). In contrast, second research year was characterised with rainfall (for example, 1st decade of June - 359%, 3rd decade of June - 219% from long -term observations).

RESULTS AND DISCUSSION

The development of leaf blotches. The severity of leaf blotches in winter wheat leaves differed significantly during both years of investigations (Fig. 3). In 2019, the total amount of precipitation was low and the lack of moisture was observed in all winter wheat growth stages; however, the severity of tan spot reached a significant level (18.7% in untreated variant). Although the first symptoms of tan spot were observed already at GS 31–32 (severity 0.03%), rapid development began only at GS 73. In contrast, the level of Septoria tritici blotch was relatively low. The first symptoms were observed later - only at the stage of early milk (severity 0.6%). Further development of the disease was slow, and at the end of vegetation period, the severity of Septoria tritici blotch in untreated plots was only 7.4%.

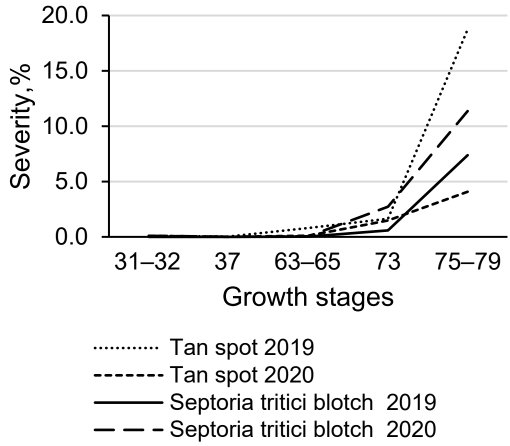

Figure 3. Severity of winter wheat leaf blotches in untreated plots in 2019–2020.

In 2020, the amount of precipitation at GS 39–65 was 81.4 mm, but at GS 65–73 - 59.8 mm (at this time in 2019 - respectively only 5.8 and 1.6 mm). These conditions promoted the development of Septoria tritici blotch. It is known that the causal agent of Septoria tritici blotch requires a moist leaf surface for infection and weather was favourable for disease development. This corresponds to the results from other studies (El Jarroudi et al., 2013; Bankina et al., 2018; Castro et al., 2018). The first symptoms were observed at an early stage of wheat development (GS 31–32) but rapid development of Septoria tritici blotch started at GS 73 (2.7% in untreated variant) and coincided with rainfall (on 29.06.2020. - 56 mm). At the end of vegetation period, the severity of Septoria tritici blotches in untreated plots reached already 11.4%. For the first time, tan spot was observed also at GS 31–32 (0.1%), but its development was slow, and at the end of vegetation, it reached only 4.1% in untreated plots. This is an unexpected result, because usually higher amounts of precipitation increase the level of tan spot (Fleitas et al., 2018; Schierenbeck et al., 2019).

Total impact of both diseases expressed as values of AUDPC (Fig. 4) differed significantly depending on year ($P < 0.001$).

Efficacy of leaf blotches control. In both years, application of fungicides significantly decreased the level of leaf blotches ($p < 0.001$ for both years). The results of the current study coincide with the results of numerous researches, i.e., fungicide treatments reduced the values of AUDPC of leaf blotches in comparison with the untreated variant (Willyerd et al., 2015; Castro et al., 2018; Fleitas et al., 2018; Schierenbeck et al., 2019).

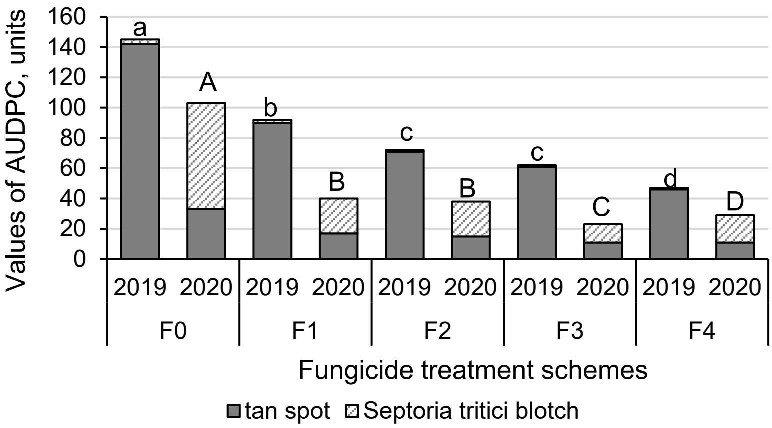

Figure 4. Values of areas under the disease progress curve (AUDPC) of leaf blotches depending on fungicide treatment schemes in 2019–2020.

Significantly different means are labelled with different letters in superscript: $^{a, b, c, d, e}$ – significant difference for average values of AUDPC for 2019; $^{A, B}$ – significant difference for average values of AUDPC for 2020.

More intensive application of fungicides was effective under conductions of higher pressure of leaf diseases. In 2019, when the differences in AUDPC values for tan spot (Fig. 4) among variants ranged between 35 and 147 (without fungicide treatment) units, the efficacy of fungicides in variant F1 (treatment frequency index (TFI) = 0.5) was lower than in variants F2 and F3. Although TFI in F2 and F3 was equal, the efficacy differed. A better efficacy was obtained in F3, where dose of fungicide was divided and the treatment was done in two applications. Variant F4, where TFI = 2, showed an even better efficacy. In 2020, when the AUDPC values ranged only between 8 and 49 units, the differences between fungicide treatment strategies on the severity of tan spot were not significant.

In both years, all fungicide treatments ensured the protection of wheat cultivars against Septoria tritici blotch ($P < 0.001$ for both years). In turn, the differences in the efficacy of fungicide treatment schemes were significant only in 2020. Although TFI in F2 and F3 varied (respectively - 0.5 and 1.0), the efficacy of those fungicide treatment schemes for limiting Septoria tritici blotch did not differ. Similar efficacy was ensured also in F4, where TFI = 2.0. A better effect was obtained in F3, where fungicide application was done two times.

Many studies revealed that used fungicide treatment schemes varied and their effectivity differed. Researches showed that one application of fungicides at the time of flag leaf formation decreased tan spot severity by 83.7% and the values of AUDPC by 86.6% (Bhatta et al., 2018). Other researchers included also early treatment until stem elongation to prevent primary infection (Schierenbeck et al., 2019; Fleitas et al., 2018). Kutcher et al. (2018) found that split fungicide application at both stem elongation (GS 30) and flag leaf (GS 39) tended to decrease the severity of leaf blotches on flag leaves and increase the yield relative to single application of fungicide applied at GS 39. Wegulo et al. (2009) obtained that the fungicides used at flowering can prevent significant yield losses. The present study confirms the results of researches in Luxembourg when in years with major tan spot outbreaks, El Jarroudi et al. (2013) found that during early grain development (at GS 75), the disease severity was well controlled by a single (at GS 55) and double (at GS 31 + GS 59) fungicide treatments, but later (at GS 85) the severity of disease increased. Those researchers used fungicide treatment schemes similar to those in our experiments but with different active ingredients.

Similarly to tan spot, the strategies used for the limiting of Septoria tritici blotch varied. In Ireland, where winter wheat fungicide programs for Septoria tritici blotch comprised even four applications, first application was done until GS 31 with the aim to slow the progression of Septoria tritici blotch in the upper canopy. Other researchers - Sylvester & Kleczewski (2018) - established that the inclusion of early treatment in fungicide programs (GS 30 + GS 37 or GS 30 + GS 60) did not result in significantly lower disease severity compared to single application at GS 37 or GS 60. Researchers found that fungicide treatment schemes with fungicide application at GS 60 resulted in the lowest leaf blotch severity on the flag leaf. Brinkman et al. (2014) confirmed that early application did not control the disease on flag leaves during grain fill and the most effective fungicide application timing was at GS 35–40 or at GS the 60–65. Triple application of fungicides resulted in the lowest leaf disease during grain fill, but efficacy of triple application did not usually differ from one application done at flowering.

Nitrogen rates. Although the development of tan spot was not influenced by nitrogen fertilizer rate ($P = 0.07$ for 2019; $P = 0.95$ for 2020), the influence of fungicide atment scheme on the development of tan spot (Table 2) depended on nitrogen fertilizer rates. In the year with higher values of AUDPC, the efficacy of treatment schemes where treatment was done in two or three applications (TFI = 1.0 and 2.0) in variants F3 and F4 was higher at all nitrogen rates. In the next year, with low pressure of tan spot, only at N210 the influence of fungicide treatment scheme was significant.

The results of present study confirm that the effectivities of fungicides on the development of tan spot increased with the increase in nitrogen dose (Castro et al., 2018).

Table 2. Values of AUDPC of tan spot depending on fungicide treatment schemes and nitrogen rate in 2019–2020

Fungicide treatment schemes	Values of AUDPC			
	N120	N150	N180	N210
	2019			
F0	146^{a}	142^{a}	147^{a}	133^{a}
F1	97^{b}	93^{b}	88^{b}	84^{b}
F2	85^{b}	$68^{b,c,d}$	$63^{b,c,d}$	70^{b}
F3	$67^{b,c}$	$65^{b,c,d}$	$56^{c,d}$	$56^{b,c}$
F4	48^{c}	46^{d}	54^{d}	35^{c}
	2020			
F0	31^{A}	40^{A}	34^{A}	26^{A}
F1	19^{B}	15^{B}	13^{B}	19^{A}
F2	18^{B}	14^{B}	15^{B}	12^{B}
F3	10^{B}	9^{B}	10^{B}	15^{A}
F4	11^{B}	12^{B}	11^{B}	10^{B}

Significantly different means are marked with different letters in superscript: a, b, c, d, – significant difference for average values of AUDPC for 2019; A, B – significant difference for average values of AUDPC for 2020.

The development of Septoria tritici blotch was not influenced by nitrogen fertilizer rate ($P = 0.67$ for 2019; $P = 0.94$ for 2020). In contrast, Jensen & Jørgensen (2016) found that severity of disease increased significantly with the increase in crop biomass in the untreated plots. The research of

Brinkman et al. (2013) revealed that severity of Septoria tritici blotch on the flag and penultimate leaves weakly associated with N rate. However, in certain years, the severity of disease increased in the untreated plots at higher N rates (32% of the leaf area was infected at a rate of 170 kg ha^{-1}, compared to 26.9% with N rate of 100 kg ha^{-1}). Castro et al. (2018) also found that weather conditions explained the differences in the effect of N fertilization on the AUDPC of Septoria tritici blotch. In the wettest year with more disease pressure, nitrogen fertilization significantly decreased disease severity. Conversely, in the driest year, no differences were detected.

Wheat yield

The average winter wheat grain yield in both trial years differed significantly ($P < 0.001$). Nitrogen fertilization significantly increased the average grain yield per both years. In 2019, a significant yield increase was observed at the nitrogen rate N180 ($P = 0.015$) (Švarta et al., 2020), but in 2020 - at the rate N150 ($P < 0.001$). Further increase of nitrogen rate did not provided a significant yield increase.

As leaf blotch severity was influenced by fungicide treatment schemes but no by nitrogen rate, this article further analyses the grain yield depending on fungicide treatment schemes at the average nitrogen background.

In our experiment, a negative moderate correlation between total AUDPC of leaf blotches and grain yield was established ($r = -0.58$). In 2019, winter wheat grain yields was 5.08–5.25 t ha^{-1} (Fig. 5) and fungicide treatment schemes did not influenced yield ($P = 0.80$). In 2020, when the average winter wheat grain yield was higher (7.82–8.64 t ha^{-1}), the using of fungicides provided significant increase of yield ($P < 0.001$) compared to untreated variant but there were no significant differences among fungicide treatment schemes. It coincides with results of research in the Baltic–Nordic region what indicate a positive yield response even after one fungicide treatment of wheat (Jalli et al., 2020). Researchers obtained that yield responses from fungicide treatment range between 0.5 and 2 t ha^{-1} and depends on region, meteorological conditions, cultivar and soil type.

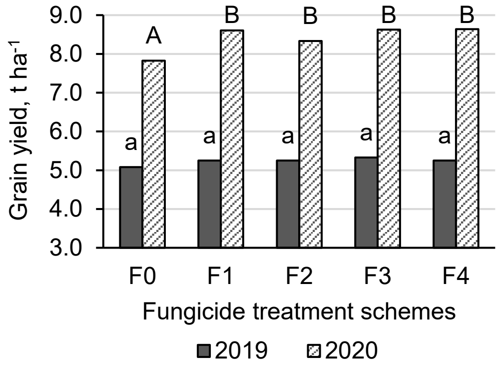

Figure 5. Winter wheat yield (t ha^{-1}) depending on fungicide treatment schemes in 2019–2020 at the average nitrogen background.

Significantly different means are marked with different letters in superscript: ^{a} – significant difference for 2019; $^{A, B}$ – significant difference for 2020.

CONCLUSIONS

1. The development of tan spot and Septoria tritici blotch differed significantly in both years and depended on meteorological conditions. In 2019, tan spot dominated and the severity of disease reached a significant level (18.7% in untreated variant). In 2020, weather conditions promoted the development of Septoria tritici blotch (11.4% in untreated variant).

2. All used schemes of fungicide treatment significantly decreased the level of tan spot and Septoria tritici blotches. More intensive fungicide application contributed better leaf blotches control, but it did not give additional yield under Latvian conditions in 2019–2020.

3. Nitrogen fertilizer rate had no significant effect on the development of leaf blotches; however, more intensive fungicide treatment was more effective in variants with higher rates of nitrogen.

4. Nitrogen fertilizer rate significantly increased the average grain yield per both years. A significant yield increase was observed: 2019 - at the nitrogen rate N180, in 2020 - at the rate N150. Further increase of nitrogen rate did not provided a significant yield increase.

5. A negative moderate correlation between total AUDPC of leaf blotches and grain yield was established. The using of fungicides increased grain yield only in year when obtained significantly higher yields (grain yields reached 7.00 t ha^{-1}) although the severity of leaf blotches was lower.

ACKNOWLEDGEMENTS. The research was supported by the EIP-Agri project 'The development of the decision-making support system for restriction of the diseases, affecting leaves and ears of winter wheat'.

REFERENCES

Bankina, B., Bimšteine, G., Arhipova, I., Kaņeps, J. & Stanka, T. 2018. Importance of agronomic practice on the control of winter wheat diseases. *Agriculture* **8**, 56. doi: 10.3390/agriculture8040056

Bhatta, M., Regassa, T., Wegulo, S.N. & Baenziger, P.S. 2018. Foliar fungicide effects on disease severity, yield, and agronomic characteristics of modern winter wheat genotypes. *Agronomy Journal* **110**(2), 1–9. doi: 10.2134/agronj2017.07.0383

Brinkman, J.M.P., Deen, W., Lauzon, J.D. & Hooker, D.C. 2014. Synergism of nitrogen rate and foliar fungicides in soft red winter wheat. *Agronomy Journal* **106**(2), 491–510. doi: 10.21354/agronj2013.0395

Central Statistical Bureau of Latvia. 2019. http://data1.csb.gov.lv/pxweb/lv/lauks/lauks__03Augk__ikgad/LAG020.px/table/tableViewLayout1/. Accessed 01.05.2021.

Castro, A.C., Fleitas, M.C., Schierenbeck, M., Gerard, G.S. & Simón, M.R. 2018. Evaluation of different fungicides and nitrogen rates on grain yield and bread-making quality in wheat affected by Septoria tritici blotch and yellow spot. *Journal of Cereal Science* **83**, 49–57. doi: 10.1016/j.jcs.2018.07.014

Cotuna, O., Paraschivu, M., Parascivu, A.M. & Sarateanu, V. 2015. The influence of tillage, crop rotation and residue management on tan spot (*Dreschlera tritici repentis* Died. Shoemaker) in winter wheat. *Research Journal of Agricultural Science* **47**(2), 13–21.

Creissen, H.E., Glynn, E., Spink, J.H. & Kildea, S. 2018. The effect of fungicides applied pre-stem extension on septoria tritici blotch and yield of winter wheat in Ireland. *Crop Protection* **104**, 7–10. doi: 10.1016/j.cropro.2017.10.003

El Jarroudi, M., Kouadio, L., Beyer, M., Giraud, F., Tychon, B. & Delfosse, P. 2013. Factors affecting tan spot on winter wheat in the grand-Duchy of Luxembourg. *Journal of Plant Pathology* **S1**(7), 1–7.

Fleitas, M.C., Schierenbeck, M., Gerard, G.S., Dietz, J.I., Golik, S.I. & Simón, M. 2018. Breadmaking quality and yield response to the green leaf area duration caudsed by fluxapyroxad under three nitrogen rates in wheat affected with tan spot. *Crop Protection* **106**, 201–209. doi: 10.1016/j.cropro.2018.01.004

Gomes, C., Costa, R., Almeida, A.S., Coutinho, J., Pinheiro, N., Coco, J., Costa, A. & Maçã, B. 2016. Septoria leaf blotch and yellow rust control by: fungicide application opportunity and genetic response of bread wheat varieties. *Emirates Journal of Food and Agriculture* **28**(7), 493–500. doi: 10.9755/ejfa.2015.04.345

Jalli, M., Kaseva, J., Andersson, B., Ficke, A., Nistrup–Jørgensen, L.N., Ronis, A., Kaukoranta, T., Ørum, J.E. & Djurle, A. 2020. Yield increase due to fungicide control to leaf blotch diseases in wheat and barley as a basis for IPM decision-making in the Nordic-Baltic region. European Journal of Plant Pathology **158**(2), 315–333. doi: 10.10007/s10658-020-02075-w

Jensen, P.K. & Jørgensen, L.N. 2016. Interactions between crop biomass and development of foliar diseasesin winter wheat and the potential to graduate the fungicide dose according to crop biomass. *Crop Protection* **81**, 92–98. doi: 10.1016/j.cropro.2015.11.016

Kremneva, O.Yu, Mironenko, V.V., Volkova, G.V., Baranova, O.A., Kin, Y.S. & Kovalenko, N.M. 2021. Resistance of winter wheat varieties to the tan spot in the North Caucasus region of Russia. *Saudi Journal of biological Sciences* **28**(3), 1787–1794. doi: 10.1016/j.sjbs.2020.12.021

Kutcher, H.R, Turkington, T.K., McLaren, D.L., Irvine, R.B. & Brar, G.S. 2018. Fungicide and cultivation management of leaf spot diseases of winter wheat in western Canada. *Plant disease* **102**(9), 1828–1833. doi: 10.1094/PDIS–12–17–1920–RE

Kuzdraliński, A., Szczerba, H., Tofil, K., Filipiak, A., Garbarczyk, E., Dziadko, P., Muszyńska, M. & Solarska, E. 2015. Early PCR detection of the *Mycosphaerella graminicola* in the leaves of winter wheat in Poland. *Romanian Agricultural Research* **32**, 273–277.

Nistrup Jørgensen, L. 2008. Resistance situation with fungicides in cereals. *Zemdirbyste-Agriculture* **95**(3), 373–378.

Simko, I. & Piepho, H.P. 2012. The area under the disease progress stairs: calculation, advantage and application. *Phytopathology* **102**, 381–389. doi: 10.1094/PHYTO–07–11–0216

Schierenbeck, M., Fleitas, M.C., Cortese, F., Golik, S.I. & Simón, M.R. 2019. Combinations of fungicide molecules and nitrogen fertilization revert nitrogen yield reductions generated by *Pyrenophora tritici-repentis* infections in bread wheat. *Crop protection* **121**, 173–181. doi: 10.1016/j.cropro.2019.04.004

Sylvester, P.N. & Kleczewski, N.M. 2018. Evaluation of foliar fungicide programs in mid-Atlantic winter wheat production systems. *Crop protection* **103**, 103–110. doi: 10.1016/j.cropro.2017.09.012

Švarta, A., Bimšteine, G., Gaile, Z., Stanka, T., Daugaviņa, L. & Plūduma–Pauniņa, I. 2020. Development of winter wheat blotches depending on fungicide treatment schemes and nitrogen rates. *In: Proceedings of annual 26th International scientific conference Research for Rural development 2020.* Latvia University of Life Science and Technologies, Jelgava, Latvia, pp. 7–13. doi: 10.22616/rd.26.2020.01

Wegulo, S.N., Breathnach, J.A. & Baenziger, P.S. 2009. Effect of growth stage on the relationship between tan spot and spot blotch severity and yield in winter wheat. *Crop Protection* **28**, 696–702. doi: 10.1016/j.cropro.2009.04.003

Willyerd, K.T., Bradley, C.A., Chapara, V., Conley, S.P., Esker, P.D., Madden, L.V., Wise, K.A. & Paul, P.A. 2015. Revisiting fungicide-based management guidelines for leaf blotch diseases in soft red winter wheat. *Plant diseases* **99**(10), 1434–1444. doi: 10.1094/PDIS-02-15-0218-RE

Willocquet, L., Meza, W.R., Dumont, B., Klocke, B., Feike, T., Kersebaum, K.C., Meriggi, P., Rossi, V., Ficke, A., Djurle, A. & Savary, S. 2021. An outlook on wheat health in Europe from a network of field eksperiments. *Crop Protection* **139**, 1–15. doi: 10.1016/j.cropro.2020.105335

Agronomy Research **20**(2), 424–436, 2022
https://doi.org/10.15159/AR.21.164

Effect of the Lactation Months on Milk Composition of the Second-Parity Lacaune Ewes

V. Tatar[1,*], A. Tänavots[1], A. Polikarpus[1], A. Sats[1], E. Arvi[1], T. Mahla[1] and I. Jõudu[1,2]

[1]Estonian University of Life Sciences, Institute of Veterinary Medicine and Animal Sciences, Chair of Food Science and Technology, Fr.R. Kreutzwaldi 1, EE51006 Tartu, Estonia
[2]Estonian University of Life Sciences, ERA Chair for Food (By-) Products Valorisation Technologies of the Estonian University of Life Sciences (VALORTECH), Fr.R. Kreutzwaldi 1, EE51006 Tartu, Estonia
[*]Correspondence: vilma.tatar@emu.ee

Received: February 24th, 2021; Accepted: December 22nd, 2021; Published: December 22nd, 2021

Abstract. This research aims to determine the chemical composition of Lacaune ewe milk produced in Estonia, as well as the correlations and the influence the stages of lactation have on milk. The study was carried out on fifty-one second-parity ewes. The analysis involved a total of 178 milk samples collected monthly from the second to the seventh month of lactation. Milk analyses included the determination of the contents of total solids, fat, total protein, casein, casein index, lactose, ash, P, Ca, K, Na, Mg, somatic cell count and pH. The Lacaune ewes' milk contained on average 18.62% total solids, 7.75% fat, 5.74% total protein, 4.32% casein, 4.76% lactose, 0.89% ash, 160.26 mg 100 g^{-1} Ca, 140.07 mg 100 g^{-1} P, 135.21 mg 100 g^{-1} K, 46.44 mg 100 g^{-1} Na, 17.66 mg 100 g^{-1} Mg. Overall means for casein index, pH value and somatic cell scores were 75.35%, 6.61 and 12.62, respectively. It was found that the month of lactation significantly affected almost all monitored traits except somatic cell score, casein index and Ca content. The contents of total solids, fat, total protein, casein, ash, P, and Mg increased, while the lactose content, and pH value decreased with the advancing lactation. Sodium content was highest and potassium content lowest value during mid-lactation. Producers must take into account that the composition of Lacaune ewe milk depends on the stage of lactation and may, therefore, affect the production process and the final quality of the product.

Key words: ewe milk, chemical composition, stage of lactation.

INTRODUCTION

The Lacaune breed has become one of the world's high-yielding ovine milk breeds, with average daily milk yields of 1.75 L (Giambra et al., 2014; Pesantez-Pacheco et al., 2018). Since dairy sheep farming is not traditional in Estonia, ewe milk products are a niche market, which is mainly influenced by the growth of consumer interest in different dairy products. Ewe milk is considered a delicacy in many countries, and ewe dairy products have gained popularity among consumers due to the quality and nutritional value of the products (Balthazar et al., 2017). Compared to the milk of other domestic mammals, high nutritional value of ewe milk is contributed to the higher concentrations of proteins, fats, vitamins, and minerals (Park et al., 2007; Barłowska et al., 2011; Balthazar et al., 2017). Ewe milk is mainly processed into traditional fine cheeses for gourmet and export markets, as well as yoghurt and ricotta (Milani & Wendorff, 2011; Pulina et al., 2017). The high levels of protein, fat, and calcium are important in cheese-making (Moatsou et al., 2004). The same reasons make ewe milk very suitable for yoghurt making. Ewe milk yoghurt possesses high gel strength and minimal syneresis, it can be produced without the need for added milk solids or stabilizers (Milani & Wendorff, 2011).

The composition of ewe milk is mainly influenced by breed, nutrition, environment and stage of lactation (Pulina et al., 2005; Park et al., 2007; Komprej et al., 2012; Inostroza et al., 2020). The stage of lactation has a significant effect on daily milk yield, pH value, somatic cell count and the content of total solids, fat, protein, casein, lactose, Ca and P (Kuchtík et al., 2017). However, studies have shown mixed results in examining the relationship between milk composition and lactation progression. There is no information on the composition and properties of ewe milk produced in Estonia. The wider purpose of this pilot study was to give an overview of the composition of Lacaune ewes' milk produced in local conditions to encourage potential farmers to take up dairy sheep farming.

The composition and the physico-chemical properties of milk vary depending on production conditions and the individual characteristics of particular animals. Fluctuations in the composition and quality of milk are also reflected in the quality of products. This research aims to identify changes in the composition and properties of milk during the lactation period in Estonia. The outcome of this work would benefit the production and valorisation efficiency of ewe milk.

MATERIALS AND METHODS

Animals

The Lacaune dairy sheep breed was introduced in Estonia in 2017, when 84 purebred Lacaune Lait sheep were imported from France. A semi-intensive system was implemented on the family-operated farm (with year-round free-range housing in modern buildings and seasonal milk production). During the sample collecting period, all ewes were kept in one flock under identical conditions under permanent veterinary supervision. The ewes did not show any signs of serious health issues, although some minor health issues were observed during the sample period and it was necessary to exclude some ewes from the study and include others from the same study group.

Lambing took place from January to March 2019. During the lactation, the ration was constant, ewes were fed twice a day with 1.1 kg of concentrate per day and *ad libitum* first cut mixed hay. The quantity and composition of the ration fed to the animals was the same throughout the sampling period. The concentrate contained 62.5% of full grain oat, 35.7% of rape seed cake, and 1.8% of vitamins and minerals. The DM content of the feed was 88%, that of crude protein 15% and 10.92 MJ kg^{-1} of metabolizable energy (ME). Hay contained 85% of dry matter, 10% of crude protein and 4.5% of minerals.

Ewes were milked twice a day at 7:00 and 17:00 using a Panazoo 1×12 parallel milking parlour (-39 kPa; 180 pulsation min^{-1}). Average milk yield was 1.8 kg per day in the first half of lactation and 0.8 kg per day in the second half of lactation, measured at the bulk milk tank. Most of the lactating ewes dried off at the end of August.

Milk sampling

Fifty one second-parity Lacaune Lait ewes, which were divided into two 25−26 ewes groups based on lambing time, participated in the study. Milk samples were collected monthly from 15 ewes within the group, from 30 ewes in total. Milk sampling started from 30 days postpartum and then monthly during the lactation period (from February to August). Milk samples were collected only at the morning milking. The total number of samples collected was 178. Individual milk samples (volume at least 250 mL) were immediately transported to the laboratory in a cooler at 4 °C. Milk sub-samples to determine fat, total protein (TP), lactose contents and somatic cell count (SCC) were preserved with Broad Spectrum Microtabs® II (Bronopol < 44%, Natamycin < 2%). Milk sub-samples for the determination of total solids (TS), casein, ash, Ca, P, K, Na and Mg contents were frozen at –20 °C using 15 and 50 mL polypropylene centrifuge tubs.

Compositional analysis

Milk fat (%), TP (%), lactose (%) and SCC ($\times 10^3$ mL^{-1}) were estimated in the Milk Analysis Laboratory of the Estonian Livestock Performance Recording Ltd with Analysers (CombiFOSS, Denmark) using the international standard IDF 141; EVS-EN ISO 13366-2 and work package PL-PR-2.

TS, casein, ash and pH were estimated in the Laboratory of the Chair of Food Science and Technology of the Estonian University of Life Sciences. TS (%) content was determined gravimetrically by oven drying at 102°C to constant weight according to the standard ISO 6731:2010. Casein (%) content was analysed by the Kjeldahl method (ISO 17997-2:2004/IDF 29-2:2004) using the wet ashing device Digestor™ 2508 and analyser Kjeltec™ 2300 (FOSS, Denmark). Ash (%) content was determined gravimetrically by incineration in a muffle furnace at 550°C (AOAC 945.46). Contents of calcium (Ca, mg 100 g^{-1}), potassium (K, mg 100 g^{-1}), sodium (Na, mg 100 g^{-1}) and magnesium (Mg, mg 100 g^{-1}) were measured according to the atomic absorption spectrometric method (ISO 8070/IDF 119:2007) by using the ContrAA® 700 device (Analytik Jena AG, Germany). The phosphorus (P, mg 100 g^{-1}) content was determined according to the standard ISO 9874:2006/IDF 42:2006 using the spectrometer Specord® 250 Plus (Analytik Jena AG, Germany). Active acidity (pH) was measured with the pH-meter SevenCompact™ S210 equipped with the electrode InLab® Expert Pro (Mettler Toledo, U.S.A).

The casein index was calculated according to the following formula (Buccioni et al., 2015):

$$Casein\ index\ \% = \left(\frac{Total\ casein\ content}{Total\ crude\ protein\ content}\right) \times 100 \qquad (1)$$

To achieve a normal distribution, the somatic cell counts (SCC) were converted to a somatic cell score (SCS) using a log base 2 function (Ali & Shook, 1980):

$$SCS = \log_2\left(\frac{SCC}{100}\right) + 3 \qquad (2)$$

Statistical analyses

Statistical analyses were performed with the statistical package R 4.0.3 (R Core Team 2021). Effect of lactation month and random effect of animals to the milk fat, TP, casein, casein index, SCS, lactose, pH, TS, ash and mineral content were studied by Linear Mixed-Effects Model (GLMM). Emmeans and multcomp packages were used to carry out pairwise comparison of the groups. Tukey's multiple comparison post-hoc test was used to determine the groups least square mean differences at the significance level of $\alpha = 0.05$. Relationships between variables and their statistical significances were calculated by rcorr function in Hmisc package (Harrell & Dupont, 2021) and reported as Pearson correlation coefficients. Significance probability levels were denoted as: * - $P < 0.05$, ** - $P < 0.01$ and *** - $P < 0.001$. In addition, principal component analysis (PCA) was performed with the procedure fviz pca in factoextra package (Kassambara & Mundt, 2020) using ewe milk composition records (fat, TP, lactose, SCS, TS, pH, ash, casein, Ca, P, K, Na and Mg) as variables and lactation month as factor.

RESULTS AND DISCUSSION

Milk composition

The ewe milk had higher contents of TS, fat, TP, casein, lactose and ash in comparison with both goat and cow milk (Park et al., 2007; Balthazar et al. 2017). This study showed that milk samples from Lacaune ewes contained on average 18.62% total solids, 7.75% fat, 5.74% total protein and 4.76% lactose (Table 1). Considerably higher contents of total solids (19.34%) and fat (8.10%) for the same breed, and distinctly lower protein (5.22%) and lactose (4.43%) contents have been found from bulk tank milk in a Brazilian study (Fava et al., 2014). Similar total solid content (18.61%) was reported in a study conducted in the Czech Republic on Lacaune ewes (individual samples, $n = 18$) at 127 days of lactation (Kuchtík et al., 2017) and in a mixture of milk (18.7%) from different breeds of sheep (Hanuš et al., 2015). The average casein and ash contents in our study were 4.32% and 0.89%, respectively (Table 1). Similar results have been found for the same breed by Kaminarides & Anifantakis (2004) and Kuchtík et al. (2017) and for the Sarda breed by Bittante et al. (2017). The mean casein index in our study was quite low, 75.35%. Commonly the casein portion of ewe milk amounts to around 80% of the total milk protein (Hejtmánková et al., 2012; Balthazar et al., 2017). The average Ca content (160.26 mg 100 g^{-1}) of Lacaune milk in this study was significantly lower (Table 1) than in some published results (Kaminarides & Anifantakis, 2004; Panayotov et al., 2018) and somewhat higher than in a Czech Republic study (Kuchtík et al., 2017). The average P content (140.07 mg 100 g^{-1}) in the current study was higher than the data reported in earlier research (Kuchtík et al., 2017; Panayotov et al., 2018). A similar trend was also found for the K content by Panayotov et al. (2018). The average K content of Lacaune milk in this study (135.21 mg 100 g^{-1}) was higher than in the milk of other ewe breeds (Park et al., 2007; Balthazar et al., 2017). The average Na and Mg contents in this study (46.44 mg 100 g^{-1} and 17.66 mg 100 g^{-1}, respectively) confirm the results from earlier research with the Lacaune (Kaminarides & Anifantakis 2004; Panayotov et al., 2018) and other ewe breeds' milk (Park et al., 2007; Balthazar et al., 2017; Aldalur et al., 2019).

Of the basic components, the fat content varied the most (CV, 19.72%), and the ash content the least over the lactation period (CV, 6.47%) (Table 1). The lactose and the casein index (CV, 7.53% and CV, 6.67% respectively) were also less variable. The variation in minerals contents was greater for Na (CV, 29.92%), K (CV, 24.89%) and Mg (CV, 21.23%) contents than for other analysed minerals. Corresponding well to the findings from earlier studies on Lacaune ewes' milk (Kaminarides & Anifantakis, 2004; Kuchtík et al., 2017; Panayotov et al., 2018), the average pH value in the present study was 6.61 and was most stable (CV, 1.72%). SCS had the highest variation (CV, 24.24%). The average number of SCS (12.62) is close to that of a Spanish study (Rovai et al., 2015) and is slightly higher than in some others studies of Lacaune milk (Barillet et al., 2001; Kuchtík et al., 2017). High SCC could refer to udder infection or some content of colostrum in the first month milk sampling. Barillet et al. (2001) and Kuchtík et al. (2017) reported that SCC can be caused by clinical, chronic or subclinical mastitis or could be linked to a reduced milk yield.

Table 1. Descriptive statistics of milk chemical composition and the coefficients of variation (CV) over the lactation period (n = 178)

Milk characteristics	Mean	SD	Minimum	Maximum	CV (%)
Fat (%)	7.75	1.53	4.23	14.75	19.72
TP (%)	5.74	0.86	4.18	8.65	15.00
Casein (%)	4.32	0.72	2.81	6.96	16.72
Casein index[1] (%)	75.35	5.03	52.32	86.53	6.67
SCS	12.62	3.06	7.32	20.89	24.24
Lactose (%)	4.76	0.36	3.42	5.44	7.53
pH	6.61	0.11	6.34	6.98	1.72
TS (%)	18.62	2.04	14.80	27.73	10.93
Ash (%)	0.89	0.06	0.75	1.11	6.47
P (mg 100 g^{-1})	140.07	19.92	80.65	206.13	14.22
Ca (mg 100 g^{-1})	160.26	18.09	118.00	229.90	11.29
K (mg 100 g^{-1})	135.21	33.65	80.50	195.90	24.89
Na (mg 100 g^{-1})	46.44	13.89	19.30	78.20	29.92
Mg (mg 100 g^{-1})	17.66	3.75	8.40	27.30	21.23

[1]Casein index: casein to protein ratio.

In the present study, the strongest and most statistically significant correlation was found between TP and casein (r = 0.91; P < 0.001) (Table 2). The TS content had a similar relationship with fat (r = 0.846; P < 0.001), TP (r = 0.846; P < 0.001) and casein (r = 0.833; P < 0.001) contents. Similar results were obtained in a study of Araucana creole ewe´s milk (Inostroza et al., 2020). In our study, the fat content had a strong positive correlation with TP (r = 0.766; P < 0.001) and casein (r = 0.757; P < 0.001). Additionally, all correlations between lactose and TS, fat, TP, casein and ash content were negative (P < 0.001), which is consistent with another study of Lacaune (Kuchtík et al., 2017) and Araucana creole ewe´s milk (Inostroza et al., 2020).

The pH value correlated positively with SCS (r = 0.429; P < 0.001) and negatively with casein and TS (r = –0.422; P < 0.001, r = –0.392; P < 0.001 respectively). This can be explained by the health condition of the udder. In case of mastitis, with an increased number of the SCC, changes in the production of milk in the mammary gland occur, e.*g*., a decrease in the casein to TP ratio also causes a fall in the acidity of milk. Similar relationship between the SCC and pH value has been found in ewe milk in Italy (Albenzio et al., 2004) and in Sarda ewes' milk (Paschino et al., 2019).

Table 2. Pearson correlation coefficients between milk parameters of Lacaune ewes

	1.	2.	3.	4.	5.	6.	7.	8.	9.	10.	11.	12.	13.	14.
1. Lactation month	1													
2. Fat	0.518 ***	1												
3. TP	0.725 ***	0.766 ***	1											
4. Casein	0.672 ***	0.757 ***	0.910 ***	1										
5. Casein index	0.042	0.141	0.001	0.409 ***	1									
6. SCS	-0.054	-0.055	-0.081	-0.192 *	-0.271 ***	1								
7. Lactose	-0.643 ***	-0.592 ***	-0.678 ***	-0.583 ***	0.069	-0.332 ***	1							
8. pH	-0.399 ***	-0.284 ***	-0.357 ***	-0.422 ***	-0.239 **	0.429 ***	0	1						
9. TS	0.527 ***	0.846 ***	0.846 ***	0.833 ***	0.13	-0.243 **	-0.429 ***	-0.392 ***	1					
10. Ash	0.224 **	0.359 ***	0.456 ***	0.326 ***	-0.207 **	0.197 **	-0.447 ***	0.151 *	0.267 ***	1				
11. P	0.255 ***	0.371 ***	0.468 ***	0.443 ***	0.033	0.007	-0.197 **	-0.306 ***	0.440 ***	0.479 ***	1			
12. Ca	0.151*	0.319 ***	0.371 ***	0.305 ***	-0.074	-0.151 *	-0.033	-0.136	0.371 ***	0.534 ***	0.537 ***	1		
13. K	-0.329 ***	-0.08	-0.282 ***	-0.247 ***	0.023	0.306 ***	0.032	0.223 **	-0.199 **	-0.08	-0.013	-0.04	1	
14. Na	0.569 ***	0.194 **	0.452 ***	0.358 ***	-0.119	0.055	-0.483 ***	-0.133	0.215 **	0.331 ***	0.141	0.015	-0.677 ***	1
15. Mg	0.770 ***	0.496 ***	0.690 ***	0.621 ***	0.003	-0.009	-0.496 ***	-0.405 ***	0.524 ***	0.345 ***	0.330 ***	0.197 **	-0.462 ***	0.637 ***

Significance probability levels are denoted as: * - $P < 0.05$, ** - $P < 0.01$ and *** - $P < 0.001$.

Correlations between the mineral content and major composition parameters of the milk were mainly moderate, but statistically significant. Higher contents of TS, fat and casein and lower contents of lactose were associated with higher contents of the analysed minerals except for K, which was lower in this case. The milk samples' major components had the strongest correlations with Mg content (Table 2). The Mg content was positively correlated with TS ($r = 0.524$; $P < 0.001$), fat ($r = 0.496$; $P < 0.001$), TP ($r = 0.690$; $P < 0.001$), casein ($r = 0.621$; $P < 0.001$), ash ($r = 0.345$; $P < 0.001$), P ($r = 0.330$; $P < 0.001$) and Na ($r = 0.637$; $P < 0.001$) contents and negatively with lactose ($r = –0.496$; $P < 0.001$), pH value ($r = –0.405$; $P < 0.001$) and K ($r = –0.462$; $P < 0.001$).

Effect of Lactation Stage

The study confirmed that the stage of lactation has a significant effect on the contents of all of the recorded components of milk, except for SCS, casein index and calcium content (Tables 2 and 3). The contents of TS, fat, TP and casein in milk increased over the lactation ($r = 0.527$; $P < 0.001$, $r = 0.518$; $P < 0.001$, $r = 0.725$; $P < 0.001$ and $r = 0.672$; $P < 0.001$ respectively), which is comparable to reports on different breeds (Othmane et al., 2002) and the Lacaune breed (Kuchtík et al., 2017), but these indicators in this study were higher than those reported for Bovec, Istrian Pramenka and Improved Bovec breeds (Komprej et al., 2012). In contrast to the TS, fat, TP and casein contents, lactose content decreased significantly during lactation in the current research ($r = –0.643$; $P < 0.001$). The same finding has been observed in studies in the Czech Republic (Kuchtík et al., 2017) and Greece (Termatzidou et al., 2020). The lactose contents in the milk of healthy animals remained fairly constant, while the decrease in the lactose content is may be attributed to udder health issues (mastitis). This suggestion is supported by the negative correlation found between lactose and SCS ($r = –0.332$; $P < 0.001$) (Table 2). However, at the sixth month of lactation the lactose content decreased while the SCS increased (Table 3). The month of lactation had a slight ($r = 0.224$), but statistically significant ($P < 0.01$) effect on the ash content, which was higher at the end of lactation. Differences in the ash content can be explained by the reduction in the milk yield over the course of lactation. Robles Jimenez et al. (2020) showed that maximum milk yield is achieved on the second month of lactation, after which the yield begins to decrease. However, the variation in the mineral contents of ewe milk depends also on several others factors such as breed, geographical location, diet, stage of lactation, parity, and farming practices (Chia et al., 2017).

The month of lactation had no significant effect on SCS ($P = 0.471$), which is in line with the findings by Kuchtík et al. (2017), where SCS in Lacaune ewe milk insignificantly increased as lactation advanced. On the other hand, Matutinovic et al. (2011) reported a significant increase in SCS during lactation in the milk from an indigenous breed in sub-Mediterranean area. In our study, the mean SCS was lowest in the fifth month of lactation, differing significantly from the first two and the sixth month of lactation ($P < 0.05$).

The pH value of ewe milk decreased ($P < 0.001$) consistently during lactation (Table 3). The same result was found by Pavić et al. (2002) and Sahan et al. (2005). It might be explained by an increase in protein content (Pellegrini et al., 1997), and especially with an increase in casein ($r = −0.422$) and P ($r = −0.306$) content during lactation. Changes in the concentration of salts and proteins, mainly the caseins in the milk also affect the acidity level (Merlin Junior et al., 2015). Kuchtík et al. (2017) reported very stable pH values in the milk of Lacaune ewes over the lactation, and the stage of lactation had no significant effect on the pH value.

Table 3. Least square means and coefficients of variations (CV) of Lacaune ewe milk parameters in different months of lactation

		Month of lactation					
		2	3	4	5	6	7
	n	29	30	30	30	30	29
Fat (%)	Mean	7.10ab	6.91a	7.8b	7.43ab	8.89c	9.13c
	CV%	14.48	17.49	14.26	13.11	20.61	15.33
TP (%)	Mean	4.9a	5.19a	5.68b	5.79b	6.4c	6.65c
	CV%	7.05	10.19	9.26	7.01	12.27	12.53
Casein (%)	Mean	3.72a	3.86a	4.2b	4.32b	4.93c	4.97c
	CV%	10.86	9.83	9.89	8.38	14.48	15.45
Casein index[1] (%)	Mean	75.71a	74.97a	74.11a	74.72a	77.35a	74.87a
	CV%	6.92	8.75	5.41	6.95	4.51	6.83
SCS	Mean	13.61a	13.16a	11.96ab	11.37b	13.07a	12.81ab
	CV%	13.45	18.47	31.52	29.27	26.14	21.55
Lactose (%)	Mean	4.96a	4.96a	4.91a	4.76b	4.48c	4.36c
	CV%	3.54	3.92	5.55	4.17	9.09	6.42
pH	Mean	6.7a	6.64b	6.62bc	6.58cd	6.56d	6.57cd
	CV%	1.37	1.19	1.80	1.30	1.84	1.80
TS (%)	Mean	17.32a	17.54ab	18.84cd	18.46bc	19.76de	20.40e
	CV%	6.85	7.95	6.06	6.40	13.21	11.23
Ash (%)	Mean	0.87a	0.89ab	0.9ab	0.89ab	0.9b	0.92b
	CV%	5.80	4.85	5.46	6.02	7.49	7.89
P (mg 100 g^{-1})	Mean	132.87a	137.94ab	136.31ab	141.28ab	145.14ab	148.6b
	CV%	22.64	13.92	10.67	9.94	12.23	11.67
Ca (mg 100 g^{-1})	Mean	156.55a	156.79a	157.46a	164.27a	164.13a	163.71a
	CV%	9.80	13.04	9.27	8.74	14.30	11.16
K (mg 100 g^{-1})	Mean	179.08a	149.19b	109.74cd	102.25c	120.62d	152.41b
	CV%	3.60	21.10	9.55	8.98	26.63	9.84
Na (mg 100 g^{-1})	Mean	26.15a	40.49b	52.85cd	56.58c	51.07cd	50.44d
	CV%	18.29	26.50	18.22	13.77	23.11	17.09
Mg (mg 100 g^{-1})	Mean	11.53a	16.36b	18.14c	18.79c	20.27d	20.89d
	CV%	14.29	17.35	9.04	10.46	11.21	9.73

[1]Casein index: casein to protein ratio.

Different superscripts indicate significant differences ($P < 0.05$, Sidak multiple comparisons post-hoc test).

Only a weak correlation was found between the month of lactation and the Ca content ($r = 0.151$; $P = 0.044$) (Table 2, 3). A stable level of Ca over the lactation period has also been found by Sevi et al. (2004), but a constantly increasing Ca content in ewe milk over the lactation has been reported in studies of Lacaune ewes by Kuchtík et al. (2017) and by Abilleira et al. (2010) for the Latxa breed's milk. These different results may have been obtained due to different feeds, parity or climate. Kuchtík et al. (2017) reported that increase in the content of Ca and P during lactation were mainly affected by the gradual increase of TP and casein contents, which were also found in our study. The P content increased slightly during lactation; the differences between the first and last months of lactation were significant ($P < 0.05$; Table 3). This is consistent with the trends reported by Kuchtík et al. (2017) and Panayotov et al. (2018) for the milk of Lacaune and Awassi breed ewes (Sahan et al., 2005). Contrary results have been found in ewe milk of the Dorset breed, where a decrease in P content during lactation was recorded (Wohlt et al., 1981).

A significant ($P < 0.001$) positive correlation was found between the lactation month and both Mg and Na contents ($r = 0.770$ and $r = 0.569$ respectively) and a negative correlation with K ($r = –0.329$), whilst Sahan et al. (2005) found significant changes only in the Na content and no significant changes in either the K or Mg contents during lactation. The mean Na content of ewe milk was higher in mid-lactation milk (Table 3). As the Na content in the milk increased, there was a decrease in the K content. A similar trend was observed elsewhere (Wohlt et al., 1981; Sahan et al., 2005). The highest average Na content and the lowest average K content were found in the fifth months of lactation.

A PCA assessment was carried out for all of the evaluated lactation months and 13 variables, which qualify milk composition. Individual traits showed high variability in the composition of milk according to the month of lactation. However, when individual components were averaged and visualized in a bi-plot (Fig. 1), lactation months can be differentiated according to the concentration of milk components.

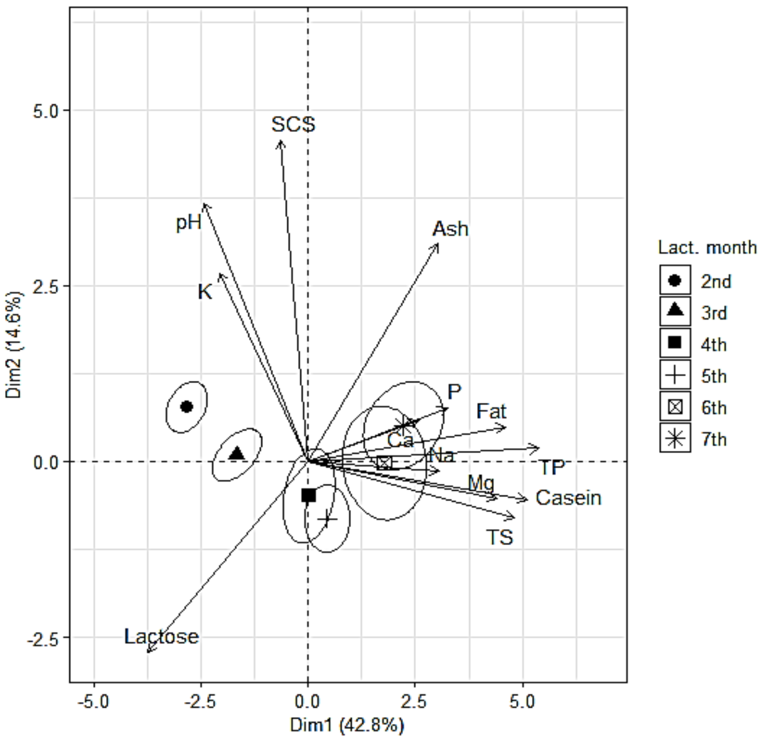

Figure 1. Bi-plot of principal component analysis with month of lactation (2^{nd}–7^{th}) and milk components in Lacaune ewes (TP – total protein; TS – total solids; SCS – somatic cell score; Dim 1 and 2 – principal components).

As the result of the PCA, six evaluated lactation months showed that 42.8% of the total variability was attributed to the first principal component (PC). The variables related to the mineral content of the milk (except K) as well as fat, casein and TP all contribute to PC1 with higher values. The PC2 aggregated 14.6% of the total variance and was related to SCS and also to pH and K. Together these two PC-s can explain over half (57.4%) of the variance.

From the location of the lactation months in Fig. 1, it can be concluded that some lactation months differ from the others, especially the second and third ones. The bi-plot reveals that the fat, casein, TP and mineral content of the milk (except K) increases throughout the lactation months. This can be explained by the changes in the milk yield within the lactation period. The milk yield was not recorded currently, but numerous studies have shown that the lactation curve of ewes is highest at the beginning of lactation, and then starts to decrease steadily (Ruiz et al., 2000; Oravcová et al., 2006; Komprej et al., 2012; Elvira et al., 2013; Inostroza et al., 2020; Robles Jimenez et al. 2020). However, according to the PC2, higher milk pH value, SCS and K were registered on the second month of lactation. In the comparison of the lactation months, the PCA showed that milk composition is quite similar on the fourth and fifth lactation months and as well as on the sixth and seventh months.

CONCLUSIONS

Lacaune ewes' milk in Estonia contained high levels of total solids, including fat, protein, casein and minerals (ash). The most variable milk traits were Na, K, SCS, Mg and fat contents and the least variable were pH value, ash and lactose contents and the casein index. The lactation stage significantly affected almost all of the measured milk traits, except for the casein index, SCS and Ca content. TS, fat, TP, casein, ash, P, and Mg contents increased, while the lactose content, and pH values decreased with advancing lactation. The mean values for K were higher and for Na lower at the beginning and at the end of lactation. Principal component analysis showed that there were small differences in the milk compositional characteristics between the fourth and fifth and between the sixth and seventh months of lactation.

Higher TS content, including the casein content, requires a higher yield of the cheese and an improvement in the structural properties of the fermented beverages in the second half of the lactation period. However, the content of Ca and P, which affects the coagulation properties of milk, remained stable or increased slightly within the lactation months. Therefore, an analysis of the coagulation properties of ewe milk during lactation would be necessary. Our results suggest that it would be possible to differentiate milk according to the lactation stage to harvest milk with key-traits for certain products.

ACKNOWLEDGEMENTS. The authors thank Viinamärdi sheep farm and its owners for supporting our sampling and recording activities.

REFERENCES

Abilleira, E., Virto, M., Najera, A.I., Salmeron, J., Albisu, M., Perez-Elortondo, F.J., Ruiz de Gordoa, J.C., de Renobales, M. & Barron, J.R. 2010. Effects of seasonal changes in feeding management under part-time grazing on the evolution of the composition and coagulation properties of raw milk from ewes. *Journal of Dairy Science* **93**, 3902–3909.

Albenzio, M., Caroprese, M., Santillo, A., Marino, R., Taibi, L. & Sevi, A. 2004. Effects of Somatic Cell Count and Stage of Lactation on the Plasmin Activity and Cheese-Making Properties of Ewe Milk. *J. Dairy Sci*. **87**, 533–542.

Aldalur, A., Bustamante, M.A. & Barron, L.J.R. 2019. Effects of technological settings on yield, curd, whey, and cheese composition during the cheese-making process from raw sheep milk in small rural dairies: Emphasis on cutting and cooking conditions. *J. Dairy Sci.* **102**, 7813–7825.

Ali, A.K.A. & Shook, G.E. 1980. An optimum transformation for somatic cell concentration in milk. *J. Dairy Sci.* **63**, 487−490.

Balthazar, C.F., Pimentel, T.C., Ferrao, L.L., Almada, C.N., Santillo, A., Albenzio, M., Mollakhalili, N., Mortazavian, A.M., Nascimento, J.S., Silva, M.C., Freitas, M.Q., Sant´Ana, A.S., Granato, D. & Cruz, A.G. 2017. Sheep Milk: Physicochemical Characteristics and Relevance for Functional Food Development. *Comprehensive Reviews in Food Science and Food Safety* **16**, 247–262.

Barillet, F., Rupp, R., Mignon-Grasteau, S., Astruc, J. & Jacquin, M. 2001. Genetic analysis for mastitis resistance and milk somatic cell score in French Lacaune dairy sheep. *Genet. Sel. Evol.* **33**, 397–415.

Barłowska, J., Szwajkowska, M., Litwi´nczuk, Z. & Krol, J. 2011. Nutritional Value and Technological Suitability of Milk from Various Animal Species Used for Dairy Production. *Comprehensive Reviews in Food Science and Food Safety* **10**, 291–302. doi: 10.1111/j.1541-4337.2011.00163.x

Bittante, G., Cipolat-Gotet, C., Pazzola, M., Dettori, M.L., Vacca, G.M. & Cecchinato, A. 2017. Genetic analysis of coagulation properties, curd firming modeling, milk yield, composition, and acidity in Sarda dairy sheep. *J. Dairy Sci.* **100**, 385–394. doi: 10.3168/jds.2016-11212

Buccioni, A., Pauselli, M., Viti, C., Minieri, S., Pallara, G., Roscini, V., Rapaccini, S., Trabalza Marinucci, M., Lupi, P., Conte, G. & Mele, M. 2015. Milk fatty acid composition, rumen microbial population, and animal performances in response to diets rich in linoleic acid supplemented with chestnut or quebracho tannins in dairy ewes. *J. Dairy Sci.* **98**, 1145–56. doi: 10.3168/jds.2014-8651

Chia, J., Burrov, K., Carne, A., McConnell, M., Samuelsson, L., Day, L., Young, W. & Bekhit, A.E.A. 2017. Minerals in Sheep Milk. *Nutrients in Dairy and their Implications on Health and Disease* 345−362. doi: 10.1016/B978-0-12-809762-5.00027-9

Elvira, L., Hernandez, F., Cuesta, P., Cano, S., Gonzalez-Martin, J.-V. & Astiz, S. 2013. Accurate mathematical models to describe the lactation curve of Lacaune dairy sheep under intensive management. *Animal* **7**(6), 1044–1052. doi: 10.1017/S175173111200239X

Fava, L.W., Külkamp-Guerreiro, I.C. & Pinto, A.T. 2014. Evaluation of physico-chemical characteristics of fresh, refrigerated and frozen Lacaune ewes' milk. *Arq. Bras. Med. Vet. Zootec.* **66**(6), 1924–1930.

Giambra, I.J., Brandt, H. & Erhardt, G. 2014. Milk protein variants are highly associated with milk performance traits in East Friesian Dairy and Lacaune sheep. *Small Ruminant Research* **121**, 382–394. doi.org/10.1016/j.smallrumres.2014.09.001

Hanuš, O., Tomáška, M., Hofericová, M., Vyletělova-Klimešová, M., Klapáčová, L., Jedelská, R. & Kološta, M. 2015. Relationship between freezing point and raw ewes' milk components as a possible tool for estimation of milk adulteration with added water. *Journal of Food and Nutrition Research* **54**, 281–288.

Harrell, F.E.Jr. & Dupont, C. 2021. Hmisc: Harrell Miscellaneous 4.6–0. https://hbiostat.org/R/Hmisc/ (accessed on 28.04.2021).

Hejtmánková, A., Pivec, V., Trnková, E. & Dragounová, H. 2012. Differences in the composition of total and whey proteins in goat and ewe milk and their changes throughout the lactation period. *Czech J. Anim. Sci.* **57**(7), 323–331.

Inostroza, K., Bravo, S., Larama, G., Saenz, C. & Sepúlveda, N. 2020. Variation in Milk Composition and Fatty Acid Profile during the Lactation of Araucana Creole Ewes in a Pasture-Based System. *Animals* **10**, 92. doi: 10.3390/ani10010092

Kaminarides, S. & Anifantakis, E. 2004. Characteristics of set type yoghurt made from caprine or ovine milk and mixtures of the two. *International Journal of Food Science and Technology* **39**, 319–324.

Kassambara, A. & Mundt, F. 2020. factoextra: Extract and Visualize the Results of Multivariate Data Analyses 1.0.7. http://www.sthda.com/english/rpkgs/factoextra (accessed on 28.04.2021).

Komprej, A., Gorjanc, G., Kompan, D. & Kovač, M. 2012. Lactation curves for milk yield, fat, and protein content in Slovenian dairy sheep. *Czech J. Anim. Sci.* **57**(5), 231–239.

Kuchtík, J., Konečná, L., Sýkora, V., Šustová, K., Fajman, M. & Kos, I. 2017. Changes of physico-chemical characteristics, somatic cell count and curd quality during lactation and their relationships in Lacaune ewes. *Mljekarstvo* **67**(2), 138–145. doi: 10.15567/mljekarstvo.2017.0206

Matutinovic, S., Kalit, S., Salajpal, K. & Vrdoljak, J. 2011. Effects of flock, year and season on the quality of milk from an indigenous breed in the sub-Mediterranean area. *Small Ruminant Research* **100**, 159–163. doi: 10.1016/j.smallrumres.2011.06.009

Merlin Junior, I.A., Sifuentes dos Santos, J., Grecco Costa, L., Grecco Costa, R., Ludovico, A., Cristine de Almeida Rego, F. & Walter de Santana, E.H. 2015. Sheep milk: physical-chemical characteristics and microbiological quality. *ARCHIVOS LATINOAMERICANOS DE NUTRICIÓN* **65**(3), 193–198.

Milani, F.X. & Wendorff, W.L. 2011. Goat and sheep milk products in the United States (USA). *Small Ruminant Research* **101**, 134–139. doi: 10.1016/j.smallrumres.2011.09.033

Moatsou, G., Samolada, M., Katsabeki, A. & Anifantakis, E. 2004. Casein fraction of ovine milk from indigenous Greek breeds. *Lait* **84**, 285–296. doi: 10.1051/lait:2004006

Oravcová, M., Margetín, M., Peškovičová, D., Daňo, J., Milerski, M., Hetényi, L. & Polák, P. 2006. Factors affecting milk yield and ewe's lactation curves estimated with test-day models. *Czech Journal of Animal Science* **51**, 483–490. doi: 10.17221/3968-CJAS

Othmane, M.H., Carriedo, J.A., De La Fuente, L.F. & Primitivo, F.S. 2002. Factors affecting test-day milk composition in dairy ewes, and relationships amongst various milk components. *Journal of Dairy Research* **69**, 53–62. doi: 10.1017/S0022029901005234

Panayotov, D., Naydenova, N., Mihaylova, G. & Iliev, T. 2018. Physico-chemical and technological characteristics of Lacaune ewe´s milk. *Bulgarian Journal of Agricultural Science* **24**(1), 101–108.

Park, Y.W., Juarez, M., Ramos, M. & Haenlein, G.F.W. 2007. Physico-chemical characteristics of goat and sheep milk. *Small Ruminant Research* **68**, 88–113.

Paschino, P., Vacca, G.M, Dettori, M.L. & Pazzola, M. 2019. An approach for the estimation of somatic cells' effect in Sarda sheep milk based on the analysis of milk traits and coagulation properties. *Small Ruminant Research* **171**, 77–81.

Pavić, V., Antunac, N., Mioč, B., Ivanković, A. & Havranek, J.L. 2002. Influence of stage of lactation on the chemical composition and physical properties of sheep milk. *Czech J. Anim. Sci.* **47**(2), 80–84.

Pellegrini, O., Remeuf, F., Rivemale, M. & Barillet, F. 1997. Renneting properties of milk from individual ewes: influence of genetic and non-genetic variables, and relationship with physicochemical characteristics. *Journal of Dairy Research* **64**, 355–366. doi:org/10.1017/S0022029997002203

Pesantez-Pacheco, J.-L., Torres-Rovira, L., Hernandez, F., Sanz-Fernandez, M.V., Villalobos, N.P., Heras-Molina, A., Garcia-Contreras, C., Vazquez-Gomez, M., Martinez-Ros, P., Gonzalez-Martin, J.V., Gonzalez-Bulnes, A. & Astiz, S. 2018. Efficiency and demographics of a high-yield dairy ewe farm with two managing systems involving five or 10 lambings per year. *Animal* **12**(10), 2181–2190. doi: 10.1017/S175173111700369X

Pulina, G., Macciotta, N. & Nudda, A. 2005. *Review article:* Milk composition and feeding in the Italian dairy sheep. *Italian Journal of Animal Science* **4**(1), 5–14. doi.org/10.4081/ijas.2005.1s.5

Pulina, G., Milán, M.J., Lavín, M.P., Theodoridis, A., Morin, E., Capote, J., Thomas, D.L., Francesconi, A.H.D. & Caja, G. 2017. *Invited review article:* Current production trends, farm structures, and economics of the dairy sheep and goat sectors. *J. Dairy Sci.* **101**, 6715−6729. doi.org/10.3168/jds.2017-14015

R Core Team (2021). R: A language and environment for statistical computing. R Foundation for Statistical Computing, Vienna, Austria. 2019. https://www.r-project.org/ (accessed on 28.04.2021).

Robles Jimenez, L.E., Angeles Hernandez, J.C., Palacios, C., Abecia, J.A., Naranjo, A., Osorio Avalos, J. & Gonzalez-Ronquillo, M. 2020. Milk Production of Lacaune Sheep with Different Degrees of Crossing with Manchega Sheep in a Commercial Flock in Spain. *Animals (Basel)* **10**(3), 520. doi.org/10.3390/ani10030520

Rovai, M., Caja, G., Quevedo, J.M., Manuelian, C.L., Saldo, J., Salama, A.A.K., Torre, P., Arana, I., Such, X. & Leitner, G. 2015. Effect of subclinical intramammary infection on milk quality in dairy sheep: II. Matured-pressed cheese (Manchego) produced from milk of uninfected and infected glands and from their blends. *Small Ruminant Research* **126**, 59–67. doi.org/10.1016/j.smallrumres.2015.03.002

Ruiz, R., Oregui, L.M. & Herrero, M. 2000. Comparison of Models for Describing the Lactation Curve of Latxa Sheep and an Analysis of Factors Affecting Milk Yield. *Journal of Dairy Science* **83(**11), 2709–2719. doi: 10.3168/jds.S0022-0302(00)75165-4

Sahan, N., Say, D. & Kacar, A. 2005. Changes in Chemical and Mineral Contents of Awassi Ewes' Milk During Lactation. *Turk. J. Vet. Anim Sci.* **29**, 589–593.

Sevi, A., Albenzio, M., Marino, R., Santillo, A. & Muscio, A. 2004. Effects of lambing season and stage of lactation on ewe milk quality. *Small Ruminant Research* **51**, 251–259. doi:10.1016/S0921-4488(03)00196-2

Termatzidou, S., Siachos, N., Kazana, P., Sotiraki, S., Saratsi, K., Achard, D., Karembe, H., Bramis, G., Kanoulas, V. & Arsenos, G. 2020. Effect of injectable eprinomectin on milk quality and yield of dairy ewes naturally infected with gastrointestinal nematodes. *Veterinary Parasitology* **286**, 109245.

Wohlt, J.E., Kleyn, D.H., Vandernoot, G.W., Selfridge, D.J. & Novotney, C.A. 1981. Effect of Stage of Lactation, Age of Ewe, Sibling Status, and Sex of Lamb on Gross and Minor Constituents of Dorset Ewe Milk. *J. Dairy Sci.* **64**, 2175–2184.

Agronomy Research **20**(2), 437–447, 2022
https://doi.org/10.15159/AR.22.025

The effect of adding carrot or beetroot powders on the quality indicators of round cracknel products

A.V. Tikhiy[1,*], N.V. Barakova[1] and E.A. Samodelkin[2]

[1]ITMO University, Faculty of Biotechnology (BioTech), 9 Lomonosov Str., RU191002 St. Petersburg, Russia
[2]Research Institution Research Center 'Kurchatov Institute'- Central Research Institute for Engineering Materials Prometheu, 49 Shpalernaya Sr., RU191015 St. Petersburg, Russia
[*]Correspondence: antontikhiy@yandex.ru

Received: February 1st, 2022; Accepted: April 5th, 2022; Published: April 28th, 2022

Abstract. The relationship between carrot/beetroot powders added, the quantity and quality of gluten in the flour and the moisture, acidity, swelling coefficient and the quality indicators of round cracknel products has been studied. The carrot and beetroot powders, produced by Vitbiokor, LLC, and the premium wheat flour were used. The powders were introduced in a dry and hydrated form. The hydration was carried out at the hydromodule of 1:5 for 40 minutes. The particle size analysis of raw materials was conducted with the laser diffraction analyzer Malvern Mastersizer 2000. The proportion of particles of less than 200 µm in the flour made 100%, in the carrot powder - 77%, in the beetroot powder - 71%. The introduction of carrot/beetroot powders in the amount of 1.5%, 3.0%, 6.0% and 9.0% by weight of the flour reduces the amount of gluten. Still, it strengthens the latter, making it possible to mold products with developed porosity. The introduction of dry carrot powder in the amount of 6% into the sourdough and the dough (1.5%, 3.0%, 6.0% and 9.0%) increases the swelling coefficient of the end products by an average of 15%, while the introduction of the hydrated powder does it by 40%. Similarly, the introduction of the dry beetroot powder leads, on average, to a 12% increase and of the hydrated powder to a 22% increase. The obtained results proved the effectiveness of introducing carrot/beetroot powders (preference given to their hydrated types) into the recipe of round cracknel products.

Key words: round cracknel products, carrot and beetroot powders, the quantity and quality of gluten, swelling coefficient.

INTRODUCTION

The consumption of functional and healthy food is growing in a modern person's diet (Mollakhalili-Meybodi et al., 2021; Amani & Aljahani, 2022). Due to the ability to benefit human health, there has recently been an increase in functional foods production. Functional foods are foods fortified with compounds providing additional health and safety benefits, e.g. vitamins, minerals, and bioactive compounds (Balakrishnaraja et al., 2021; Zarzycki et al., 2022). A high amount of the required components is contained in the vegetable powders. Therefore, such mass consumption foods as bakery products are enriched (Gryazyina et al., 2016; Nevskaya et al., 2020).

Among the range of goods produced by the baking industry, a special place is occupied by round cracknel products. Round cracknel products belong to the low humidity products with a moisture content of no more than 19% (GOST 32124, 2013). They are products with a longer shelf life (25 or more days) than bread (3–5 days), making them very attractive for consumers. Moreover, the round cracknel products retain their original properties throughout the entire shelf life.

The important indicator of the round cracknels' quality is their swelling coefficient. The swelling coefficient, i.e. hydrophilicity of bagels is the ability to swell and soften in warm water without destroying the structure. To make this happen, water must penetrate as much as possible through the crust of the product, fill the internal space and be retained in it. Therefore, the appropriate product structure must be created: a sufficiently large number of pores with thin, but at the same time strong walls, evenly distributed over the entire inner surface of the product (Shirokova & Veselova, 2016).

The formation of the product structure occurs during the dough preparation process. It involves the following ingredients: flour (which contains natural high-molecular compounds with a large number of functional groups), yeast-microorganisms (which are natural leavening agents of the dough emitting carbon dioxide, which forms the porous structure of the product), and water (which dissolves high-molecular flour compounds and participates in complex physico-chemical and colloidal processes when making bakery products).

At the initial stage of the dough preparation, it is necessary to arrange the homogeneity of the mass. Its formation depends on the dispersion degree of the ingredients added to the flour. The difference between the particle size of the ingredient and the degree of flour dispersion should be as minor as possible (Karama et al., 2016; Taniguchi et al., 2022). When mixing the dough, it is important to wet the flour and the ingredients included in its composition, i.e. vegetable powders. To increase the water absorption properties of the flour, vegetable powders should have good moisture binding capacity (Rudnev et al., 2021).

During the dough preparation, the interaction of flour components (carbohydrates and proteins) with water forms the gluten quality. For the round cracknels production, flour with strong gluten is needed.

The sourdough is also involved in the formation of the qualitative properties of gluten. Its quantity regulates the strength of gluten (Akhmetzhanova & Savkina, 2017).

If the flour with poor gluten is used, the amount of sourdough added should be increased. The yeast used in the preparation should have a high fermentation activity, i.e. release as much carbon dioxide as possible with less flour added. The vegetable powder components contain the necessary nutrients stimulating the yeast biochemical system.

The speed of the fermentation process at these stages depends on the readiness of the powder components for the interaction with the yeast, i.e., the degree of solubility or the ability to dissolve quickly. It is possible to increase the degree of solubility of these components by the pretreatment of the powders, such as hydration. Hydration provides the process of swelling of the powder components. Water penetrates the high-molecular components of plant materials while maintaining powder integrity. A part of the water molecule binds by absorption to macromolecular substances of the powder while a part of the molecules penetrates the internal structure of the swelling substance due to diffusion (Douglass & Harrowell, 2018; Drake et al., 2018). As a result, there is a significant increase in the powder volume.

As a result, some of the low-molecular components of the swelling substance can go into a dissolved state, affecting the process of powder components penetration into the yeast cell and the entire fermentation process (Allert & Adshevskaya, 2017; Koryachkina et al., 2018).

Osmotically bounded water is water bound with ions, which forms hydration shells around the charged particles and water associated with the well-dissolved low molecular weight compounds (Murashov, 2013). After interacting with the osmotic water, the end round cracknels must not fall apart. This requirement is ensured by the state of the colloidal system and the quality of flour gluten: it should be elastic but strong enough.

One more important indicator of the bakery products' quality is acidity because it shows the readiness of the fermented semi-finished product, i.e. sourdough or dough. The dough is loosened with carbon dioxide. During the fermentation period, there is an accumulation of products determining the taste and aroma of bakery products made from the well-fermented dough.

The previous studies have shown that the formed organic acids or the additionally introduced ones contribute to the swelling of gluten proteins, affecting the physical and colloidal properties of the dough (Gatko, 2004).

Promising vegetable raw materials with several advantages are dry carrot and beetroot powders (Hobbs et al., 2014; Zubkova & Zakharov, 2016). The advantage of these powders is that they are made from the vegetables that are widely grown in all regions of the world, relatively cheap, rich in vitamins C, B1, B2, B5, B6, PP, E, folic acid, provitamin A, and also include a high content of colouring substances, e.g. betaine, betanin, beta-carotene (Dombrovskaya et al., 2017; Kapoor & Feng 2022).

This study aims to investigate the effect of carrot and beetroot powders on the quality of gluten, evaluate the prospects of carrying out carrot and beetroot powders hydration, and estimate their effect on the swelling acidity of round cracknels.

MATERIALS AND METHODS

The dry carrot and beetroot powders produced by Vitbiokor, LLC (the Republic of Belarus) were used for the experiment. The chemical composition is presented in Table 1 (Godunov, 2021).

Moreover, the following ingredients were used: premium wheat flour *Predportovaya* (Saint Petersburg Mill Plant, JSC), pressed bakery yeast (Combinat Food Products, JSC), refined deodorized sunflower oil (MEZYugRusi, LLC), common salt (Araltuz, JSC), and granulated sugar (Prodimeks, LLC).

Table 1. The chemical composition of raw materials

Nutrient	Sample name	
	Carrot powder	Beetroot powder
Protein, %	10.0	9.9
Fats, %	0.8	0.7
Carbohydrates, %	55.2	59.8

The particle size distribution of raw materials has been analyzed with the help of the laser diffraction analyzer *Malvern Mastersizer 2000.*

The amount of gluten in flour was determined according to GOST 27839-2013 standard. The raw gluten was extracted from the dough produced with pure wheat to flour and from that made of wheat flour with carrot and beetroot powders added in the ratio of 1.5%, 3.0%, 6.0%, 9.0% by weight of flour and water (Table 2).

Table 2. Dough recipe for calculating the amount of gluten

Raw material	Sample type				
	Control sample	1.5%	3.0%	6.0%	9.0%
Premium wheat flour, g	30.00	29.55	29.1	28.20	27.30
Drinking water, g	17.00	17.05	17.08	17.16	17.25
Dry carrot/beetroot powder, g	0	0.45	0.90	1.80	2.70
TOTAL, g	47.00	47.05	47.08	47.16	47.25

The prepared dough samples were washed with the gluten washing machine (*U1-MOK-1MT)*. Water-soluble substances, as well as starch and bran, were removed from the dough. The raw gluten washed out was weighed and calculated as a proportion of the total mass of the sample analyzed.

The quality of gluten was determined with the gluten deformation measuring device (*IDK-3M*). To determine the value of resistance to compressive load deformation, the raw gluten was formed into a ball of 120 g. The measuring process took 30 seconds.

For preparing the round cracknel products, the sponge-and-dough method was used. The sourdough recipe is shown in Table 3. The amount of dry or hydrated carrot or beetroot powder introduced made up 6% of the flour weight based on previous research findings (Tikhiy et al., 2021). Powders were hydrated at a ratio of 1:5 powder to water, at the water temperature of 30 °C, for 40 min. The thick sourdough with a moisture content of about 40% was prepared.

The amount of water introduced into the sponge was adjusted according to the moisture-binding ability of the powders (Koryachkina et al., 2015) and the amount of water used for hydration (if hydrated powders were introduced).

Table 3. Sourdough recipe with powders added and with no powders added

Raw material	Sample type		
	No powders	With dry powders	With hydrated powders
Premium wheat flour, g	50.0	50.0	50.0
Pressed yeast, g	1.25	1.25	1.25
Drinking water, g	25.0	26.45	26.45
Dry carrot/beetroot powder, g	0	3.0	0
Hydrated carrot/beetroot powder, g	0	0	3.0
TOTAL, g	76.25	80.70	80.70

A KitchenAid 5KSM175PSECA mixer mixed the sourdough for 2 minutes at the first speed rate and 1 minute at the second speed rate. The fermentation process took 120 min. After it, the dough was mixed. The dough recipe is shown in Table 4.

The amount of water added to the dough was adjusted according to the moisture-binding ability of the powders and the amount of water used for hydration (if hydrated powders were introduced) so that the humidity was 32.5%.

The dough was mixed on a *KitchenAid 5KSM175PSECA* mixer at the first speed rate for 3 minutes and 1 minute at the second speed rate. After it, it was held for 10 min and divided into 43 g blanks. Then, they were rounded and molded into round cracknels.

Table 4. The round cracknels recipe

Raw material	Sample type				
	Control sample	1.5%	3%	6%	9%
Premium wheat flour, g	200.0				
Sunflower oil, g	20.0				
Salt, g	3.75				
Sugar, g	22.5				
Sourdough, g	76.25	80.7	80.7	80.7	80.7
Dry carrot/beetroot powder*, g	0.00	0.75	4.50	12.00	19.50
Drinking water, g	85.00	85.20	86.90	90.10	92.10
TOTAL, g	407.50	412.90	418.35	429.05	438.55

*When mixing the dough and the dry powder, the dry powder was added to the dough. When mixing the dough with the addition of the hydrated powder, the hydrated powder was added to the dough.

The products were baked at a temperature of 214 °C for 11 minutes. At the end of baking, the products were cooled to a temperature of 23 °C. After that, the physical and chemical properties of the end products were analyzed. During the experiment, the proofing time for all samples was 55 min.

The sourdough acidity was calculated by dissolving 5 g of the sample and then potentiometric titration with the standardized sodium hydroxide (NaOH) to pH 8.0. Acidity was determined using the titration method, and the results were presented in degrees according to GOST 5670 (1996); the pH was measured with a pH meter *Testo 206-pH1* (Kobus-Cisowska et al., 2020).

To determine the acidity of the end products, 10 g of crumb and 100 cm^3 of distilled water at a temperature of 18–25 °C were placed in a volumetric flask of 250 cm^3. Subsequently, the sample was shaken to reach homogeneity and allowed to settle for 15 min. 25 cm^3 of the filtrate were extracted and exposed to potentiometric titration with the standardized solution of sodium hydroxide (NaOH) to pH 8.0 (GOST 5670, 1996).

The moisture of the sourdough, the dough, and the end products was determined by drying test portions at 160 °C for 5 min and calculating the percent of the weight difference between the original sample and the dry one (GOST 21094, 1975).

The swelling coefficient of the end products was determined by comparing the weights of dry pieces of the product (2 cm long) to the weights of the swollen parts, which had been held in a water bath for 5 minutes, at a water temperature of 60 °C (GOST 32124, 2013).

In the study, conventional research methods were used. All the values were reported as mean ± SD. All treatments and analyses were performed in triplicate for each sample. The statistical processing of the obtained results was carried out by conventional methods (assessing the significance according to Fisher's and Student's criteria) using the *Microsoft Excel* software package.

RESULTS AND DISCUSSION

The particle size of powders and flour affects the quality and mode of dough preparation and the biochemical and colloidal processes occurring when the powders and the flour are interacting with the water (Qin et al., 2021).

The results of the particle size distribution analysis for flour and carrot/beetroot powders are presented in Table 5.

The beetroot powder has a more acceptable particle size than the carrot powder. As shown in the table, 100% premium flour particle size range from 0 µm to 200 µm. 77% of the carrot powder particles and 71% of beetroot powder particles range from 0 µm to 200 µm (the same diapason), comparable to the flour particle size.

Table 5. The particle size distribution analysis of the premium wheat flour and carrot/beetroot powders

Particle size, µm	Percentage of particles in the grind, %		
	Flour	Carrot	Beetroot
0–50	41.85	39.20	45.89
50–100	27.86	19.32	21.97
100–200	30.29	18.96	3.33
200–500	-	6.67	-
500–1,000	-	8.21	-
1,000–2,000	-	7.64	28.81

To study the impact of the powders on the structural and mechanical properties of the dough, their effect on the quantity and quality changes of gluten was determined.

The flour samples without and with dry powders of carrots or beetroots added in 1.5%, 3.0%, 6.0% and 9.0% were prepared (Table 6).

As shown in the table, when dry carrot powder is added to the flour in an amount of 1.5%, 3.0%, 6.0% and 9.0%, the gluten content decreases from 31.3% to 30.2%; 29.1%; 28.8%; 27.5% respectively, and when adding beetroot powder in the same amount - from 31.3% to 30.6%; 29.7%; 29.0%; 28.3% respectively.

Table 6. Indicators of the quantity and quality of gluten in samples with and without powders

Indicator	Sample type								
	No powder	Carrot powder				Beetroot powder			
		1.5%	3.0%	6.0%	9.0%	1.5%	3.0%	6.0%	9.0%
Dry gluten quantity, %	31.30	30.21	29.12	28.83	27.52	30.63	29.75	29.02	28.34
Gluten quality, units	68.73 ± 0.48	59.80 ± 0.54	58.50 ± 0.40	58.00 ± 0.52	55.35 ± 0.54	66.90 ± 0.51	60.00 ± 0.53	55.30 ± 0.46	50.05 ± 0.54

The partial replacement of the premium wheat flour with the carrot and beetroot powders caused a decrease in the total gluten content of the test samples.

The change in the gluten elastic properties was measured with the gluten deformation measuring device and expressed in units (gluten quality units). When carrot powder is added to the flour in an amount of 1.5%, 3.0%, 6.0% and 9.0%, the quality of gluten, and its deformation, measured with the gluten deformation measuring device, decreases from 68.7 to 55.3 units. When the same amount of beetroot powder is added to the flour, the gluten deformation index decreases from 68.7 down to 50.0 units, depending on the amount of powder added.

The decrease in the deformation index increases the elastic properties of gluten and indicates its strengthening according to GOST R 54478 (2011), which is crucial to the formation of product porosity. Due to carbon dioxide released during the fermentation, gluten is stretched, and the structure and porosity are formed. In the technology of round cracknels preparation, the fermentation process occurs when preparing the dough and during the after fermentation process while proofing. The influence of vegetable powders on the fermentation of sourdough was estimated by the change in acidity (Table 7).

Table 7. Physical and chemical properties of the sourdough with and without powders added

Indicator	Sample type				
	No powder	Carrot powder		Beetroot powder	
		dry	hydrated	dry	hydrated
Moisture, %	35.82 ± 0.46	36.21 ± 0.55	35.92 ± 0.48	36.34 ± 0.42	35.90 ± 0.51
Acidity, deg.	3.80 ± 0.11	4.00 ± 0.12	4.20 ± 0.10	4.00 ± 0.11	4.20 ± 0.10

The change in the dough acidity when introducing the dry powders is insignificant and is within the margin of error. The dough acidity changed by 0.2 deg when submitting to the hydrated powders. In powder hydration, some components pass into a dissolved state. It explains the increase in the rate of nutrient entry into the yeast cell, the activation of the vital activity of yeast and, as a result, the increase in the amount of organic acids produced by the yeast cell.

The dough was mixed according to the recipe (Table 4). The effect of vegetable powders on the dough fermentation process was estimated by the change in the acidity of the end dough (Tables 8 and 9).

Table 8. Physical and chemical properties of the dough with and without carrot powder added

Indicator	Sample type								
	Control sample	Carrot powder							
		Dry				Hydrated			
		1.5%	3.0%	6.0%	9.0%	1.5%	3.0%	6.0%	9.0%
Moisture, %	32.51 ± 0.51	32.71 ± 0.54	32.84 ± 0.49	33.12 ± 0.50	33.21 ± 0.51	32.42 ± 0.53	32.54 ± 0.51	32.71 ± 0.50	32.91 ± 0.54
Acidity, deg.	2.80 ± 0.10	3.00 ± 0.11	3.00 ± 0.10	3.20 ± 0.12	3.20 ± 0.11	2.80 ± 0.11	3.00 ± 0.10	3.20 ± 0.11	3.20 ± 0.11

After the mixture process, the dough with carrot and beetroot powders added was smooth and elastic, with no under mixing.

Table 9. Physical and chemical properties of the dough with and without beetroot powder added

Indicator	Sample type								
	Control sample	Beetroot powder							
		Dry				Hydrated			
		1.5%	3.0%	6.0%	9.0%	1.5%	3.0%	6.0%	9.0%
Moisture, %	32.51 ± 0.51	32.52 ± 0.50	32.72 ± 0.51	33.01 ± 0.52	33.13 ± 0.51	32.46 ± 0.54	32.65 ± 0.51	32.80 ± 0.53	32.91 ± 0.50
Acidity, deg	2.80 ± 0.10	3.00 ± 0.10	3.20 ± 0.12	3.20 ± 0.11	3.40 ± 0.11	3.00 ± 0.10	3.20 ± 0.12	3.20 ± 0.10	3.40 ± 0.11

The results presented in Tables 8 and 9 showed increased acidity when the dry and the hydrated powders were used. In the sample with no powders added, the acidity is 2.8 deg. With the introduction of the powders, the acidity increases to an average of 3.0–3.2 deg.

The organic acids added to the carrot and beetroot powders caused the increase in dough acidity. Moreover, the fermentation process occurs during the proofing. The microelements, which are parts of the powders (including organic acids), cause the vital activity of the yeast, leading to an increase in the new organic acids formation (Garzon et al., 2021). Acidity is determined at the end of the proofing process. Therefore, a faster increase in acidity causes a reduction in the technological operation time. Moreover, the rise in dough acidity leads to an increase in organoleptic characteristics of the end products.

The fermentation process activation when adding the vegetable powders leads to an increase in dough acidity and a change in the dough structure and its porosity (Yano et al., 2017). The addition of pectin and dietary fiber to the vegetable powders affects the interaction processes of finished products with water, their wettability and swelling. There will be a decrease in the amount of carbohydrates and flour proteins, which affects the colloidal system of the dough and the end products. Porosity, wettability and the state of the colloidal system affect swelling, an essential indicator for round cracknel products.

The acidity and the swelling coefficient of the end round cracknels are presented in Tables 10 and 11.

Table 10. Physical and chemical properties of the end products with and without carrot powder added

Indicator	Sample name								
	No powder	Carrot powder							
		Dry				Hydrated			
		1.5%	3.0%	6.0%	9.0%	1.5%	3.0%	6.0%	9.0%
Moisture, %	20.10 ± 0.50	19.71 ± 0.53	20.45 ± 0.51	20.37 ± 0.54	20.70 ± 0.51	19.74 ± 0.51	19.85 ± 0.52	19.97 ± 0.50	19.71 ± 0.51
Acidity, deg	2.60 ± 0.10	2.80 ± 0.11	2.80 ± 0.12	3.00 ± 0.12	3.00 ± 0.11	2.60 ± 0.10	2.80 ± 0.11	3.00 ± 0.10	3.00 ± 0.12
Swelling coefficient	4.12 ± 0.11	5.78 ± 0.12	5.52 ± 0.14	5.44 ± 0.12	4.65 ± 0.16	6.76 ± 0.11	6.15 ± 0.14	5.14 ± 0.12	4.86 ± 0.11

Table 11. Physical and chemical properties of the end products with and without beetroot powder added

Indicator	Sample name								
	No powder	Beetroot powder							
		Dry				Hydrated			
		1.5%	3.0%	6.0%	9.0%	1.5%	3.0%	6.0%	9.0%
Moisture, %	20.10 ± 0.50	20.75 ± 0.5	20.54 ± 0.5	20.87 ± 0.5	20.62 ± 0.5	20.28 ± 0.5	19.83 ± 0.5	19.94 ± 0.5	19.84 ± 0.5
Acidity, deg	2.60 ± 0.10	3.00 ± 0.11	2.80 ± 0.10	3.00 ± 0.12	3.00 ± 0.10	2.60 ± 0.10	2.80 ± 0.12	3.00 ± 0.11	3.00 ± 0.1
Swelling coefficient	4.12 ± 0.11	4.84 ± 0.13	4.77 ± 0.14	4.4 ± 0.12	4.12 ± 0.1	5.53 ± 0.15	4.84 ± 0.12	4.62 ± 0.11	4.15 ± 0.13

The results presented in Tables 10 and 11 show that the dry carrot powder added in an amount of 1.5% increases the swelling coefficient of the end product from 4.1 to 5.7. When the hydrated powder is added, it increases from 4.1 to 6.7. The increase in the swelling coefficient after adding the hydrated powder can be explained by an increase in the yeast fermentation activity (the data on increased acidity are presented in Table 7, Table 8 and Table 9). Therefore, by the amount of carbon dioxide released, the formation of a more porous structure of the product and the swelling coefficient increase. The difference between the swelling coefficient in the end products when dry and hydrated carrot powders are added remains even with an increase in the powder application dose. But with an increase in the powder application dose, this difference will decrease, which is explained by a decrease in the amount of carbohydrates and proteins introduced with the flour, which affects the colloidal system of the product and, as a result, the swelling.

The tendency remains when the dry and the hydrated beetroot powders are added to the sourdough and the dough. Still, the difference between the swelling coefficient increase and the addition of the hydrated beetroot powder is less than with the hydrated carrot powder added. The introduction of dry carrot powder leads to an increase in the swelling coefficient of the end products by an average of 15%. In comparison, introducing the hydrated carrot powder in the same amount into the sourdough and the dough increases the swelling coefficient by 40%. The introduction of the dry beetroot powder leads to an increase in the swelling coefficient of the end products by an average of 12%. In comparison, introducing the hydrated beetroot powder in the same amount in the sourdough and the dough increases the swelling coefficient by 22%. This is due to the different chemical compositions of the carrot and beetroot powders and the different amounts of polar and non-polar substances.

CONCLUSIONS

The results obtained in this study prove the effectiveness of introducing vegetable powders, particularly carrot and beetroot ones, into the recipe of round cracknel products. The introduction of powders increased the quality indicators of the end products, i.e. acidity and swelling. The introduction of powders in a dry and prehydrated form, particularly into the sourdough and the dough, increased the quality of gluten and its elasticity, making it possible to increase the swelling of the round cracknels. The study has demonstrated the positive effect of the preliminary hydration of dry carrot and beetroot powders before adding them to the sourdough and the dough in round cracknels production. Thus, according to the results, further research is needed to study the feasibility of pre-hydration of the powders obtained from the other types of vegetable crops and provide evidence of the effectiveness of including hydrated vegetable powders in various bakery products.

REFERENCES

Akhmetzhanova, A.T. & Savkina, O.A. 2017. The influence of starter cultures on the quality of bread made from wheat flour with strong gluten. *Almanac of scientific works of young scientists of ITMO University*, 22–25 (in Russian).

Allert, A.A. &Alshevskaya, M.N. 2017.Scientific substantiation of using vegetable masses of beetroot, carrot, parsley in bakery products technology. *KSTU News*. **45**, 125–135 (in Russian).

Amani, H. Aljahani. 2022. Wheat-yellow pumpkin composite flour: Physico-functional, rheological, antioxidant potential and quality properties of pan and flat bread. *Saudi Journal of Biological Sciences* **29**(5), 3432–3439.

Balakrishnaraja, R., Swetha, V., Srivigneswar, S., Sakthi Priyaa, S.S. &Gowrishankar, L. 2021. Formulation and development of functionally enriched onion (*Allium cepa*) bread *Materials Today: Proceedings* **47**(9), 1835–1841.

Dombrovskaya, Ya.P., Aralova, S.I., Tekutieva, Y.A. & Denisova, A.A. 2017. Prospects of use of nonconventional vegetable raw materials to improve the biological value of flour culinary products.*Food industry* **7**, 19–21 (in Russian).

Douglass, I. & Harrowell, P. 2018. Kinetics of Dissolution of an Amorphous Solid. *J. Phys Chem B*, **122**(8), 2425–2433. doi: 10.1021/acs.jpcb.7b12243

Drake, A.C., Lee, Y., Burgess, E.M., Karlsson, J.O.M., Eroglu, A. & Higgins, A.Z. 2018. Effect of water content on the glass transition temperatureof mixtures of sugars, polymers, and penetrating cryoprotectants in physiological buffer, *PLoS One*. **13**(1).

Garzon, R., Skendi, A., Lazo-Velez, M.A., Papageorgiou, M. & Rosell, C.M. 2021. Interaction of dough acidity and microalga level on bread quality and antioxidant properties, *Food Chemistry*, **344**.

Gatko, N.N. 2004. The impact of additives on the quality of bakery products. *Proceedings of universities: Food technology* **5(**6), 37–39 (in Russian).

Godunov, O.A. 2021. *Improving the technology of obtaining polydisperse vegetable* powders *from vegetables and their use to increase the nutritional value of bakery products*. PhD Thesis, Moscow State University of Food Production, Moscow, Russia, 135 pp. (in Russian).

GOST 32124. 2013. 'Ring-shaped rolls. General specifications'. Federal Technical Regulation and Metrology Agency, Russian Federation.

GOST 27839. 2013. 'Wheat flour. Methods of determination quantity and quality of gluten'. Federal Technical Regulation and Metrology Agency, Russian Federation.

GOST R 54478. 2011. 'Grain. Methods for determination of quantity and quality of gluten in wheat'. Technical committee for standardization, Russian Federation.

GOST 5670. 1996. 'Bread, rolls and buns. Methods for determination of acidity'. Gosstandart of Russia, Russian Federation.

GOST 21094. 1975. 'Bread and bakery products. Method for the determination of moisture'. USSR Ministry of Food Industry, USSR.

Gryazyin, F.I., Danilova, O.A. & Emelyanova, T.N. 2016. Use of natural supplements in technology of bakery products of low humidity. *Vestnik of the Mari State University. Chapter 'Agriculture.Economics'* **2**(6), 15–19 (in Russian).

Hobbs, D.A., Ashouri, A., George, T.W., Lovegrove, J.A. & Methven, L. 2014. The consumer acceptance of novel vegetable-enriched bread products as a potential vehicle to increase vegetable consumption, *Food Research International* **58**, 15–22.

Kapoor, R. & Feng, H. 2022. Characterization of physicochemical, packing and microstructural properties of beet, blueberry, carrot and cranberry powders: the effect of drying methods, *Powder Technology* **395**, 290–300.

Karama, M.C., Petit, J., Zimmera, D., Djantoub, E.B. & Schera, J. 2016. Effects of drying and grinding in production of fruit and vegetable powders: A review. *Journal of Food Engineering* **188**, 32–49.

Kobus-Cisowska, J., Szymanowska-Powałowska, D., Szymandera-Buszka, K., Rezler, R., Jarzębski, M., Szczepaniak, O., Marciniak, G., Jędrusek-Golińska, A. & Kobus-Moryson, M. 2020. Effect of fortification with calcium from eggshells on bioavailability, quality, and rheological characteristics of traditional Polish bread spread. *Journal of Dairy Science* **103**(8), 6918–6929.

Koryachkina, S.Ya. 2015. The use of finely dispersed vegetable and fruit powders in pasta production. *Modern Science and Innovation* **1**, 57–62 (in Russian).

Koryachkina, S.Ya., Ladnova, O.L., Lobok, I.S. & Mikaelyan, A.V. 2018. Justification of functional bakery products creation using a mixture of pumpkin and carrot powders. *Bread products*, 60–62.

Murashov, S.V. 2013. Osmotically bound water. *Scientific Journal of National Research ITMO University: Processes and Food Production Equipment*, **4** (in Russian).

Mollakhalili-Meybodi, N., Arab, M., Nematollahi, A. & Khaneghah, A.M. 2021. Prebiotic wheat bread: Technological, sensorial and nutritional perspectives and challenges. *LWT*, **149**.

Nevskaya, E.V., Zueva, A.G. & Belyaev, A.G. 2020. Extract and powder of EpilobiumAngustifolium in bakery products. *Food processing: Techniques and Technology* **50(**1), 61–69 (in Russian).

Qin, W., Lin, Z., Wang, A., Chen, Z., He, Y., Wang, L., Liu, L., Wang, F. & Tong, L.T. 2021. Influence of particle size on the properties of rice flour and quality of gluten-free rice bread. *LWT*, **151**.

Rudnev, S.D, Shevchenko, T.V., Ustinova, Yu.V., Kruk, R.V., Ivanov, V.V. & Chistyakov, A.M. 2021.Technological features and theoretical justification for the use of mechanically activated water in the production of flour products. *Food processing: Techniques and Technology* **51(**4), 768–778 (in Russian).

Shirokova, L.O. & Veselova, A.Yu. 2016. Formation of structural and mechanical properties of donut products at certain stages of the technological process. *Khleboproducty* **3**, 56–57 (in Russian).

Taniguchi, A., Miura, M., Ikeda, M.T., Kaneko, S. & Kobayashi, R. 2022. Factors affecting rheological properties of barley flour-derived batter and dough examined from particle properties. *Food hydrocolloids*. doi: 10.1016/j.foodhyd.2022.107645

Tikhiy, A.V., Barakova, N.V. & Sergacheva, E.S. 2021.Expansion of the range of round cracknel recipes. *SEWAN conference proceedings*, 341–342 (in Russian).

Yano, H., Fukui, A., Kajiwara, K., Kobayashi, I., Yoza, K., Satake, A. & Villeneuve, M. 2017. Development of gluten-free rice bread: Pickering stabilization as a possible batter-swelling mechanism. LWT.*Food Science and Technology* **79**, 632–639.

Zarzycki, P., Wirkijowska, A., Nawrocka, A., Kozłowicz, K., Krajewska, M., Kłosok, K. & Krawęcka, A. 2022. Effect of Moldavian dragonhead seed residue on the baking properties of wheat flour and bread quality. *LWT*, **155**.

Zubkova, T.V. & Zakharov, V.L. 2016.The use of finely dispersed carrot and pumpkin powders in baking technology. *Bulletin of Michurinsk State Agricultural University***1**, 84–89 (in Russian).

Agronomy Research **20**(2), 448–456, 2022
https://doi.org/10.15159/AR.22.032

Risk factors for honey bee (*Apis mellifera* L.) mortality in Estonian apiaries during 2012–2013

L. Tummeleht*, T. Orro and A. Viltrop

Estonian University of Life Sciences, Institute of Veterinary Medicine and Animal Sciences, Friedrich Reinhold Kreutzwaldi 62, EE51006 Tartu, Estonia
*Correspondence: lea.tummeleht@emu.ee; https://orcid.org/0000-0002-6478-7047

Received: January 4th, 2022; Accepted: May 11th, 2022; Published: May 19th, 2022

Abstract. In light of the global increase in honey bee colony losses, risk factors regarding beekeeping management practices and honey bee diseases have been studied intensively during the last decade. Some risk factors have been outlined, but the correlation of evidence between relevant factors coinciding with honey bee mortality still needs to be clarified. The current study used the two-year data collected in frames of the European Commission EPILOBEE project. Previously, the data from Estonian apiaries were analysed together with the data from all 17 participating European countries in the consortium. In the current study, data from Estonian apiaries were targeted separately. In total, 196 apiaries containing 2,439 colonies all over Estonia were included in this dataset. The study aimed to clarify the risk factors that would predict colony losses in Estonia. The main factors increasing colony mortality after winter were the size of the apiary, *Varroa destructor* mite count, infestation with *Paenibacillus larvae,* and lack of farmlands around the apiary. No significant risk factors in relation to honey bee summer mortality were detected.

Key words: American foulbrood, Beekeeping management practices, EPILOBEE, honey bee breeds, *Varroa destructor.*

INTRODUCTION

Beekeeping in Estonia is important and widespread but operated rather in small-scale establishments. Estonia is situated in the northern temperate zone that is characterized by the cold winters and summers that tend to have brief warm period. In temperate climates, weather conditions during winter can put substantial pressure on honey bee colony survival (Switanek et al., 2017; Brodschneider et al., 2019). Again, weather conditions during summer can influence the winter survival of honey bees, as shown in a recent study conducted in the northeastern United States (Calovi et al., 2021). Consequently, high colony losses can also occur during the summer following noticeable losses in the winter (Jacques et al., 2017).

However, the climatic conditions *per se* are not responsible for honey bee survival. The mortality of managed honey bee colonies has been explained by a multicausal aetiology. Variable interactions between the causal agents contribute to the presence of honey bee pathogens, chemical pollution, pesticides and factors related to housing, beekeeping management practices, and the environment surrounding apiaries (Dennis vanEngelsdorp & Meixner, 2010; Clermont et al., 2015; Goulson et al., 2015; Wilfert et al., 2016; Switanek et al., 2017; Bird et al., 2021; El Agrebi et al., 2021). In addition, honey bees should have managed to accumulate an adequate amount of food reserves for surviving the winter (Döke et al., 2015; Lemanski et al., 2020). Honey bee colony losses in Europe exhibit fluctuating patterns depending on the year and several other factors (Jacques et al., 2017; Buendia et al., 2018; Gray et al., 2019; Gray et al., 2020).

The factor often contributing to honey bee survival is the size of the apiary, which reflects the type of beekeeping operation (hobby or commercial) and experience of the beekeepers (Jacques et al., 2017). Most studies find the highest mortality rates in small apiaries operated by hobby beekeepers (Chauzat et al., 2016; Gray et al., 2019).

Although honey bee mortality can vary depending on the year, beekeeping management practices, and the combination of stressors, the most strongly contributing factors are probably pathogens such as varroa mites (*Varroa destructor*) together with associated viruses and the microsporidians *Nosema* spp. (D. vanEngelsdorp et al., 2009; Dennis vanEngelsdorp & Meixner, 2010; Jacques et al., 2017; Thaduri et al., 2019).

Varroa mites not only burden bees mechanically by feeding on their brood and adult honey bees' haemolymph and fat body tissue (Ramsey et al., 2019) but are also effective vectors for many bee viruses, such as deformed wing virus (Wilfert et al., 2016). Nearly 100% of Estonian apiaries are infested with varroa mites (Mõtus et al., 2016).

The current study aimed to analyse risk factors for winter and summer mortality. The data were collected in framesof the pan-European epidemiological project on active surveillance of honey bee colony losses (EPILOBEE 2012–2014) coordinated by the EU Reference Laboratory for Honey Bee Health.

The EPILOBEE project included data from 17 European countries, with overwinter losses from 2% to 32%. Estonia, along with Finland, Latvia, and Sweden, was clustered according to its honey bee mortality rates. It was found to have upper-middle mortality rates in 2012 and 2013. In 2012, Poland was included in the same cluster; Portugal and Denmark were included in 2013 (Jacques et al., 2017). Although the data from Estonian apiaries were analysed within the consolidated dataset, we suspected that the local trends might be overshadowed. In addition, there has been no other broad-based epidemiological study before or after that in Estonian apiaries. Therefore, in this current paper, we only examined the specifics of Estonian colony losses.

MATERIALS AND METHODS

Study population

The used data were collected in frames of a pan-European EPILOBEE project, 2012–2014. The detailed epidemiological study design was described by Chauzat et al. (2016) and Jacques et al. (Jacques et al., 2017).

In total, 196 apiaries containing 2439 colonies throughout Estonia were randomly selected from the beekeeper register managed by The Agricultural Registers and Information Board of Estonia (EARIB). In 2012 the total number of registered apiaries in Estonia was 8,488 (EARIB database, 2012). Within each apiary, the sample size calculator assigned a random and representative number of colonies. The number of honey bee colonies in the selected apiaries ranged from 1 to 170 (median 14; 75% quartile 19). The Estonian Veterinary and Food Board carried out a sampling of the apiaries during three visits: the first visit in September 2012 (before winter), the second visit in April 2013 (after winter), and the third visit in July 2013, in the middle of the beekeeping season. The sample to detect infectious diseases and parasites consisted of adult honey bees collected from randomly selected colonies within the apiary. Every visit was accompanied by a questionnaire described in detail in the study by (Mõtus et al., 2016).

The colonies sampled for this study were used to estimate the mortality in every apiary. Mortality was calculated as the proportion of colonies the beekeepers reported as lost from all the sampled colonies in an apiary due to any reason excluding predation (brown bear, rodents, woodpecker, etc.). Apiaries were grouped according to the quartiles of the number of colonies in apiary.

Data analysis

To identify factors associated with honey bee winter mortality, a Tobit regression model was used. Winter mortality within apiary (% of colonies lost) was used as a response variable. Tobit regression was used because 35% of apiaries did not have honey bee winter mortality (0%). In the Tobit regression, all cases falling above (or below) a specified threshold value are censored, although these cases remain in the analysis (Tobin, 1958). The outcome variable (winter mortality %) was transformed logarithmically to achieve a normal distribution of variable. The winter mortality minimum was 3% loss of the colonies, maximum was 100%. Univariable analyses were performed, and variables with a P-value < 0.2 were included in the full model. For categorical variables with more than two levels, the Wald test P-value was used. The possible confounding effect of the size of the apiary (categorized into four groups according to quartiles) was individually assessed for every independent variable in separate models. The full model included the size of the apiary, the presence of American foulbrood (yes/no), the average count of varroa mites (categorized into 4 groups according to quartiles), farmlands around the apiary (yes/no), town near the apiary (yes/no), orchards near the apiary (yes/no), type of beekeeping (hobby, part-time or professional), the beekeeper's experience, which was defined by the number of years in beekeeping business, and the bee breed (Buckfast, Carnica, hybrid, Ligustica, and the race Dark European Honey Bee). Backwards stepwise elimination of the variables was used for the final model. Possible interactions and confounders (change of the coefficient over 15% after variable elimination) were controlled.

To identify factors associated with honey bee summer mortality (minimum was 3% loss of the colonies, maximum 50%), a logistic regression model was used. Honey bee summer mortality, as either present (15% of apiaries) or not, was used as a response variable. Model building strategies were the same as in the honey bee winter mortality model (univariable models with apiary size included, followed by backwards stepwise elimination from the full model). The initial full model included four variables: the size of the apiary, farmland around the apiary, town near the apiary, and the average count of varroa mites.

The statistical program STATA 14.2 (StataCorp LP, College Station, TX, USA) was used for the described Tobit regression and logistic regression models.

RESULTS AND DISCUSSION

Winter mortality

The results of the regression analysis to test associations between honey bee winter mortality and the investigated risk factors are presented in Table 1. There was a significant positive association between the size (number of colonies) of the apiary and honey bee winter mortality ($P = 0.001$). The relationship became stronger with the increasing number of colonies in the apiary (Table 1). The group of the largest apiaries contained apiaries with 20–65 colonies but also had one outlier - an apiary with 170 colonies. Removing the outlier from the model did not change the result, so we still consider the results valid (Fig. 1). When included in the consortium, the results of the data analysis of 17 European countries previously reported by Jacques et al. (2017) showed the opposite result as the small hobby beekeepers had a mortality risks twice as high as professional beekeepers. This result could be explained by a lack of experience and professionalism by hobby beekeepers harbouring a smaller number of colonies. The same dataset for all the participants from the first study year showed a negative relationship between winter mortality and apiary size (Chauzat et al., 2016). Like the EPILOBEE consortium study, the four-year survey of beekeepers in China showed that commercial beekeepers operating larger apiaries tended to have a lower rate of colony losses than did hobby beekeepers. However, there was a significant year effect as the mortality trends in different sizes of beekeeping operations in a certain year were not always consistent with the overall trend (Tang et al., 2020). Additionally, a COLOSS survey involving data from 2017–2018 from 36 countries reported significantly higher losses in small apiaries up to 50 colonies (Gray et al., 2020). A study in Austria showed no connection between apiary size and colony losses (Morawetz et al., 2019).

The varroa mite count in colonies significantly affected honey bee winter mortality according to the Tobit regression model, where varroa mite-infected honey bee colonies were grouped using the quartiles of the data ($P < 0.001$). The association became stronger when the average count of varroa mites increased (Table 1).

Guzmán-Novoa et al. (2010) studied the effect of parasite levels, the strength of the colony, and the food reserves on winter mortality in Canada. They found that varroa mite burden could be the main factor explaining the death and reduced populations of honey bee colonies in northern climates.

In case varroa mite infestation is controlled, weather conditions, particularly high temperatures in summer and precipitation in the past year, were the strongest predictors of overwintering survival, as shown in the north-eastern United States while using European honey bee colonies in the study (Calovi et al., 2021). The data on Switzerland's honey bee population support the idea that *V. destructor* is a keyplayer in colony losses, interacting in combination with other pathogens and the effect of the particular year (Dainat et al., 2012).

Apparently, honey bees have also become more sensitive to varroa parasites as evidenced by changes in the *Varroa* infestation rate causing colony loss since 1980, as discussed elsewhere (vanEngelsdorp & Meixner, 2010). VanEngelsdorp & Meixner (2010) reported that a honey bee colony could withstand a couple of thousand mites; currently, 10% infestation indicates imminent colony loss.

Table 1. Results of the Tobit regression model to test associations between honey bee winter mortality (ln percentage) and various parameters of the apiary. The total sample size was 186 apiaries. In the model, 68 of the observations were left-censored (winter mortality 0%) and 118 were uncensored observations (winter mortality 3.2–100%). Apiaries were grouped by quartiles of number of colonies in apiary and the average count of varroa mites per colony data

Variable (n = number of apiaries)	Coefficient (SE)	95% confidence interval (CI)	P-value	Wald test P-value
Size of the apiary				0.001
1–7 colonies (43)	0			
8–13 colonies (48)	1.39 (0.47)	0.46; 2.32	**0.003**	
14–19 colonies (47)	1.14 (0.47)	0.22; 2.07	**0.016**	
≥ 20 colonies (48)	1.95 (0.48)	0.99; 2.91	**< 0.001**	
Average count of varroa mites				< 0.001
0–1.09 (47)	0			
1.1–2.99 (45)	1.26 (0.46)	0.36; 2.16	**0.007**	
3.0–8.19 (50)	1.06 (0.45)	0.17; 1.95	**0.019**	
≥ 8.2 (44)	2.15 (0.47)	1.22; 3.07	**< 0.001**	
American foulbrood				
negative (175)	0			
positive (11)	1.67 (0.64)	0.40; 2.95	**0.010**	
Farmlands around the apiary				
no (22)	0			
yes (164)	-1.02 (0.47)	-1.95; -0.09	**0.032**	
Honey bee breed or race				0.142*
Buckfast (20)	0			
Carnica (54)	-0.90 (0.54)	-1.96; 0.16	0.094	
Hybrid (48)	-0.76 (0.56)	-1.88; 0.35	0.176	
Ligustica (46)	-1.14 (0.55)	-2.23; -0.05	**0.041**	
Dark European honey bee (18)	-1.73 (0.72)	-3.15; -0.31	**0.017**	
Constant	0.94 (0.75)	-0.53; 2.42	0.210	

* Variable retained in model as confounder.

Winter mortality of honey bee colonies was significantly higher in colonies infected with American foulbrood (P = 0.010) (Fig. 2). American foulbrood, caused by gram+ bacteria *Paenibacillus larvae,* is widespread globally and often results in colony death even in light of sufficient knowledge about this dangerous bee pathogen (Forsgren et al., 2018; Bulson et al., 2021). Lindstrom et al. (Lindstrom et al., 2008) showed that the *P. larvae* spore load in adult honey bee samples was significantly linked to larval mortality in a study conducted in Southern Finland. American foulbrood along with *Nosema* spp. and varroa mite infections were the leading causes of mortality in an Algerian study on seasonal mortality of the cultured honey bee *Apis mellifera intermissa* (Adjlane & Haddad, 2018).

Assessed winter mortality was lower in apiaries located near farmlands (rapeseed, grain, legumes, or grasslands) (P = 0.032). It is usually assumed that honey bees are supported by the natural environment around apiaries. Our data reveal the opposite, winter mortality of honey bees was lower when there were farmlands surrounding the apiary.

A statistically significant negative relationship between honey bee breed and winter mortality was found for the honey bees breed Ligustica ($P = 0.041$) and Dark European honey bee ($P = 0.017$) in the model, whereas the overall association between the honey bee breed and winter mortality was not statistically significant ($P = 0.142$).

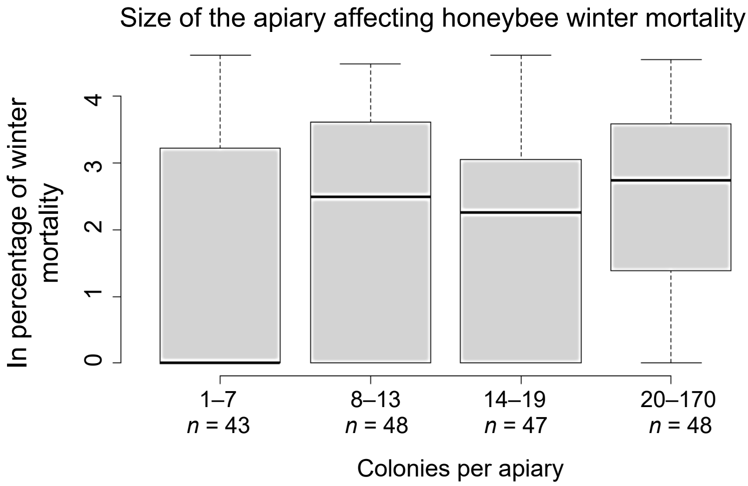

Figure 1. The apiaries were grouped according to the quartiles of the number of colonies in apiary. The last group contains the outlier of apiaries with 170 colonies. Removing the outlier did not change the results, so it was included in the analysis.

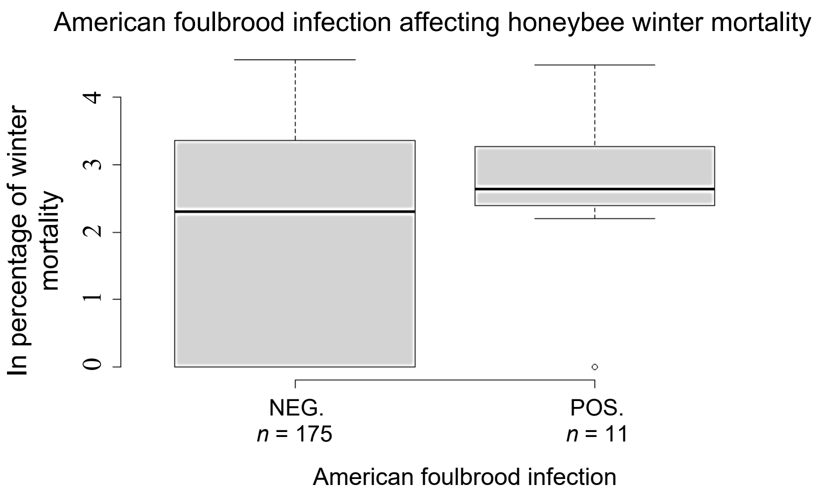

Figure 2. American foulbrood infection significantly increased honey bee winter mortality ($P = 0.010$).

Summer mortality

The summer mortality of honey bees was not affected by the size of the apiary ($P = 0.274$) in the multivariate logistic regression model, where crop production around the apiary showed a trend ($P = 0.078$) in reducing summer mortality. However, there was a positive trend in the association between summer mortality and large apiaries harbouring over 20 colonies (P = 0.056) (Table 2).

Table 2. Results of the multivariate logistic regression model to test associations between honey bee summer mortality, apiary size, and crop production around the apiary (n = 193)

Variable (number of apiaries)	OR	95% confidence interval (CI)	P-value	Wald test P-value
Size of the apiary				0.274*
1–7 colonies (49)				
8–13 colonies (49)	1.89	0.51; 7.01	0.339	
14–19 colonies (48)	1.61	0.42; 6.18	0.485	
20–170 colonies (50)	3.32	0.97; 11.42	0.056	
Farmlands around the apiary				
No (23)				
Yes (173)	0.39	0.14; 1.11	0.078	

* Variable retained in model as confounder.

The lack of accordance with consolidated data and overall trends can be explained by the rather modest size of apiaries in general in Estonia (median value of 13.5 colonies per apiary). Nevertheless, our honey bee summer mortality was also not affected by varroa mites. Additionally, the summer mortality tended to be lower in apiaries located near farmlands. This may be an indication that farmlands better support the nutritional needs of honey bees compared to other landscapes and that the previously proven harmful effects of insecticides and pesticides used on farmlands did not have chronic effects on honey bee survival in Estonia. Since no causal relationships were studied, we cannot provide any other speculation for this result.

CONCLUSIONS

The results of this study shed light on the potential risk factors that increase mortality in Estonian apiaries. Honey bee winter mortality was significantly affected by the size of the apiary. Whereby there was only a positive trend in the association between summer mortality and large apiaries harbouring over 20 colonies. Parasitic mite *Varroa destructor* and American foulbrood caused by bacteria *Paenibacillus larvae* significantly affected the honey bee winter mortality. In contrast to the common view that honey bee health is supported by natural environments, there was lower winter mortality detected when there were farmlands around the apiaries. Similarly, the summer mortality tended to be lower in apiaries located near farmlands.

In conclusion, there were more risk factors affecting honey bee winter mortality than summer mortality in 2012–2013. However, the number of apiaries affected by summer mortality in our study was low, meaning that the power of our study was not high enough to be able to identify the significant risk factors. Most probably, the effect of the conditions of the particular year was playing a role.

Studies approaching beekeeping management practices and risk factors for honey bee health in Estonia are rather scarce. Further studies giving us longitudinal data on this field are needed.

ACKNOWLEDGEMENTS. This work was supported by the European Commission and the EU Reference Laboratory EPILOBEE project (2012–2014) and by funding from the Estonian Research Council project no L190001VLVB (RITA1/02-10-10 "Opportunities for mitigation of bee losses (2019−2021)). The authors are grateful to the specialists in Estonian Agriculture and Food Board for data collection and management, to the technicians in Estonian Veterinary and Food Laboratory for laboratory analysis and to the project coordinators in EU reference laboratory for honey bee health for designing and organizing the work of EPILOBEE project.

REFERENCES

Adjlane, N. & Haddad, N. 2018. Effect of Some Honeybee Diseases on Seasonal Mortality of Apis mellifera intermissa in Algeria Apiaries. [Article]. *Proceedings of the Zoological Society* **71**(1), 83–87. doi: 10.1007/s12595-016-0188-5

Bird, G., Wilson, A.E., Williams, G.R. & Hardy, N.B. 2021. Parasites and pesticides act antagonistically on honey bee health. [https://doi.org/10.1111/1365-2664.13811]. *Journal of Applied Ecology* **58**(5), 997–1005. doi: https://doi.org/10.1111/1365-2664.13811

Brodschneider, R., Brus, J. & Danihlík, J. 2019. Comparison of apiculture and winter mortality of honey bee colonies (Apis mellifera) in Austria and Czechia. *Agriculture, Ecosystems & Environment* **274**, 24–32. doi: https://doi.org/10.1016/j.agee.2019.01.002

Buendia, M., Martin-Hernandez, R., Ornosa, C., Barrios, L., Bartolome, C. & Higes, M. 2018. Epidemiological study of honeybee pathogens in Europe: The results of Castilla-La Mancha (Spain). *Spanish Journal of Agricultural Research* **16**(2). doi: 10.5424/sjar/2018162-11474

Bulson, L., Becher, M.A., McKinley, T.J. & Wilfert, L. 2021. Long-term effects of antibiotic treatments on honeybee colony fitness: A modelling approach. *Journal of Applied Ecology* **58**(1), 70–79. doi: https://doi.org/10.1111/1365-2664.13786

Calovi, M., Grozinger, C.M., Miller, D.A. & Goslee, S.C. 2021. Summer weather conditions influence winter survival of honey bees (Apis mellifera) in the northeastern United States. *Scientific Reports* **11**(1), 1553. doi: 10.1038/s41598-021-81051-8

Chauzat, M.-P., Jacques, A., consortium, E., Laurent, M., Bougeard, S., Hendrikx, P. & Ribiere-Chabert, M. 2016. Risk indicators affecting honeybee colony survival in Europe : one year of surveillance. *Apidologie* **47**, 348–378 doi: doi.org/10.1007/s13592-016-0440-z

Clermont, A., Eickermann, M., Kraus, F., Hoffmann, L. & Beyer, M. 2015. Correlations between land covers and honey bee colony losses in a country with industrialized and rural regions. *Science of The Total Environment* **532**, 1–13. doi: https://doi.org/10.1016/j.scitotenv.2015.05.128

Dainat, B., Evans, J.D., Chen, Y.P., Gauthier, L. & Neumann, P. 2012. Predictive Markers of Honey Bee Colony Collapse. *Plos One* **7**(2). doi: 10.1371/journal.pone.0032151

Döke, M.A., Frazier, M. & Grozinger, C.M. 2015. Overwintering honey bees: biology and management. [Review]. *Current Opinion in Insect Science* **10**, 185–193. doi: 10.1016/j.cois.2015.05.014

El Agrebi, N., Steinhauer, N., Tosi, S., Leinartz, L., de Graaf, D.C. & Saegerman, C. 2021. Risk and protective indicators of beekeeping management practices. *Science of The Total Environment* **799**, 149381. doi: https://doi.org/10.1016/j.scitotenv.2021.149381

Forsgren, E., Locke, B., Sircoulomb, F. & Schäfer, M.O. 2018. Bacterial Diseases in Honeybees. *Current Clinical Microbiology Reports* **5**(1), 18–25. doi: 10.1007/s40588-018-0083-0

Goulson, D., Nicholls, E., Botías, C. & Rotheray, E.L. 2015. Bee declines driven by combined stress from parasites, pesticides, and lack of flowers. **347**(6229), 1255957. doi: 10.1126/science.1255957 %J Science

Gray, A., Brodschneider, R., Adjlane, N., Ballis, A., Brusbardis, V., Charrière, J.-D., … & Soroker, V. 2019. Loss rates of honey bee colonies during winter 2017/18 in 36 countries participating in the COLOSS survey, including effects of forage sources. *Journal of Apicultural Research* **58**(4), 479–485. doi: 10.1080/00218839.2019.1615661

Gray, A., Noureddine, A., Arab, A., Ballis, A., Brusbardis, V., Charrière, J.-D., … & Uzunov, A. 2020. Honey bee colony winter loss rates for 35 countries participating in the COLOSS survey for winter 2018–2019, and the effects of a new queen on the risk of colony winter loss. *Journal of Apicultural Research*. doi: 10.1080/00218839.2020.1797272

Guzmán-Novoa, E., Eccles, L., Calvete, Y., McGowan, J., Kelly, P.G. & Correa-Benítez, A. 2010. *Varroa destructor* is the main culprit for the death and reduced populations of overwintered honey bee (*Apis mellifera*) colonies in Ontario, Canada. *Apidologie,* **41** 443–450.

Jacques, A., Laurent, M., Ribière-Chabert, M., Saussac, M., Bougeard, S., Budge, G., Hendrikx, P. & Chauzat, M.-P. 2017. A pan-European epidemiological study reveals honey bee colony survival depends on beekeeper education and disease control. *PLoS ONE* **12**. doi: doi.org/10.1371/journal.pone.0172591

Lemanski, N.J., Bansal, S. & Fefferman, N.H. 2020. The sensitivity of a honeybee colony to worker mortality depends on season and resource availability. *BMC Evolutionary Biology* **20**(1), 139. doi: 10.1186/s12862-020-01706-4

Lindstrom, A., Korpela, S. & Fries, I. 2008. Horizontal transmission of Paenibacillus larvae spores between honey bee (Apis mellifera) colonies through robbing. *Apidologie* **39**(5), 515–522. doi: 10.1051/apido:2008032

Morawetz, L., Köglberger, H., Griesbacher, A., Derakhshifar, I., Crailsheim, K., Brodschneider, R. & Moosbeckhofer, R. 2019. Health status of honey bee colonies (Apis mellifera) and disease-related risk factors for colony losses in Austria. *PLOS ONE* **14**(7), e0219293. doi: 10.1371/journal.pone.0219293

Mõtus, K., Raie, A., Orro, T., Chauzat, M.P. & Viltrop, A. 2016. Epidemiology, risk factors and varroa mite control in the Estonian honey bee population. *Journal of Apicultural Research* **55**(5), 396–412. doi: 10.1080/00218839.2016.1251081

Ramsey, S.D., Ochoa, R., Bauchan, G., Gulbronson, C., Mowery, J.D., Cohen, A., Lim, D., Joklik, J., Cicero, J.M., Ellis, J.D., Hawthorne, D. & vanEngelsdorp, D. 2019. *Varroa destructor* feeds primarily on honey bee fat body tissue and not hemolymph. *Proc Natl Acad Sci U S A.* Jan 29, **116**(5), 1792–1801. doi: 10.1073/pnas.1818371116. Epub 2019 Jan 15. PMID: 30647116; PMCID: PMC6358713.

Switanek, M., Crailsheim, K., Truhetz, H. & Brodschneider, R. 2017. Modelling seasonal effects of temperature and precipitation on honey bee winter mortality in a temperate climate. *Science of The Total Environment* **579**, 1581–1587. https://doi.org/10.1016/j.scitotenv.2016.11.178

Tang, J., Ma, C., Shi, W., Chen, X., Liu, Z., Wang, H. & Chen, C. 2020. A National Survey of Managed Honey Bee Colony Winter Losses (Apis mellifera) in China (2013–2017). *Diversity* **12**(9), 318. https://doi.org/10.3390/d12090318

Thaduri, S., Stephan, J.G., de Miranda, J.R. & Locke, B. 2019. Disentangling host-parasite-pathogen interactions in a varroa-resistant honeybee population reveals virus tolerance as an independent, naturally adapted survival mechanism. *Scientific Reports* **9**. doi: 10.1038/s41598-019-42741-6

Tobin, J. 1958. Estimation of Relationships for Limited Dependent Variables. *Econometrica* **26**(1), 24–36. doi: 10.2307/1907382

vanEngelsdorp, D., Evans, J.D., Saegerman, C., Mullin, C., Haubruge, E., Nguyen, B.K., … & Pettis, J.S. 2009. Colony Collapse Disorder: A Descriptive Study. *Plos One* **4**(8). doi: 10.1371/journal.pone.0006481

vanEngelsdorp, D. & Meixner, M.D. 2010. A historical review of managed honey bee populations in Europe and the United States and the factors that may affect them. *Journal of Invertebrate Pathology* **103**, S80–S95. doi: https://doi.org/10.1016/j.jip.2009.06.011

Wilfert, L., Long, G., Leggett, H.C., Schmid-Hempel, P., Butlin, R., Martin, S.J.M. & Boots, M. 2016. Deformed wing virus is a recent global epidemic in honeybees driven by Varroa mites. *Science* **351**(6273), 594–597. doi: 10.1126/science.aac9976

Agronomy Research **20**(2), 457–468, 2022
https://doi.org/10.15159/AR.22.017

Evaluation of the honey bee colonies weight gain during the intensive foraging period

A. Zacepins[1,*], N. Ozols[2], A. Kviesis[1], J. Gailis[2], V. Komasilovs[1], O. Komasilova[1] and V. Zagorska[2]

[1]Department of Computer Systems, Faculty of Information Technologies, Latvia University of Life Sciences and Technologies, Liela iela 2, LV-3001 Jelgava, Latvia
[2]Institute of Plant Protection Research 'Agrihorts', Latvia University of Life Sciences and Technologies, Paula Lejina iela 2, LV-3004 Jelgava, Latvia
[*]Correspondence: aleksejs.zacepins@llu.lv

Received: March 5th, 2022; Accepted: April 1st, 2022; Published: April 13rd, 2022

Abstract. Beekeeping in Latvia has a long tradition and it is a classical branch of agriculture. In Latvia, there is no traditional beekeeping region, and beekeeping is performed in all regions. Honey yield is influenced by various factors - variety of crops (nectar plants) around the apiary, man-made changes in land/forests (deforestation), climate change, beekeepers' actions, etc. Application of information and communication technologies (ICT) in the field of beekeeping can bring benefits to the beekeepers. To be more specific, continuous remote monitoring of certain bee colony parameters can improve beekeeper's apiary management, by informing timely about the nectar flow (or even provide information on bee colony states, e.g., swarming). In such a way, beekeepers can plan their next actions - prepare supers or even choose to move the apiary to a different geographical location. Within this research, weight gain of the ten honey bee colonies was remotely monitored and analysed during two-week period at the beginning of the summer 2021 in Vecauce, Latvia, using the precision beekeeping approach. This monitoring period corresponded to intensive flowering of the winter rapeseed and field beans. Colonies were equipped with the automatic scales. In addition, colony and environmental temperature was monitored. Measurements were taken every thirty minutes. Analysing the obtained data, weight increase can be observed in all colonies, from 17 to 48 kg. As well, based on weight data, swarming event can be identified. Constant monitoring of weight change can also help to identify daily patterns in honey bee activity.

Key words: precision beekeeping, weight monitoring, foraging activity, honey bees, winter rapeseed, field beans.

INTRODUCTION

According to (Crane, 1990), only 16% of the world's flowering plant species contribute to honey bees (*Apis* spp.) as food sources. Moreover, not all bee plants are equally important to bees and honey production (Adgaba et al., 2017). This indicates that, for every local geographical region, there are very few important honey source plants. Based on comprehensive studies, it was possible to estimate the honey production potentials of some major honey source plants: such as *Trifolium pratense* L. (red clover) (883 kg of honey ha^{-1} flowering season; Szabo & Najda, 1985); *Asclepias syriaca* L. (milkweed) (500–600 kg honey ha^{-1} per flowering season; Zsidei, 1993) and *Phacelia tanacetifolia* Benth (60–360 kg honey ha^{-1} per flowering season; Nagy, 2002). Average honey production per hive is 20 kg throughout the world (Kizilaslan & Kizilaslan, 2007).

Beekeeping in Latvia is a long-standing agricultural industry developing rapidly along with other industries. The only honey bee species used in Latvian beekeeping is *Apis mellifera* (Zacepins et al., 2021).

Latvia is located in a mixed forest area, which occupies 48.21% of the entire territory, while 35.44% is arable land, meadows, pastures and gardens, 1.61% - shrubs and 3.34% - marshes[1], but the remaining areas (land under waters, roads, etc.) are not suitable for beekeeping. The natural foraging base does not provide the honey yield evenly throughout the whole season, thus the average honey yield in Latvia is about 20 kg per colony. In some periods, at the end of May and in the second half of summer, natural yield decreases (Liepniece, 2015).

A very rich composition of plants is found in Latvia, therefore bees have an opportunity to bring very diverse nectar into their hive (Lapina, 2016). One of the important cultivated plants for the honey bees in Latvia is rape (*Brassica napus* L.). This is a 60–130 cm high annual herbaceous plant belonging to the family of cruciferous plants (Brassicaceae). Rape is a good nectar crop with a high yield. In rape flowers, nectar is released continuously, so bees can visit one flower repeatedly (Liepniece, 2015). Oilseed rape honey crystallizes very rapidly after the honey extraction, as there is more glucose than fructose in the plant nectar, which influences the fructose/glucose ratio in honey (Bertazzini & Forlani, 2016). This honey becomes almost white, as there are practically no minerals. Some other field crops important for honey bees also should be mentioned. For instance, two legumes (Fabaceae) species - faba bean (*Vicia faba* L.) and winter vetch (*Vicia villosa* Roth) - are relatively popular in Latvia.

Honey production of the colonies is under the effect of many factors, such as the performance of the bee queen, colony strength and climate and pasture conditions (Genç & Aksov, 1993). A high honey yield can be obtained by having strong colonies at the beginning of honey flow. Honey yield can also be affected by the professionality of the beekeepers and colony health status, as well selection of the apiary location is important (Komasilova et al., 2020).

Nowadays, the evaluation of a honey bee colony foraging activity can be done remotely and continuously, thanks to achievements in the precision beekeeping. Precision beekeeping allows to remotely monitor individual bee colonies using the information and communication technologies (Zacepins, 2015). One of the colony parameters that is important for the beekeepers is its weight. Weight dynamics can provide the beekeeper with essential information on several important colony events (Buchmann & Thoenes, 1990; Meikle et al., 2006, Komasilovs et al., 2019). Colony weight should be monitored in order to: identify the beginning and the end of nectar flow or daily gain in nectar stores (Meikle et al., 2008; Okada et al., 2012; Human & Brodschneider, 2013); monitor food consumption during passive period (Seeley & Visscher, 1985; Stalidzans et al., 2017); to detect swarming event (Meikle et al., 2008; Linton, 2012). The application of colony

[1] The State Land Service (https://www.vzd.gov.lv/lv/zemes-sadalijums-zemes-lietosanas-veidos) [last accessed: 15.12.2021]

scales is well-established in the beekeeping industry, as they are used to determine the gains and losses of the hive mass and, in this way, indirectly indicate an increase or decrease in honey growth in a bee colony (Bratek & Dziurdzia, 2021).

Precision beekeeping in Latvia also started to be a part of the beekeeping practice, thus the benefits of such an approach should be presented to the beekeeper community (Zacepins et al., 2021).

The main aim of this research was to monitor and analyse the honey bee colonies weight dynamics during the oilseed winter rape and beans flowering period in one location in Latvia using the automated bee colony scales.

MATERIALS AND METHODS

Location description

Experiment and measurements were carried out at LLU (Latvia University of Life Sciences and Technologies) apiary (Fig. 1), located in Vecauce, Latvia (GPS coordinates: 56.46753585940729, 22.88788600517433) during spring-summer period 2021 (from 07.05.2021 until 07.09.2021). For this publication, data from 04.06.2021 until 21.06.2021 was analysed, as this period corresponds to the intensive winter rapeseed, faba beans and winter vetch flowering period.

Within a radius of three kilometres, various habitats were found around the studied *apiary*: agricultural land, forests, small town, roads, railways, small rivers and ditches. Most of this area was occupied by agricultural land, which was mostly used for various arable crop growing.

Figure 1. Honey bee apiary in Vecauce, Latvia.

Among these, winter oilseed rape was grown in the fields with a total area of 182.79 ha, faba beans - 106.47 ha and winter vetch - 25.99 ha (Fig. 2).

Apiary description

Ten honey bee (*Apis mellifera*) colonies from the 40 colony apiary were chosen (based on a beekeeper's suggestion) for the remote monitoring. Colonies were placed in Latvian design type hives made from wood with frame dimensions of 300 mm (height) and 435 mm (width) for brood, and frames with dimensions of 146.5 mm (height) and 435 mm (width) for honey. All hives were put in the same location in an open environment with the distance of at least 5 m between hives in a one column and 3.5–4.5 m between hives in a one row. Hive volume for the brood is 81.7 L, but if additional honey frames (twelve frames) are added then volume increase to 120 L. Weight and temperature of the colonies were continuously measured with the time interval of 30 minutes between two measurements by the automated bee colony scales (including inside thermometer), and in addition environmental temperature was monitored. For some analysis (Table 2) author's used average values per day to decrease the potential error if using one value at exact moment.

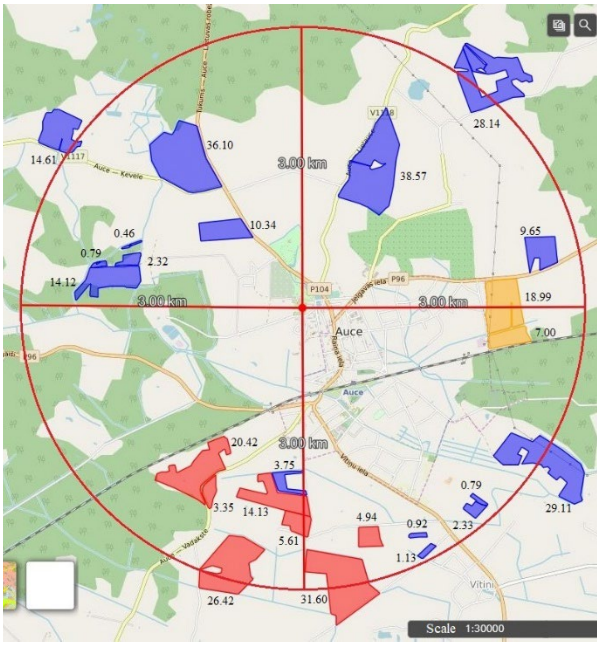

Figure 2. Topographic map of Vecauce area. The center of the red circle indicates the apiary that was studied. The red circle delimits the area within a radius of 3 km around the apiary. Fields in which winter rape, faba beans and winter vetch were grown in 2021 are painted in violet, red and yellow, respectively. The numbers next to these fields indicate their area in hectares.

Monitoring device

All colonies were equipped with bee colony monitoring system based on the ESP8266 microchip inspired by the monitoring system developed within the SAMS project (Wakjira et al., 2021). For weight monitoring, a single-point load cell Bosche H30A was used. For the bee colony temperature monitoring DS18S20 1-Wire® sensors were used. Load cell accuracy and precision were empirically evaluated by (Kviesis et al., 2020). The precision of the scale measurement system (single point load cell H30A together with the 24-bit HX711 A/D converter) was observed to be around 10 g.

One temperature sensor (Dallas DS18S20) per colony was installed inside the hive above the hive body (brood frames) as suggested by (Stalidzans & Berzonis, 2013).

The monitoring system was powered by a Sony Li-ion 18650 3.7 V 3120 mAh battery. Data about the bee colony, battery charging status and wi-fi signal were collected every 30 minutes and sent to the remote cloud platform. The screenshot below (Fig. 3) demonstrates how the summary of the colony monitoring was shown to the beekeeper on the cloud platform in real-time:

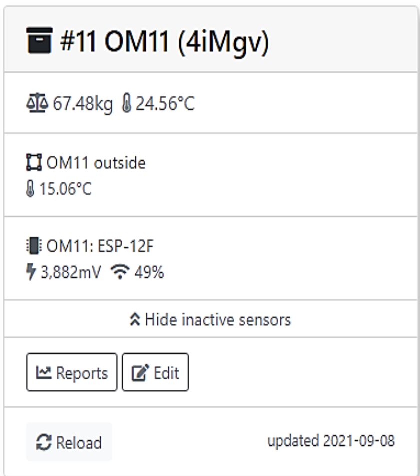

Figure 3. Data demonstration to the end users.

For the internet connection, local Wi-Fi network was used. Distance from the Wi-Fi router to the monitoring nodes was around

70 m, and the signal strength was considered as below average. To prevent data loss due to the Wi-Fi router failure (or bad signal strength caused by weather or other obstacles), each monitoring device was equipped with an SD card.

Description of environmental parameters

Weather conditions during the observation period were suitable for successful foraging activities (see Table 1). Data about environmental parameters were collected from nearest public weather station from www.meteo.lv. Table below summarises the average values for temperature, humidity, wind and rain during the observation period.

Based on the literature data (Komasilova et al., 2021) the observed conditions are considered as great for the foraging process. Ideal conditions are considered when temperature is between 20 °C and 30 °C, humidity between 60% and 80%, wind speed less than 5 m s^{-1}, and there is no rain.

Table 1. Meteorological data during the observation period

Date	Average values (time period: 5:00–22:00)			
	Air temperature, °C	Humidity, %	Wind, m s^{-1}	Rain, mm
04.06.2021	18.38	62.33	1.88	0.00
05.06.2021	19.18	57.47	3.72	0.00
06.06.2021	19.56	55.06	3.25	0.00
07.06.2021	20.66	57.00	4.03	0.00
08.06.2021	19.12	68.75	3.46	0.00
09.06.2021	18.98	68.89	2.98	0.00
10.06.2021	19.51	66.72	2.78	0.00
11.06.2021	20.15	68.50	2.25	0.00
12.06.2021	16.73	84.42	3.32	2.32
13.06.2021	15.84	66.67	7.10	0.07
14.06.2021	17.40	55.25	2.97	0.00
15.06.2021	17.80	62.61	4.38	0.00
16.06.2021	18.15	55.36	2.29	0.00
17.06.2021	20.43	59.50	2.64	0.00
18.06.2021	23.58	57.44	3.19	0.00
19.06.2021	25.28	58.84	3.27	0.00
20.06.2021	26.40	62.64	3.69	0.00
21.06.2021	27.34	61.53	4.06	0.00

Pollen analysis methodology

Pollen was collected in apiary using pollen traps placed outside the beehive entrance. The beekeeper took pollen samples (400 g) from five hives every two weeks, thus these samples contained pollen collected during two-week period of time. The samples were stored in a freezer at –18 °C until the middle of August when they were prepared for further analysis. All samples were then divided into two parts. One part of each sample was placed in a dryer at 35 degrees and dried for 24–36 hours, then sent to Quality Services International GMbH in Germany for analysis of the botanical composition. The second part of each sample was sent frozen to the Water & Life Lab analytical laboratory in Italy to identify pesticide residues in the pollen. The botanical composition of pollen was determined using microscopy, and the pesticide residues were determined using GC/MS/MS, LC/MS/MS methods with the lowest analytical limit of 0.01 mg kg^{-1}.

RESULTS AND DISCUSSION

Time period from 04.06.2021 till 21.06.2021 was taken for the detailed analysis of the weight gain of the ten monitored bee colonies.

Table 2. Average weight per day for all colonies

Date	Average weight per date, kg									
	#1	#2	#3	#4	#5	#6	#7	#8	#9	#10
04.06.2021	104.53	117.78	89.58	118.08	94.72	98.28	113.02	108.02	113.76	107.12
05.06.2021	106.29	118.15	91.72	115.89	95.84	100.47	114.96	108.85	116.57	111.29
06.06.2021	107.33	126.23	90.40	121.74	96.84	98.57	121.78	114.43	121.88	116.85
07.06.2021	110.94	132.36	89.40	127.03	100.05	97.80	126.85	119.47	128.63	119.46
08.06.2021	113.47	137.80	91.57	130.44	102.13	99.89	129.54	122.25	130.79	120.93
09.06.2021	114.50	139.37	92.21	133.07	103.85	100.88	131.37	123.34	132.66	121.32
10.06.2021	115.27	140.72	93.02	134.86	105.05	101.98	132.12	124.31	134.01	121.16
11.06.2021	115.96	142.56	93.74	136.23	105.40	102.67	132.81	125.06	134.82	119.02
12.06.2021	116.64	144.82	94.98	137.66	106.76	103.78	134.29	126.07	136.59	118.48
13.06.2021	116.38	140.19	93.91	137.28	106.26	101.09	133.62	125.86	136.18	118.23
14.06.2021	116.48	138.80	90.94	138.06	106.59	99.37	133.88	126.27	136.09	117.76
15.06.2021	118.52	142.37	91.75	141.10	110.47	100.24	136.27	128.26	138.72	118.19
16.06.2021	120.59	145.86	92.95	144.22	112.39	101.66	138.75	130.51	141.70	118.91
17.06.2021	123.61	150.31	95.15	150.16	116.17	104.19	142.26	133.87	*145.84**	120.59
18.06.2021	126.90	154.32	97.82	155.09	119.91	107.41	145.99	137.40	*123.78**	123.10
19.06.2021	130.43	157.57	100.98	159.65	123.28	111.01	149.49	140.72	*114.41**	125.96
20.06.2021	134.24	160.00	104.26	163.67	125.91	114.19	152.77	143.75	117.55	128.54
21.06.2021	137.34	161.36	107.03	166.41	127.79	116.81	155.08	146.09	120.04	130.68

* On 18.06.2021 and 19.06.2021 beekeeper extracted some amount of honey from colony #9.

Table 2 and Fig. 4 below demonstrate average weight gain for all colonies. Average weight is calculated considering 30 minutes individual measurements intervals.

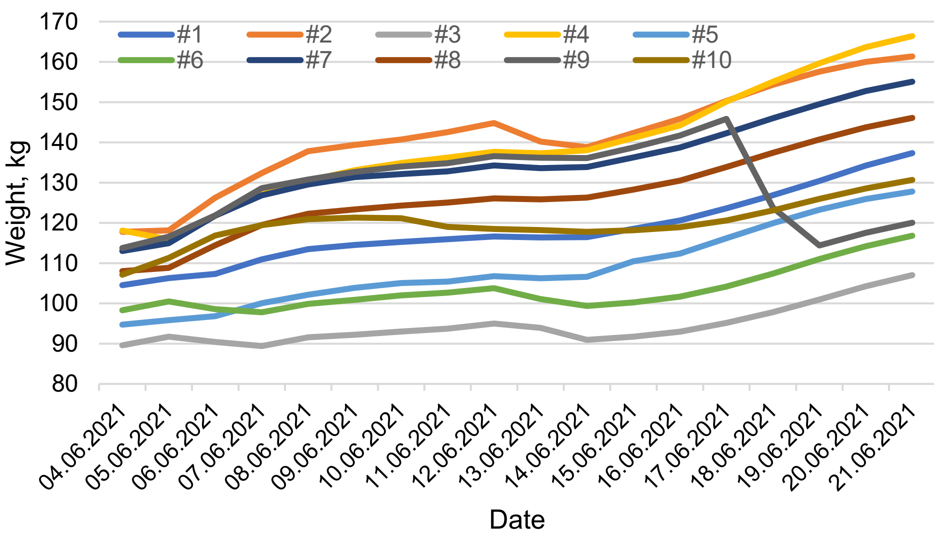

Figure 4. Weight dynamics of the monitored bee colonies.

It should be emphasised that weight gain for each colony differs, which can be explained by the fact, that colonies differ in strength, and it is also dependent on the starting weight of the colony (Table 3). Starting weight included the weight of the hive itself and the bees, brood and their food storages.

Table 3. Weight change of the hives for the whole period

	Weight change of the colonies									
	#1	#2	#3	#4	#5	#6	#7	#8	#9	#10
Starting weight, kg	104.53	117.78	89.58	118.08	94.72	98.28	113.02	108.02	113.76	107.12
End weight, kg	137.34	161.36	107.03	166.41	127.79	116.81	155.08	146.09	145.84	130.68
Change in weight, kg	32.81	43.58	17.45	48.33	33.07	18.53	42.06	38.07	32.08	23.56
Change in weight, %	31%	37%	19%	41%	35%	19%	37%	35%	28%	22%

Average weight change for all colonies - 31%.

It can be observed that the heaviest bee colony increased its initial weight by 41%, but on average bee colonies increased their weight by 31%.

Changes in the weight for all colonies per day are summarised in Table 4 below:

Table 4. Weight change of all tested colonies per day

Date	Weight change per date, kg									
	#1	#2	#3	#4	#5	#6	#7	#8	#9	#10
04.06.2021	0.000	0.000	0.000	0.000	0.000	0.000	0.000	0.000	0.000	0.000
05.06.2021	1.769	0.372	2.140	-2.192	1.119	2.188	1.938	0.828	2.815	4.170
06.06.2021	1.038	8.086	-1.321	5.851	1.002	-1.907	6.822	5.583	5.307	5.558
07.06.2021	3.604	6.128	-0.997	5.296	3.212	-0.769	5.073	5.044	6.753	2.608
08.06.2021	2.531	5.438	2.170	3.410	2.078	2.096	2.683	2.781	2.153	1.470
09.06.2021	1.032	1.570	0.631	2.627	1.718	0.988	1.833	1.086	1.878	0.389
10.06.2021	0.775	1.347	0.817	1.786	1.197	1.101	0.752	0.968	1.350	-0.161
11.06.2021	0.685	1.844	0.714	1.376	0.353	0.689	0.692	0.755	0.809	-2.133
12.06.2021	0.676	2.255	1.239	1.423	1.363	1.107	1.481	1.012	1.762	-0.544
13.06.2021	-0.259	-4.626	-1.063	-0.374	-0.498	-2.690	-0.673	-0.215	-0.401	-0.248
14.06.2021	0.101	-1.390	-2.971	0.779	0.328	-1.715	0.255	0.413	-0.096	-0.473
15.06.2021	2.044	3.565	0.805	3.042	3.875	0.863	2.393	1.993	2.637	0.435
16.06.2021	2.067	3.489	1.203	3.120	1.920	1.421	2.481	2.249	2.978	0.722
17.06.2021	3.025	4.458	2.204	5.935	3.784	2.536	3.511	3.356	4.139	1.676
18.06.2021	3.286	4.010	2.669	4.932	3.743	3.213	3.730	3.531	*2.514**	2.505
19.06.2021	3.533	3.243	3.155	4.564	3.366	3.603	3.495	3.320	*2.514**	2.868
20.06.2021	3.808	2.435	3.284	4.019	2.632	3.184	3.280	3.027	3.136	2.577
21.06.2021	3.102	1.355	2.768	2.741	1.884	2.622	2.316	2.347	2.494	2.142

* For colony #9 on the days, when honey was extracted, we used the average weight increase values observed on previous days.

Fig. 5 demonstrates average daily weight change of the whole group of colonies with the standard deviation. Weight change is directly related to the amount of possible foraging resources, also weather conditions has effect on the foraging activity.

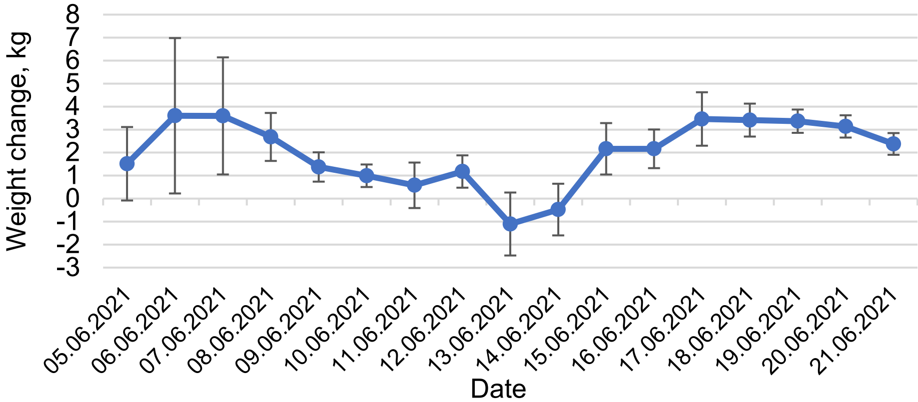

Figure 5. Average daily weight change of the whole group of colonies with the standard deviation.

Table 5. below shows maximum weight gain during one day for all colonies. It can be seen that individual bee colony can gain up to 8kg per day, depending on the foraging resources, environmental conditions and colony strength.

Table 5. Maximum weight gain per day

Max weight per day, kg									
#1	#2	#3	#4	#5	#6	#7	#8	#9	#10
3.808	8.086	3.284	5.935	3.875	3.603	6.822	5.583	6.753	5.558

Daily routine of the bee colony

Continuous monitoring of the honey bee colony weight allows to identify daily patterns of their activity during sunny summer days. Based on the weight data, honey bee day can be split into 3 periods: nectar processing by reducing the water content during the night; flying out and foraging; coming back with collected nectar (see Fig. 6).

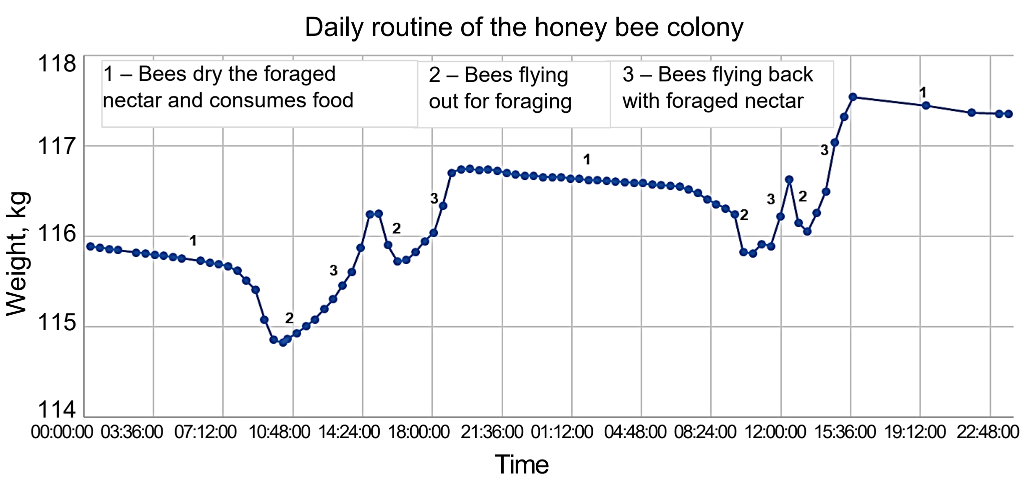

Figure 6. Daily routine of the honey bee colony.

Identification of the swarming event

In addition to the foraging activity, weight data monitoring can provide also information about the swarming event of the colony. During the observation period, one bee colony swarmed, and Fig. 7 below demonstrates this event. Suddenly #10 colony weight dropped by 2.6 kg: from 120.54 kg to 117.91 kg, and beekeeper on-site approved that the colony swarmed. This weight change during the swarming agrees with swarm weight identified by (Villa, 2004).

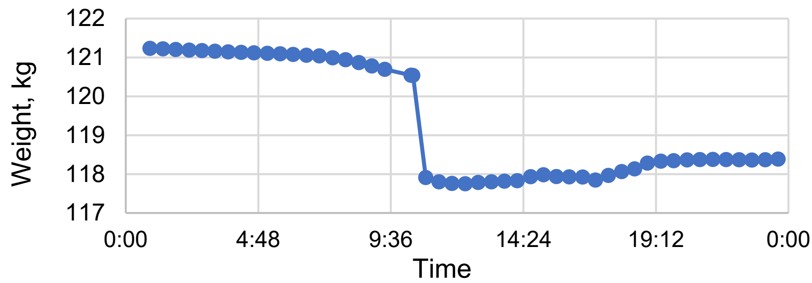

Figure 7. Weight change during the bee colony swarming event.

Effect of the rain on the foraging activity

During the foraging period weather conditions were excellent, without much precipitation. Rain was observed only on 12.06 and 13.06. Analysing bee colony average weight gain per day, it can be seen that weight decreased on 13.06 and 14.06.

This could be explained by the fact that rain affect the quality of nectar by dilution and washing out (Lawson & Rands, 2019). Authors assume that plants needed some time to produce new nectar.

Evaluation of the system battery life for the continuous monitoring

The developed bee colony monitoring system was powered by the one Sony Li-ion 18650 3.7 V 3120 mAh battery. It was evaluated that the system can operate up to 40 days with a fully charged battery. Fig. 8 below demonstrates the battery discharging dynamics during the continuous measurements with 30 minutes intervals.

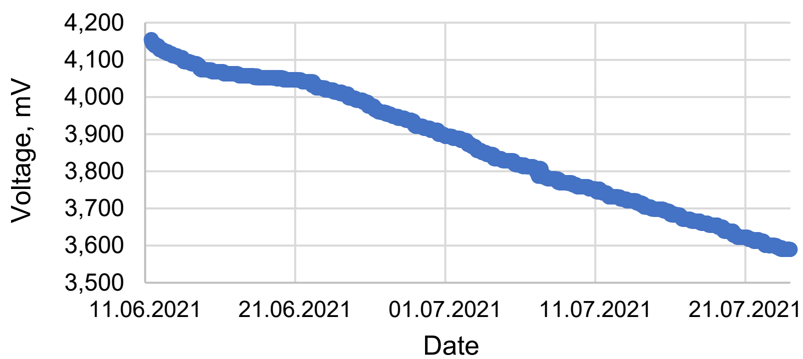

Figure 8. Battery discharge dynamics during the measurements.

Some authors report of similar system operation of 131 days with a standard deviation of 30 days (Bratek & Dziurdzia, 2021), but the measurement interval was 6 hours, not 30 minutes as done in this authors' research. However, 40 days of operation is considered to be relevant in this particular case, as beekeeper anyway visits the apiary for managemental tasks, so the change of batteries is possible.

Pollen analysis results

At the beginning of June, pollen from Brasicaceae plants predominated in the samples (58%). The bees had also collected pollen from poppies (*Papaver* spp.), dandelions (*Taraxacum* spp.), pears (*Pyrus* spp.) and other plants. During this period, the rape fields close by the apiary were in full bloom. This also explains the high proportion of pollen from Brasicaceae plants in bee yields. In the middle and second half of the month, rape had finished blooming, but field beans and vetch began to bloom. Pollen from these plants predominated in samples collected in the second half of June. Their proportion was 66%. The bees had also collected pollen from clover (*Trifolium* spp.), raspberries (*Rubus* spp.), umbellifers (Apiaceae spp.) and other plants.

Analysis of the test results for the botanical composition of the collected pollen shows that, during the period from 1st of June till 7th of June (winter rapeseed blooming period 17.05.2021-07.06.2021), bees were collecting the nectar mostly from the field where the rapeseed was grown. As pollen sample for the dates from 1st till 14th of June featured 56% of pollens containing Brassicaceae family pollens. But, in the next two weeks, field beans and winter vetch were more attractive for the bees - 66% of field bean pollens were in the sample collected from the 14th till 28th of June (field bean flowering period was from the 14th of June till 28th of June. This fact was unexpected, as usually bees choose the closest place with more intensively blooming and bright flowers (distance to rapeseed was 1.6 km closer than distance to field beans, blooms of yellow colour for bees are more attractive (Papiorek et al., 2016)).

Analysis of the plant protection product residues showed no active substrance for the field beans. For the Winter rapeseed two active substrances were found: Azoxystrobin (29 mg kg^{-1}) and Difenoconazole (0.11 mg kg^{-1}).

CONCLUSIONS

For the first time remote and continuous monitoring of the bee colony weight dynamics during the winter rapeseed and field beans flowering was performed in Latvia. The data collected, showed that if foraging conditions are good, then colony can intensively gain weight and perform active foraging process.

In conditions of the present study it was calculated for the tested period that an average of 31% weight gain was obtained.

An additional benefit of the real-time weight monitoring of the bee colonies can be the swarming event identification.

Taking into account the data obtained, by using the electronic hives, the beekeeping areas can be remotely monitored in order to evaluate accurately the honey flows at different crops, honey production or necessity of artificial feedings. Thus, the beekeepers can decide on the necessity to move the apiary to another geographical location.

ACKNOWLEDGMENTS. Scientific research activities were conducted during the s396 project ('Evaluation and identification of the most effective control methods for topical pests of legumes and identification of factors influencing the viability of pollinators important for agriculture'). This research work was also supported by the project HIVEOPOLIS which has received funding from the European Union's Horizon 2020 research and innovation programmes under grant agreement No. 824069.

REFERENCES

Adgaba, N., Al-Ghamdi, A., Tadesse, Y., Getachew, A., Awad, A.M., Ansari, M.J., Owayss, A.A., Mohammed, S.E.A. & Alqarni, A.S., 2017. Nectar secretion dynamics and honey production potentials of some major honey plants in Saudi Arabia. *Saudi Journal of Biological Sciences* **24**(1), 180–191.

Bertazzini, M. & Forlani, G. 2016 Intraspecific Variability of Floral Nectar Volume and Composition in Rapeseed (Brassica napus L. var. oleifera). *Frontiers in Plant Science* **7**, 288. doi: 10.3389/fpls.2016.00288

Bratek, P. & Dziurdzia, P. 2021. Energy-Efficient Wireless Weight Sensor for Remote Beehive Monitoring. *Sensors* **21**(18), 6032.

Buchmann, S. & Thoenes, S. 1990. The electronic scale honeybee colony as a management and research tool. *Bee Science* **1**, 40–47.

Crane, E. 1990. *Bees and Beekeeping: Science, Practice and World Resources Heinemann Newnes*. Oxford. 614 pp. ISBN: 9780801424298

Genç, F. & Aksoy, A., 1993. Some of the correlations between the colony development and honey production on the honeybee (Apis mellifera L.) colonies. *Apiacta* **28**(2), 33–41.

Human, H. & Brodschneider, R. 2013. Miscellaneous standard methods for Apis mellifera research. *Apicultural Research* **52**(4), 1–53.

Kizilaslan, H. & Kizilaslan, N. 2007. Factors affecting honey production in apiculture in Turkey. *Journal of Applied Sciences Research* **3**(10), 983–987.

Komasilova, O., Komasilovs, V., Kviesis, A., Bumanis, N., Mellmann, H. & Zacepins, A. 2020. Model for apiary location evaluation. *Agronomy Research* **18**(S2), 1350–1358. https://doi.org/10.15159/ar.20.090

Komasilovs, V., Zacepins, A., Kviesis, A., Fiedler, S. & Kirchner, S. 2019. 'Modular sensory hardware and data processing solution for implementation of the precision beekeeping', *Agronomy Research* **17**(2), 509–517. doi: 10.15159/AR.19.038

Kviesis, A., Zacepins, A., Fiedler, S., Komasilovs, V. & Laceklis-Bertmanis, J. 2020. Automated system for bee colony weight monitoring. *Agrofor international journal* **5**(2), 42–53.

Lapina, L. 2016. Diversity of honey in Latvia. *Harmonious Agriculture* **3**, 134–138.

Lawson, D.A. & Rands, S.A., 2019. The effects of rainfall on plant–pollinator interactions. *Arthropod-Plant Interactions* **13**(4), 561–569.

Liepniece, M. 2015. Nectar plnats (Latvian: Nektarāugi). Publisher: Latvian Beekeepers Association, 2015, p.104.

Linton, F. 2012. Hive Monitoring Technology: High Tech Hives. *American Bee Journal* **152**(8), 767–769.

Meikle, W., Hoist, N. & Mercadier, G. 2006. Using balances linked to data loggers to monitor honeybee colonies. *Journal of Apicultural Research* **45**, 39–41.

Meikle, W., Rector, B., Mercadier, G. & Holst, N. 2008. Within-day variation in continuous hive weight data as a measure of honeybee colony activity. *Apidologie* **39**, 694–707.

Okada, R., Akamatsu, T. & Iwata, K. 2012. Waggle dance effect: dancing in autumn reduces the mass loss of a honeybee colony. *The Journal of Experimental Biology* **215**, 1633–1641.

Papiorek, S., Junker, R.R., Alves-dos-Santos, I., Melo, G.A., Amaral-Neto, L.P., Sazima, M., Wolowski, M., Freitas, L. & Lunau, K., 2016. Bees, birds and yellow flowers: pollinator-dependent convergent evolution of UV patterns. *Plant Biology* **18**(1), 46–55.
Seeley, T.D. & Visscher, P.K. 1985. Survival of honeybees in cold climates: the critical timing of colony growth and reproduction. *Ecological Entomology* **120**(1), 826–88.
Stalidzans, E. & Berzonis, A. 2013. Temperature changes above the upper hive body reveal the annual development periods of honey bee colonies. *Computers and electronics in agriculture* **90**, pp.1–6.
Stalidzans, E., Zacepins, A., Kviesis, A., Brusbardis, V., Meitalovs, J., Paura, L., Bulipopa, N. and Liepniece, M. 2017. Dynamics of weight change and temperature of Apis mellifera (Hymenoptera: Apidae) colonies in a wintering building with controlled temperature. *Journal of economic entomology* **110**(1), 13–23.
Szabo, T.I. & Najda, H.G. 1985. Flowering, nectar secretion and pollen production of some legumes in the Peace River Region of Alberta, Canada. *J. Apic. Res*. **24**(2), 102–106.
Villa, J. D. 2004. Swarming behavior of honey bees (Hymenoptera: Apidae) in southeastern Louisiana. *Annals of the Entomological Society of America* **97**(1), 111–116.
Wakjira, K., Negera, T., Zacepins, A., Kviesis, A., Komasilovs, V., Fiedler, S., Kirchner, S., Hensel, O., Purnomo, D., Nawawi, M. & Paramita, A., 2021. Smart apiculture management services for developing countries-the case of SAMS project in Ethiopia and Indonesia. *PeerJ Computer Science* **7**, 484.
Zacepins, A., Brusbardis, V., Meitalovs, J. & Stalidzans, E. 2015. Challenges in the development of Precision Beekeeping. *Biosystems Engineering* **130**, 60–71.
Zacepins, A., Kviesis, A., Komasilovs, V., Brusbardis, V. & Kronbergs, J. 2021. Status of the Precision Beekeeping Development in Latvia. *Rural Sustainability Research* **45**(340), 86–92.
Zsidei, B. Méhészeti ismeretek. Fazekas és fiai nyomdája, Szarvas Nectar production for the Hungarian Honey Industry (1993) Reviewed by Farkas, A., Zajácz, E., 2007. *Eur. J. Plant Sci. Biotech. Global Science Book*, 125–151.

INSTRUCTIONS TO AUTHORS

Papers must be in English (British spelling). A proof-reader will revise English, but authors are strongly urged to have their manuscripts reviewed linguistically prior to submission. Contributions should be sent electronically. Papers are considered by referees before acceptance. The manuscript should follow the instructions below.

Structure: Title, Authors (initials & surname; an asterisk indicates the corresponding author), Authors' affiliation with postal address (each on a separate line) and e-mail of the corresponding author, Abstract (up to 250 words), Key words (not repeating words in the title), Introduction, Materials and methods, Results and discussion, Conclusions, Acknowledgements (optional), References.

Layout, page size and font
- Use preferably the latest version of **Microsoft Word**, doc., docx. format.
- Set page size to **ISO B5 (17.6×25 cm)**, all **margins at 2 cm**. All text, tables, and figures must fit within the text margins.
- Use single line spacing and **justify the text**. Do not use page numbering. Use **indent 0.8 cm** (do not use tab or spaces instead).
- Use font Times New Roman, point size for the title of article **14 (Bold)**, author's names 12, core text 11; Abstract, Key words, Acknowledgements, References, tables, and figure captions 10.
- Use *italics* for Latin biological names, mathematical variables and statistical terms.
- Use single ('…') instead of double quotation marks ("…").

Tables
- All tables must be referred to in the text (Table 1; Tables 1, 3; Tables 2–3).
- Use font Times New Roman, regular, 10 pt. Insert tables by Word's 'Insert' menu.
- Do not use vertical lines as dividers; only horizontal lines (1/2 pt) are allowed. Primary column and row headings should start with an initial capital.

Figures
- All figures must be referred to in the text (Fig. 1; Fig. 1 A; Figs 1, 3; Figs 1–3). Avoid 3D charts, background shading, gridlines and excessive symbols. Use font **Arial, 10 pt** within the figures. Make sure that thickness of the lines is greater than 0.3 pt.
- Do not put caption in the frame of the figure.
- The preferred graphic format is Excel object; for diagrams and charts EPS; for half-tones please use TIFF. MS Office files are also acceptable. Please include these files in your submission.
- Check and double-check spelling in figures and graphs. Proof-readers may not be able to change mistakes in a different program.

References
- **Within the text**

In case of two authors, use '&', if more than two authors, provide first author 'et al.':

Smith & Jones (2019); (Smith & Jones, 2019);
Brown et al. (2020); (Brown et al., 2020)

When referring to more than one publication, arrange them by following keys: 1. year of publication (ascending), 2. alphabetical order for the same year of publication:

(Smith & Jones, 2019; Brown et al., 2020; Adams, 2021; Smith, 2021)

- **For whole books**

Name(s) and initials of the author(s). Year of publication. *Title of the book* (*in italics*). Publisher, place of publication, number of pages.

Behera, K.B. & Varma, A. 2019. *Bioenergy for Sustainability and Security*. Springer International Publishing, Cham, pp. 1–377.

- **For articles in a journal**

Name(s) and initials of the author(s). Year of publication. Title of the article. *Abbreviated journal title* (*in italic*) volume (in bold), page numbers.
Titles of papers published in languages other than English, should be replaced by an English translation, with an explanatory note at the end, e.g., (in Russian, English abstr.).

Bulgakov, V., Adamchuk, V., Arak, M. & Olt, J. 2018. The theory of cleaning the crowns of standing beet roots with the use of elastic blades. *Agronomy Research* **16**(5), 1931–1949. doi: 10.15159/AR.18.213

Doddapaneni, T.R.K.C., Praveenkumar, R., Tolvanen, H., Rintala, J. & Konttinen, J. 2018. Techno-economic evaluation of integrating torrefaction with anaerobic digestion. *Applied Energy* **213**, 272–284. doi: 10.1016/j.apenergy.2018.01.045

- **For articles in collections:**

Name(s) and initials of the author(s). Year of publication. Title of the article. Name(s) and initials of the editor(s) (preceded by In:) *Title of the collection (in italics)*, publisher, place of publication, page numbers.

Yurtsev, B.A., Tolmachev, A.I. & Rebristaya, O.V. 2019. The floristic delimitation and subdivisions of the Arctic. In: Yurtsev, B.A. (ed.) *The Arctic Floristic Region*. Nauka, Leningrad, pp. 9–104 (in Russian).

- **For conference proceedings:**

Name(s) and initials of the author(s). Year of publication. Name(s) and initials of the editor(s) (preceded by In:) *Proceedings name (in italics)*, publisher, place of publishing, page numbers.

Ritchie, M.E. & Olff, H. 2020. Herbivore diversity and plant dynamics: compensatory and additive effects. In: Olff, H., Brown, V.K. & Drent R.H. (eds) *Herbivores between plants and predators. Proc. Int. Conf. The 38th Symposium of the British Ecological Society*, Blackwell Science, Oxford, UK, pp. 175–204.

Please note

- Use '.' (not ',') for decimal point: 0.6 ± 0.2; Use ',' for thousands – 1,230.4;
- Use '–' (not '-') and without space: pp. 27–36, 1998–2000, 4–6 min, 3–5 kg
- With spaces: 5 h, 5 kg, 5 m, 5 °C, C : D = 0.6 ± 0.2; p < 0.001
- Without space: 55°, 5% (not 55 °, 5 %)
- Use 'kg ha^{-1}' (not 'kg/ha');
- Use degree sign ' ° ' : 5 °C (not 5 ^{O}C).